Great Lakes Water Quality Agreement
Nutrient Annex Objectives and Targets Task Team
Ensemble Modeling Report
DRAFT

Prepared for:

GLWQA Nutrient Annex 4 Objectives and Targets Task Team

By the Modeling Subgroup

March 15, 2015

Annex 4 Ensemble Modeling Report
DRAFT

Prepared for:

GLWQA Nutrient Annex 4 Objectives and Targets Task Team

By the Modeling Subgroup

March 15, 2015

Disclaimer

This report was supported by EPA, through a contract with Battelle, and Environment Canada.

This document is a preliminary draft. It has not been formally released by the U.S. Environmental Protection Agency (EPA) and should not at this stage be construed to represent Agency policy. It is being circulated for comments on its technical merit and policy implications. EPA, through its Great Lakes Program Office, funded and managed this work under Contract No. EP-R5-11-07, Task Order 21.

Questions concerning this document or its application should be addressed to:

Jean Chruscicki
U.S. Environmental Protection Agency
Region 5
77 Jackson Boulevard
Mail Code: WW-16J
Chicago, IL 60604-3507
312-353-1435
Chruscicki.jean@EPA.gov

Modeling Subgroup

Donald Scavia, Co-Principal Investigator, University of Michigan
Joseph DePinto, Co-Principal Investigator and Investigator for WLEEM, LimnoTech

University of Michigan
Hongyan Zhang, Technical Lead for 2D EcoLE Model
Daniel Obenour, Technical Lead for Probabilistic Cyanobacteria Model
Serghei Bocaniov, ELCOM-CAEDYM 3D Model
Isabella Bertani, Probabilistic Cyanobacteria model and report preparation
Cara Steger, Probabilistic Cyanobacteria model and report preparation

LimnoTech Inc.
Daniel Rucinski, 1D Central Basin Hypoxia Model

Michigan Technological University
Martin Auer, Great Lakes *Cladophora* Model

Tufts University
Stephen Chapra, TP Mass Balance Model

Environment Canada
Ram Yerubandi, 9-Box Model and ELCOM-CAEDYM 3D Model
Louis Leon, 9-Box Model and ELCOM-CAEDYM 3D Model
Craig McCrimmon, 9-Box Model

National Oceanographic and Atmospheric Administration
Richard Stumpf, Harmful Algal Bloom Model

Battelle
Harry Stone

Annex 4 Ensemble Modeling Report

Contents

1. Introduction

The U.S. Environmental Protection Agency (U.S. EPA), Environment Canada (EC) and other partners are using multiple existing models, in an ensemble of models approach, to provide load-response relationships for Eutrophication Response Indicators (ERIs) of concern. This report describes the approach and results of technical analysis of models included in the ensemble approach as applied to Lake Erie (see Figure 1). The report includes the results from a range of phosphorus load-response curves for Lake Erie, generated by models that relate phosphorus loads to objectives outlined in Annex 4 of the 2012 Great Lakes Water Quality Agreement (GLWQA). The results of the technical evaluation and modeled load-response curves provide objective information and an ensemble modeling approach for recommendations to the Annex 4 Objectives Task Team.

The Lake Erie ecosystem objectives of Annex 4 (Nutrients) in the Amendment to the GLWQA (September 7, 2012) are summarized as follows:

1. minimize hypoxic zones related to excessive phosphorus loading;
2. prevent nuisance levels of algal biomass;
3. maintain healthy nearshore ecosystems as indicated by algal communities;
4. prevent harmful algal blooms that produce toxins posing a human or ecosystem health threat; and
5. ensure that the open waters of the Western and Central Basins of Lake Erie maintain mesotrophic conditions and oligotrophic conditions are maintained in the Eastern Basin of Lake Erie.

Four Eutrophication Response Indicators (ERIs) reflecting the Annex 4 objectives for Lake Erie were evaluated and modeled by applying one or more models for potential inclusion in an ensemble modeling approach. The ERIs included: (1) basin-wide phytoplankton biomass as represented by chlorophyll-*a* (chl-*a*) (indicates lake trophic status); (2) Western Basin basin-wide cyanobacteria biomass; (3) Central Basin hypoxia extent and duration; and (4) Eastern Basin extent of nuisance levels of the green algae *Cladophora*.

Figure 1. Map of Lake Erie showing the locations of the various basins, rivers, and municipalities

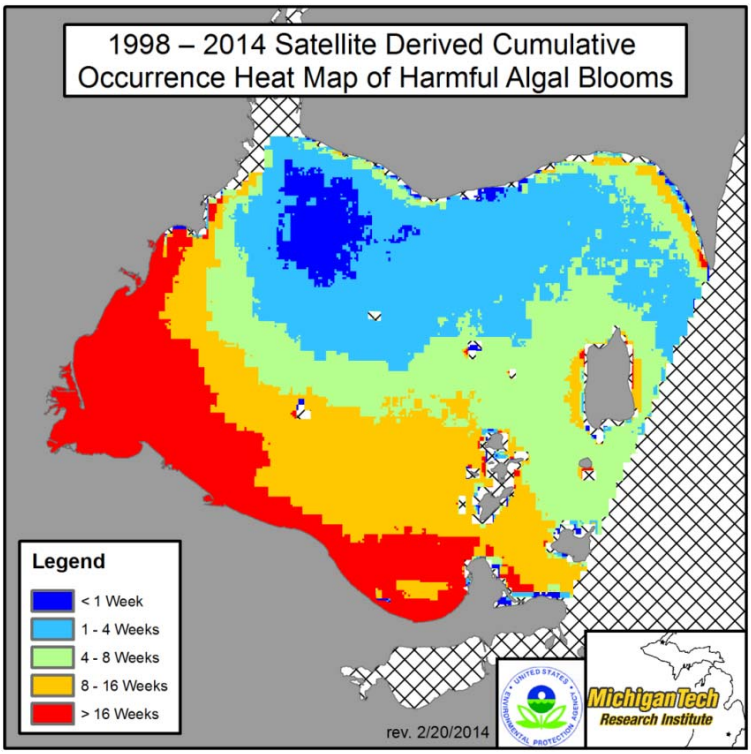

Figure 2. Map of cumulative durations of HABs for 1998-2014 for the Western Basin of Lake Erie, generated from SeaWiFS data and MODIS data (source: Michigan Tech Research Institute).

1.1 Background

In the late 1970s, a series of contemporary Great Lakes eutrophication models were applied to establish and confirm the target phosphorus loads for each of the Great Lakes and large embayments and basins to eliminate excess algae growth and improve areas of low dissolved oxygen, with the objective of limiting chlorophyll-*a* and algal indicators of eutrophication. Those target loads were codified in Annex 3 of the 1978 Amendment to the GLWQA. The models used for that analysis ranged from quite simple empirical relationships to kinetically complex, process-oriented models, including in order of increasing complexity: Vollenweider's empirical total phosphorus (TP) model (all lakes), Chapra's semi-empirical model (all lakes), Thomann's Lake 1 process model (Lake Ontario and Lake Huron), DiToro's process model (Lake Erie), and Bierman's process model (Saginaw Bay). The results of these model applications have been documented in the International Joint Commission (IJC) Task Group III report (Vallentyne and Thomas, 1978) and in Bierman (1980). The post-audit of several of these models in the mid-1980s confirmed that they had established a good relationship between total phosphorus (TP) loading to a lake/basin/embayment and its system-wide averaged TP and chlorophyll-*a* concentration.

In 2006 as part of the Parties' (U.S. EPA, Environment Canada) review of the GLWQA, a sub-committee of Great Lakes modelers (co-chaired by Joe DePinto at LimnoTech, and David Lam at Environment Canada) was charged to conduct an examination of the data and models used to support the phosphorus target loads specified in Annex 3 of the 1978 Agreement relative to the current status of the Lakes. The charge to that sub-group was to address three questions:

(1) Have we achieved the target phosphorus loads in all of the Great Lakes?
(2) Have we achieved the water quality objectives in all of the Great Lakes?
(3) Can we define the quantitative relationships between phosphorus loads and lake conditions with existing models? Are the models still valid on a whole lake basis or have ecosystem changes to the phosphorus (P) - chlorophyll relationship occurred such that new or updated models need to be run?

The findings were that those models were aimed at whole lake eutrophication symptoms as they were manifested at the time, but were not sufficiently spatially resolved to capture the nearshore eutrophication being observed throughout the lakes. The models did not represent the process formulations required to capture the impacts of ecosystem structure and function changes (e.g., impacts from Dreissenid mussels and other aquatic invasive species) relative to phosphorus processing and eutrophication responses in the lakes (DePinto *et al.*, 2006). The sub-committee of Great Lakes modelers recommended a new, concerted research, monitoring, and model enhancement effort to:

- Quantify the relative contributions of various environmental factors (TP loads, changes in the bioavailability of phosphorus, hydrometeorological impacts on temperature conditions and hypolimnion (dense, colder water below the thermocline) structure and volume, Dreissenid-induced alterations of nutrient-phytoplankton-light conditions and oxygen demand functions) to the nearshore re-eutrophication of the Great Lakes; and
- Develop a revised quantitative relationship between these stressors and the recently observed eutrophication indicators such as cyanobacteria blooms, enhanced hypoxia (defined

as dissolved oxygen levels below 4 mg/L) and nuisance benthic algal (e.g., *Cladophora*, *Lyngbya*) growth.

The 2012 Protocol for the GLWQA (United States and Canada, 2012) includes Annex 4 on Nutrients, in particular on phosphorus control to achieve ecosystem objectives related to eutrophication symptoms. The Annex sets "interim" phosphorus concentration objectives and loading targets that are identical to those established in the 1978 Amendment. However, it requires that the "Parties, in cooperation and consultation with State and Provincial Governments, Tribal Governments, First Nations, Métis, Municipal Governments, watershed management agencies, other local public agencies, and the Public, shall:

(1) For the open Waters of the Great Lakes:
   a. Review the interim Substance Objectives for phosphorus concentrations for each Great Lake to assess adequacy for the purpose of meeting Lake Ecosystem Objectives, and revise as necessary;
   b. Review and update the phosphorus loading targets for each Great Lake; and
   c. Determine appropriate phosphorus loading allocations, apportioned by country, necessary to achieve Substance Objectives for phosphorus concentrations for each Great Lake;

(2) For the nearshore Waters of the Great Lakes:
   a. Develop Substance Objectives for phosphorus concentrations for nearshore waters, including embayments and tributary discharge for each Great Lake;
   b. Establish load reduction targets for priority watersheds that have a significant localized impact on the Waters of the Great Lakes."

The Annex calls for research and other programs aimed at setting and achieving the revised nutrient objectives. It also calls for the Parties to take into account the bioavailability of various forms of phosphorus, related productivity, seasonality, fisheries productivity requirements, climate change, invasive species, and other factors, such as downstream impacts, as necessary, when establishing the updated phosphorus concentration objectives and loading targets. Finally, it calls for the Lake Erie objectives and loading target revisions to be completed within three years of the 2012 GLWQA entry into force.

To assist the Parties in accomplishing these mandates, an ensemble modeling team collaborating with the Annex 4 Objectives Group (referenced hereinafter as "Modeling Team"), developed an approach to evaluate the interim phosphorus objectives and load targets for Lake Erie and to provide information to update those targets using new research, monitoring and modeling in the lake. The plan that is developed for Lake Erie can serve as a general template for the other Great Lakes in meeting the 2012 GLWQA Protocol Annex 4 mandates.

2. Approach and scope

The Annex 4 Objectives Task Group requested that initial considerations of phosphorus load reduction targets be guided by the Modeling Team in the Fall of 2014. The Modeling Team convened during two workshops: a model evaluation and planning workshop in April 2014 and an ensemble modeling workshop in September 2014. These efforts were designed to identify eutrophication response indicators and models currently available to address them; to provide an internal peer review of the models; and to assemble model results into an ensemble capable of informing phosphorus load target-setting decisions.

There is precedent for using this ensemble (i.e., multiple) modeling approach for this type of assessment. A range of models with a range of complexities and approaches that use the same basic input data afford a comparison of results that can be very instructive. Reconciling differences among results in terms of the different assumptions used in various models provides insights about the most important sources and processes for a given system. Bierman and Scavia (2013) identified a number of benefits of applying multiple models of different complexity:

- Problems are viewed from different conceptual and operational perspectives;
- The same datasets are utilized in different ways;
- Multiple lines of evidence are provided;
- The level of risk in environmental management decisions is reduced; and
- Model diversity adds more value to the decision process than model multiplicity.

As described above, this approach was used in the late 1970's to establish the original target phosphorus loads for the Great Lakes (Bierman, 1980). Examples of other ensemble approaches to support management decisions regarding large ecosystems include:

- The Multiple Management Models (M3) approach being developed for Chesapeake Bay by the Chesapeake Bay Program's Scientific and Technical Advisory Committee (STAC) (http://www.chesapeake.org/stac/workshop.php?activity_id=222);
- The IJC project that compared three different mass balance models for PCBs in Lake Ontario to assess the state-of-the-art modeling of hydrophobic organic chemicals in large lakes (IJC, 1988);
- The use of multiple models to assess load – response relationships for hypoxia in the Gulf of Mexico (Scavia *et al*., 2004; Bierman and Scavia, 2013); and
- The use of multiple models to inform a nutrient TMDL for the Neuse River Estuary (Stow *et al*., 2003).

All of these efforts have provided new management insights and added confidence in using models for supporting management decisions.

2.1 Process

The Modeling Team and agency personnel were first assembled on April 9-10, 2014 to assess the capabilities of existing Lake Erie models to develop response curves for nutrient loads and the objectives identified by the Annex 4 group (See *Appendix A-1* for a workshop agenda and participant list and *Appendix A-3* for a report of that workshop). The objective of the workshop was to develop "[a] plan (scope, schedule, and budget) for conducting an ensemble modeling effort to develop recommendations to the Annex 4 Objectives Task Team for revised Lake Erie target P loads and objectives by the end of September, 2014." Models were initially evaluated in the April workshop on the basis of presentations by each modeler and by review of documentation reports/publications of development and application of each model.

The output from the workshop was used by EPA as the basis of a contract (EP-R5-11-07, Task Order 21) with Battelle through its Great Lakes Program Office. The contract envisioned that the models identified in the April Workshop plan would be evaluated and applied to develop load-response curves based on phosphorus load adjustment scenarios. Through this contract, Battelle subcontracted university and private sector members of the Modeling Team who were responsible for the identified models to execute elements of the workshop plan in order to provide objective data on performance of the models, and to develop an ensemble modeling approach. Dr. Don Scavia, University of Michigan, was subcontracted to serve as the Lead Principal Investigator. Dr. Scavia invited and secured collaboration by other members of the Modeling Team with identified models who were employed by the U.S. government or EC and therefore not funded via the EPA contract. Modelers and models in this project include:

- Richard Stumpf, National Oceanic and Atmospheric Administration (NOAA), Great Lakes Environmental Research Laboratory (GLERL): "NOAA/GLERL Western Lake Erie Harmful Algal Bloom (HAB) Model"
- Daniel Obenour, University of Michigan (UM): "UM/GLERL Western Lake Erie HAB Model"
- Steven Chapra, Tufts University: "TP Mass Balance Model"
- Daniel Rucinski, LimnoTech: "1-D Central Basin Hypoxia Model"
- Hongyan Zhang, University of Michigan: "Ecological model of Lake Erie" (EcoLE)
- Luis Leon and Ram Yerubandi, Environment Canada: "9-Box Model"
- Joseph DePinto, LimnoTech: "Western Lake Erie Ecosystem Model" (WLEEM)
- Serghei Bocaniov, University of Michigan, Luis Leon, Environment Canada, and Ram Yerubandi, Environment Canada: "Estuary, Lake and Coastal Ocean Model - Computational Aquatic Ecosystem Dynamics Model" (ELCOM-CAEDYM)
- Martin Auer, Michigan Technological University: "Great Lakes *Cladophora* Model".

[These modelers, representing a subset of the Modeling Team, are hereafter referenced as the "Modelers".]

During Summer and early Fall 2014, the Modelers prepared documentation, primarily from previous publications: complete documentation of model equations, coefficients, driving variables, assumptions, and time step of predictions; comparisons between model output and observations used in the model calibration; final model evaluation performance values; validation, and

assessments of model uncertainty/sensitivity. The Modelers also used a common set of phosphorus loads and meteorological variables as inputs to develop load-response curves for selected ERIs using their respective models.

The models all used data from 2008 as a baseline. The common set of phosphorus loads included six loading scenarios: 0 %, 25%, 50%, 75%, 100%, and 125% Total Phosphorus (TP); the 2008 baseline loading is defined as a 100% TP load. Reductions were made at 0%, 25%, 50%, and 75%, and one scenario increased current TP loading by 25% (125% scenario). Some of the models also evaluated the effects of reductions of selected external sources, including:

- TP from all tributaries and the Detroit River,
- TP from only the Maumee River,
- TP and dissolved reactive phosphorus (DRP) loads (by reducing concentration) from only the Detroit River,
- only DRP loads (by reducing concentration) from all tributaries and the Detroit River,
- only DRP loads (by reducing concentration) from only the Maumee River, and
- producing a baseline with no sediment feedback, either by re-suspension or pore water diffusion.

At the September 29-30, 2014 workshop, the modeling team presented, evaluated, and discussed the individual response curves. (See *Appendix A-2* for a workshop agenda and participant list). Each modeler presented calibration/confirmation results or other model skill assessment, described how the load-response curves were developed, showed load-response curves and any supporting diagnostic analyses, and described the level of uncertainty or sensitivity associated with the model. The details of each model formulation, calibration, confirmation, and sensitivity/uncertainty, as well as the construction of the load-response curves are provided in *Appendix B*.

On the second day of the workshop, discussions focused on the most appropriate ways to compare the models to produce ensemble guidance for developing load reduction targets. Once the individual models were applied to produce their respective load-response relationships, decisions had to be made on how best to synthesize these results into an ensemble. Ideally, each model would have been calibrated to the same data sets and driven by the same inputs (nutrient loads, meteorological drivers, etc.) to afford the opportunity to "average" results in forming the ensemble. However, given the limited time and resources available for this effort, the Modelers relied primarily on existing models that were built and tested with a range of conditions (See *Appendix B*). This deadline did not afford the modeling team time for a formal model comparison, vetting, and evaluation process by comparing all models using the identical input and measured response data set. Given this limitation, below we show the load-response curves for each modeled ERI with all inputs being as similar as possible.

2.2 Selecting Ecosystem Response Indicators

Selecting appropriate ERIs of concern for Lake Erie, along with metrics used to model and track them, was a critical step. The group selected four ERIs and defined how each metric was to be measured and what spatial and temporal scale would be used for each measurement.

(1) Overall phytoplankton biomass as represented by chlorophyll-a

- Basin-specific, summer average chlorophyll-*a* concentration

This is a traditional indicator of lake trophic status ranging from lakes with normoxic conditions and limited nutrient matter, to those with low dissolved oxygen and high nutrient concentration (i.e., oligotrophic, mesotrophic, eutrophic, respectively).

(2) Cyanobacteria blooms in the Western Basin

- Maximum 30-day average basin-wide cyanobacteria biomass

This metric gives an indication of the worst condition relative to harmful algal blooms (HABs) in the Western Basin. Blooms were quantified with an index that uses satellite imagery of biomass, based on chl-*a* as the surrogate for biomass. A Cyanobacteria Index (CI) was determined using composites of imagery to remove interference and biasing from clouds and to provide the best estimate of biomass. Estimates or averages were calculated in a variety of time intervals.

(3) Hypoxia (defined as bottom-layer dissolved oxygen concentrations <4 mg/L; Zhou et al. 2013) in hypolimnion of the Central Basin

- Number of hypoxic days
- Average areal extent of hypoxic area during summer
- Average hypolimnion dissolved oxygen (DO) concentration during a specified period (typically August and September)

These metrics are quantitatively correlated based on Central Basin monitoring and analysis, but they are different manifestations of the hypoxia problem. Each metric has a bearing on the impact on the ecosystem (especially fish communities), and on the relative impact of physical conditions versus nutrient-algal growth conditions.

(4) Cladophora in the nearshore areas of the Eastern Basin

- Algal dry weight biomass
- Stored phosphorus content

While beach fouling by sloughed *Cladophora* would likely be a desirable metric, there is neither an acceptable monitoring program to measure and report progress against such a metric, nor a scientifically credible model to relate it to nutrient loads and conditions. There are, however, models that can relate *Cladophora* growth to ambient DRP concentration and models that can estimate nearshore DRP as a function of TP loads and biophysical dynamics. Linking these models would allow *Cladophora* growth to be evaluated as a function of TP loads. Given the limited time available, the *Cladophora* growth as a function of TP loads was evaluated through a TP model developed for this effort (Chapra, Dolan, and Dove) and an empirical model relating DRP and TP based on EC measurements.

Models capable of estimating the impact of TP loads on each of the ERIs were identified. The models are summarized in Table 1 below and briefly described in section 2.4.

Table 1. Models included in the ensemble modeling effort

Model	Response Indicators			
	Overall basin-wide phytoplankton biomass	***Western Basin cyanobacteria blooms***	***Central Basin hypoxia***	***Eastern Basin Cladophora (nearshore)***
NOAA Western Lake Erie HAB Model (Stumpf)		X		
U-M/GLERL Western Lake Erie HAB Model (Obenour)		X		
TP Mass Balance Model (Chapra, Dolan, and Dove)	X (using empirical P-chlorophyll a relationship)			
1-D Central Basin Hypoxia Model (Rucinski)	X		X	
Ecological Model of Lake Erie (EcoLE) (Zhang)	X		X	
9-Box Model (McCrimmon, Leon, and Yerubandi)			X	
Western Lake Erie Ecosystem Model (LimnoTech)	X (Western Basin only)	X		
ELCOM-CAEDYM (Bocaniov, Leon, and Yerubandi)	X		X	
Great Lakes *Cladophora* Model (Auer)				X

2.3 Model Evaluation Criteria

The following criteria were adopted to assess the ability of each modeling effort to address the goals.

Ability to develop load-response curves and/or provide other output important for quantitative understanding of the questions/requirements posed in Annex 4: A key function of the models used in this effort is to establish relationships between phosphorus loads and the metric defined by the Annex 4 subgroup for each objective. As such, models were evaluated for their ability to generate load-response curves as the highest evaluation criterion. Other models were also evaluated for their utility in providing additional information to help understand phosphorus-chlorophyll dynamics, justify production relationships, or otherwise inform the response curves or targets.

Applicability to objectives/metrics provided by the Annex 4 subgroup: The models were evaluated for their ability to address the spatial, temporal, and kinetic characteristics of the objectives and metrics outlined by the Annex 4 subgroup. While models that address other objectives and metrics can be additionally informative, the highest priority models are those that can address them directly.

Extent/quality of calibration and confirmation: *Calibration* **-** Given the broad range in model type and complexity, a wide range of skill assessments was used. Models were evaluated as to their ability to reproduce state-variables that matched the objective metrics, as well as internal process dynamics. *Post-calibration testing* – Models were also measured against their ability to replicate conditions not represented in the calibration data set.

Extent of model documentation (peer review or otherwise): Models were evaluated based on the extent of their written documentation. Full descriptions of model kinetics calculations, inputs, calibration, confirmation, and applications were reviewed. Model documentation was available in peer-reviewed journal articles, government reports, or other documentation (e.g. white papers).

Level of uncertainty analysis available: Models were evaluated as to the extent they were able to quantify aspects of model uncertainty, including uncertainties associated with observation measurement error, model structure, parameterization, and aggregation, as well as uncertainty associated with characterizing natural variability.

2.4 Models

Models used in the ensemble effort are described briefly here. See *Appendix B* for more in depth information about each model application.

NOAA Western Lake Erie HAB Model (Stumpf) - In Stumpf *et al.*(2012) the authors present an empirical regression between spring TP load and flow from the Maumee River and maximum 30-day cyanobacteria index (CI) for Western Lake Erie as calculated by the European space satellite, MERIS. This method applies an algorithm to convert raw satellite reflectance around the 681 nm band into an index that correlates with cyanobacteria density. Ten day composites were calculated by taking the maximum CI value at each pixel within a given 10-day period to remove clouds and capture areal biomass. The authors conclude that spring flow or TP load can be used to predict bloom magnitude. Maumee River TP load from March to July was used as a predictor of CI utilizing data from 2002 to 2013. For more information see *Appendix B-1*.

U-M/GLERL Western Lake Erie HAB Model (Obenour) - A probabilistic empirical model was developed to relate the size of the Western Basin cyanobacteria bloom to spring bioavailable phosphorus loading (Obenour *et al.*, 2014). The model is calibrated to multiple sets of bloom observations, from previous remote sensing and *in situ* sampling studies. A Bayesian hierarchical framework is used to accommodate the multiple observation datasets, and to allow for rigorous uncertainty quantification. Furthermore, a cross validation exercise demonstrates the model is robust and would be useful for providing probabilistic bloom forecasts. The model suggests that there is a threshold loading value, below which the bloom remains at a baseline (i.e., background level). However, this may be an artifact of the lack of sufficient cyanobacteria observations at low loads. Above this threshold, bloom size increases proportionally to phosphorus load from the Maumee River. The model includes a temporal trend component indicating that response for a given load has been increasing over the study period (2002-2013), such that the lake is now more susceptible to cyanobacteria blooms than it was a decade ago. For more information see *Appendix B-2*.

Total Phosphorus Mass Balance Model (Chapra, Dolan, and Dove) - Chapra and Dolan (2012) have developed an update to the original TP mass balance model that was used (along with other models) to establish phosphorus loading targets for the 1978 Great Lakes Water Quality Agreement. Annual TP estimates were generated from year 1800 to 2010. The model is designed to predict the annual average concentrations in the offshore waters of the Great Lakes as a function of external loading and does not attempt to resolve finer-scale temporal or spatial variability. For Lake Erie this model computes the basin-wide annual average TP concentration as a function of all external TP loads. Calibration data for this model were obtained from Environment Canada and the Great Lakes

National Program Office. The model can be expanded to include chlorophyll-*a* and potentially Central Basin hypoxia through available empirical relationships with TP. For more information see *Appendix B-3*.

1-Dimensional Central Basin Hypoxia Model (Rucinski) - A one-dimensional model with 50 half-meter layers, calibrated to observations in the Central Basin of Lake Erie, was used to develop load-response curves relating chlorophyll-*a* concentrations and hypoxia to phosphorus loads in the Western Basin and Central Basin. The model is driven by a 1D hydrodynamic model that provides temperature and vertical mixing profiles (Rucinski *et al.*, 2010). The biological portion of the coupled hydrodynamic-biological model incorporates phosphorus and carbon loading, internal phosphorus cycling, carbon cycling (in the form of algal biomass and detritus), algal growth and decay, zooplankton grazing, oxygen consumption and production processes, and sediment interactions. The model has been applied to 19 years (1983 – 2003) of physical conditions to understand the relative contribution of stratification conditions versus phosphorus loading on the severity of hypoxia in the Central Basin. For more information see *Appendix B-4*.

Ecological Model of Lake Erie - EcoLE (Zhang) - Zhang *et al*. (2008) developed and applied a 2D hydrodynamic and water quality model to Lake Erie termed the Ecological Model of Lake Erie (EcoLE), which is based on the CE-QUAL-W2 framework. The purpose of the model application was to estimate the impact that Dreissenids are having on phytoplankton populations. The model was calibrated against data collected in 1997 and verified against data collected in 1998 and 1999. Model results indicate that Dreissenid mussels have weak direct grazing impacts on algal biomass and succession, while their indirect effects through nutrient excretion have much greater and profound impacts on the system (Zhang *et al.*, 2011). The model can produce load-response curves for chlorophyll-*a* concentrations and dissolved oxygen. For more information see *Appendix B-5*.

Nine-Box model (McCrimmon, Leon, and Yerubandi) - This model is a coarse grid (9-box) phosphorus mass balance model for quantitative understanding of Lake Erie eutrophication and related hypoxia (Lam *et al.*, 1983). The model is extensively calibrated and validated against observations in the past. Re-calibrations were conducted for a post-zebra mussel period and found that 9-box model is able to express offshore Lake Erie concentrations reasonably well. The model can be expanded to include empirically derived chlorophyll-*a* relationships for given TP concentrations. For more information see *Appendix B-6*.

Western Lake Erie Ecosystem Model (WLEEM) (LimnoTech) - The Western Lake Erie Ecosystem Model (WLEEM) has been developed as a 3D fine-scale, process-based, linked hydrodynamic-sediment transport-advanced eutrophication model, with the aim of providing a quantitative relationship between loadings of water, sediments, and nutrients to the Western Basin of Lake Erie from all sources and its response in terms of turbidity/sedimentation and algal biomass (three different phytoplankton functional groups, including cyanobacteria, are modeled separately). The model operates on a daily time scale and can produce time series outputs and spatial distributions of either total chlorophyll and/or cyanobacteria biomass as a function of loading. Therefore, it can produce load-response plots for several potential endpoints of interest in the Western Basin (the Western Basin model domain is bounded by a line connecting Pointe Pelee with Marblehead). It can also produce mass balances for the Western Basin for any one of its ~30 state variables; therefore, it has computed the daily loading of Western Basin nutrients and oxygen-demanding materials to the Central Basin as a function of loads to the Western Basin. This provided valuable information on how

load reductions to the Western Basin impact hypoxia development in the Central Basin. For more information see *Appendix B-7*.

ELCOM-CAEDYM (Bocaniov, Leon, and Yerubandi) - ELCOM-CAEDYM is a three-dimensional hydrodynamic and bio-geochemical model that consists of two coupled models: a three-dimensional hydrodynamic model - the Estuary, Lake and Coastal Ocean Model (Hodges *et al.*, 2000), and a bio-geochemical model - the Computational Aquatic Ecosystem Dynamics Model (Hipsey and Hamilton, 2008). The ELCOM-CAEDYM model has shown a great potential for modeling of biochemical processes and has been successfully used for in-depth investigations into variable hydrodynamic and biochemical processes in many lakes throughout the world including the Laurentian Great Lakes. In Lake Erie it has been used to study nutrient and phytoplankton dynamics (Leon *et al.*, 2011; Bocaniov *et al.*, 2014), the effect of mussel grazing on phytoplankton biomass (Bocaniov *et al.*, 2014), the sensitivity of thermal structure to variations in meteorological parameters (Liu *et al.*, 2014), and even winter regime and the effect of ice on hydrodynamics and some water quality parameters (Oveisy *et al.*, 2014). The application of the ELCOM-CAEDYM model to study oxygen dynamics and understand the Central Basin hypoxia is a subject of ongoing work. In this ensemble modeling process, ELCOM-CAEDYM is being applied to develop load-response curves for total chlorophyll-*a* in all three basins and Central Basin hypoxia. For more information see *Appendix B-8*.

Great Lakes Cladophora model (Auer) - The Great Lakes *Cladophora* Model (GLCM) is a revision of the original *Cladophora* model developed by Auer and Canale in the early 1980s in response to the need to understand the causes of large *Cladophora* blooms around the Great Lakes, especially in Lake Huron (Tomlinson *et al.*, 2010). The new model reflects current understandings of *Cladophora* ecology and a new set of tools and software to allow others to quickly run the model and view output. The updated model was calibrated and verified against data from Lake Huron (1979) and new data collected by the authors in 2006 in Lake Michigan. The model allows users to simulate standing crop of *Cladophora* as influenced by environmental parameters such as depth, light, and phosphorus concentrations. For this ensemble modeling process, the model is being applied generically to conditions in the Eastern Basin of Lake Erie. For more information see *Appendix B-9*.

2.5 Total phosphorus loadings to Lake Erie

Because the goal of this ensemble modeling exercise is to generate load-response relationships for the above eutrophication metrics in Lake Erie, it is instructive to review the Lake Erie loading behavior and characteristics to understand the dependent variables used for these relationships. Over the past 20 years external TP loadings to Lake Erie showed large year-to-year variation but no clear long-term trend (Figure 3). Interannual variability is largely driven by hydrometeorological conditions, which modulate the timing and magnitude of surface runoff and ultimately the amount of nutrients delivered to the lake by tributaries. For example, the large loads recorded in 1996-1998 have been associated with exceptionally high tributary loads due to increased precipitation (Dolan and Richards, 2008). Over the most recent ten years for which detailed data on Lake Erie TP loads are available (2002-2011), phosphorus from non-point sources, transported to the lake by runoff and rivers, contributed on average 78% of the total annual load to the lake (Dolan and Chapra, 2012; Dolan, pers. comm. 2012).

Basin-wide phosphorus loads are remarkably different among basins, with the Western Basin receiving on average 61% of the whole lake load, while loads to the Central and Eastern basins make up 28% and 11% of the average annual lake load, respectively (Figure 3). In the years 2002-2011 the annual loads to the three basins have ranged between 792-1175 MT (metric tonnes) in the Eastern Basin (average: 952 MT), 1769-3723 MT in the Central Basin (average: 2556 MT), and 3870-7103 MT in the Western Basin (average: 5514 MT).

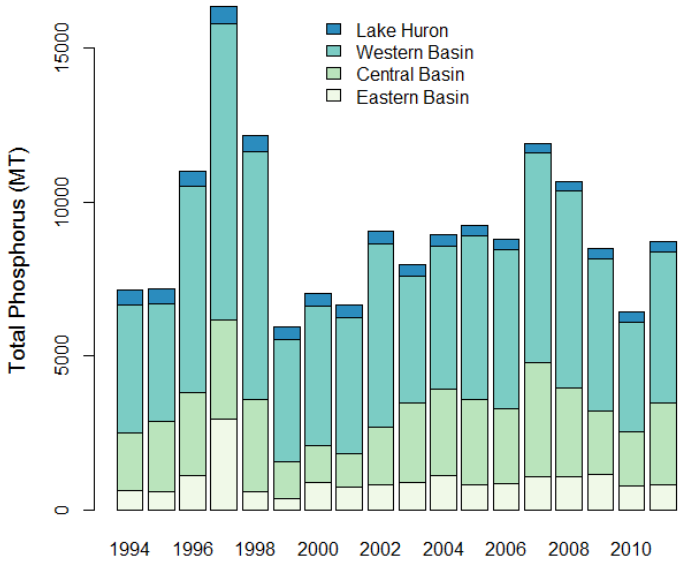

Figure 3. Total phosphorus loads to Lake Erie divided by basin for water years 1994-2011. A water year runs from October-September (sources: Dolan and Chapra, 2012; Dolan, pers. comm., 2012).

The large TP loads delivered annually to the Western Basin derive primarily from the Maumee and Detroit rivers (Figure 4). The vast majority of the phosphorus delivered by the Maumee River into the Western Basin originates from agricultural activities, which dominate the watershed, and are the primary cause of the extremely high TP concentrations in the Maumee compared to the Detroit River. As a result, although the Maumee River only contributes about 5% of the total flow discharging annually into the Western Basin, it contributes approximately

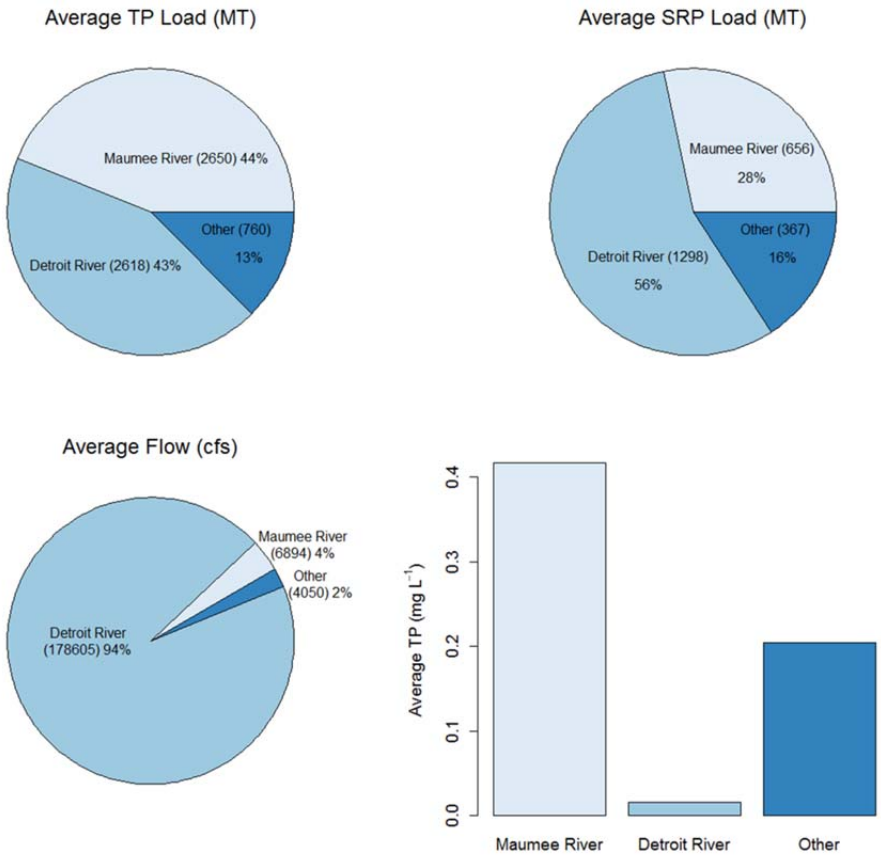

Figure 4. Annual average TP and DRP loads delivered to the Western Basin by major tributaries (upper panel), with corresponding flow (lower left panel) and flow weighted average TP concentration (lower right panel). Data are averaged over the years 2008, 2011, 2012 and 2013 (see *Appendix B-7*).

45% of the TP load, a percentage similar to that of the Detroit River, which accounts for over 90% of the total flow to the basin (Figure 4).

While the TP load from the Detroit River remained relatively constant over the years, the load from the Maumee River showed considerable interannual variability. Over the period 2002-2010, the annual Maumee TP load varied between 1426 - 4123 MT, with an average of 2455 MT (sources: Heidelberg University's National Center for Water Quality Research and United States Geological Survey). A more detailed analysis of the seasonal dynamics of the Maumee River TP loadings in the years 2002-2010 indicated that about 50% of the annual load is discharged on average during spring (March-June; average: 1155 MT), while this percentage decreased to 35% when considering only the loads delivered in April-July (average: 791 MT).

It is also important to recognize that even though DRP load has increased significantly since the mid-1990s (Richards, pers. comm., Scavia *et al.*, 2014), it is still a relatively small portion of the TP load to Lake Erie (Figure 5), and the models reflect this relative influence. DRP was approximately 30% of the TP load in 2008 and 2011, the two years where complete data were available. DRP load to the Western Basin was 33% and 34% of TP in those years, 26% to the Central Basin, and 23% and 16% to the Eastern Basin. However, the DRP is considerably more bioavailable than the PP+DNRP, making the relative contribution of the two fractions to ERI indicators approximately equal. This is an important consideration when exploring means for load reduction. The models do consider this reality in establishing loading targets.

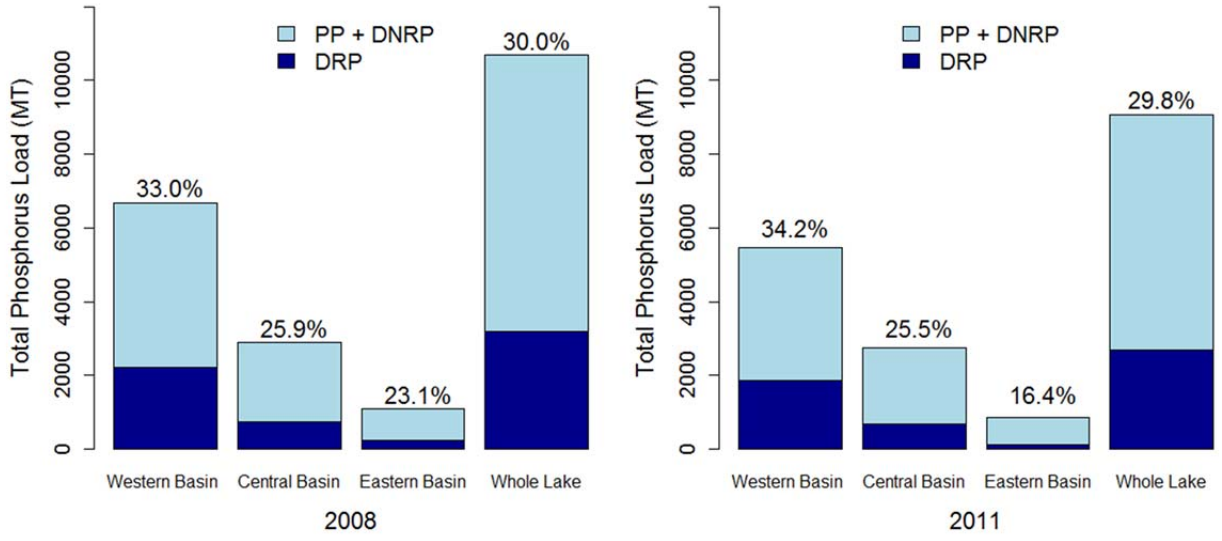

Figure 5. Average DRP load as a percent of TP load for 2008 and 2011 (see *Appendix B-7*).

3. Results

In reviewing model capabilities and the relevant eutrophication indicators, the Modelers concluded that the most reliable information can be provided for Western Basin total phytoplankton biomass, Western Basin cyanobacteria blooms, Central Basin hypoxia, and Eastern Basin *Cladophora*. Central Basin phytoplankton biomass was also investigated, but observations and model results indicate that concentrations are already low and further load reductions, based on that indicator, are not needed.

3.1 Western Basin Phytoplankton Biomass

Based on analysis of model performance (*Appendix B*), four models are suitable for exploring the relationship between total phytoplankton biomass (as chl-*a*) and external TP loading (Figures 6-9). Direct comparisons are made difficult because the models used different averaging periods for reporting summer average chl-*a*. To help in the comparison, each model output was converted to a percent of the value determined for the highest loads. While some models reported Western Basin chl-*a* as a function of whole lake annual TP loads, nutrient loads delivered to the Central and Eastern basins are assumed to have a negligible influence on phytoplankton growth in the Western Basin. The whole lake loads reported in each original load-response curve were converted to the corresponding Western Basin loads based on the Western Basin-to-Whole Lake load ratio recorded for the year used by each model as baseline scenario (Figure 10).

Comparison of load reductions is summarized in Section 4. Variability among results from different models is partly expected when modeling multiple interacting bio-physical factors such as those that influence phytoplankton growth, and partly derives from the varying degree of complexity and output characteristics of the adopted models. For example, Chapra *et al*. (*Appendix B-3*) compute chl-*a* concentrations based on a relatively simple empirical relationship between chl-*a* in August and TP concentrations in a given basin, and resulting chl-*a* concentrations are representative of August epilimnetic conditions (see *Appendix B-3*). On the other hand, ELCOM-CAEDYM, EcoLE, and WLEEM account for several ecological drivers in addition to phosphorus concentration when predicting chlorophyll-*a* levels in the Western Basin, and their results are averaged over summer months (June-August for ELCOM-CAEDYM and EcoLE, and July-September for WLEEM). As a result of these differences, the annual TP loads to the Western Basin needed to achieve, for example, a 50% decrease in the maximum chl-*a* concentration reported by each model range between 1130 MT and 3010 MT.

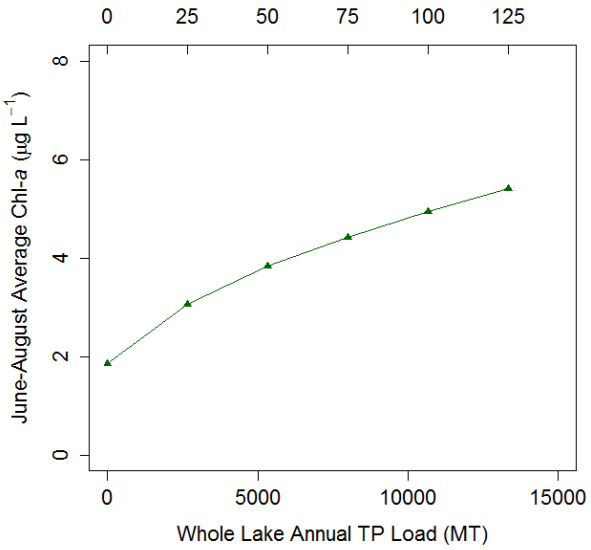

Figure 6. June – August average chlorophyll-*a* concentration in the Western Basin as a function of whole lake annual TP load, according to ELCOM-CAEDYM (*Appendix B-8*). The top x-axis shows TP load as a percent of the 2008 baseline load.

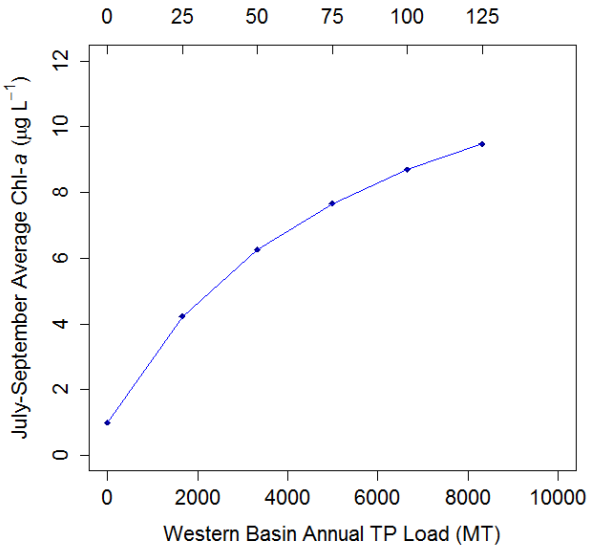

Figure 7. July – September average chlorophyll-*a* concentration in the Western Basin as a function of Western Basin annual TP load, according to WLEEM (*Appendix B-7*). The top x-axis shows TP load as a percent of the 2008 baseline load.

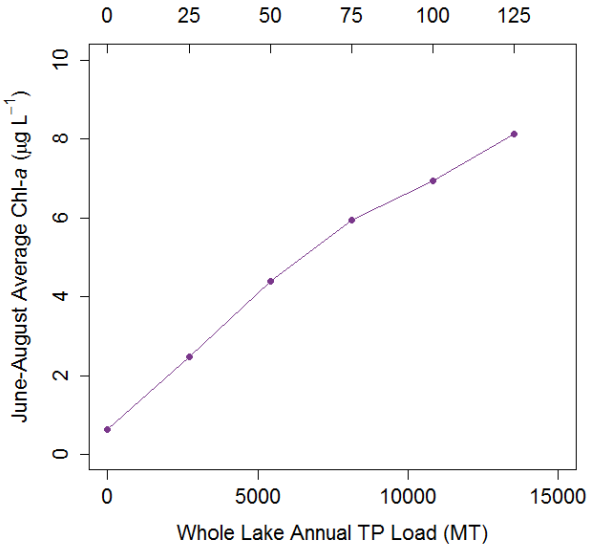

Figure 8. June – August average chlorophyll-*a* concentration in the Western Basin as a function of whole lake annual TP load, according to EcoLE (*Appendix B-5*). The top x-axis shows TP load as a percent of the 2008 baseline load.

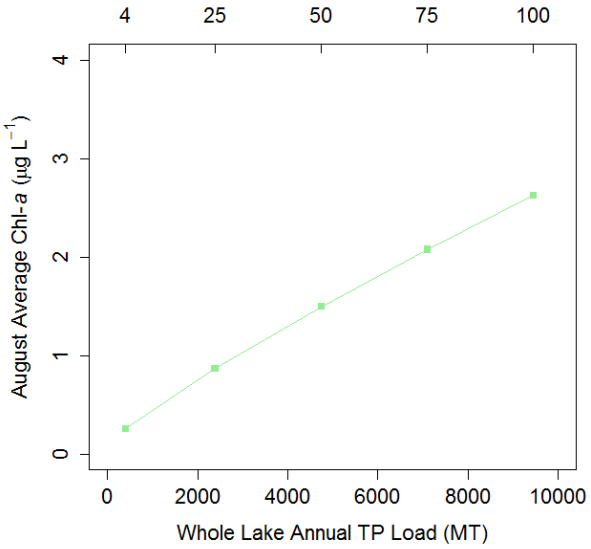

Figure 9. August average chlorophyll-*a* concentration in the Western Basin as a function of whole lake annual TP load, according to the Chapra *et al*. model (*Appendix B-3*). The top x-axis shows TP load as a percent of the 2008 baseline load. The 125% scenario was not calculated by the Chapra *et al.* model.

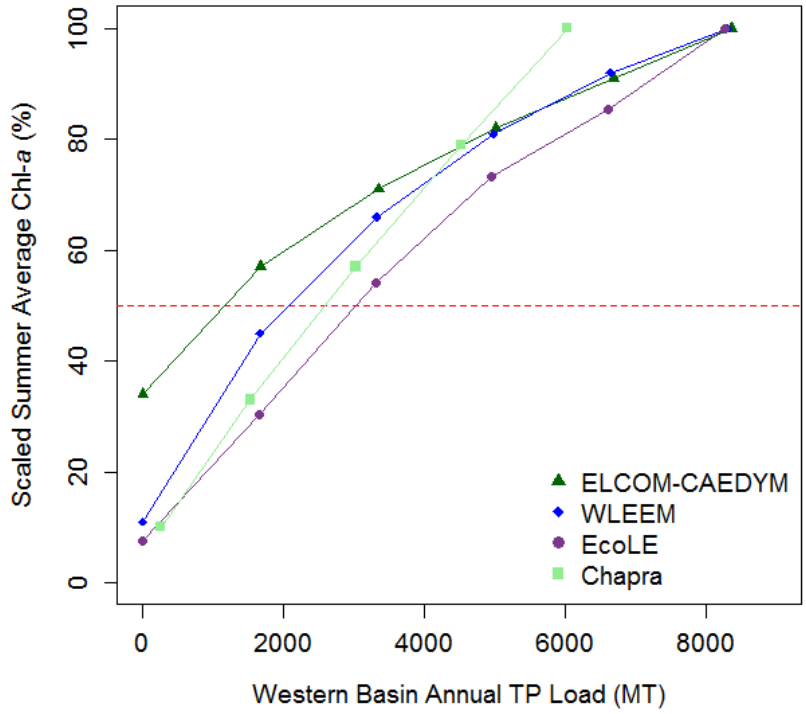

Figure 10. Average summer chlorophyll–*a* concentration in the Western Basin predicted by different models as a function of annual Western Basin TP loads. Each response curve has been scaled to 100% at its maximum chlorophyll value to facilitate comparisons. Maximum chlorophyll value corresponds to the 125% TP load scenario for all models except for Chapra *et al*., which only considered TP load scenarios up to 100% of the 2008 baseline. Red horizontal line represents a 50% reduction in maximum chlorophyll concentration.

3.2 Western Basin Cyanobacteria Blooms

The load-response curves for peak cyanobacteria biomass in the Western Basin for the three models which simulate this metric are shown in Figures 11-13. All models identified spring TP loading from the Maumee River as the main driver of HABs, although the Obenour model is actually driven by an estimate of bioavailable phosphorus (estimated in that simple model as approximately 50% of particulate phosphorus plus 100% of DRP; *Appendix B-2*). WLEEM is driven by actual measured particulate and dissolved phosphorus forms, so it explicitly accounts for bioavailable phosphorus and the kinetic conversions of one phosphorus form to another within the model domain (e.g., mineralization of organic phosphorus to orthophosphate, gradient-driven desorption of orthophosphate from inorganic particulate phosphorus). This Maumee focus is especially evident when comparing the WLEEM load-response results based on varying TP loads from all Western Basin sources with that obtained by reducing Maumee River TP load alone (Figure 13). The two curves are very similar, indicating that a reduction in TP loadings from sources other than the Maumee River results in a relatively minor decrease in HAB severity. WLEEM exploration of response to Detroit River TP reductions also confirms the negligible role it plays in HAB formation, although loads from the Detroit River do influence ecosystem indicators such as TP, DRP, and total chlorophyll-*a* levels in the whole Western Basin (see *Appendix B-7*).

Direct comparison of response curves from the three models is made difficult because they used different averaging periods for loads, and WLEEM used a different method than the two satellite-driven empirical models for determining the peak cyanobacteria biomass. The Obenour and Stumpf models are fit to the same set of satellite-derived bloom observations (plus additional *in situ* observations in the case of Obenour). The satellite estimates are maximum 30-day values, as determined from three consecutive 10-day composites, which in turn are derived by taking the highest biomass value observed at each image pixel over each 10-day period (Stumpf *et al.*, 2012). WLEEM, on the other hand, simulates daily average basin-wide cyanobacteria biomass, from which a 30-day moving average is calculated over summer months and then the maximum consecutive 30-day value is reported for each year (see *Appendix B-7*). As a result, WLEEM biomass estimates are significantly lower than those used by Stumpf and Obenour, which makes the "severe" bloom threshold of 9600 MT of cyanobacteria offered by Stumpf in *Appendix B-1* incompatible with WLEEM estimates.

To account for this and provide a bloom threshold consistent with WLEEM's biomass estimates and equivalent to 9600 MT, the ratio of the Stumpf modeled 2008 biomass (the baseline year and also a severe bloom year) to the 9600 MT value was calculated, and then that ratio was applied to the 2008 biomass predicted by WLEEM to obtain an "equivalent" threshold of 7990 MT cyanobacteria biomass for WLEEM (green line in Figure 13).

The Obenour model includes a temporal component that suggests increased susceptibility of Western Lake Erie to bloom formation (see *Appendix B-2*). Accordingly, the same TP load is predicted to trigger a larger bloom under present-day conditions compared to earlier years, as evidenced by the two different response curves obtained when running the model under 2013 versus 2008 conditions (Figure 11). While an important finding statistically, a mechanism for this trend is not yet clear and it is not known if the trend will continue. As a result, the Obenour model predicts that under 2008 lake conditions a total maximum spring (March-June) Maumee TP load of 1230 MT is needed to achieve a peak summer cyanobacteria biomass of 9600 MT, while the same cyanobacteria biomass level requires a much lower maximum load (500 MT) under 2013 lake conditions (Figure 11 and Table 2). Considering that over the period 2002-2011 the March-June Maumee load was on average 50% of the total annual river load, these spring loads correspond to annual maximum Maumee loads of 2460 MT (2008 conditions) and 1000 MT (2013 conditions). The Stumpf model, which does not include a temporal trend, indicates that a maximum annual Maumee load of 2038 MT is necessary to reach the 9600 MT threshold, and WLEEM suggests a maximum annual Maumee load of 1926 MT to achieve a comparable peak biomass based on its estimation method.

The Obenour model and WLEEM were also used to explore the impact of DRP load reductions. Both models predict that even 100% removal of the Maumee DRP load alone (without changing the PP+DNRP load) would not be enough to produce peak cyanobacteria bloom formation below the "severe" threshold (see *Appendices B-2* and *B-7*).

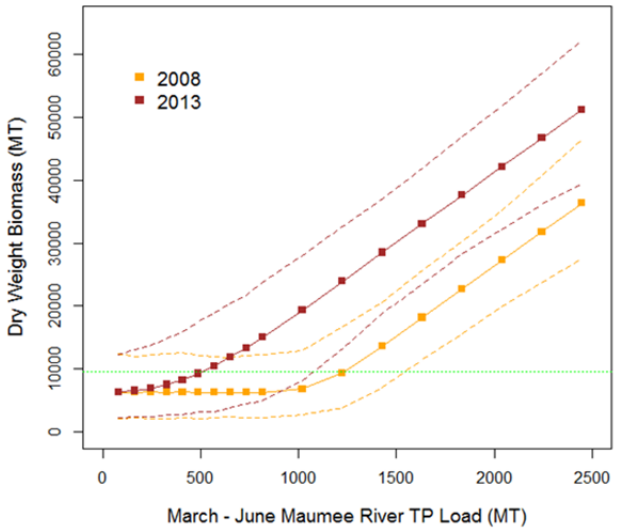

Figure 11. Cyanobacteria bloom size (peak 30-day average biomass) predicted by the Obenour *et al.* model in the Western Basin as a function of spring Maumee River TP load. Solid lines are mean predictions under 2008 and 2013 lake conditions (see *Appendix B-2* for details), while dashed lines are 95% predictive intervals. The green dotted line indicates the threshold for "severe" blooms as devised by Stumpf in *Appendix B-1*.

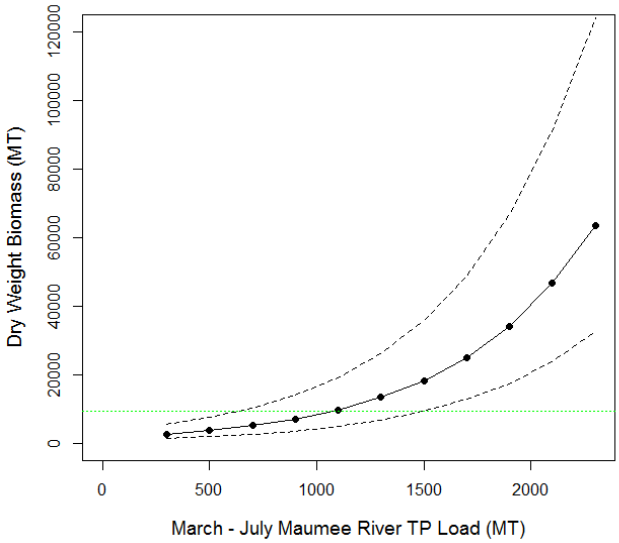

Figure 12. Cyanobacteria bloom size (peak 30-day average biomass) predicted by the Stumpf model in the Western Basin as a function of spring Maumee River TP load. The solid line represents mean predictions, while dashed lines are 95% confidence intervals. The green dotted line indicates the threshold for "severe" blooms as devised by Stumpf in *Appendix B-1*.

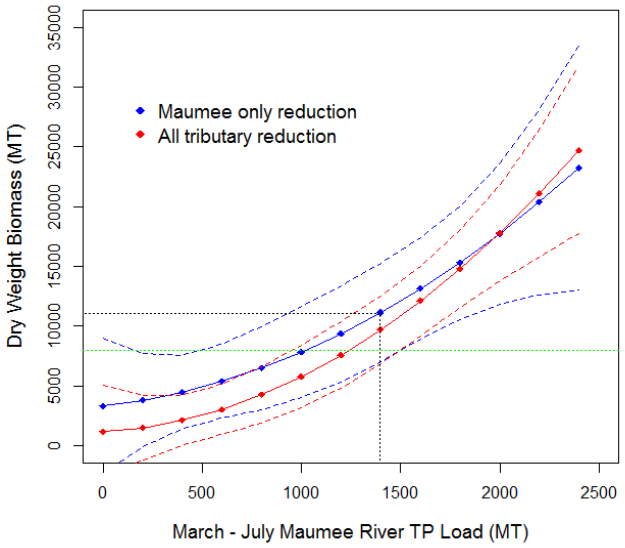

Figure 13. Cyanobacteria bloom size (peak 30-day rolling average biomass) predicted by WLEEM in the Western Basin in relation to changes in annual TP loads from all external sources (red lines) and from the Maumee River only (blue lines). Solid lines are mean predictions, while dashed lines are 95% confidence intervals around the regression fitted through results of model simulations using 2008, 2011-13 (see *Appendix B-7*). The black dotted line marks the 2008 TP load and corresponding bloom prediction. The green dotted line indicates the biomass level corresponding to a decrease in the 2008 bloom prediction equivalent to the percentage reduction of Stumpf`s 2008 predicted value down to 9600 MT.

3.3 Central Basin Hypoxia

Previous studies have shown that the hypolimnetic oxygen depletion rates in the Central Basin of Lake Erie are driven by both the sediment oxygen demand (SOD) and water column oxygen demand (WOD) and summer stratification. Since the full effect of nutrient load changes cannot be seen with short simulations of the models, SOD rates are adjusted to capture the nutrient load reductions (*Appendices B4-B8*).

The response curves for hypolimnetic dissolved oxygen from the various models (Figure 14) show similar decreasing trends with increasing loads, though there are some discrepancies at the lowest loads. The 9-Box model is the only one that was run for three consecutive years to approximate a steady-state response to the load reductions, and this could partially explain some of the differences. Additional differences among model output include the fact that Rucinski models and the 9-Box model report hypolimnetic averaged DO, while the other two report concentrations from the models' bottom layer (0.5-1.0 m for ELCOM-CAEDYM; 1.0 and 1-3 m for EcoLE). Rucinski_WB (constant P retention of Western Basin load in the Western Basin) and Rucinski_WLEEM use two representations of flux from the Western Basin to the Central Basin; the Rucinski WB uses a net apparent attenuation loss rate due to settling as the loads are transported from the Western basin to the Central Basin, the Rucinski WLEEM uses outputs from the WLEEM model for loading that enters the Central Basin from the Western Basin. Figures in *Appendix B-4* show that the two methods yield similar results. In addition, all response curves were plotted as a function of Western + Central basin TP loads. Whenever necessary, whole lake loads originally reported by each modeler were converted to Western + Central basin loads based on the Western + Central load-to-whole lake load ratio recorded in the baseline year used by each modeler.

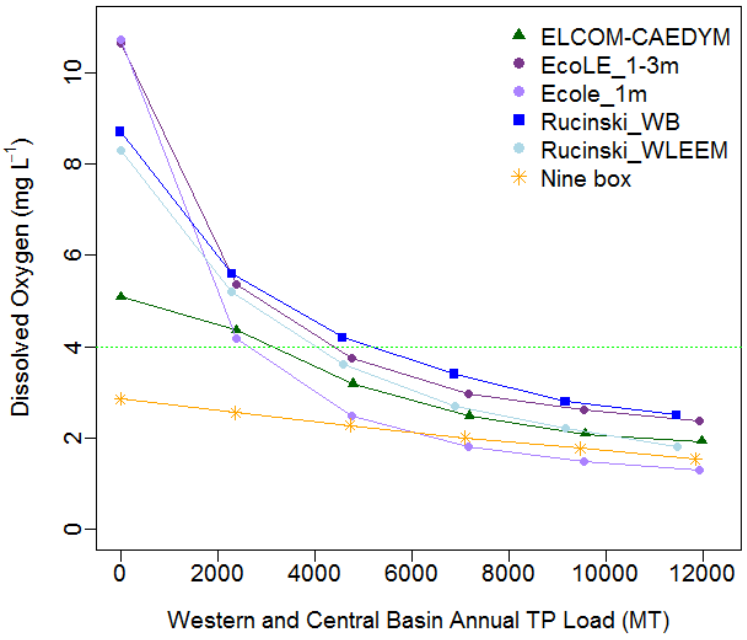

Figure 14. August-September average hypolimnetic dissolved oxygen concentration predicted by different models in the Central Basin as a function of annual TP loads. The green line represents the average concentration corresponding to initiation of statistically significant hypoxic area (Zhou *et al*. 2013)

While the typical definition of hypoxia is for dissolved oxygen concentrations below 2 mg/L, Zhou *et al*. (2013) showed that statistically significant hypoxic areas begin for average bottom water DO concentrations below approximately 4.0 mg/L. Using that as an indicator, for example, suggests a need to keep Western + Central basin loads below 2600 to 5100 MT (Table 2).

Several models estimate hypoxic area. ELCOM-CAEDYM does this directly through a detailed 3-dimensional model; 9-Box does this by using hypolimnetic DO concentration and the area intersecting the bottom of the thermocline; EcoLE and Rucinski use the Zhou *et al*. (2013) relationship between hypoxic area and bottom-layer DO concentration. All models show that the extent of the hypoxic zone will increase with increasing TP loads (Figure 15). The primary cluster of models suggest that a decrease in annual Western + Central basin TP load to 3415 – 5955 MT/year (9-Box suggests 1150 MT/year) is necessary to reduce the average extent of the Central Basin hypoxic zone to 2000 km^2 (Figure 15 and Table 2), a value typical of the mid-1990s, which coincides with recovery of several recreational and commercial fisheries in Lake Erie's Western and Central basins (Ludsin *et al*., 2001, Scavia *et al*., 2014). This corresponds to a 39-52% TP decrease from the 2002-2011 average of 8070 MT/year.

If a maximum TP load of 3415 to 5955 MT/year were achieved, the models indicate a decrease in the total number of hypoxic days (days where average bottom water dissolved oxygen is < 2 mg/L) to values between 14 - 42 days (Figure 16). The relative scatter among models at the low end of the range is likely due to the coarse resolution among load scenarios. This is different from the use of a 4 mg/l bottom layer (not hypolimnion average) concentration to define the onset of statistically significant hypoxic area (see Zhou *et al*., 2013).

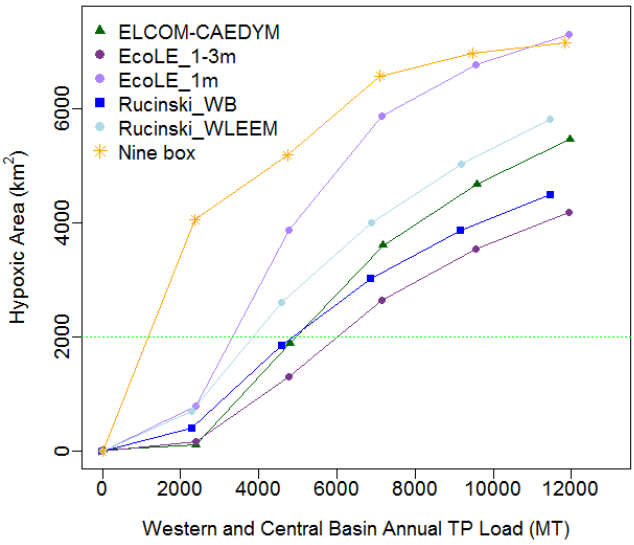

Figure 15. August-September average extent of the hypoxic area predicted by different models in the Central Basin as a function of annual TP loads to the Western and Central Basin. The green horizontal dotted line indicates a suggested threshold of 2000 km^2.

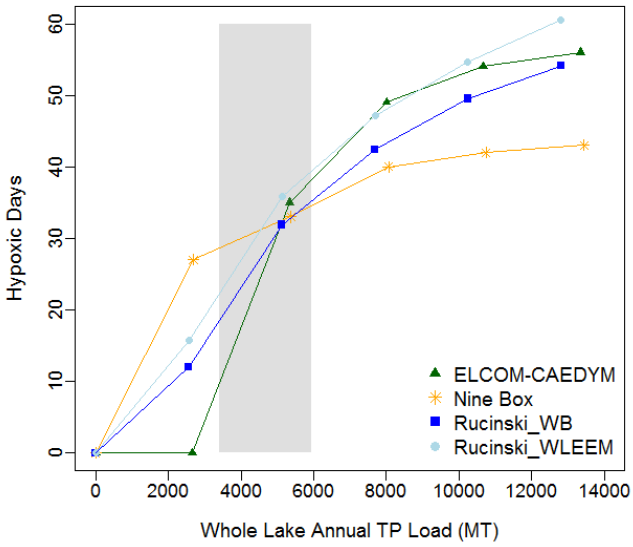

Figure 16. Number of hypoxic days predicted by different models in the Central Basin as a function of annual TP loads. The shaded area indicates the range of loads required to achieve the hypoxic area threshold of 2000 km^2 (Figure 15), excluding predictions from the 9-Box model.

3.4 Eastern Basin Cladophora *(nearshore)*

As described in *Appendix B-9*, several steps and models were required to establish a quantitative relationship between TP loads and the *Cladophora* indicator. These models include one that relates standing stock *Cladophora* biomass to Eastern Basin DRP concentrations, one that relates DRP to TP concentrations, and one that relates Eastern Basin TP concentrations to TP loads. Given those relationships, and assuming, for example, a threshold value for the *Cladophora* ERI of 30 gDW/m^2 (a threshold expected to eliminate nuisance growth of the alga in the Eastern Basin), the models indicate this corresponds to a DRP concentration of 0.9 µgP/L. A regression model indicates that a 0.9 µgP/L DRP concentration corresponds to a TP concentration of 6.3 µgP/L, and the Chapra TP model indicates that a 6.3 µgP/L TP concentration in the Eastern Basin corresponds to a total TP load for Lake Erie of 7000 MT/Year, requiring a 22% reduction from the 2002-2011 average.

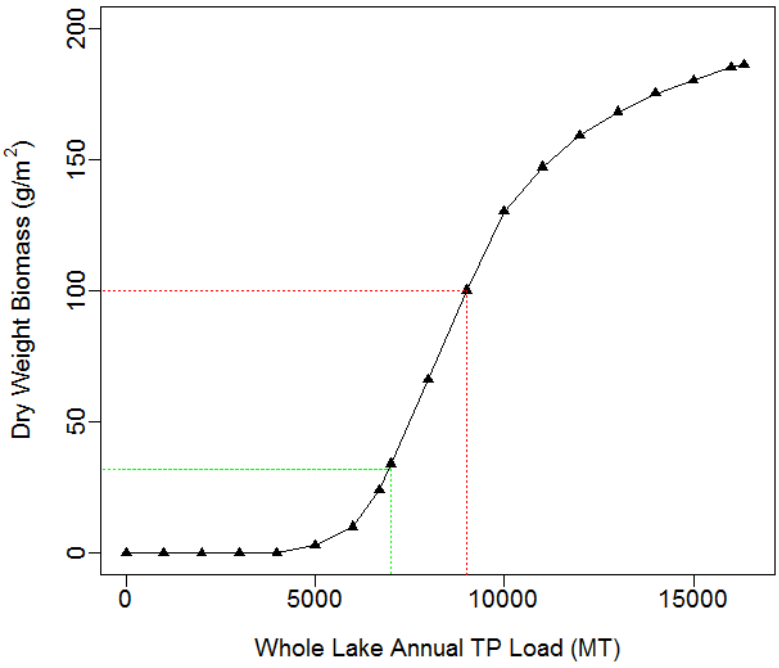

Figure 17. *Cladophora* biomass predicted by the Great Lakes *Cladophora* model (GLCM) in the Eastern Basin as a function of annual TP loads. The green dotted line represents the author's suggested TP loading target (7000 MT), while the red dotted line shows the average annual TP load to Lake Erie over the period 2002-2011 (9022 MT).

This load results in an offshore DRP concentration that should not stimulate nuisance growth of *Cladophora.* As offshore DRP concentrations are reduced, control of *Cladophora* growth will shift to direct inputs to the nearshore (e.g. wastewater treatment plant effluents and tributary runoff). For the Eastern Basin of Lake Erie, this means that loads from direct inputs to the nearshore such as the Grand River will determine whether nuisance growth of *Cladophora* occurs.

4. Conclusions

The load-response curves presented above represent our current best estimates of how the lake eutrophication response metrics will respond to phosphorus loads. The loadings necessary to achieve example thresholds were calculated and are summarized in Table 2 below.
Results of the ensemble modeling approach to date suggest:

- Achieving cyanobacteria biomass reduction requires a focus on reducing TP loading from the Maumee River, with an emphasis on high-flow event loads in the period from March – July. Results suggest that focusing on Maumee DRP load alone will not be sufficient and that phosphorus load from the Detroit River is not a driver of cyanobacteria blooms.

- Reducing hypoxia in the Central Basin requires a Central + Western Basin annual load reduction greater than is needed to achieve Western Basin cyanobacteria biomass reduction. Load reductions focused on dissolved oxygen concentration and hypoxic areal extent also drive shorter hypoxia duration.

- The whole lake load for achieving a *Cladophora* threshold is higher (i.e., lower percent reduction) than computed for the hypoxia threshold. These results offer several different strategies for recommending load reductions for the GLWQA. As illustrated by the example thresholds in Table 2, the models enable decision-makers to evaluate the levels of loads and load reductions necessary to achieve target values they may choose.

Table 2. TP loads (MT) associated with example ERI thresholds. For cyanobacteria, the threshold differs among models (see text). March - June Maumee River loads were assumed to be 50% of the annual river load, while March– July Maumee River loads were 53% of the annual load, which was in turn assumed to be 45% of the whole Western Basin annual load. For phytoplankton, Western Basin annual loads correspond to a 50% reduction in maximum chlorophyll-*a* concentration reported by each model. The threshold for Central Basin hypoxic area extent was set to 2000 km^2, while a threshold for Central Basin dissolved oxygen was set to 4 mg/L. For *Cladophora*, a threshold for total dry weight biomass was set at less than 30 g/m^2.

Model	Maumee spring load to achieve threshold	Maumee annual load to achieve threshold	WB annual load to achieve threshold	WB + CB annual load to achieve threshold	Whole lake annual load to achieve threshold
Cyanobacteria					
Obenour_2008	1230	2460	5467		
Obenour_2013	500	1000	2222		
Stumpf	1080	2038	4528		
WLEEM	1021	1926	4281		
Western Basin Phytoplankton					
Chapra			2600		
EcoLE			3010		
ELCOM-CAEDYM			1130		
WLEEM			2030		
Hypoxic Area					
EcoLE_1-3m				5955	
EcoLE_1m				3415	
ELCOM-CAEDYM				4920	
9-Box				1150	
Rucinski				4830	
Rucinski_WLEEM				3880	
Dissolved Oxygen					
EcoLE_1-3m				4400	
EcoLE_1m				2600	
ELCOM-CAEDYM				3100	
Rucinski				5100	
Rucinski_WLEEM				4000	
Cladophora					
Auer					7000

References

Bierman,V.J., 1980. A Comparison of Models Developed for Phosphorus Management in the Great Lakes. Conference on Phosphorus Management Strategies for the Great Lakes. pp. 1-38.

Bierman, V.J., Jr. and D. Scavia. 2013. Hypoxia in the Gulf of Mexico: Benefits and Challenges of Using Multiple Models to Inform Management Decisions. Presentation at Multiple Models for Management (M3.2) in the Chesapeake Bay, Annapolis MD, February 25, 2013.

Bocaniov, S.A., Smith, R.E.H, Spillman, C.M., Hipsey, M.R., Leon, L.F., 2014. The nearshore shunt and the decline of the phytoplankton spring bloom in the Laurentian Great Lakes: insights from a three-dimensional lake model. *Hydrobiol*. 731: 151-172.

Chapra, S.C., Dolan,D.M., 2012. Great Lakes total phosphorus revisited: 2. Mass balance modeling. *J. Great Lakes Res*. 38 (4): 741-754.

Conroy, J.D., Boegman, L., Zhang, H., Edwards, W.J., Culver, D.A., 2011. "Dead Zone" dynamics in Lake Erie: the importance of weather and sampling intensity for calculated hypolimnetic oxygen depletion rates. *Aquat. Sci.* 73:289-304.

DePinto, J.V., Lam, D., Auer, M.T., Burns, N., Chapra, S.C., Charlton, M.N., Dolan, D.M., Kreis, R., Howell, T., Scavia, D., 2006. Examination of the status of the goals of Annex 3 of the Great Lakes Water Quality Agreement. Rockwell, D., VanBochove, E., Looby, T. (eds). pp. 1-31.

Dolan, D.M., Chapra, S.C., 2012. Great Lakes total phosphorus revisited: 1. Loading analysis and update (1994-2008). *J. Great Lakes Res*. 38 (4): 730-740.

Dolan, D.M., Richards, R.P., 2008. Analysis of late 90s phosphorus loading pulse to Lake Erie. In: Munawar, M., Heath, R. (Eds.), Checking the Pulse of Lake Erie: Ecovision World Monograph Series, Aquatic Ecosystem Health and Management Society, Burlington, Ontario, pp. 79–96.

Hipsey, M.R., Hamilton, D.P., 2008. Computational aquatic ecosystems dynamics model: CAEDYM v3 Science Manual. Centre for Water Research Report, University of Western Australia.

Hodges, B.R., Imberger, J., Saggio, A., Winters, K., 2000. Modeling basin scale waves in a stratified lake. *Limnol.Oceanogr*. 45: 1603–1620.

International Joint Commission. 1988. *Report on Modeling the Loading-Concentration Relationship for Critical Pollutants in the Great Lakes*. IJC Great Lakes Water Quality Board, Toxic Substances Committee, Task Force on Toxic Chemical Loadings.

Lam, D.C.L., Schertzer, W.M., Fraser, A.S., 1983. Simulation of Lake Erie water quality responses to loading and weather variations. Burlington, Ont.: Environment Canada, Scientific series /Inland Waters Directorate; no. 134

Leon, L.F., Smith, R.E.H., Hipsey, M.R., Bocaniov, S.A., Higgins, S.N., Hecky, R.E., Antenucci, J.P., Imberger, J.A., Guildford, S.J., 2011.Application of a 3D hydrodynamic–biological model for seasonal and spatial dynamics of water quality and phytoplankton in Lake Erie. *J. Great Lakes Res*. 37: 41-53.

Liu, W., Bocaniov, S.A., Lamb, K.G., Smith, R.E.H., 2014.Three dimensional modeling of the effects of changes in meteorological forcing on the thermal structure of Lake Erie. *J. Great Lakes Res*. http://dx.doi.org/10.1016/j.jglr.2014.08.002.

Ludsin, S.A., Kershner, M.W., Blocksom, K.A., Knight, R.L., Stein, R.A., 2001. Life after death in Lake Erie: nutrient controls drive fish species richness, rehabilitation. *Ecol. Appl*. 11: 731–746

Obenour, D.R., Gronewold, A.D., Stow, C.A., Scavia, D., 2014.Using a Bayesian hierarchical model to improve Lake Erie cyanobacteria bloom forecasts. *Water Resour. Res.* 50.

Oveisy, A., Rao, Y.R., Leon, L.F., Bocaniov, S.A., 2014. Three-dimensional winter modelling and the effects of ice cover on hydrodynamics, thermal structure and water quality in Lake Erie. *J. Great Lakes Res.* http://dx.doi.org/10.1016/j.jglr.2014.09.008

Rucinski, D.R., Beletsky, D., DePinto, J.V., Schwab, D.J., Scavia, D., 2010. A simple 1-dimensional, climate based dissolved oxygen model for the central basin of Lake Erie. *J. Great Lakes Res.* 36: 465-476.

Scavia, D., Justić, D., Bierman V.J., 2004.Reducing Hypoxia in the Gulf of Mexico: Advice from Three Models. *Estuaries* 27: 419-425.

Scavia, D., J. D. Allan, K. K. Arend, S. Bartell, D. Beletsky, N. S. Bosch, S. B. Brandt, R. D. Briland, I. Daloğlu, J. V. DePinto, D. M. Dolan, M. A. Evans, T. M. Farmer,D. Goto, H. Han, T. O. Höök, R. Knight, S. A. Ludsin, D. Mason, A. M. Michalak, R. P. Richards, J. J. Roberts, D. K. Rucinski, E. Rutherford, D. J. Schwab, T. Sesterhenn, H. Zhang, Y. Zhou., 2014. Asssessing and addressing the re-eutrophication of Lake Erie: Central Basin Hypoxia. *J. Great Lakes Res.* 40: 226–246.

Stow C.A., Roessler C., Borsuk M.E., Bowen, J.D. &Reckhow K.H., 2003. Comparison of Estuarine Water Quality Models for Total Maximum Daily Load Development in Neuse River Estuary.*Journal of Water Resources Planning and Management* 129 (4): 307-314.

Stumpf, R.P., Wynne, T.T., Baker, D.B., Fahnenstiel, G.L., 2012.Interannual Variability of Cyanobacterial Blooms in Lake Erie. *PLoSONE* 7 (8): 1-11.

Tomlinson, L.M., Auer, M.T., Bootsma H.A., 2010. The Great Lakes *Cladophora* Model: Development and application to Lake Michigan. *J. Great Lakes Res.* 36: 287-297.

United States and Canada 2012.2012 Great Lakes Water Quality Agreement. USEPA and Environment Canada (ed). p. Annex 4. http://www.epa.gov/glnpo/glwqa/.

Vallentyne, J.R., Thomas, N.A., 1978. Fifth Year Review of Canada-United State Great Lakes Water Quality Agreement Report of Task Group III A Technical Group to Review Phosphorus Loadings. pp. 1-100.

Zhang, H., Culver, D.A., Boegman, L., 2008. A Two-Dimensional Ecological Model of Lake Erie: Application to Estimate Dreissenid Impacts on Large Lake Plankton Populations. *Ecol. Model.* 214: 219-241.

Zhang, H., Culver, D.A., Boegman, L. 2011. Dreissenids in Lake Erie: an algal filter or a fertilizer? *Aq. Inv.* 6 (2): 175-194.

Zhou, Y., D.R. Obenour, D. Scavia, T.H. Johengen, A.M. Michalak (2013) Spatial and Temporal Trends in Lake Erie Hypoxia, 1987-2007. Environ. Sci. Technol.47 (2), pp 899-905 Supporting Information; Correction

Appendix A.

A-1. Agenda and Participant List: April 9-10, 2014 Ensemble Modeling Planning Workshop
A-2. Agenda and Participant List: September 29-30, 2014 Ensemble Modeling Implementation Workshop
A-3. Report from April 9-10 Workshop

Appendix B.

B-1. NOAA Western Basin HAB Model (Stumpf)
B-2. U-M/GLERL Western Basin HAB Model (Obenour)
B-3. Total Phosphorus Mass Balance Model (Chapra, Dolan, and Dove)
B-4. 1-Dimensional Central Basin Hypoxia Model (Rucinski)
B-5. Ecological Model of Lake Erie (EcoLE) (Zhang)
B-6. Nine Box Model (McCrimmon, Leon, and Yerubandi)
B-7. Western Lake Erie Ecosystem Model (WLEEM) (LimnoTech)
B-8. ELCOM-CAEDYM (Bocaniov, Leon, and Yerubandi)
B-9. Great Lakes *Cladophora* Model (Auer)

Appendix A-1. Agenda and Participant List: April 9-10, 2014 Ensemble Modeling Planning Workshop

GLWQA PHOSPHORUS LOAD RESPONSE MODELING WORKSHOP

April 9-10, 2014, University of Michigan

Registered Participants

First Name	Last Name	Affiliation
Eric	Anderson	NOAA-GLERL
Martin	Auer	Michigan Technological University
Sarah	Becker	Ohio EPA
Dmitry	Beletsky	University of Michigan, CILER
Steven	Chapra	Tufts University (remote participant)
Joe	DePinto	LimnoTech
Mary Anne	Evans	USGS Great Lakes Science Center
Joe	Fillingham	UW-Milwaukee, School of Freshwater Sciences
Russ	Kreis	U.S. EPA
Anika	Kuczynski	Michigan Technological University
Luis	Leon	Environment Canada
Daniel	Obenour	University of Michigan, Water Center
Pete	Richards	Heidelberg University
Daniel	Rucinski	LimnoTech
Donald	Scavia	University of Michigan, Graham Institute
Dave	Schwab	University of Michigan, Water Center
Craig	Stow	NOAA-GLERL
Richard	Stumpf	NOAA Center for Coastal Monitoring and
Ed	Verhamme	LimnoTech
Dale	White	Ohio EPA
Ram	Yerubandi	Environment Canada
Hongyan	Zhang	University of Michigan, CILER

GLWQA PHOSPHORUS LOAD RESPONSE MODELING WORKSHOP

April 9-10, 2014, University of Michigan
214 S. State Street, Ann Arbor, MI

Meeting Objective

The group will assess the capabilities of existing models in their abilities to develop response curves between nutrient loads and the objectives being identified by the Annex 4 group. It is desirable to include to the extent possible a range of model complexities in the model ensemble used for this analysis.

Desired Outcome

A plan (scope, schedule, and budget) for conducting an ensemble modeling effort to develop recommendations to the Annex 4 Objectives Task Team for revised Lake Erie target P loads and objectives by the end of September, 2014.

AGENDA

APRIL 9, 2014

10:00 AM	Convene, welcome, introductions, workshop goals	Don Scavia, University of Michigan
10:20 AM	P-loading trends and analysis over past 10-15 years	Pete Richards, Heidelberg University
10:40 AM	Review and discuss • Model evaluation criteria • Decisions needed to implement ensemble modeling effort	Don Scavia
12:00 PM	Lunch (provided)	
1:00 PM	Model presentations: HABs and Cladophora	Don Scavia
	Probabilistic cyanobacteria bloom forecasting model for western Lake Erie	Dan Obenour, University of Michigan
	Relating cyanobacterial blooms to phosphorus loads	Richard Stumpf, NOAA Center for Coastal Monitoring and Assessment
	Western Lake Erie Ecosystem Model	Joe DePinto, LimnoTech
	Modeling Cladophora in the Great Lakes: A Management Perspective	Martin Auer, Michigan Technological University
2:40 PM	Break	

3:00 PM	Model Presentations: Hypoxia/P/Chl	Joe DePinto
	Modeling Lake Erie's hypoxia response to nutrient loads and physical variability	Dan Rucinski, LimnoTech
	Great Lakes phosphorus modeling	Steven Chapra, Tufts University (remote)
	A 2D Ecological model of Lake Erie - An application of CE-QUAL-W2 to simulate Lake Erie water qualities	Hongyan Zhang, University of Michigan
	Environment Canada lake modeling	Luis Leon and Ram Yerubandi, Environment Canada
4:20 PM	Discussion, plans for day two	Joe DePinto
5:00 PM	Adjourn	

APRIL 10, 2014

8:30 AM	Morning refreshments	
9:00 AM	Group discussion: • What can current models do now? What do they need to do? • What minor modifications to some models will make them more useful/appropriate? • What common baseline/questions/assumptions/ output formats should be established among models	Don Scavia, Joe DePinto
12:00 PM	Lunch	
1:00 PM	Next steps Develop plan (scope, schedule, and budget) for ensemble modeling effort	Don Scavia, Joe DePinto

Appendix A-2. Agenda and Participant List: September 29-30, 2014 Ensemble Modeling Implementation Workshop

GREAT LAKES WATER QUALITY AGREEMENT PHOSPHORUS LOAD RESPONSE ENSEMBLE MODELING WORKSHOP

September 29-30, 2014, University of Michigan

Registered Participants

Modelers

Auer	Martin	Michigan Tech
Bertani	Isabella	University of Michigan
Bocaniov	Serghei	University of Michigan
Chapra	Steve	Tufts University
Depinto	Joe	LimnoTech
Leon	Luis	Environment Canada
McCrimmon	Craig	Environment Canada
Obenour	Daniel	University of Michigan
Rucinski	Daniel	LimnoTech
Scavia	Don	University of Michigan
Stumpf	Richard	NOAA
Verhamme	Ed	LimnoTech
Yerubandi	Ram	Environment Canada
Zhang	Hongyan	University of Michigan

Observers/Advisors

Chruscicki	Jean	US EPA
George	Sandra	Environment Canada
Perkins	Sarah	Battelle
Redder	Todd	LimnoTech
Schlea	Derek	LimnoTech
Stow	Craig	NOAA-GLERL
Warren	Glenn	US EPA
Wortman	Santina	US EPA

September 29-30, 2014, University of Michigan
214 South State Street, Ann Arbor, MI

September 29, 2014

10:00 AM	Convene, welcome, opening discussion (process, planned outcomes, and evaluation criteria)	Don Scavia
11:00 AM	*Modeling group presentations and discussion	
11:00	Western Basin bloom severity index	Rick Stumpf
11:15	Western Basin probabilistic cyanobacteria model	Dan Obenour
11:30	Great Lakes *Cladophora* model	Marty Auer
12:00 PM	Lunch (provided)	
1:00 PM	*Modeling group presentations and discussion, continued	
1:00	TP Mass Balance Model	Steve Chapra
1:30	1D Central Basin hypoxia model	Dan Rucinski
2:00	EcoLE	Hongyan Zhang
2:30	Lam's 9-Box Model	Craig McCrimmon
3:00 PM	Break	
3:15 PM	*Modeling group presentations and discussion, continued	
3:15	WLEEM	Joe DePinto
4:00	ELCOM-CAEDYM	Ram Yerubandi, Luis Leon, Serghei Bocaniov
4:45	Day 1 Recap, Day 2 Preview	Don Scavia
5:00	Adjourn	
5:30 PM	Group dinner at Sava's Restaurant	

September 30, 2014

8:30 AM	Continental breakfast (provided)	
9:00 AM	Comparison and discussion of response curves	Don Scavia
	Phytoplankton biomass	Steve Chapra
	Western Basin Cyanobacterial blooms	Joe DePinto
	Central Basin Hypoxia	Serghei Bocaniov
	Eastern Basin *Cladophora*	Marty Auer
10:30 AM	Break	
10:45 AM	Assembling the ensemble model	Joe DePinto
12:30 PM	Lunch (provided)	
1:15 PM	Group Discussion	
	Individual Model Deliverables Uncertainty in models and ensemble Updates needed Next steps, deadlines, writing assignments	Don Scavia
3:00 PM	Adjourn	

Appendix A-3. Report from April 9-10 Workshop

GLWQA PHOSPHORUS LOAD RESPONSE MODELING WORKSHOP REPORT

April 9-10, 2014, University of Michigan
214 South State Street, Ann Arbor, MI

1. Introduction

The purpose of this report is to outline an approach to use a series of modeled response curves relating phosphorus loads and objectives outlined in Annex 4 of the 2012 Great Lakes Water Quality Agreement.

Background

In the late 1970s a series of contemporary Great Lakes eutrophication models were applied to establish and confirm the target phosphorus loads for each of the Great Lakes and large embayments/basins. Those target loads were codified in Annex 3 of the 1978 Amendment to the Great Lakes Water Quality Agreement. The models applied for that analysis ranged from quite simple empirical relationships to kinetically complex, process-oriented models, including in order of increasing complexity: Vollenweider's empirical total phosphorus (TP) model (all lakes), Chapra's semi-empirical model (all lakes), Thomann's Lake 1 process model (Lake Ontario and Lake Huron), Ditoro's process model (Lake Erie), and Bierman's process model (Saginaw Bay). The results of these model applications have been documented in the IJC Task Group III report (Vallentyne and Thomas, 1978) and in Bierman (1980). The post-audit of several of these models in the mid-1980s confirmed that they had established a good relationship between total phosphorus loading to a lake/basin/embayment and its system-wide averaged TP and chlorophyll a concentration.

In 2006 as part of the Parties' (U.S. EPA, Environment Canada) review of the Great Lakes Water Quality Agreement, a sub-committee of Great Lakes modelers (co-chaired by Joe DePinto, LimnoTech, and David Lam, Environment Canada) was charged to conduct an examination of the data and models that were used to support the phosphorus target loads specified in Annex 3 of the Agreement relative to the current status of the Lakes. The charge to this sub-group was to address three questions:

(4) Have we achieved the target phosphorus (P) loads in all of the Great Lakes?
(5) Have we achieved the water quality objectives in all of the Great Lakes?
(6) Can we define the quantitative relationships between P loads and lake conditions with existing models? Are the models still valid on a whole lake basis or have ecosystem changes to the P- chlorophyll relationship occurred such that new or updated models need to be run?

The findings of this sub-group were basically that those models were aimed at whole lake eutrophication symptoms as they were manifested at the time, but were now not sufficiently spatially resolved to capture the nearshore eutrophication being observed throughout the lakes

and did not represent the process formulations to capture the impacts of ecosystem structure and function changes (e.g., Dreissenid impacts) relative to phosphorus processing and eutrophication responses in the lakes (DePinto et al., 2006) There was a general recommendation for a concerted research, monitoring, and model enhancement effort:

- to quantify the relative contributions of various environmental factors (total phosphorus loads, changes in the availability of phosphorus loads, hydrometeorological impacts on temperature conditions and hypolimnion structure and volume, *Dreissena*-induced alterations of nutrient-phytoplankton-light conditions and oxygen demand functions) to the nearshore re-eutrophication of the Great Lakes; and
- to develop a revised quantitative relationship between these stressors and the recently observed eutrophication indicators such as cyanobacteria blooms, enhanced hypoxia and nuisance benthic algal (e.g., *Cladophora*, *Lyngbya*) growth.

The recent publication of the 2012 Protocol amending the Great Lakes Water Quality Agreement (United States and Canada, 2012) includes an Annex 4 on nutrients, in particular on phosphorus control to achieve ecosystem objectives related to eutrophication symptoms. At this point the Annex has set "interim" phosphorus concentration objectives and loading targets that are identical to the Annex 3 values established in the 1978 Amendment. However, it requires that the "Parties, in cooperation and consultation with State and Provincial Governments, Tribal Governments, First Nations, Métis, Municipal Governments, watershed management agencies, other local public agencies, and the Public, shall:

(3) For the open Waters of the Great Lakes:
   a. Review the interim Substance Objectives for phosphorus concentrations for each Great Lake to assess adequacy for the purpose of meeting Lake Ecosystem Objectives, and revise as necessary;
   b. Review and update the phosphorus loading targets for each Great Lake; and
   c. Determine appropriate phosphorus loading allocations, apportioned by country, necessary to achieve Substance Objectives for phosphorus concentrations for each Great Lake;

(4) For the nearshore Waters of the Great Lakes:
   a. Develop Substance Objectives for phosphorus concentrations for nearshore waters, including embayments and tributary discharge for each Great Lake; and
   b. Establish load reduction targets for priority watersheds that have a significant localized impact on the Waters of the Great Lakes.

The Annex also calls for research and other programs aimed at setting and achieving the revised nutrient objectives. It also calls for the Parties to take into account the bioavailability of various forms of phosphorus, related productivity, seasonality, fisheries productivity requirements, climate change, invasive species, and other factors, such as downstream impacts, as necessary, when establishing the updated phosphorus concentration objectives and loading targets. Finally, it calls for the Lake Erie objectives and loading target revisions to be completed within three years of the 2012 Agreement entry into force.

To assist the Parties in developing and applying an approach for accomplishing these mandates, we developed the approach outlined in this paper to evaluate the interim phosphorus objectives and load targets for Lake Erie and to propose an approach for updating those targets in light of the new research and monitoring and modeling in the lake. The plan that is developed for Lake Erie can serve as a template for the other Great Lakes in meeting the 2012 Great Lakes Water Quality Agreement Protocol Annex 4 mandates.

Approach and Scope

On April 9-10, 2014, LimnoTech and University of Michigan's Graham Sustainability Institute convened a meeting of Lake Erie modelers, agency personnel, and others to assess the capabilities of existing models to develop response curves between nutrient loads and the objectives being identified by the Annex 4 group. This group's goal was to develop a plan for conducting an ensemble modeling effort, leading to recommendations to the Annex 4 Objectives Task Team for revised Lake Erie objectives and associated target P loads by the end of September 2014. A meeting agenda and list of participants are included in *Appendix A-1*.

2. Model Evaluation Criteria

During the meeting, we used the following criteria to assess the ability of each modeling effort to address the goals. While some level of assessment was done during the meeting, final assessments and decisions on appropriate use will be completed as part of the final product.

Ability to develop load-response curves and/or provide other output important for quantitative understanding of the questions/requirements posed in Annex 4: A key function of the models to be used in this effort is to establish relationships between phosphorus loads and the metric defined by the Annex 4 subgroup for each objective. As such, models will be evaluated as to their ability to establish load-response curves as the highest priority. Other models were also evaluated as to their utility to provide additional information to help understand dynamics, justify relationships, or otherwise inform the response curves or targets.

Applicability to objectives/metrics to be provided by the Annex 4 subgroup: The models will be evaluated as to their ability to address the specific spatial, temporal, and kinetic resolution characteristics of the objectives and metrics outlines by the Annex 4 subgroup. While models that address other objectives and metrics can be additionally informative, the highest priorities are those that can address them directly.

Extent/quality of calibration and confirmation: *Calibration* - Given the expected range in model type and complexity, there will likely be a range of skill assessments to be used. Models will be evaluated as to their ability to reproduce state-variables that match the objective metrics, as well as internal process dynamics. ***Post-calibration testing*** – Models will also be measured against their ability to replicate conditions not represented in the calibration data set.

Extent of model documentation (peer review or otherwise): Models will be evaluated based on the extent of their documentation. Full descriptions of model kinetics, inputs, calibration, confirmation, and applications are expected. This can be done through copies of peer reviewed journal articles, government reports, or other documentation, but it must be in writing.

Level of uncertainty analysis available: Models will be evaluated as to the extent they are able to quantify aspects of model uncertainty, including uncertainties associated with observation measurement error, model structure, parameterization, and aggregation, as well as uncertainty associated with characterizing natural variability.

3. Current modeling efforts to address response indicators

As mentioned above an initial recommendation must be put forth by the Annex 4 Objectives Task Group by the Fall of 2014. This deadline did not afford the time to go through a formal model comparison, vetting and evaluation process; hence this workshop was held to identify the eutrophication response indicators of concern and the models currently available to address those indicators. It also provided for an informal vetting of these models.

The first task related to the short-term goal is to identify the Eutrophication Response Indicators (ERIs) of concern for Lake Erie. We have identified the following four ERIs, along with metrics used to model and track them. This involves defining the metric in terms of how it is measured and what spatial and temporal scale will be used for that metric measurement.

(1) Overall phytoplankton biomass as represented by chlorophyll a

- Basin-specific, summer (June-August) average chlorophyll concentration

This is a traditional indicator of lake trophic status (i.e., oligotrophic, mesotrophic, eutrophic).

(2) *Cyanobacteria blooms (including Microcystis sp.) in the Western Basin*

- Maximum basin-wide cyanobacteria biomass (mass dry weight)
- Summer total basin-wide cyanobacteria biomass (mass dry weight integrated over summer bloom period)

The first metric gives an indication of the worst condition relative to HABs in the Western Basin, while the second factors in the cumulative effects of multiple drivers (loads, hydrology, wind, temperature, etc.) in producing a season-long cumulative production of HABs. The length of the "summer bloom period" referred to in this metric can vary from one scenario to another.

(3) Hypoxia in hypolimnion of the Central Basin

- Number of hypoxic days
- Average areal extent during summer
- Average hypolimnion DO concentration during stratification

All three of these metrics are quantitatively correlated based on Central Basin monitoring and analysis, but they are different manifestations of the problem that each has a bearing on the assessment of the impact on the ecosystem (especially fish communities) and on the relative impact of physical conditions and nutrient-algal growth conditions on the indicator.

(4) *Cladophora in the nearshore areas of the Eastern Basin*

While beach fouling by sloughed *Cladophora* is likely the most important metric, there is neither an acceptable monitoring program to measure and report progress, nor a scientifically credible model to relate it to nutrient loads and conditions. There are models that can relate *Cladophora* growth to ambient DRP concentration and models that can estimate near shore DRP as a function of loads and biophysical dynamics. Linking these models could allow us to then relate loads to *Cladophora* growth, but the accumulation of errors across models minimizes the utility as a predictor. Instead, what would be useful is to use these models to explore the relative impacts of loads recommended for other objectives eutrophication response indicators on *Cladophora* growth potential.

The models capable of addressing each of these indicators have been identified and described briefly below and summarized in Table A3-1.

Table A3-1: Models considered for ensemble modeling effort, organized according to capability to address selected ecosystem response indicators.

Model	**Response Indicators**			
	Overall phytoplankton biomass	**Western basin cyanobacteria blooms**	**Central basin hypoxia**	**Eastern basin *Cladophora* (nearshore)**
Total Phosphorus Mass Balance Model (Chapra, Dolan, and Dove	X		X	
Western Lake Erie Ecosystem Model (WLEEM) (LimnoTech)	X (Western)	X	X (provide organic matter load)	
ELCOM-CAEDYM (Bocaniov, Leon, and Yerubandi)	X	X	X	X (boundary conditions)
Ecological Model of Lake Erie (EcoLE) (Zhang)	X	X	X	
U-M/GLERL Western Lake Erie		X		

HAB Forecasting Model (Obenour)				
NOAA Total Phosphorus Reduction Model (Stumpf)		X		
Nine Box model (McCrimmon, Leon, and Yerubandi)	X		X	
1-Dimensional Central Basin Hypoxia Model (Rucinski)	X (Central)		X	
Great Lakes *Cladophora* model (Auer)				X
Cladophora growth model (Higgins)				X

Overall phytoplankton biomass (Chlorophyll)

A possible metric for the overall phytoplankton biomass indicator is a basin-specific, summer (June – August) average chlorophyll a concentration. The following models could be applied for this metric:

Total Phosphorus Mass Balance Model (Chapra, Dolan, and Dove)

Chapra and Dolan (2012) presented an update to the original mass balance model that was used (along with other models) to establish phosphorus loading targets for the 1978 Great Lakes Water Quality Agreement. Annual TP estimates were generated from 1800 to 2010. The model is designed to predict the annual average concentrations in the offshore waters of the Great Lakes as a function of external loading and does not attempt to resolve finer-scale temporal or spatial variability. Calibration data for this model were obtained from EC and GLNPO. The model can be expanded to include chlorophyll and potentially central basin hypoxia.

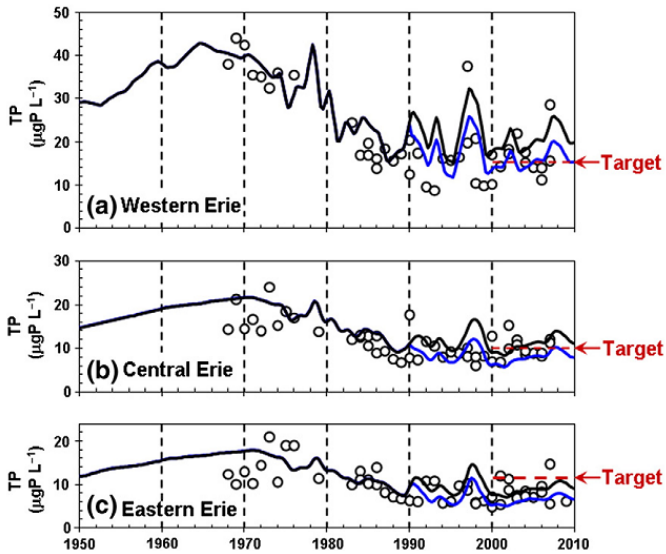

Figure A3-1: Model and data comparison of TP concentration for the three basins of Lake Erie (adapted from Chapra and Dolan (2012)).

Western Lake Erie Ecosystem Model (WLEEM) (LimnoTech)

The Western Lake Erie Ecosystem Model (WLEEM) has been developed as a 3D fine-scale, process-based, linked hydrodynamic-sediment transport-advanced eutrophication model to provide a quantitative relationship between loadings of water, sediments, and nutrients to the Western Basin of Lake Erie from all sources and its response in terms of turbidity/sedimentation and algal biomass. The model operates on a daily time scale and can produce time series outputs and spatial distributions of either total chlorophyll and/or cyanobacteria biomass as a function of loading. Therefore, it can produce load-response plots for several potential endpoints of interest in the Western Basin. The Western Basin model domain is bounded by a line connecting Pointe Peele with Marblehead. It will also produce mass balances for the Western Basin for any one of its ~30 states variables; therefore, it can compute the daily loading of Western Basin nutrients and oxygen-demanding materials to the Central Basin as a function of loads to the Western Basin. This will provide valuable information on how load reductions to the Western Basin will impact hypoxia development in the Central Basin.

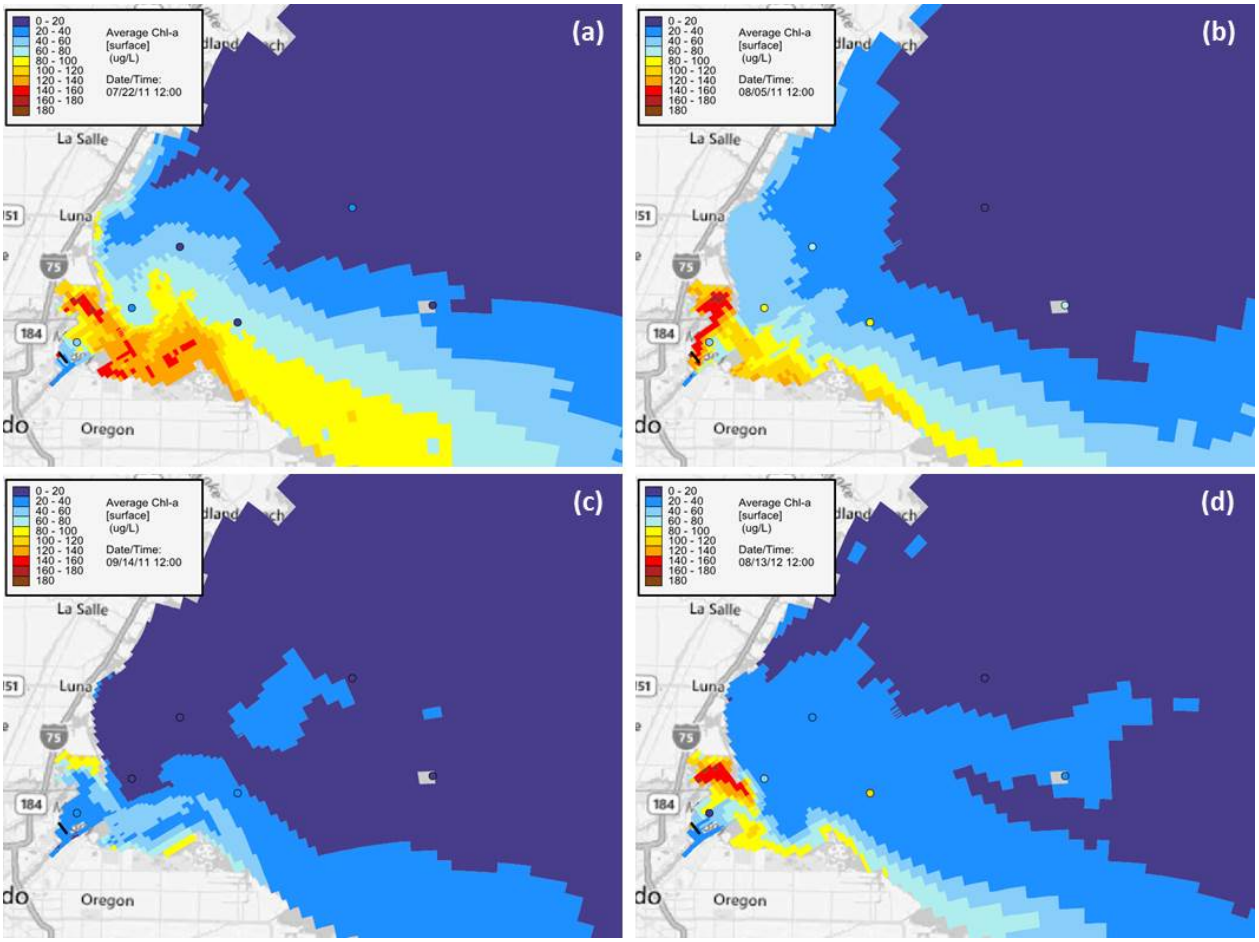

Figure A3-2: WLEEM produced total chlorophyll a concentration in Western Lake Erie on (a) 7/22/2011, (b) 8/5/2011, (c) 9/14/2011, and (d) 8/13/2012.

ELCOM-CAEDYM (Bocaniov, Leon, and Yerubandi)

ELCOM-CAEDYM is a three-dimensional hydrodynamic and bio-geochemical model that consists of two coupled models: a three-dimensional hydrodynamic model - the Estuary, Lake and Coastal Ocean Model (ELCOM; Hodges et al., 2000), and a bio-geochemical model - the Computational Aquatic Ecosystem Dynamics Model (CAEDYM; Hipsey and Hamilton, 2008). The ELCOM-CAEDYM model has shown a great potential for modelling of biochemical processes and been successfully used for in-depth investigations into variable hydrodynamic and biochemical processes in many lakes all over the world including the Laurentian Great Lakes. In Lake Erie it has been used to study nutrient and phytoplankton dynamics (Leon et al., 2011; Bocaniov et al., 2014), the effect of mussel grazing on phytoplankton biomass (Bocaniov et al., 2014), the sensitivity of thermal structure to variations in meteorological parameters (Liu et al., in revision) and even winter regime and the effect of ice on hydrodynamics and some water quality parameters (Oveisy et al., in revision). The application of ELCOM-CAEDYM model to study the oxygen dynamics and understand the central basin hypoxia is a subject of the ongoing work.

The first application of a coupled model (ELCOM-CAEDYM) to Lake Erie was for the year of 2002 (early/mid-April to mid-October). It included eleven major tributaries accounting for 97.5 % of total lake inflow and one outflow (Niagara River). The model was calibrated by the adjustment of model parameters and constants to improve the agreement between model output and observations. The adjustment of the parameters was within the range of published values. The model was validated for its ability to reproduce thermal structure, surface and near-bottom temperatures, light attenuation coefficients, nutrients including their fractions (e.g. TP, soluble reactive phosphorus - SRP, TDP, NO3 and NO2, NH4, soluble reactive silica- SRSi, etc.) and phytoplankton (Leon et al., 2011; Bocaniov et al., 2014).

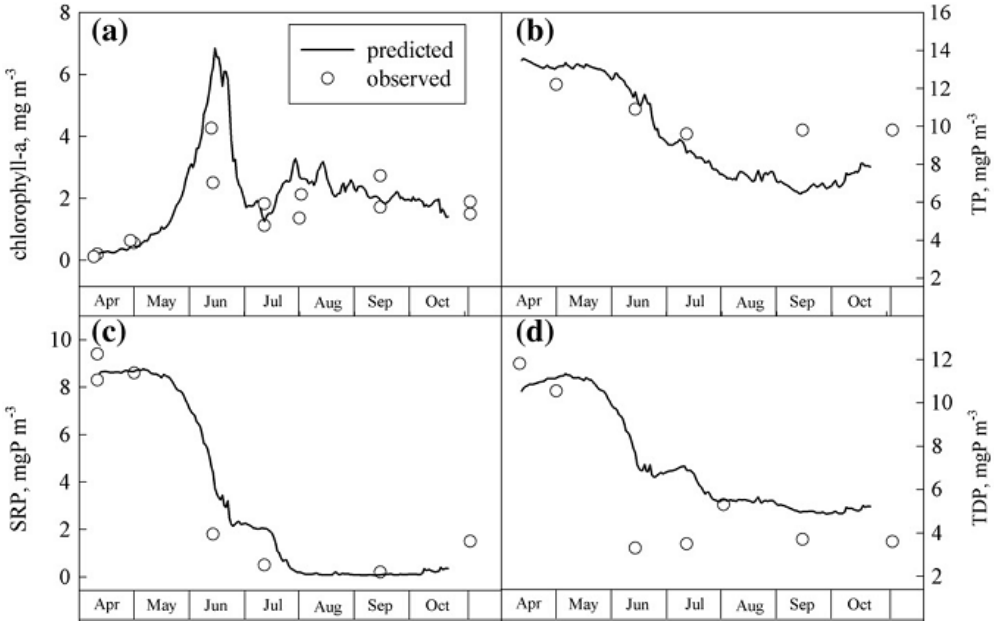

Figure A3-3: Time series output of predicted concentrations of Chl-a, TP, TDP, SRP for the top 5 m together with observations for station 938 (east basin) in 2002. (From Leon et al., 2011)

Ecological Model of Lake Erie - EcoLE (Zhang)

Zhang et al. (2008) developed and applied a 2D hydrodynamic and water quality model to Lake Erie termed the Ecological Model of Lake Erie (EcoLE), which is based on the CE-QUAL-W2 framework. The purpose of the model application was to estimate the impact that dreissenids are having on phytoplankton populations. The model was calibrated against data collected in 1997 and verified against data collected in 1998 and 1999. Model results indicate that mussels can filter approximately 20% of the water column per day in the western basin and 3% in the central and eastern basins. Because phytoplankton are not evenly distributed in the water column and mussels reside on the bottom, this translates to approximately 1% and 10% impact on phytoplankton biomass in the central/eastern and western basins, respectively. Dreissenid mussels have weak direct grazing impacts on algal biomass and succession, while their indirect effects through nutrient excretion have much greater and profound negative impacts on the system (Zhang et al., 2011). Algal biomass output can be converted to chlorophyll concentrations. The model also dynamically simulates dissolved oxygen in the lake, and has been applied to evaluate the importance of weather and sampling intensity for calculated hypolimnetic oxygen depletion rates in the western-central basin (Conroy et al., 2011).

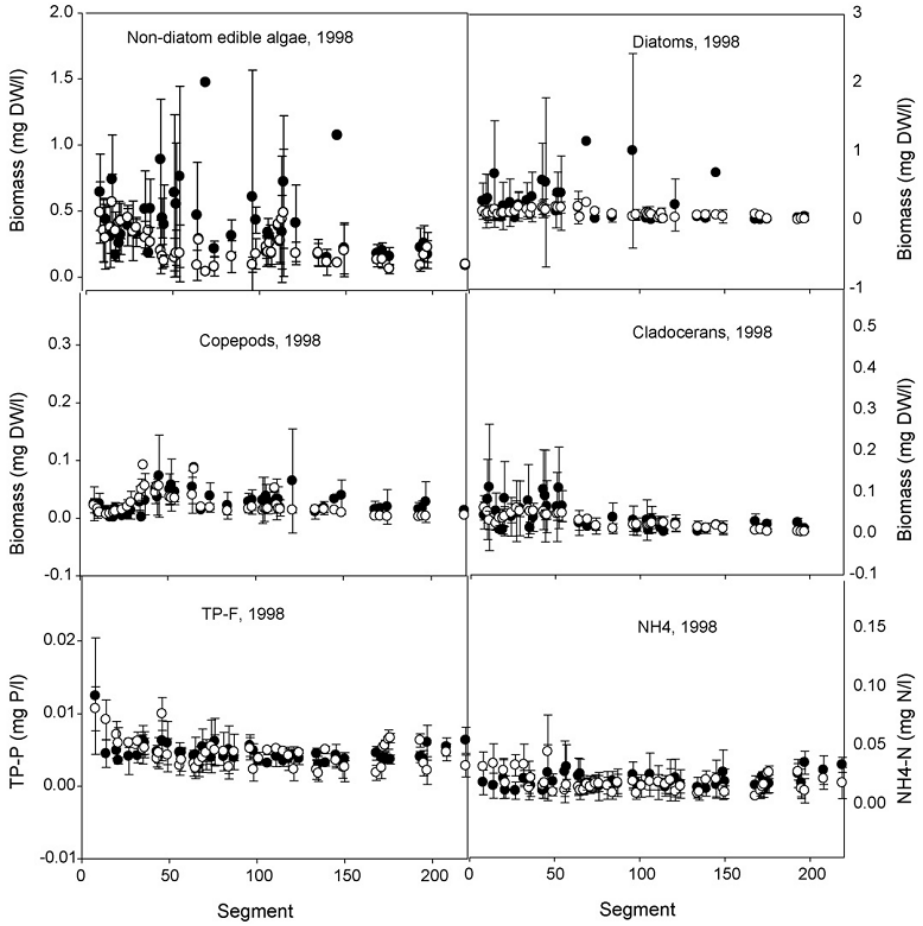

Figure A3-4: EcoLE model verification of 1998 for non-diatom edible algae, diatoms, copepods, cladocerans, total dissolved phosphorus (TP-F), and ammonia (NH4).

Western Basin cyanobacterial blooms

Possible metrics for the Western Basin cyanobacterial blooms indicator could include: maximum basin-wide cyanobacteria biomass or summer average cyanobacteria biomass in the basin. This metric therefore requires a model that is specific for the cyanobacteria functional group and either provides a time-variable simulation of that functional group or an empirical relationship for the metric in question. The Obenour and Stumpf models produce empirical relationships between spring loading (approximately March-June) from the Maumee River and the maximum cyanobacteria biomass. The ELCOM-CAEDYM, WLEEM and EcoLE models all compute the cyanobacteria biomass on a time-variable basis and at a spatial resolution such that they can compute both maximum and summer average cyanobacteria biomass.

U-M/GLERL Western Lake Erie HAB Forecasting Model (Obenour)

A probabilistic model was developed to relate the size of the western basin cyanobacteria bloom to spring phosphorus loading (Obenour et al., in review). The model is calibrated to multiple sets of bloom observations, from previous remote sensing and in situ sampling studies. A Bayesian hierarchical framework is used to accommodate the multiple observation datasets, and to allow for rigorous uncertainty quantification. Furthermore, a cross validation exercise demonstrates the model is robust and would be useful for providing probabilistic bloom forecasts (Figure A3-5). The deterministic form of the model suggests that there is a threshold loading value, below which the bloom remains at a baseline (i.e., background level). Above this threshold, bloom size increases proportionally to phosphorus load. Importantly, the model includes a temporal trend component indicating that this threshold has been decreasing over the study period (2002-2013), such that the lake is now significantly more susceptible to cyanobacteria blooms than it was a decade ago.

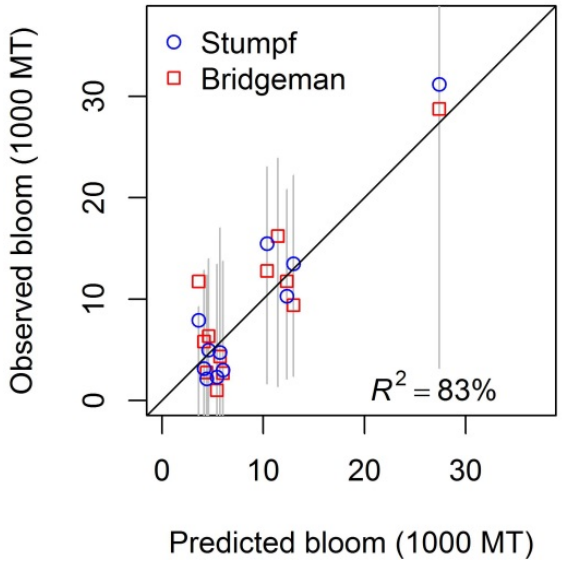

Figure A3-5: Predicted vs. Observed Bloom intensity (U-M/GLERL Western Lake Erie HAB model).

NOAA Total Phosphorus Reduction Model (Stumpf)

In Stumpf et al. (2012) the authors present a regression between spring TP load and flow from the Maumee River and mean summer cyanobacteria index (CI) for western Lake Erie as calculated by the European space satellite, MERIS. This method applies an algorithm to convert raw satellite reflectance around the 681 nm band into an index that correlates with cyanobacteria density. Ten day composites were calculated by taking the maximum CI value at each pixel within a given 10-day period to remove clouds and capture areal biomass. The authors conclude that spring flow or TP load can be used to predict bloom magnitude. Average flow from March to June was the best predictor of CI utilizing data from 2002 to 2011 (Figure A3-6).

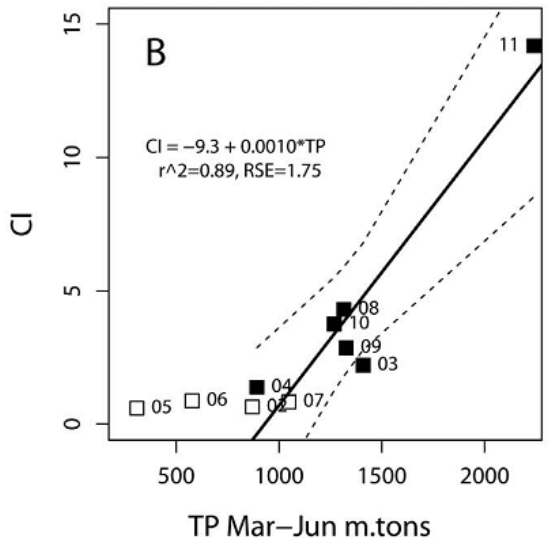

Figure A3-6: Maumee River TP load (March to June) versus cyanobacteria index (CI) from 2002 to 2011 (NOAA Total Phosphorus Reduction Model).

Western Lake Erie Ecosystem Model (WLEEM) (LimnoTech) (described above)

ELCOM-CAEDYM (Bocaniov ,Leon, and Yerubandi) (described above)

Ecological Model of Lake Erie - EcoLE (Zhang) (described above)

Central Basin hypoxia

Possible metrics for the Central Basin hypoxia indicator include the number of hypoxic days in the Central Basin during a given summer stratification period, and/or the average areal extent of the hypoxic zone during a given summer month, and/or the average hypolimnion DO concentration during the summer stratified period. The following existing models can provide estimates of the relationship between these metrics and external phosphorus loads.

1-Dimensional Central Basin Hypoxia Model (Rucinski)

A model, calibrated to observations in the Central Basin of Lake Erie, was used to develop response curves relating chlorophyll concentrations and hypoxia to phosphorus loads. The model is driven by a 1D hydrodynamic model that provides temperature and vertical mixing profiles (Rucinski et al., 2010). The biological portion of the coupled hydrodynamic-biological model incorporates phosphorus and carbon loading, internal phosphorus cycling, carbon cycling (in the form of algal biomass and detritus), algal growth and decay, zooplankton grazing, oxygen consumption and production processes, and sediment interactions.

The 1-dimensional model has been corroborated with data from 1987-2005 for dissolved oxygen (DO), total phosphorus (TP) and chlorophyll a (chl-a). This corroboration was performed with loads estimated from Pete Richards and Dave Dolan, with the assumption that the "available nutrient" pool was comprised exclusively of dissolved reactive phosphorus (DRP). The "unavailable nutrient" pool was therefore assumed to be the difference between TP and DRP. Response curves of DO (hypolimnion oxygen demand, hypoxia days, hypoxic area, bottom DO) vs TP and DRP have been developed, and published, based on the existing calibration.

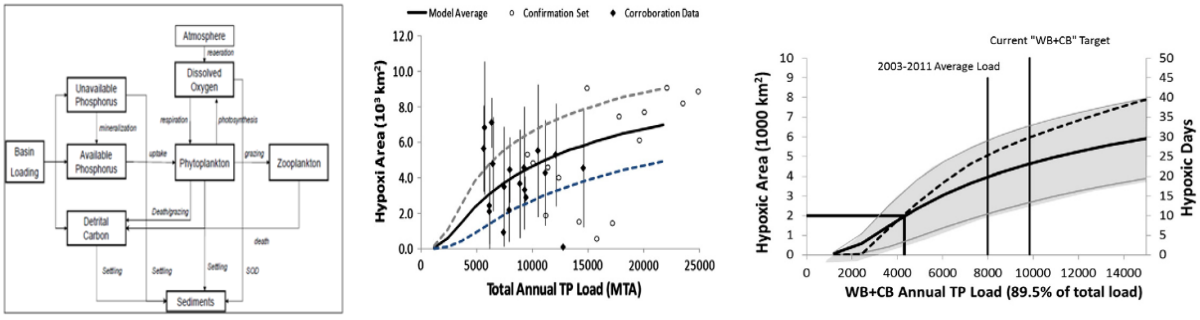

Figure A3-7: Conceptual diagram of state variables and kinetic interactions of the Lake Erie DO Model (Rucinski et al., 2010), calibration, and response curves.

Nine Box model (McCrimmon, Leon, and Yerubandi)

This is a 9-box model for quantitative understanding of the eutrophication and related hypoxia (Lam et al., 1983). The model is extensively calibrated and validated against observations in the past. Re-calibrations were conducted for post-zebra mussel period and found that 9 box model is able to express offshore Lake Erie concentrations reasonably well. The model can be expanded to include empirically derived chlorophyll relations for given TP concentrations.

Total Phosphorus Mass Balance Model (Chapra, Dolan, and Dove) (described above)

The TP mass balance model is described in 3.1.1.

ELCOM-CAEDYM (Bocaniov ,Leon, and Yerubandi) (described above)

Ecological Model of Lake Erie - EcoLE (Zhang) (described above)

Eastern Basin *Cladophora* (nearshore)

The indicator of concern for the Eastern Basin is *Cladophora* growth in nearshore areas. Here the two *Cladophora* growth models of Auer and Higgins are candidates for this analysis. Both models could provide estimates of biomass per unit area and areal coverage; however, both models require estimates of nearshore DRP concentrations. Those concentrations could potentially be provided by the ELCOM-CAEDYM (Leon/Bocaniov) model.

Great Lakes Cladophora Model (Auer)

The Great Lakes *Cladophora* Model (GLCM) is a revision of the original *Cladophora* model developed by Auer and Canale in the early 1980s in response to the need to understand the causes of large *Cladophora* blooms around the Great Lakes, especially in Lake Huron (Tomlinson et al., 2010). The new model reflects current understandings of *Cladophora* ecology and a new set of tools and software to allow others to quickly run the model and view output. The updated model was calibrated and verified against data from Lake Huron (1979) and new data collected by the authors in 2006 in Lake Michigan. The model allows users to simulate standing crop of *Cladophora* as influenced by environmental parameters such as depth, light, and phosphorus concentrations.

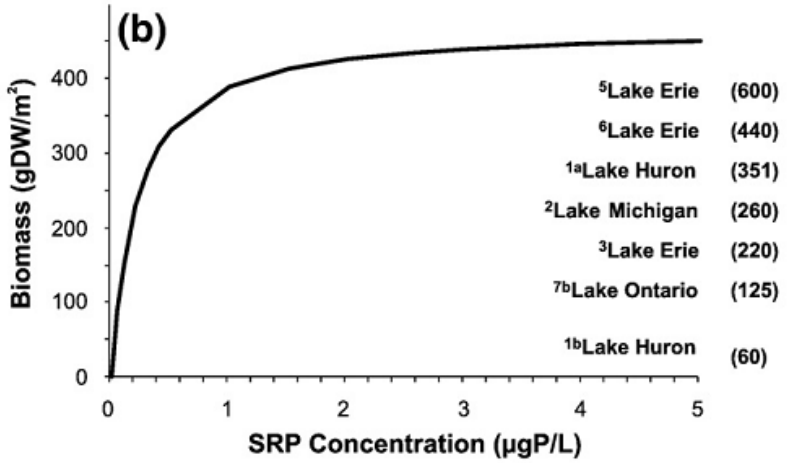

Figure A3-8: Excerpt from Tomlinson et al. (2010) showing relationship between *Cladophora* biomass and ambient SRP concentration.

Cladophora growth model (Higgins)

Another revision of the "Canale and Auer" *Cladophora* model mentioned in the previous section was undertaken by Higgins et al. (Higgins et al., 2005). The *Cladophora* Growth Model (CGM), as

termed by the authors, includes several revisions to the Canale and Auer model that were identified when applying the model to eastern Lake Erie. The revisions include further refinements of *Cladophora* response to changes in light extinction (Kpar) and maximum biomass (Xmax).

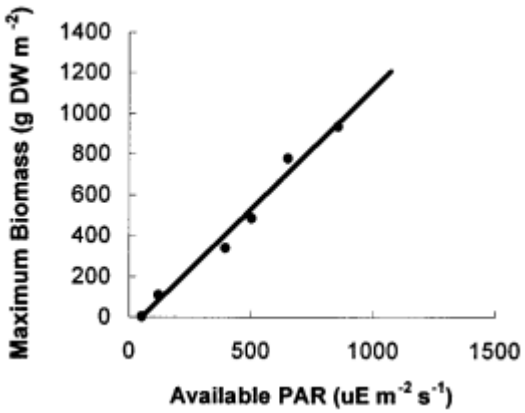

Figure A3-9: Relationship between available light (PAR) and maximum *Cladophora* biomass (from Higgins et al., 2005)

4. Proposed process for applying ensemble modeling

Our recommendation for revision of the Annex 4 objectives and associated target phosphorus loads is to use an approach similar to the multiple model application used to establish and confirm the target P loads in Annex 3 of the 1978 Amended GLWQA. The general philosophy is to begin with identifying the eutrophication response indicators (ERIs) of concern and to use multiple models to compute appropriate load-response relationships for each of the indicators. Then once the target/threshold measure of the eutrophication response indicators has been established, the load-response relationships can be used to compare and recommend loads corresponding to that threshold. Models that compute in-lake nutrient concentrations along the way to producing the load-response relationship can potentially be used to extract the temporal and spatial profile of river mouth, nearshore, and open-lake nutrient concentrations consistent with a given target load.

The ensemble of models proposed to be applied have all been developed to address the current Lake Erie ecosystem structure and function, including the potential to address both nearshore and offshore conditions. The models also represent a range of complexities and assumptions. This ensemble approach within which all models use the same basic input data (i.e., forcing functions) to create common load-response relationships provides several benefits over relying on a single model. First, by reconciling differences among results in terms of the different assumptions and model construction and parameterization, it provides insights into the most important sources and processes for a given system and management issue. Also, a given management question can be viewed from different conceptual and operational perspectives. The same datasets are mined in different ways. Multiple lines of evidence are compiled. All of this reduces the level of risk in environmental management decision-making.

In the end, having great model diversity can add more value to the analysis than having a multiplicity of very similar models.

Short term efforts

The models capable of addressing each of these indicators have been identified and described briefly above. Each of those models will be applied using a series of tasks to produce a set of results to be used in making the target load and objectives recommendations. These tasks are described below.

Tasks required for each response indicator

Task 1: Define metrics (state variables) to be modeled

Each modeling team will define the modeled metric/s (i.e., state variable) that will be computed to represent the ERIs that they are addressing (see metric descriptions above).

Task 2: Identify the models to be applied to each ERI

Table A3-1 above lists five models to be used for the overall phytoplankton biomass ERI, five models to be used for the Western Basin cyanobacteria bloom ERI, five models to be used for the Central Basin hypoxia ERI, and a blending of two *Cladophora* models to be used for the Eastern Basin *Cladophora* ERI. Based on the workshop all of these models appear to be a valuable part of the multiple modeling effort to address the short-term Annex 4 goal stated above; however the final assessment will be made once individual model results are delivered (e.g., more complete documentation of response to the evaluation criteria outlined above). Each modeling effort will be required to provide the following information to serve as the basis for the final evaluation:

- Complete documentation of model equations, coefficients, and driving variables
- Documented comparisons between model output and observations (state variables, processes) used in calibration
- Documentation of post-calibration testing (e.g., comparison of model performance for observations not used in the calibration)
- Documentation of formal and/or informal assessments of model uncertainty/sensitivity
- The response curves relating nutrient loads to the objective metrics.

Task 3: Apply models to develop load-response and other output analyses

This task describes the individual short-term activities that are planned for each of the models.

General

Prior to applying the models, a common (baseline) Lake Erie input data set needs to be developed for all models to have a common baseline input data set for their analysis. The proposed approach is to select a single year that contains the most complete representation of the necessary data and also represents a “typical” year with respect to such forcing functions as hydrology, wind, temperature, and Dreissenid densities. This year should come from the past 10 years or so of observations, so these conditions can be said to be “recent”. Then load alterations that might be analyzed in producing load-response curves would use all of the same

inputs but simply adjust the concentration of phosphorus in the hydrologic inputs to the system.

Possible years for developing this baseline are 2008, which according to Dolan and Chapra, is a good representation of average loading conditions to the lake. Another possibility would be 2013, which is a very recent year that provides conditions between the extreme western basin years of 2011 and 2012. We will collaborate with the Parties (EPA and EC) to produce data sets for both the input and in-lake response data for the selected common year.

The group will also decide on the suite of independent P load variables to use for the x-axis in the load-response analysis curves. These independent variable loads could have spatial and temporal specifications (e.g., basin loads, tributary loads, or seasonal loads) and they can have P form specifications (e.g., TP, DRP, Bioavailable P).

Total Phosphorus Mass Balance Model (Chapra, Dolan, and Dove)

In the short term, this model would be used in its present version to develop basin-specific load-response curves for TP and chlorophyll a (Chapra and Dolan, 2012). Chapra would also investigate the feasibility of extending his model framework to compute hypolimnetic oxygen and sediment nutrient release in the Central Basin (Chapra and Canale, 1991).

ELCOM-CAEDYM (Bocaniov, Leon, and Yerubandi)

In the short-term, Environment Canada and Bocaniov will collaborate to undertake the following ELCOM-CAEDYM model application activities:

1. Using the common, baseline year selected by the modeling group, assess ELCOM-CAEDYM performance with respect to observed nutrient and phytoplankton concentrations during that year.
2. Control experiments with different loading scenarios similar to those suggested for WLEEM.
3. Generate Load (TP, SRP) vs Total Chl-a curves
4. Generate Load (TP, SRP) vs Cyanobacteria Chl-a
5. Generate Load (TP) vs Hypolimnetic oxygen concentration
6. Generate Load (TP) vs hypoxia area

Nine Box model (McCrimmon, Leon, and Yerubandi)

In the short-term, the Lam et al. 9-box model will also be applied by Environment Canada with the following steps:

1. Using the common, baseline year selected by the modeling group, assess 9 Box model performance with respect to observed nutrient during that year
2. Run NWRI vertical temperature model for providing stratification to hypoxia model
3. Generate Load (TP) vs concentrations in west, central and east basins
4. Generate Load (TP) vs DO concentrations
5. Generate Load (TP) vs hypoxia area (NWRI method)

1-Dimensional Central Basin Hypoxia Model (Rucinski)

This model can produce a range of hypoxia conditions (any of the selected metrics) for a given load as a function of a range of observed or hypothesized physical forcing conditions that might affect the duration and magnitude and depth of stratification. The short-term application will do the following steps:

- Using the existing model parameterization and the common, baseline year a series of hypoxia load-response curves will be developed for the three metrics. These curves will be driven by the same load reduction scenarios suggested for the WLEEM model (applied to both the Western Basin and Central Basin inputs). The load of phosphorus and organic material from the Western Basin to the Central Basin for those scenarios will be computed by WLEEM.
- Chlorophyll a load-response curves will be produced using the same series of P load reduction scenarios. This will provide an input to the overall phytoplankton biomass metric.
- Using loads of phosphorus and oxygen-demanding material from the Western Basin based on WLEEM may require re-calibration/corroboration of the model prior to its application for the first two bullets above.

Ecological Model of Lake Erie - EcoLE (Zhang)

The Zhang short term activities will first have to examine how to initialize and run the model for the common, baseline year. They will then check the model against total chlorophyll a, cyanobacteria chlorophyll a, and central basin DO for that year, and possibly recalibrate. The recalibrated model will then be used to generate load-response curves for total chlorophyll a in each basin, cyanobacteria biomass in the Western Basin, and hypoxia in the central basin.

Western Lake Erie Ecosystem Model (WLEEM) (LimnoTech)

WLEEM will be run for the common baseline year using nutrient and solids loads to the Western Basin from all sources estimated in the same way that Dolan estimated the loads for the EcoFore project. The model will produce spatial and temporal profile outputs of TP, DRP, NO_3, TNH_3, TKN, total phytoplankton biomass (as mgC/L and chlorophyll a), functional phytoplankton group biomass (e.g., cyanobacteria), and several ancillary state variables (T, chloride, TSS and VSS, K_e, DO). The concentration of all state variable outputs will be expressible as either volumetric concentration in a given 3D model cell or as a depth averaged concentration for every horizontal grid cell. The state variables can also be expressed as a mass of the constituent in a given volume of water, thus facilitating the development of Western Basin mass balances from the model output. These mass balances can be developed on any spatial and temporal basis, including the total mass of cyanobacteria in the Western Basin integrated over the entire growing season. In summary, concentration or mass balance outputs can then be averaged or aggregated over any desired time and space (e.g., basinwide, August average of cyanobacteria chlorophyll a).

The following scenarios will be run with the model using the common baseline year (additional scenarios may be run based on suggestions from managers):

- Baseline loads and flows and other forcing functions;
- Reduce TP and DRP loads (by reducing concentration) from all tributaries and the Detroit River by 25%, 50%, 75%, 100%;
- Reduce TP and DRP loads (by reducing concentration) from only the Maumee River by 25%, 50%, 75%, 100%;

- Reduce TP and DRP loads (by reducing concentration) from only the Detroit River by 25%, 50%, 75%, 100%;
- Reduce only DRP loads (by reducing concentration) from all tributaries and the Detroit River by 25%, 50%, 75%, 100%;
- Reduce only DRP loads (by reducing concentration) from only the Maumee River by 25%, 50%, 75%, 100%;
- Baseline with no sediment feedback, either by resuspension or pore water diffusion).

The output from these scenarios will permit the production of a large suite of load-response plots with TP or DRP load (either annual or cumulative over some specified time period, like March-June) on the x-axis and any one of the state variables on the y-axis (again averaged over any specified time and/or space designation for the Western Basin). The output will also be used to compute net fluxes (loads) of phosphorus and decomposable organic carbon to the Central Basin by various load management options.

U-M/GLERL Western Lake Erie HAB Forecasting Model (Obenour)

In the short term, the application of the Obenour model will include the following steps:

1. **Recalibrate model to 'bioavailable' phosphorus loads.** Bioavailable phosphorus loads will be determined by applying 'bioavailable fraction coefficients' to the DRP and non-DRP phosphorus loads from the Maumee River. The coefficients will be initialized based on prior information developed through literature review, and the coefficients will be updated based on bloom model calibration, through Bayesian inference. This revise calibration will be compared with those generated using TP and DRP loads.

2. **Expand scope of the model.** The bloom forecasting model will be re-calibrated to an expanded dataset of harmful algal bloom observations, covering 1979-1987 and 1998-present. Observations prior to 2002 will be derived from SeaWiFs and CZCS satellite imagery. By expanding the calibration dataset, it will be possible to consider additional biophysical drivers of the temporal variability in harmful algal blooms. In addition to Maumee River nutrient loads, water column mixing, sea surface temperature, and Detroit River nutrient loads will be added to the analysis as potential bloom predictors. The resulting model will refine our understanding of the causes of cyanobacteria blooms, and may suggest new management measures, beyond Maumee River phosphorus load reductions.

NOAA Total Phosphorus Reduction Model (Stumpf)

In the short term, Stumpf will apply their bloom severity forecasting model to suggest TP and DRP load targets using the Maumee River as the surrogate for the loading of influence in the western basin.

First, they will update the model published in Stumpf et al., 2012.Then they will produce load-response curves for the Western Basin cyanobacteria metrics using the revised model. The load-response plots will also provide estimates of uncertainty for the various relationships examined.

Great Lakes *Cladophora* Model (Auer)

The modeling effort in the short-term will be to model the change in *Cladophora* biomass production in a model domain along the north shoreline of the Eastern Basin in response to changes in external loading to the lake under various loading scenarios. Specifically, this effort will include:

- Adapt the Great Lakes *Cladophora* Model (GLCM, Tomlinson et al., 2010) to accommodate selected features of the *Cladophora* Growth Model (Higgins et al., 2005), the only other attached algae modeling tool presently available;
- Perform sensitivity analyses with the GLCM to facilitate the assignment of uncertainty estimates to the P-loading/*Cladophora* response relationship;
- Apply a whole lake modeling framework such as ELCOM-CAEDYM to establish the (spatiotemporal) phosphorus regime of the eastern basin for baseline and projected tributary and point source bioavailable P loads and for a range of bioavailable P concentrations at the eastern basin – central basin boundary;
- Apply the GLCM to establish a load-response relationship between bioavailable P levels at the eastern basin – central basin boundary and *Cladophora* growth and estimates of uncertainty in the *Cladophora* response at each P level.

Task 4: Evaluation of deliverables against the criteria

The modeling team will use the evaluation criteria outlined above and the deliverables from each group to assess which model results will be used in the ensemble.

Task 5: Conduct comparison analysis among models for each ERI

For each ERI, load-response outputs will be compared among the models to identify significant differences and to understand those differences in terms of model formulation and inherent assumptions. A modeling group decision will be made on how to represent the various models in establishing a target load to meet a given ERI metric.

This task will also include, if appropriate, producing an *in-lake* nutrient concentration profile in space and time for each target load to demonstrate its variability and to stress the resources necessary to monitor compliance on that basis.

Task 6: Synthesize results and formulate recommended initial target loads

This task would be accomplished in cooperation with the entire Annex 4 Objectives Task Group. The modeling sub-group will synthesize and document the results of the first five tasks with a sub-group meeting. Then the documented results will be shared with the entire Objectives Task Group and another face-to-face meeting will take place with the goal of developing a report to be sent forward to the Annex 4 Committee.

APPENDIX B: INDIVIDUAL MODEL REPORTS

APPENDIX B-1: NOAA Western Lake Erie HAB Model

R.P. Stumpf, NOAA National Centers for Coastal Ocean Science

Summary

Reducing spring, March to July, total phosphorus to less than 1150 m.tons should result in only mild blooms. Reducing the load by 40% will eliminate most blooms, however, 2011 and 2013 would still have substantial, although greatly reduced, blooms. A reduction of 40% or greater in 2008 would result in a mild bloom (CI < 2).

1. Model Description

Overview

Stumpf et al. (2012) examined the role of phosphorus loading on the severity of the summer cyanobacterial bloom in western Lake Erie. Bloom severity was quantified from satellite with a "cyanobacteria index" (CI). The CI is a measure of total biomass of cyanobacteria, with chlorophyll as the surrogate for biomass. Phosphorus data came from Heidelberg University, converted to monthly mean loads. Stumpf et al. (2012) found that TP from the Maumee River provides a better metric of variation in biomass than does dissolved reactive phosphorus, probably due to the importance of discharge, which influences TP more than soluble reactive phosphorus (SRP). The Maumee River, as the major Lake Erie tributary produces most of the load into southwestern Lake Erie, 10-fold greater TP than the next largest tributary (Raisin River; Dolan and Richards, 2008). The original model used loads from March to June to explain variations from 2002-2011. Starting in 2012, NOAA has produced an annual prediction of bloom severity based on the model. The model prediction for 2013, which had a large July load, was underestimated. Previously July was not considered because 2003 and 2008 had large July loads, yet did not have blooms that were substantively different from the other major bloom years of 2009 and 2010. An evaluation of temperature (Stumpf, unpublished) found that while all years have similar temperatures in July and August, 2003 and 2008 had the coldest average June (Figure B1-1).

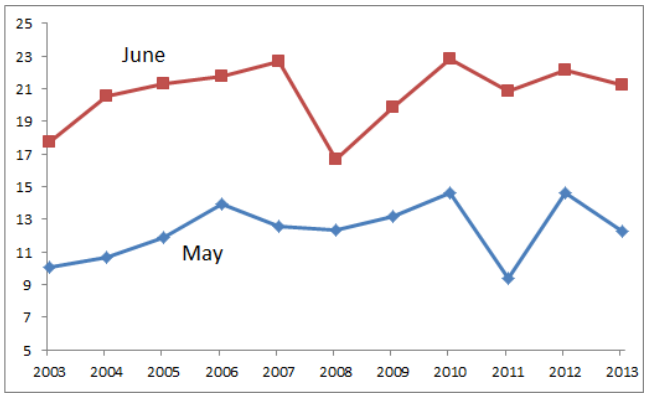

Figure B1-1: Average temperature for western Lake Erie basin for May and June.

Structure/state variables/relationship

The model for estimating load-response is a non-linear (exponential or semi-log) relationship between TP and CI. The TP input is total m.tons for March to July for all years, except 2003 and 2008, when only March to June is used. The condition for switching is June average temperature < 18 C. July temperatures are similar between years.

The response curve was derived from linear regression of log(CI) vs TP. Thresholds classifying "mild" or "significant" blooms were derived by identifying a threshold separating years into those having blooms

of concern and those years having mild blooms. Blooms with CI<2 were considered mild or ignorable. Those with CI>2, such as 2003, have been reported as "significant". All mild blooms occurred for TP load of <1100 m.tons, and all significant blooms occurred with TP load >1200 m.tons, suggesting a TP threshold of about 1150 m.tons determines bloom severity.

2. Data used for model input and evaluation

CI is based on MERIS from Stumpf et al. 2012, with 2012-2013 added from MODIS (Wynne et al., 2013). The CI is determined in 10-day composites to remove interference and biasing from clouds and to provide the best estimate of biomass for each 10-day period. The annual CI used to define the bloom severity is the average of the three 10-day periods around the maximum severity of the bloom, so it is effectively a 30-day average. MERIS produces a more sensitive measure with less noise than MODIS. The nominal uncertainty in the CI for MERIS is about 10%, and about 25% for MODIS. A CI of 1 is equivalent to about 10^{20} cells. Conversion to biomass can vary. Obenour used a conversion of 4800 m.tons per CI, which we will use here.

3. Calibration and confirmation approach and results.

The response curve is based on the regression:

$\log(CI) = a_0 + a_1 * TP$

Where (slope), $a_1 = 6.744 \times 10^{-4}$, and (intercept) $a_0 = -0.42899$.

The R-square is 0.62, standard error of the slope is 1.673×10^{-4} (24% of the slope). Residual standard error of the estimates is 0.29 in log space which corresponds to an uncertainty factor of 1.95. Essentially, the modeled CI is correct within a factor of 2.

CI_adj is CI calculated from a reduction in TP along the response curve:

$CI\_adj = 10^{(-M*TP*a_1)}$

Where M is the proportional reduction in TP (e.g., 10% is M=0.1).

4. Application Results

<u>Load-Response curves and diagnosis</u>

Load response curves are shown in Figure B1-2 for 10-40% reductions. The results indicate that a 40% reduction will eliminate four of the six severe bloom years, and cause a substantial reduction in the 2011 bloom.

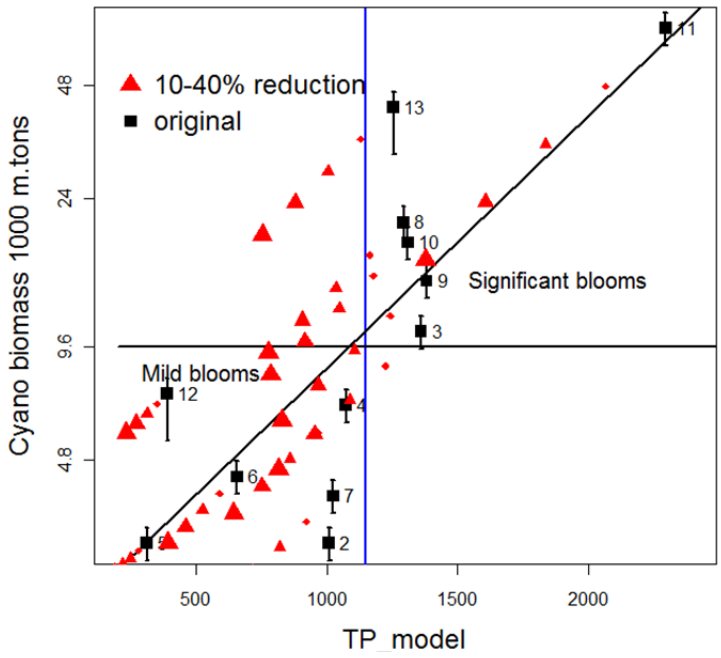

Figure B1-2: Load and response of CI-based biomass against TP load. Triangles increase in size for the amount of % reductions (10%, 20%, 30%, 40%). Potential error in the actual (original) CI is shown as vertical line. Response curve is shown as black line. Blooms with CI> 2 were perceived as significant, <2 were not. Vertical TP line shows the TP threshold between the two, significant and mild.

Uncertainty/Sensitivity assessment

"Leave-one-out" regression was conducted to determine how sensitive the model slope is to any individual year. Excluding any one year, except 2012 resulting in a range of values of a_1 (the slope) of 6.449×10^{-4} to 6.969×10^{-4} (vs the response value of 6.744×10^{-4}), a variation in the response slope of < ±5%. 2012 skewed the relationship, excluding 2012 resulted in an increase in slope to 7.849×10^{-4}. If the response curve without 2012 were used, a greater reduction in CI would be expected for the same TP. We prefer the conservative solution here.

The largest uncertainty is the variation between the significant bloom years. This probably results from variations in other influencing factors. Hydrodynamic factors that reinforce the TP model will influence the apparent uncertainty in the large bloom years (Stumpf et al., 2012). The balance of dissolved phosphorus to total phosphorus may also influence the relationship.

The statistical uncertainty (standard error) in the slope is shown in the analysis for selected years in Figure B1-3.

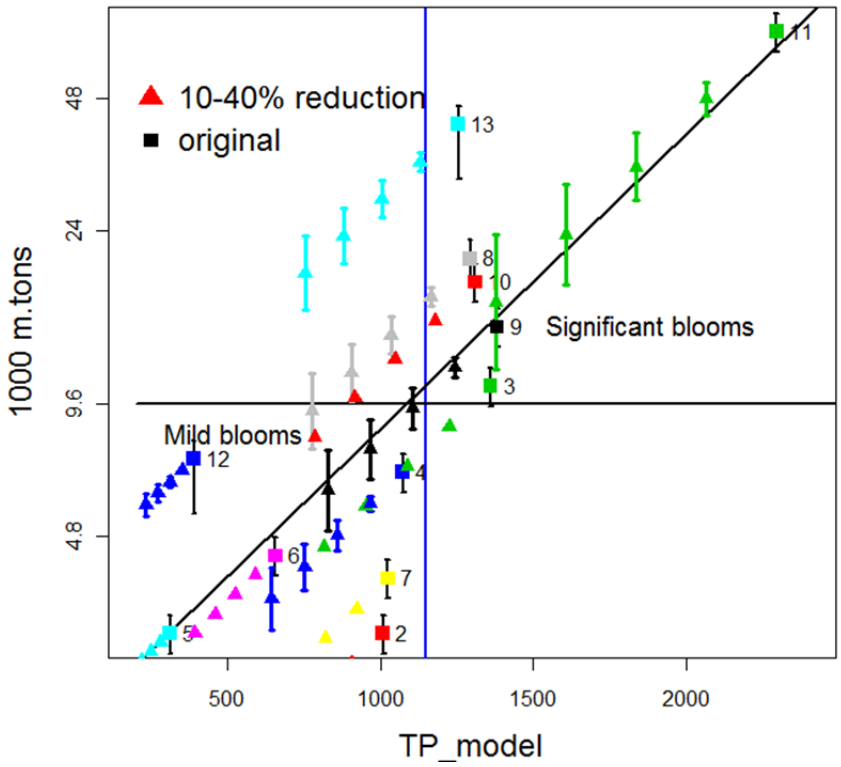

Figure B1-3: Figure B1-2 repeated with estimated response curve uncertainty included on each of the 4 reduction scenarios. Not shown for all years in order to help readability of the graph. Each year is marked with a different color.

5. Conclusions/recommendations

A 40% load reduction will reduce the bloom biomass by more than ½. For most bloom years, this would result in a mild bloom. When river discharge is extremely high, such as 2011, a significant bloom would remain, although smaller than what occurred in 2011.

6. References

Dolan, D. M., & Richards, R. P. (2008). Analysis of late 90s phosphorus loading pulse to Lake Erie. *Checking the Pulse of Lake Erie. Ecovision World Monograph Series, Aquatic Ecosystem Health and Management Society*, 79-96.

Stumpf, R. P., Wynne, T. T., Baker, D. B., & Fahnenstiel, G. L. (2012). Interannual variability of cyanobacterial blooms in Lake Erie. *PloS one*, *7*(8), e42444.

Wynne, T. T., Stumpf, R. P., & Briggs, T. O. (2013). Comparing MODIS and MERIS spectral shapes for cyanobacterial bloom detection. International Journal of Remote Sensing, 34(19), 6668-6678.

APPENDIX B-2: UM/GLERL Western Lake Erie HAB Forecasting Model

Daniel Obenour, North Carolina State University

1. Model Description

Overview

The UM/GLERL Western Lake Erie HAB forecasting model is a probabilistic model developed by Obenour et al. (2014) to predict peak summer HAB size in Western Lake Erie as a function of spring total phosphorus (TP) loading from the Maumee River. The model also includes a temporal term that captures changes in the lake`s susceptibility to HAB formation over time. Within the Annex 4 modeling effort, the original model version has been updated to utilize the (estimated) bioavailable fraction of the Maumee TP load as the HAB predictor. An additional set of remote sensing bloom observations was also added to the calibration dataset.

Structure/forcing functions/state variables/key relationship/conceptual model

The deterministic form of the bloom forecasting model is as follows:

$$\hat{z}_i = \begin{cases} \beta_b + \beta_0 + \beta_w W_i + \beta_t T_i & \text{for} \beta_0 + \beta_w W_i + \beta_t T_i > 0 \\ \beta_b & \text{for} \beta_0 + \beta_w W_i + \beta_t T_i < 0 \end{cases} \quad (1)$$

where β_b, β_0, β_w, and β_t are model parameters that predict bloom size, $\hat{z}_i$, in year *i*, in terms of the bioavailable fraction of the spring TP load, W_i, and model year, T_i. The parameter β_b is a background bloom level representing the bloom size in years of minimal phosphorus loading. The parameter β_0 is an intercept term, and β_t represents how that intercept changes over time. Parameters β_b and β_0 have units of 1000 MT bloom (dry weight) and β_t has units of (1000 MT bloom)/year. The parameter β_w represents the unit increase in bloom size per unit increase in P load (1000 MT/mo). The 'time step' of the model is yearly.

Predicted values are related to bloom observations, $z_{i,j}$, through the following two probabilistic expressions:

$$z_{i,j} \sim Gamma[(\hat{z}_i + \gamma_i)^2/\sigma_\epsilon^2,\ (\hat{z}_i + \gamma_i)/\sigma_\epsilon^2] \quad (2)$$

$$\gamma_i \sim Gamma\left(\hat{z}_i{}^2/\sigma_\gamma^2, \hat{z}_i/\sigma_\gamma^2\right) - \hat{z}_i \quad (3)$$

The gamma distributions have shape (g_α) and rate (g_β) parameters (i.e., *Gamma*(g_α, g_β)) such that the mean and variance are g_α/g_β and $g_\alpha/g_\beta{}^2$, respectively. Model prediction errors (γ_i) are drawn from a gamma distribution with variance σ_γ^2, and observation measurement errors are drawn from a gamma distribution with variance σ_ϵ^2. Here, subscript *j* differentiates between multiple observations of the same bloom, i.e., observations from remote sensing (Stumpf et al., 2012 and SeaWiFS satellite imagery, see below) and from in-lake sampling (Bridgeman et al., 2013). For brevity, we refer to these different

sets of observations as the “Stumpf observations”, the “SeaWiFS observations”, and the “Bridgeman observations”.

For each year, spring P load is determined as a weighted average of January to June (m = 1 to 6) monthly loads, based on the following equations:

$$W_i = \frac{1}{\sum \psi_m} \sum_{m=1}^{6} w_{i,m} \psi_m \quad (4)$$

$$\psi_m = \begin{cases} 0 & \text{for } m \leq (\beta_\psi - 1) \\ m + 1 - \beta_\psi & \text{for} (\beta_\psi - 1) < m < \beta_\psi \\ 1 & \text{for } m \geq \beta_\psi \end{cases} \quad (5)$$

where β_ψ is a weighting parameter.

The bioavailable fraction of the TP load was estimated as the sum of the bioavailable fractions of Dissolved Reactive Phosphorus (DRP) and Particulate Phosphorus (PP) loads:

$$\text{Bioavailable P} = \eta * \text{DRP} + \theta * \text{PP}$$

The PP load was approximated as the difference between the TP and DRP loads (Baker et al., 2014). Based on a review of the literature on the bioavailability of different P forms in the Maumee River, DRP is expected to be 100% readily available to algae (η =1; Lambert, 2012), while only a fraction θ of the PP load is expected to be available to algae (DePinto et al., 1981; Lambert, 2012). The parameter θ was estimated probabilistically, together with other model parameters, through Bayesian inference (see “Calibration and confirmation approach and results”).

2. Data used for model input and evaluation (calibration, confirmation)

Phosphorus loads (TP and DRP) are generated from Maumee River nutrient concentration data collected by Heidelberg University’s National Center for Water Quality Research (NCWQR, http://www.heidelberg.edu/academiclife/distinctive/ncwqr/data), and stream flow data collected by the United States Geological Survey (USGS, http://www.usgs.gov/water) at Waterville, Ohio (USGS Station 04193500). Currently, we use nutrient and flow data from 1998-present, and the time interval is daily (or less).

Three sets of bloom observations are used in this study. The first set is developed from MERIS satellite remote sensing imagery, per a procedure developed by NOAA (Wynne et al., 2010; Stumpf et al., 2012). The second set of observations is developed from a University of Toledo field monitoring program (Bridgeman et al., 2013). The third set is developed from SeaWiFS satellite remote sensing imagery by MTRI under contract to the Water Center, using procedures similar to Shuchman et al. (2006). Together, these sources cover the period of 1998-present.

3. Calibration and confirmation approach and results

The model was jointly calibrated to the three sets of bloom observations by means of a Bayesian hierarchical approach, using R and WinBUGs software. Detailed information on the Markov Chain Monte Carlo algorithm settings used can be found in Obenour et al. (2014). Non-informative uniform distributions were used for most parameters. Vague normal prior distributions were used for the parameters β_0 and θ. In order to develop a loosely informative prior for the parameter θ, we considered the bioavailable PP fractions reported in P speciation analyses and algal bioavailability assays conducted in the Maumee River (DePinto et al., 1981; Young et al., 1985; Lambert, 2012; Baker et al., 2014). In setting the prior, we also took into account the evidence that mussels significantly enhance the rate at which PP is recycled into the water column as DRP in Western Lake Erie, thereby decreasing P turnover times and further increasing PP bioavailability to algae (Mellina et al., 1995; Arnott & Vanni, 1996; Conroy et al., 2005; Johengen et al., 2014). As a result, we used a vague normal prior N(0.3,0.7) that is constrained to be between 0.2 and 1, as at least 20% of the PP discharged from tributaries is expected to be readily bioavailable (Baker et al., 2014), and more PP may become bioavailable throughout the summer.

The posterior probability distributions of model parameters resulting from the calibration process are shown in Figure B2-1, together with the corresponding priors. The replacement of TP with the bioavailable fraction of TP as the bloom predictor, and the expansion of the calibration dataset through the inclusion of the SeaWIFS bloom observations did not substantially change the posterior distributions reported for the original model version (Obenour et al., 2014). The updated model estimate for θ suggests that over 40% of the Maumee PP loading is (or becomes) bioavailable, though the uncertainty surrounding this estimate is large (Figure B2-1).

Observed and predicted bloom sizes are compared in Figure B2-2 (left panel). The model explains over 91% of the variability in bloom observations. To assess the model`s predictive performance when predicting data not included in the calibration process, a leave-one-year-out cross-validation was carried out. Briefly, observations from each year were removed from the dataset, in turn, with the model being re-calibrated to the remaining data and then used to forecast the excluded observations. Results of cross-validation are illustrated in Figure B2-2 (right panel).

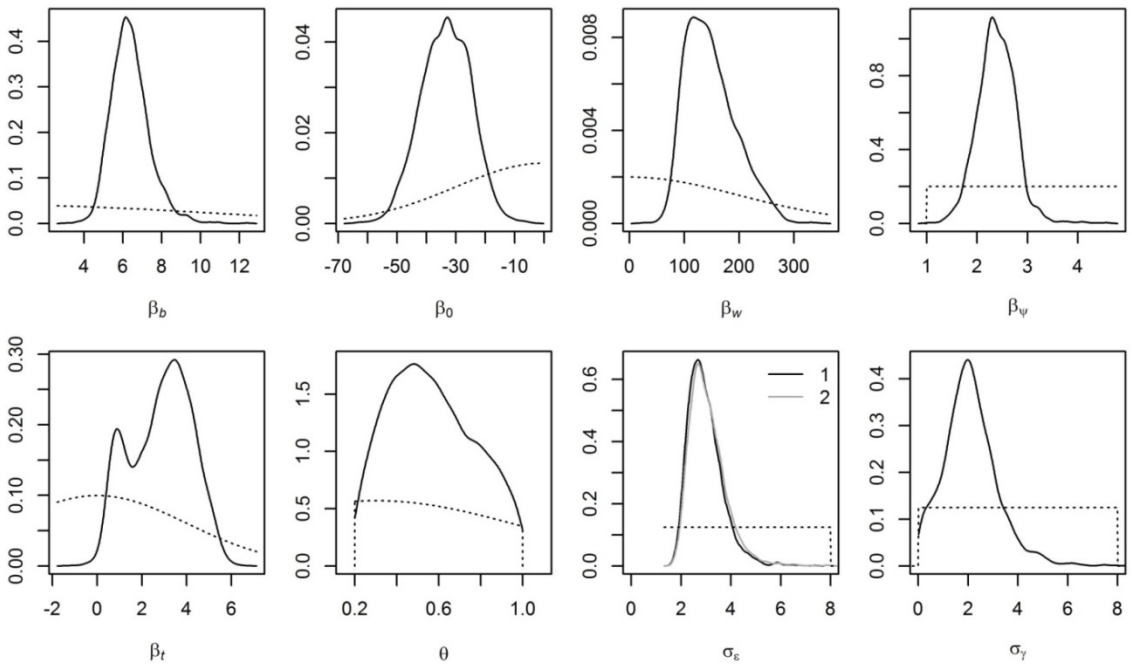

Figure B2-1: Prior (dashed) and marginal posterior (solid) model parameter distributions. The two distributions for σ_ϵ represent the measurement error for (1) Stumpf and Bridgeman observations and (2) SeaWiFS observations.

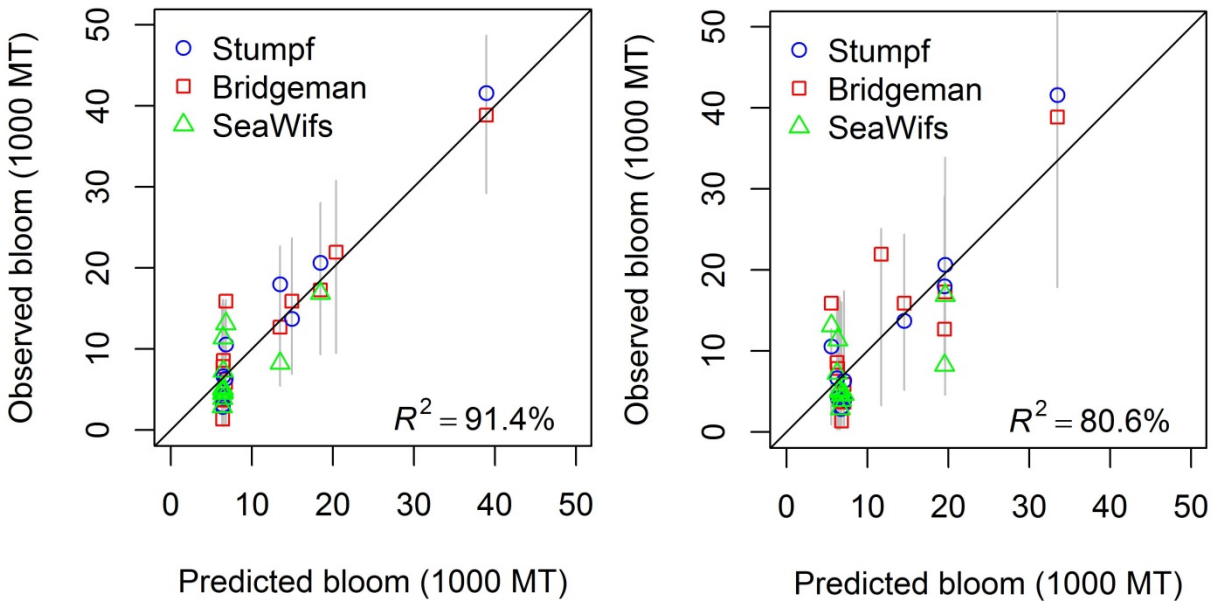

Figure B2-2: Observed versus predicted bloom with 95% predictive intervals. Left panel: full model performance; right panel: cross-validation model performance (the less-certain SeaWiFS observations are not included in R^2 determination).

4. Application Results

Load-Response Curves

The updated UM/GLERL HAB forecasting model was used to generate loading response curves showing the expected range of bloom sizes corresponding to different P load reduction scenarios.

The following scenarios were implemented:

1. We varied TP load (PP and DRP) between 20 and 612 MT/mo, roughly corresponding to 5% - 150% of the TP load value (396 MT/mo) measured in 2008 (Figure B2-3 and Table B2-1).
2. We varied the PP load between 16 and 494 MT/mo, roughly corresponding to 5% - 150% of the PP value (313 MT/mo) estimated in 2008, while holding the DRP load constant at 2008 levels (Figure B2-4 and Table B2-2).
3. We varied the DRP load between 4 and 118 MT/mo, roughly corresponding to 5% - 150% of the DRP value (83 MT/mo) measured in 2008, while holding PP constant at 2008 levels (Figure B2-5 and Table B2-3).

Because the model includes a temporal trend component, reflecting the system's apparent increasing susceptibility to large algal blooms, we develop response curves for both 2008 (year used as baseline scenario in other models) and 2013 (approximately current) lake conditions.

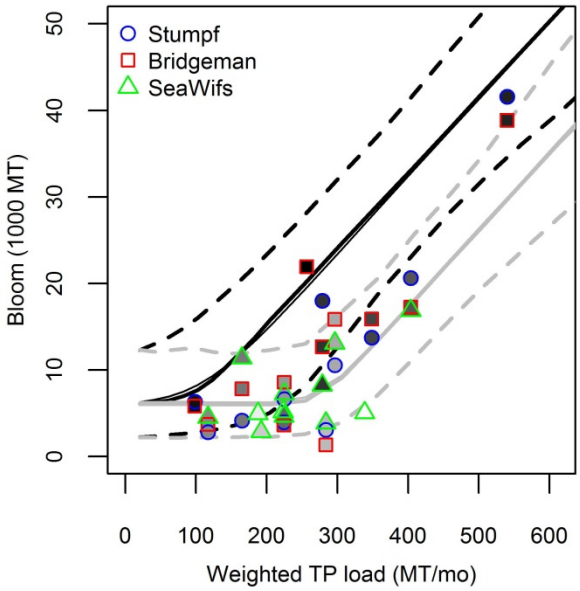

Figure B2-3: Relationship between bloom size and weighted TP load, with median prediction (thick lines), mean prediction (thin lines), and 95% predictive intervals (dashed). Grey lines: 2008 lake conditions, black lines: 2013 lake conditions. The corresponding bioavailable P loads estimated by the model and used to generate the response curves are reported in Table B2-1. Bloom observations are shaded on a linear gradient from white (1998) to black (2013).

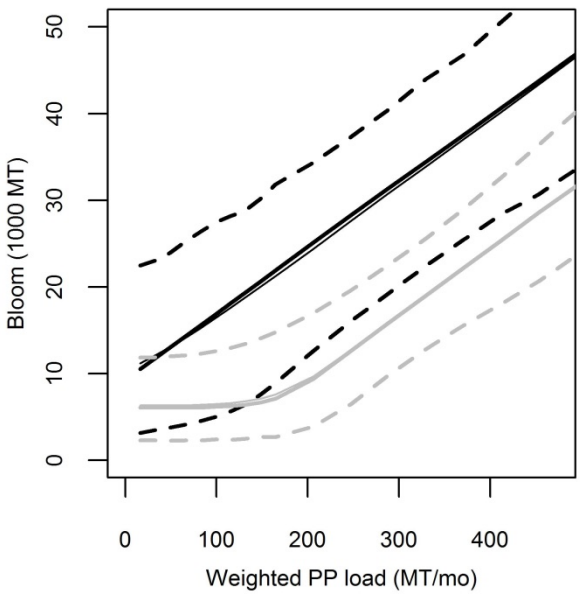

Figure B2-4: Relationship between bloom size and weighted PP load, with median prediction (thick lines), mean prediction (thin lines), and 95% predictive intervals (dashed). Grey lines: 2008 lake conditions, black lines: 2013 lake conditions. The corresponding bioavailable P loads are reported in Table B2-2. Weighted DRP load is held to the 2008 value (83 MT/mo).

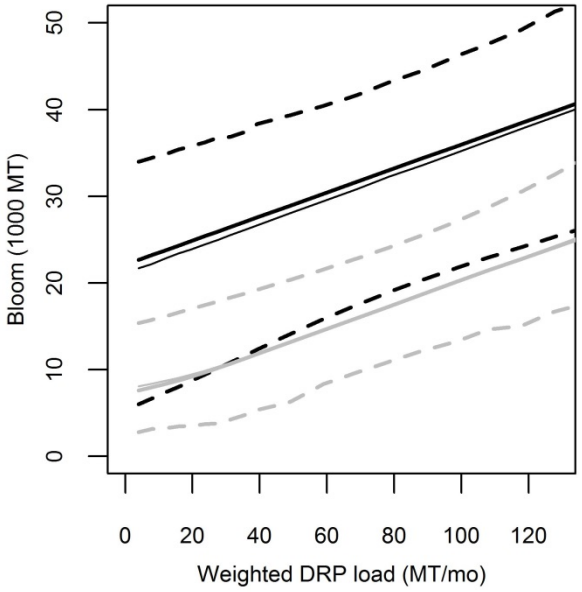

Figure B2-5: Relationship between bloom size and weighted DRP load, with median prediction (thick lines), mean prediction (thin lines), and 95% predictive intervals (dashed). Grey lines: 2008 lake conditions, black lines: 2013 lake conditions. The corresponding bioavailable P loads are reported in Table B2-3. Weighted PP load is held to the 2008 value (313 MT/mo).

Table B2-1: TP loads and corresponding bioavailable P loads, along with mean and median predicted bloom size, and 95% predictive intervals under 2008 and 2013 lake conditions.

TP load (MT/mo)	Bioavail. P load (MT/mo)	2013 Median predictions (1000 MT)	2013 Mean predictions (1000 MT)	2013 95% Pred. Interval (1000 MT)	2008 Median predictions (1000 MT)	2008 Mean predictions (1000 MT)	2008 95% Pred. Interval (1000 MT)
20	13	6.1	6.4	2.2 – 12.3	6.0	6.3	2.2 – 12.4
41	27	6.3	6.6	2.4 – 13.1	6.1	6.3	2.3 – 12.0
61	40	6.5	6.9	2.4 – 13.7	6.0	6.4	2.1 – 12.3
82	54	7.0	7.5	2.7 – 14.8	6.1	6.3	2.2 – 12.4
102	67	7.7	8.3	2.8 – 15.9	6.1	6.4	2.3 – 12.6
122	81	8.8	9.3	3.2 – 17.6	6.0	6.3	2.2 – 12.1
143	94	10.4	10.5	3.2 – 18.9	6.0	6.3	2.2 – 11.9
163	108	12.1	11.9	3.9 – 20.4	6.0	6.3	2.4 – 11.9
184	121	13.8	13.3	4.4 – 21.9	6.0	6.3	2.2 – 12.2
204	135	15.7	15.1	5.0 – 23.7	6.0	6.3	2.3 – 12.4
255	168	20.1	19.3	8.1 – 28.0	6.5	6.8	2.7 – 13.0
306	202	24.6	23.9	13.3 – 32.6	9.1	9.4	3.8 – 16.7
357	236	29.0	28.5	18.8 – 37.0	13.4	13.6	7.1 – 20.5
408	269	33.4	33.1	23.4 – 41.9	17.9	18.2	11.5 – 25.7
459	303	37.9	37.6	28.3 – 46.9	22.5	22.7	15.7 – 30.2
510	337	42.4	42.1	32.2 – 51.7	27.0	27.3	20.0 – 35.2
561	370	46.9	46.7	36.2 – 57.0	31.6	31.8	23.7 – 40.8
612	404	51.3	51.2	39.5 – 62.1	36.1	36.4	27.6 – 46.5

Table B2-2: PP loads and corresponding bioavailable P loads (holding DRP at 2008 value), along with mean and median predicted bloom size, and 95% predictive intervals under 2008 and 2013 lake conditions.

PP load (MT/mo)	Bioavail. P load (MT/mo)	2013 Median predictions (1000 MT)	2013 Mean predictions (1000 MT)	2013 95% Pred. Interval (1000 MT)	2008 Median predictions (1000 MT)	2008 Mean predictions (1000 MT)	2008 95% Pred. Interval (1000 MT)
16	95	10.6	11.2	3.2 – 22.5	6.1	6.4	2.3 – 12.0
33	105	11.8	12.1	3.5 – 23.0	6.1	6.4	2.3 – 12.1
49	114	13.0	13.1	3.8 – 24.0	6.1	6.3	2.3 – 11.7
66	124	14.4	14.1	4.1 – 25.2	6.1	6.4	2.3 – 12.5
82	133	15.5	15.2	4.6 – 26.4	6.1	6.4	2.3 – 12.1
99	143	16.8	16.4	5.0 – 27.5	6.2	6.5	2.4 – 12.5
115	153	18.1	17.6	5.7 – 28.2	6.3	6.6	2.4 – 12.9
132	162	19.4	18.8	6.3 – 28.8	6.4	6.8	2.5 – 13.6
148	172	20.6	20.1	7.6 – 30.2	6.6	7.1	2.7 – 13.8
165	181	21.9	21.3	8.9 – 31.8	7.1	7.6	2.7 – 14.9
206	205	25.1	24.3	12.7 – 34.3	9.4	9.6	3.9 – 16.8
247	229	28.3	27.6	16.0 – 37.3	12.6	12.8	6.4 – 19.8
288	253	31.5	30.7	19.2 – 40.4	15.8	15.9	9.8 – 22.6
329	276	34.4	33.9	22.5 – 44.0	19.0	19.1	12.8 – 25.5
370	300	37.4	37.0	25.4 – 46.8	22.2	22.2	15.6 – 28.9
411	324	40.6	40.1	28.5 – 50.5	25.3	25.4	18.0 – 32.7
453	348	43.7	43.3	30.6 – 54.3	28.6	28.6	20.6 – 36.3
494	372	47.0	46.6	33.6 – 58.1	31.6	31.7	23.6 – 40.2

Table B2-3: DRP loads and corresponding bioavailable P loads (holding PP at 2008 values), along with mean and median predicted bloom size, and 95% predictive intervals under 2008 and 2013 lake conditions.

DRP load (MT/mo)	Bioavail. P load (MT/mo)	2013 Median predictions (1000 MT)	2013 Mean predictions (1000 MT)	2013 95% Pred. Interval (1000 MT)	2008 Median predictions (1000 MT)	2008 Mean predictions (1000 MT)	2008 95% Pred. Interval (1000 MT)
4	190	22.6	21.7	6.2 – 34.0	7.7	8.1	2.8 – 15.6
8	194	23.1	22.2	6.5 – 34.4	8.0	8.4	3.2 – 15.7
12	198	23.9	22.8	7.5 – 34.9	8.3	8.7	3.2 – 15.9
16	202	24.2	23.4	8.1 – 35.4	8.8	9.1	3.5 – 16.8
20	206	24.8	23.9	8.4 – 35.8	9.2	9.5	3.5 – 16.8
24	209	25.5	24.4	9.3 – 36.2	9.7	9.9	3.7 – 17.1
28	213	26.0	24.9	9.9 – 36.8	10.2	10.3	3.8 – 18.0
31	217	26.5	25.5	10.9 – 36.9	10.8	10.8	4.3 – 18.5
35	221	27.0	26.1	11.7 – 37.4	11.2	11.3	4.7 – 18.9
39	225	27.6	26.7	12.6 – 38.4	11.9	12.0	5.3 – 19.5
49	235	28.8	28.1	13.9 – 39.4	13.2	13.2	6.3 – 20.0
59	245	30.3	29.4	16.0 – 40.4	14.5	14.7	8.3 – 21.5
69	255	31.8	30.8	17.5 – 41.7	16.0	16.0	9.7 – 23.1
79	265	33.1	32.3	18.8 – 43.2	17.3	17.3	10.9 – 24.0
89	274	34.3	33.6	20.6 – 44.5	18.7	18.7	12.2 – 25.3
98	284	35.7	35.0	21.7 – 6.1	20.1	20.1	13.2 – 27.3
108	294	37.1	36.4	22.9 – 47.6	21.5	21.6	14.6 – 28.7
118	304	38.6	37.8	24.0 – 49.2	22.8	22.9	15.1 – 30.5

Diagnosis/Interpretation

Under approximately current (2013) conditions, the model predicts a bloom size of 15700 MT (95% predictive interval: 5000-23700) associated with a spring weighted TP load of 204 MT/mo, which approximately corresponds to 50% of the weighted TP load observed in 2008 (Figure B2-3 and Table B2-1). If only the PP fraction of the TP load is reduced, while holding DRP constant, the model estimates that a 60% decrease in the 2008 weighted spring PP load would be necessary to achieve a comparable bloom size (Figure B2-4 and Table B2-2). Finally, under the hypothetical scenario of a decrease in DRP load only, the model predicts that even if highly unrealistic low levels of 4 MT/mo were reached, bloom size would still be as high as 21700 MT (95% predictive interval: 6200-34000, Figure B2-5 and Table B2-3).

Uncertainty/Sensitivity Assessment

The adopted hierarchical approach allowed us to characterize both model prediction error and observation measurement error, in addition to parameter uncertainty (Obenour et al., 2014). However, only model prediction error is of interest when using the model to develop loading response curves that can inform load reduction management plans. Hence, the 95% predictive intervals associated with the curves reported in Figures B2-3 through B2-5 quantify model parameter and predictive uncertainty. The width of the predictive intervals indicates that the uncertainty associated with model predictions needs to be taken into careful consideration when setting loading targets based on these loading response curves. It should be emphasized that the uncertainty in predicting a long-term mean (not shown) would be less than the uncertainty for predictive individual years.

5. Conclusions/Recommendations

Our model confirms the crucial role played by spring phosphorus loading from the Maumee River in triggering HABs in Western Lake Erie. As such, policies aimed at minimizing HAB size should primarily focus on reducing phosphorus loads in the Maumee watershed. Also, our analysis of the impact of different bioavailable fractions of the TP load suggests that particulate P may represent a substantial component of the phosphorus pool that becomes available to algae over the course of the summer. Reductions in DRP loads alone are predicted to be insufficient to reduce HAB size to desired levels. As pointed out in more detail in the next section, further research and modeling efforts are needed to assess potential interactions between anthropogenic nutrient loading and other environmental stressors, primarily climate change and invasive species, in promoting HAB development in Western Lake Erie.

6. References

Arnott, D. L., & Vanni, M. J. (1996). Nitrogen and phosphorus recycling by the zebra mussel (*Dreissena polymorpha*) in the western basin of Lake Erie. *Canadian Journal of Fisheries and Aquatic Sciences*, 53, 646–659.

Baker, D. B., Confesor, R., Ewing, D. E., Johnson, L. T., Kramer, J. W., & Merryfield, B. J. (2014). Phosphorus loading to Lake Erie from the Maumee, Sandusky and Cuyahoga rivers: the importance of bioavailability. *Journal of Great Lakes Research*. doi: 10.1016/j.jglr.2014.05.001

Bridgeman, T. B., Chaffin, J. D., & Filbrun, J. E. (2013). A novel method for tracking western Lake Erie *Microcystis* blooms, 2002–2011. *Journal of Great Lakes Research*, 39(1), 83-89.

Conroy, J. D., Edwards, W. J., Pontius, R. A., Kane, D. D., Zhang, H., Shea, J. F., Richey, J. N., & Culver, D. A. (2005). Soluble nitrogen and phosphorus excretion of exotic freshwater mussels (*Dreissena* spp.): potential impacts for nutrient remineralisation in western Lake Erie. *Freshwater Biology*, 50(7), 1146–1162.

DePinto, J. V., Young, T. C., & Martin, S. C. (1981). Algal-available phosphorus in suspended sediments from lower Great Lakes tributaries. *Journal of Great Lakes Research,* 7(3), 311-325.

Johengen, T. H., Vanderploeg, H. A., & Liebig, J. R. (2014). Effects of algal composition, seston stoichiometry, and feeding rate on zebra mussel (*Dreissena polymorpha*) nutrient excretion in two Laurentian Great Lakes. In T. F. Nalepa & D. W. Schloesser (Eds.), *Quagga and Zebra Mussels - Biology, Impacts, and Control* (2nd ed., pp. 445–459). Boca Raton, FL: CRC Press, Taylor & Francis Group.

Lambert, R.S. (2012). Great Lakes tributary phosphorus bioavailability. Master`s Thesis. Michigan Technological University.

Mellina, E., Rasmussen, J. B., & Mills, E. L. (1995). Impact of zebra mussel (*Dreissena polymorpha*) on phosphorus cycling and chlorophyll in lakes. *Canadian Journal of Fisheries and Aquatic Sciences*, 52, 2553–2573.

Michalak, A. M., Anderson, E. J., Beletsky, D. et al. (2013). Record-setting algal bloom in Lake Erie caused by agricultural and meteorological trends consistent with expected future conditions. *Proceedings of the National Academy of Sciences of the United States of America*, 110, 6448–6452.

Obenour, D. R., Gronewold, A. D., Stow, C. A., & Scavia, D. (2014). Using a Bayesian hierarchical mode to improve Lake Erie cyanobacteria bloom forecasts.*Water Resources Research*. DOI: 10.1002/2014WR015616

Paerl, H. W., & Huisman, J. (2009). Climate change: a catalyst for global expansion of harmful cyanobacterial blooms. *Environmental Microbiology Reports*, 1, 27–37.

Shuchman, R., Korosov, A., Hatt, C., Pozdnyakov, D., Means, J., & Meadows, G. (2006). Verification and application of a bio-optical algorithm for Lake Michigan using SeaWiFS: a 7-year inter-annual analysis. *Journal of Great Lakes Research*, *32*(2), 258-279.

Stumpf, R. P., Wynne, T. T., Baker, D. B., & Fahnenstiel, G. L. (2012). Interannual variability of cyanobacterial blooms in Lake Erie. *PLOS ONE*, 7, e42444.

Vanderploeg, H. A., Liebig, J. R., Carmichael, W. W., Agy, M. A., Johengen, T. H., Fahnenstiel, G. L., & Nalepa, T. F. (2001). Zebra mussel (*Dreissena polymorpha*) selective filtration promoted toxic *Microcystis* blooms in Saginaw Bay (Lake Huron) and Lake Erie. *Canadian Journal of Fisheries and Aquatic Sciences*, 58(6), 1208-1221.

Wynne, T. T., Stumpf, R. P., Tomlinson, M. C., & Dyble, J. (2010). Characterizing a cyanobacterial bloom in western Lake Erie using satellite imagery and meteorological data. *Limnology and Oceanography*, 55(5), 2025-2036.

Young, T. C., DePinto, J. V., Martin, S. C., & Bonner, J. S. (1985). Algal-available particulate phosphorus in the Great Lakes basin. *Journal of Great Lakes Research*, 11(4), 434-446.

APPENDIX B-3: Total Phosphorus Mass-Balance Model

Steve Chapra, Civil and Environmental Engineering Department, Tufts University, Medford, MA 02155
Dave Dolan Natural and Applied Sciences, University of Wisconsin-Green Bay, Green Bay, WI 54311
Alice Dove, Water Quality Monitoring and Surveillance, Environment Canada, Burlington, ON L7R 4A6

1. Model description

Thirty-five years ago, a parsimonious total phosphorus (TP) budget model was developed to assess the impact of population and land-use trends on Great Lakes eutrophication (Chapra 1977, Chapra and Robertson, 1977, Chapra and Sonzogni, 1979). The framework was then used, along with several other models, to establish phosphorus loading targets for the 1978 Great Lakes Water Quality Agreement (International Joint Commission 1978; Bierman, 1980). The IJC TP loading and concentration targets are listed in Table B3-1.

Table B3-1. Total phosphorus target loads and concentrations. Note that the target loads include phosphorus inputs from upstream lakes.

Basin	Target TP Load (MTA)	Target TP Concentration ($\mu g P L^{-1}$)
Lake Erie	11,000	
Western Erie		15
Central Erie		10
Eastern Erie		10
Lake Ontario	7,000	10

A positive initial confirmation of the model's predictive ability was made for Lake Ontario in the early 1980s when reductions in detergent and wastewater phosphorus had induced a significant downward trend in that lake's TP concentration (Chapra, 1980). Additional confirmation of model performance was established for the entire system through 1987 (Lesht et al., 1991). We recently expanded the time frame of the previous modeling considerably by extending the analysis to 2010 (Chapra and Dolan, 2012). In so doing, a more complete and comprehensive assessment was provided of whether the model adequately simulated the water-quality improvements observed from the mid-1970's to the present.

A number of refinements were adopted to improve model performance. First, a more detailed segmentation scheme was employed with finer resolution for the embayments. A chloride budget model was developed to better parameterize transport with particular emphasis on quantifying the magnitude of mixing across open boundaries. Then, the TP budget model was used to compute concentration trends and compare them with modern TP data for the period from 1965 to the present. Up until about 1990, simulation results for all the lakes generally conformed to observations and indicated that these lakes have exhibited significant improvement on a whole-lake basis consistent with load reductions due primarily to the implementation of the Great Lakes Water Quality Agreement (GLWQA). After 1990, although the simulation results for Lake Superior continued to follow the data, the observations for the offshore waters of the other lakes indicated somewhat lower TP concentrations

than predicted by the model. The largest divergence took place in Lake Ontario with less dramatic divergences occurring in the offshore waters of lakes Michigan, Huron and Erie. In order to simulate these outcomes, the model's apparent settling velocity, which parameterizes the rate that total phosphorus is permanently lost to the lake's deep sediments, was increased after 1990. This result supported the hypothesis that Dreissenid mussels have enhanced the Great Lakes phosphorus assimilation capacity.

Overview

In the present report we use the same model developed by Chapra and Dolan (2012) to evaluate the impact of total phosphorus loadings on the eutrophication of the Lower Great Lakes. Although Lake Erie is our primary focus, we have included Lake Ontario in order to provide a more comprehensive assessment of the impacts of load reductions. In particular, we believe it is important to recognize that Lake Erie controls will have a measurable effect on Lake Ontario.

Structure/forcing functions/state variables/key relationship/conceptual model

The current section provides a mathematical description of the mass-balance model used for the current analysis. Before proceeding, it is important to stress that our model is primarily designed to predict the annual average concentrations of the offshore waters of the Lower Great Lakes as a function of external loadings. Whereas this approach is certainly consistent with the time and space scales employed for the establishment of target loads in the GLWQA, it is important to stress that our model does not attempt to resolve finer-scale temporal (e.g., diel or seasonal) or spatial (e.g., nearshore-offshore) variability.

As with the original model (Chapra, 1977), Lake Ontario is represented as a single well-mixed system, whereas Lake Erie is divided into its 3 major subsegments to better resolve horizontal gradients. TP mass balances for each basin can be written as (Chapra, 1975, 1977, 1997):

Western Lake Erie (*w*):

$$V_w \frac{dp_w}{dt} = W_w + Q_h p_h - Q_w p_w + E_{wc}'\left(p_c - p_w\right) - v_{s,w} A_w p_w \quad \textbf{(1)}$$

Central Lake Erie (*c*):

$$V_c \frac{dp_c}{dt} = W_c + Q_w p_w - Q_c p_c + E_{wc}'\left(p_w - p_c\right) + E_{ce}'\left(p_e - p_c\right) - v_{s,c} A_c p_c \quad \textbf{(2)}$$

Eastern Lake Erie (*e*):

$$V_e \frac{dp_e}{dt} = W_e + Q_c p_c - Q_e p_e + E_{ce}'\left(p_c - p_e\right) - v_{s,e} A_e p_e \quad \textbf{(3)}$$

Ontario (*o*):

$$V_o \frac{dp_o}{dt} = W_o + Q_e p_e - Q_o p_o - v_{s,o} A_o p_o \quad \textbf{(4)}$$

where V_i = volume of segment i (km^3), p_i = concentration of segment i ($\mu gP\ L^{-1}$), W_i = the mass loading rate to segment i (metric tonnes per annum or MTA), Q_i = outflow from segment i ($km^3\ yr^{-1}$), Q_i = advective outflow from segment i ($km^3\ yr^{-1}$), $E'_{i,j}$ = bulk horizontal eddy diffusion coefficient at interface between segments i and j ($km^3\ yr^{-1}$), $v_{s,i}$ = apparent settling velocity for TP for segment i ($km\ yr^{-1}$), A_s = the segment's bottom sediment surface area across which TP is permanently lost from the system (km^2). Note that by setting v_s to zero, Eqs. (1) through (4) apply to conservative substances such as chloride in which case loadings and concentrations are expressed in kMTA and $mg\ L^{-1}$, respectively.

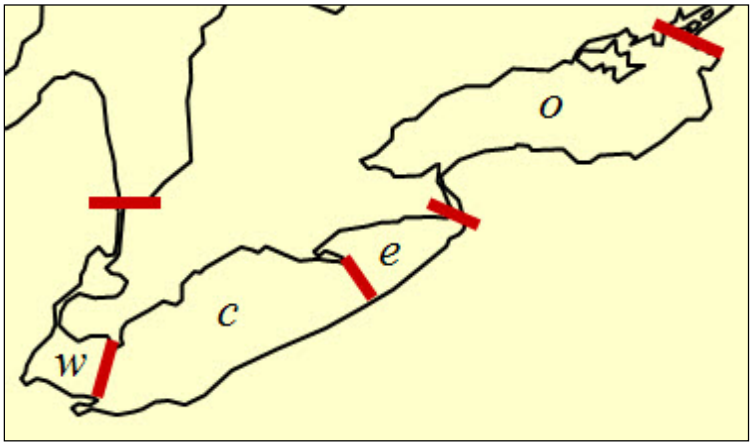

Figure B3-2: Segmentation scheme for chloride and total phosphorus models for the Lower Great Lakes.

The bulk mixing coefficient is a phenomenological parameter that represents the large-scale diffusive exchange across open boundaries. As described by Chapra (1979) this parameter accounts for all transport mechanisms over and about advective outflow. These include but not limited to exchange due to large-scale eddy diffusion, and dispersion due to shear flow and spatial non-uniformities. It is related to more fundamental quantities by (Chapra, 1979)

$$E' = \frac{EA_c}{\ell} \qquad \textbf{(5)}$$

where E = horizontal eddy diffusive mixing coefficient ($km^2\ yr^{-1}$), A_c = interface cross-sectional area (km^2), and ℓ = mixing length (km). The mixing length parameterizes the length of the zone defining the gradient between adjacent volumes (Chapra, 1997).

The complete system of differential equations provides a quantitative framework to analyze trends of chloride and TP. Given parameters, loading time series, and initial conditions, the equations can be integrated to obtain concentrations as a function of time. To do this, we use a constant-step, 4^{th}-order Runge-Kutta method (Chapra, 2011). Employing a 4th-order scheme tends to minimize the temporal component of numerical diffusion.

Model Parameters and Forcing Functions

This section provides a description of the model parameters and forcing functions.

Morphometry. Morphological parameters (volumes, areas and lengths) for the model segments and interfaces are listed in Tables B3-2 and B3-3. These are based on previously published estimates (e.g., Chapra and Sonzogni, 1979, Quinn, 1992).

Table B3-2. Segment parameters for the Lower Great Lakes. The volumes and sediment areas represent measured values whereas the TP settling velocity is based on calibration. The settling velocities in parentheses are used starting in 1990.

Segment	Symbol	Volume km^3	Sediment area km^2	Settling velocity $m\ yr^{-1}$
West Erie	WE	28	3680	30 (50)
Central Erie	CE	274	15390	22 (30)
East Erie	EE	166	6150	27 (32)
Ontario	ONT	1631	18960	19 (29)

Table B3-3. Interface parameters for the lower Great Lakes. The areas and lengths represent measured values whereas the diffusion coefficients are based on calibration.

Interface	Cross-sectional area km^2	Mixing length km	Diffusion $10^6\ cm^2\ s^{-1}$	Bulk diffusion $km^3\ yr^{-1}$
WE-CE	0.464	66.14	1	22.1
CE-EE	1.144	91.35	5	197.5

Intersegment flows. From 1860 through 2010, the annual outflows for connecting channels are based on measurements reported by the Army Corps of Engineers (Keith Kompoltowicz, personal communication) and NOAA's Great Lakes Environmental Research Laboratory (Croley and Hunter, 1994, GLERL 2010). Within-lake intersegment flows are derived from annual water balances consisting of measured tributary flows, changes in lake level, and estimates of net over-lake precipitation (precipitation minus evaporation). The flows prior to 1860 are set to constant values equal to the average flows for the pre-diversion period (1860-1899).

Loadings. Time series of annual chloride and TP loadings were determined for each model segment for the period from 1800 to early 2010 based on historical estimates (Chapra, 1977), reports to the International Joint Commission (IJC) by the Great Lakes Water Quality Board (as summarized for the State of the Lakes Ecosystem Conference, SOLEC, by Nielso et al., 1995), and recent direct measurements for the period from 1994 to 2008 (Dolan and Chapra, 2012).

Concentrations. The concentration data can be divided into two categories: historical (prior to the mid-1960s) and modern (after the mid-1960s). Historical chloride concentration data were taken from a number of sources as previously summarized by Chapra et al. (2009, 2012). Historical TP concentration data were taken from a number of published sources [Great Lakes Water Quality Board (1974, 1975,

1976, 1977a, 1977b, 1978a, 1978b, 1979, 1987)]. For the historical data, values either represented single samples (especially for the earliest chloride data) or annual averages.

Beginning in the late 1960s, much more systematic data collection efforts were instituted under the auspices of Environment Canada (EC). Because they involved more rigorous quality control, this "modern" data set exhibits considerably less uncertainty than the historical data. Hence, it provides a better basis for separating long-term, emerging trends from interannual natural variability.
EC conducts ship-based cruises to collect water-quality samples on the Lower Great Lakes. Briefly, EC conducts monitoring in each of the Lower Great Lakes. Each lake is generally monitored every second year, with multiple cruises conducted during that year. All regions (nearshore, offshore and major embayments) are monitored for the EC program. Methods for EC's Great Lakes Surveillance Program are described in Dove et al. (2009). The data collection and analysis methods used for chloride are also described in additional detail in Chapra et al. (2009, 2012).

For TP, the current investigators were provided with access to the individual measurements for the EC data. This was initially done as part of a sub-group charged with examination of the status of the goals of Annex 3 of the GLWQA (DePinto et al., 2007) but has continued so that we currently have access to the individual measurements from both datasets.

For the current analysis, we have employed these datasets to compute open-lake annual median values for both chloride and TP concentrations. We have used latitude and longitude data to compute annual medians for our model segments. Medians, rather than average values, are chosen because the former is less sensitive to outliers. Finally, we systematically excluded near-shore samples. This was done under the assumption that open-lake (offshore) waters best indicate long-term trends because they are less influenced by local pollutant discharges than shallower nearshore waters. It should also be mentioned that using offshore values is consistent with the current GLWQA. For example, the Agreement's TP concentration targets are for open-lake concentrations (Table B3-1).

2. Calibration and confirmation approach and results

Model Calibration

This section outlines how the model was calibrated including the final values of the key calibration parameters used for the subsequent simulations. These are the bulk mixing coefficient (chloride) and the apparent settling velocity (TP).

The model calibration consists of adjusting the free parameters - the bulk mixing coefficients and the apparent settling velocities - so that the final simulation results fit measured chloride and TP concentrations, respectively. Because the chloride simulations only depend on the former, the calibration is conducted in two steps. The diffusion coefficients can be estimated by first adjusting them to fit the chloride data. These values along with the other parameters and the measured TP loadings can then be employed to estimate the apparent settling velocities by adjusting them to fit the TP data. This sequential calibration strategy of calibrating the transport first and then the transformations second, is commonplace in water-quality modeling (Chapra, 2003) and for the present case has the advantage of parsimony in that each calibration step involves adjusting a single free parameter. Thus, because there is

only one degree of freedom, the model is actually being used to address the inverse problem. That is, the mass-balance provides a framework to directly estimate each of the unknown parameters by difference.

Diffusion calibration. Initial estimates of the intersegment eddy diffusion were based on previously published estimates (Ahrnsbrak and Ragotzgie, 1970; Richardson, 1974, 1976; Saylor and Sloss, 1976; Quinn, 1977; Chapra and Sonzogni, 1979). In addition, we also computed a first estimate for each boundary based on the Okubo (1971) diffusion diagram as computed with the following equation:

$$E_{j,k} = 6260\ell_{j,k}^{4/3} \quad \textbf{(6)}$$

where *j* and *k* designate the two segments straddling the open interface, $E_{j,k}$ = the horizontal eddy diffusion coefficient ($cm^2\ s^{-1}$), and $\ell =$ a characteristic length representing the approximate size of the eddies contributing to the turbulent mixing across the interface (km). For the present system, we assumed that the mixing length provide a reasonable estimate of the characteristic length for each interface.

Using these values as a starting point, the diffusion coefficient was then adjusted to minimize the sum of the squares of the residuals between the measured and simulated chloride concentrations for the period from 1994 through 2008. The final values are listed in Table B3-3.

Of course, more refined hydrodynamic models as well as much higher resolution spatial and temporal data would be required to definitively describe the complex mixing regimes for such systems. Nevertheless, because they are primarily dependent on the observed annual chloride concentrations, the values in Table B3-3 provide reasonable estimates of annual mixing for the present lumped, mean annual model.

Apparent settling velocity calibration. As stated previously, once the chloride balance has been used to estimate of mixing across the model's open boundaries, the remaining free parameter (i.e., not directly measured) needed to simulate total phosphorus is the apparent settling velocity. As was the case for diffusion, initial estimates for some segments can be based on previous studies (Chapra and Sonzogni, 1979, Lesht et al., 1991). These values, along with those for segments that had not been modeled previously, were then adjusted so that simulated TP concentrations were consistent with measured values.

In so doing, we again adopted a two-step approach. The model was first run for the period from 1800 to 2010 and the settling velocities set at constant values in order that the model yielded TP concentrations consistent with observations collected just before loading reductions were implemented in the early 1970s. This was done to be consistent with the approach employed during establishment of target loads for the GLWQA. In addition, it was considered valid because then the subsequent model test (i.e., whether the model would follow measurements after load reductions were implemented) would start with minimal error. As described previously, this approach resulted in a good fit (as measured by the

residual sum of the squares between the measurements and the simulated TP concentrations) for Lake Superior. However, for the main bodies of the other lakes, the modeled and measured concentrations began to diverge after about 1990 with the most glaring discrepancy in Lake Ontario. We, therefore, recalibrated the model by increasing the post-1990 apparent settling velocity in order to yield model output better matching current measured TP concentrations. It should be noted that we limited these increases to the main-lake, open-water segments (i.e., excluding the embayments) in an effort to be parsimonious, but also because of the higher likelihood that deep water sedimentation would not be heavily influenced by resuspension as might be the case in the shallower embayments.

The resulting calibrated values are listed in Table B3-2 with the post-1990 values in parentheses. Although these values are quite variable, their range is not atypical of literature estimates. Data analyses by a number of individuals (e.g., Chapra, 1975, Dillon and Rigler, 1975, Thomann and Mueller, 1987) have determined that the settling velocity can range over about an order of magnitude from about 3 to 30 m yr^{-1}. However, values have been reported from less than 1 to over 200 m yr^{-1}.

Results

The following summary of results focuses on total phosphorus concentrations for the main bodies of each of the Lower Great Lakes. Detailed results for the chloride simulations as well as for the major embayments are presented elsewhere (Schmitt Marquez, 2010; Dolan et al., 2011; Maccoux et al., 2012).

Total phosphorus concentration trends. Although the model simulations are generated for the entire post-settlement period (1800-2010), the results presented here are limited to 1950 to 2010. This was done in order to better visualize the behavior of the model output and data.

Fit statistics. In addition to the plots, we have also computed two fit statistics in order to quantify the residual error between the data points and the model simulations. These are an average percent relative error and a root mean error.

The average percent relative error is computed for each segment as

$$\text{Average Error} = \frac{\sum_{i=1}^{n}\left(\frac{\left|\hat{c}_i(t_i) - c(t_i)\right|}{\hat{c}_i(t_i)}\right)}{n} \times 100\% \qquad \textbf{(7)}$$

where t_i = the time corresponding to the i^{th} TP concentration measurement; $\hat{c}_i(t_i) =$ the i^{th} TP concentration measurement (μgP L^{-1}); $c(t_i) =$ the model calculated TP concentration at time t_i (μgP L^{-1}), and n = the number of measurements.

The standard error is computed for each segment as

$$\text{RME} = \sqrt{\frac{\sum_{i=1}^{n}\left(\hat{c}_i(t_i) - c(t_i)\right)^2}{n-1}} \qquad \textbf{(8)}$$

Note that this formulation assumes that one degree of freedom is lost due to the fact that each segment's fit is primarily dictated by a single estimated parameter, the apparent settling velocity. Of course, because the system is coupled, each segment's concentration is also dictated by other segment settling velocities as well as the model's other estimated parameter, the open-interface turbulent mixing coefficients. Nevertheless, we believe that Eq. (7) provides a reasonable estimate of the magnitude of the scatter around the best-fit line represented by the calibrated model.
As listed in Table B3-4, the results for most parts of the system indicate a good fit with root mean and percent relative errors on the order of 1 μgP L^{-1} and 20%, respectively. The highest errors occur for Green Bay, Saginaw Bay and Lake Erie. This is a reflection of the fact that these segments are most impacted by basin tributary loadings due to the size of the tributaries relative to their volumes.

Table B3-4. Fit statistics for the calibrated model as calculated with the final calibrated model (i.e., with higher post-1990 settling velocities). The average TP concentrations for 1970 and 2010 computed with the calibrated model are also included to provide a basis for assessing the RME.

			Average TP		Average
Segment	***n***	**RME**	**1970**	**2010**	**error**
West Erie	43	5.4	39.6	15.5	26%
Central Erie	47	3.7	20.8	7.9	26%
East Erie	48	3.6	19.6	7.2	29%
Ontario	53	1.5	21.5	6.2	13%

The trends and variability of the model simulations can also be directly assessed by examining the time series of the model output and data shown in Figures B3-2 and B3-3. In order to relate the TP levels in the plots to trophic state, the present analysis uses values of 10 and 20 μgP L^{-1} as bounds for mesotrophy, as originally suggested by Dillon (1975) and confirmed for the Great Lakes by Chapra and Dobson (1981). In addition, we have classified segments with TP < 5 μgP L^{-1} as being ultraoligotrophic (Homa and Chapra, 2011).

Lake Erie. After having experienced severe cultural eutrophication during the 1950s and 1960s, both the data and model simulations indicate that TP levels for all three basins of Lake Erie have dropped significantly over the following decades (Figure B3-2). Nevertheless, the target concentration levels are still exceeded for some years. This is partly due to the fact that although Lake Erie's TP loadings have been reduced, they still sometimes exceed the established annual target loads (Dolan and Chapra, 2012). Further, the exceedances are exacerbated by the fact that Lake Erie's response exhibits higher interannual variability than for the main bodies of Lake Ontario. As described elsewhere for chloride (Chapra et al., 2009), this variability is in large part due to Lake Erie's short residence time relative to the other Great Lakes.

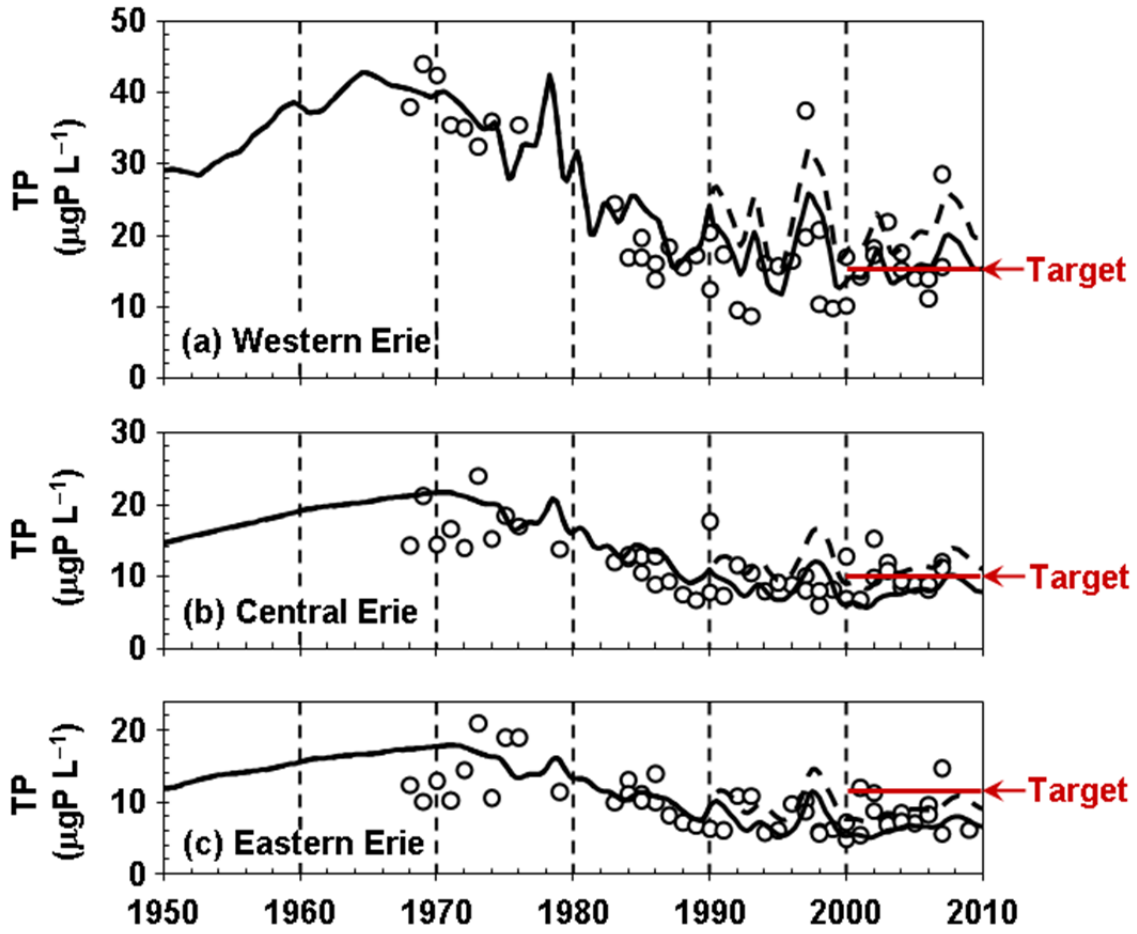

Figure B3-2: Simulation results for TP concentration (µgP L^{-1}) versus year for the three basins of Lake Erie. Model simulations are designated by lines and measured data by markers. Two model simulations are shown for each basin. The upper dashed line on each plot employs a constant apparent settling velocity whereas the lower solid line uses a higher apparent settling velocity after 1990. The IJC target concentrations are indicated at the right of each plot.

As noted previously, we have employed constant and increased post-1990 settling velocities for each of the basins. As depicted in Figure B3-2, the range of the two scenarios is comparable to the range of the observations with the heightened case doing a somewhat better job of representing the current 2010 levels.

Lake Ontario. Whereas the foregoing results suggest that Lake Erie may have experienced stronger post-1990 TP assimilation, the simulations for Lake Ontario are much more conclusive. As depicted in Figure B3-3, the observations indicate a much greater improvement for Lake Ontario than predicted by the model with a constant apparent settling velocity. Whereas the model predicts that the load reductions should bring the lake to oligo-mesotrophic levels, the data indicate that it is solidly oligotrophic with a minimum mean annual TP concentration of approximately 5.4 µgP L^{-1} in 2002. In order to simulate this outcome, a higher post-1990 apparent settling velocity must be employed. As listed in Table B3-2, a value of 29 m yr^{-1} after 1990 yields a model simulation that minimizes the sum of the squares of the residuals between the model output and measured values.

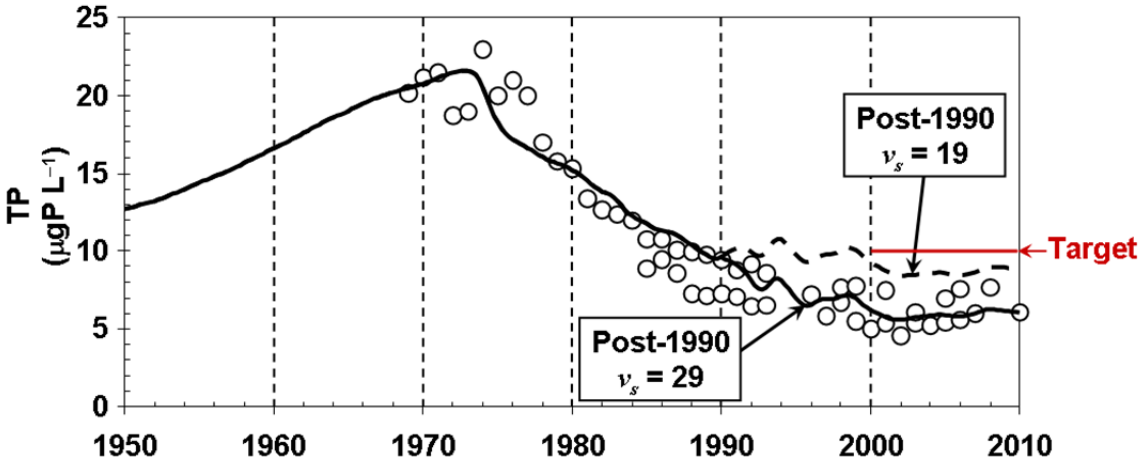

Figure B3-3: Simulation results along with data for TP concentration (µgP L^{-1}) versus year for Lake Ontario. Model simulations are designated by lines and measured data by markers. Two versions of the model are indicated. The upper dashed line employs a constant apparent settling velocity of 19 m yr^{-1} for the entire simulation. The lower solid line uses the same value until 1990 when the settling velocity is increased to 29 m yr^{-1}. The IJC target concentration is indicated at the right of the plot.

As a final note regarding in-lake trends for the lower Great Lakes, after reaching minimum levels in about 2000, there is a suggestion that TP levels may now be increasing, albeit at a slow rate. Although the interannual variability obscures any such trend in western Lake Erie, the recent data for central and eastern Lake Erie as well as for Lake Ontario hint at a possible increase. Because at best we are dealing with less than 10 data points, a statistically-significant trend cannot yet be substantiated. Nevertheless, the fact that such increases have been documented for conservative ions such as chloride and sodium (Chapra et al., 2009, Chapra et al., 2012) implies that such TP trends bear watching.

3. Application Results

Load-Response curves

The calibrated model was run at steady state using average flows and total phosphorus (TP) loadings (Dolan and Chapra, 2012) from water years 2001-2010. The following average values resulted:

Lake	Index	TP (µgP/L)	Chl *a* (µg/L)	SD (m)
Western Erie	**1**	**16.00**	**2.63**	**1.55**
Central Erie	**2**	**8.15**	**1.49**	**2.27**
Eastern Erie	**3**	**7.03**	**1.31**	**2.46**
Ontario	**4**	**6.37**	**1.21**	**2.60**

The model can then be used to compute the response of three water-quality indicators to levels of the total Lake Erie TP loading (Figure B3-4).

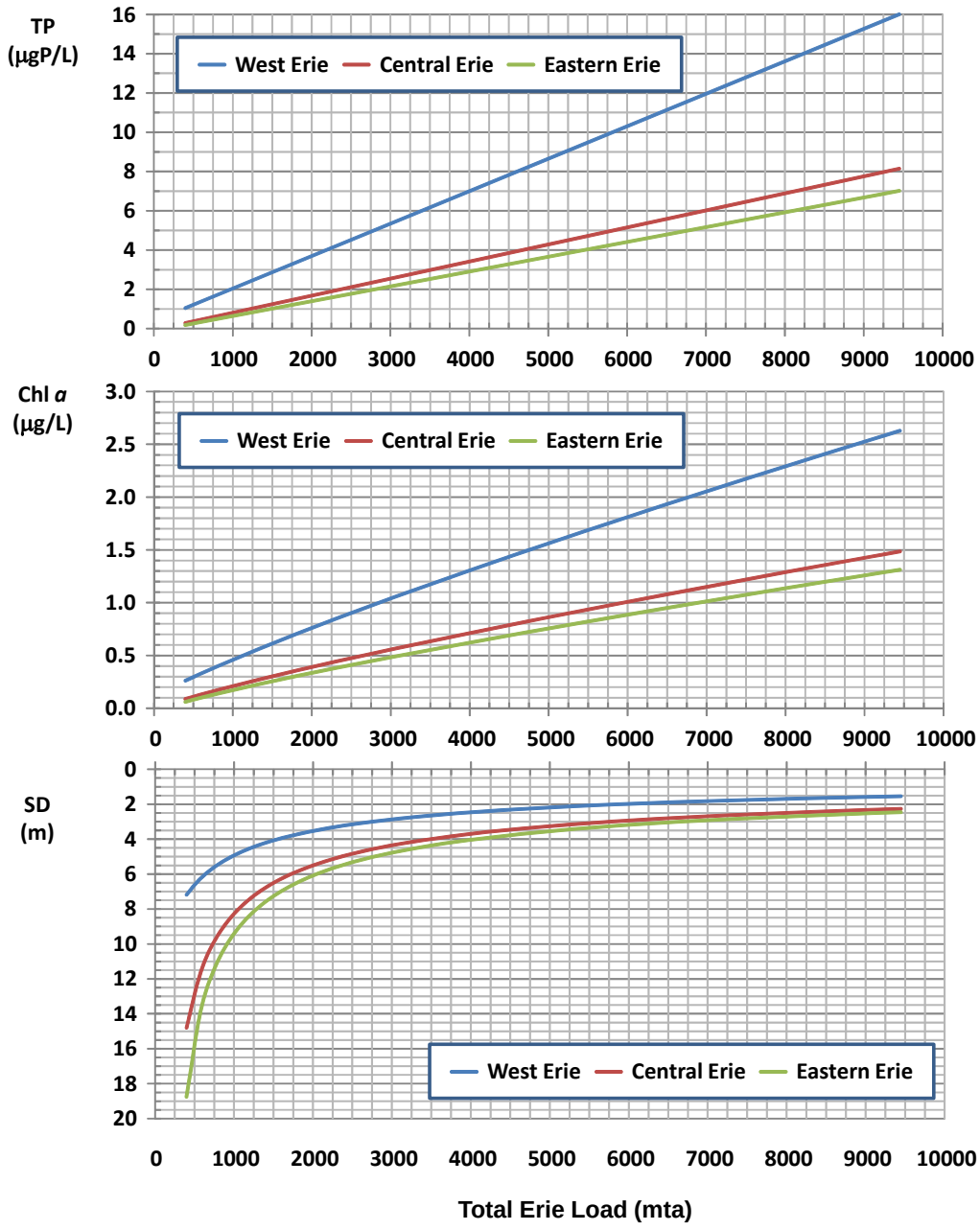

Figure B3-4: Loading response plots for TP concentration, summer chlorophyll *a* concentration, and summer Secchi depth for the three basins of Lake Erie plotted versus the total Lake Erie TP loadings.

Uncertainty/Sensitivity assessment

At this time, a full uncertainty/sensitivity assessment has yet to be conducted. It is hoped that this would be implemented in the future (see Sec. 6).

A simple sensitivity analysis is provided by computing the steady-state system response matrix for TP. As depicted in Figure B3-5, each element $a_{i,j}^{(-1)}$ gives the response of lake *i* to a unit load to lake *j* (μgP/L per 1,000 mta). Thus, because the model is linear, each element provides the sensitivity of each basin's concentration response to a 1,000 mta load change for each other basin. For example, the plot indicates that if the loading to the Western Basin were lowered by 1,000 mta, then the TP concentrations of Western Erie, Central Erie, Eastern Erie and Ontario would be lowered 2.62, 0.722, 0.474, and 0.117 μgP/L, respectively.

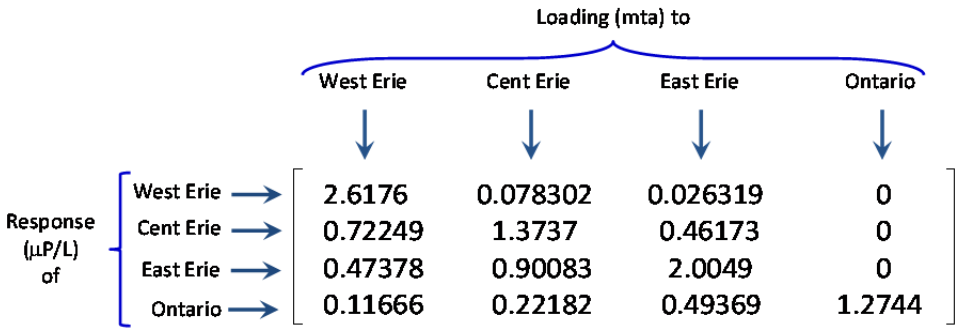

Figure B3-5: The TP system response matrix for the Lower Great Lakes.

Aside from such sensitivity calculations, the matrix can be employed to provide a detailed breakdown of how each lake's TP loads impact every other lake as displayed in the following table:

	From Huron	Western Erie	Central Erie	Eastern Erie	Total Erie	From Erie	Ontario Direct	Total Ontario
Loads (mta) →	**397.8**	**5633.3**	**2426.5**	**990.4**	**9448.0**	**1358.2**	**3641.3**	**4999.4**
Western Erie	**1.04**	**14.75**	**0.19**	**0.03**	**16.00**	**0.70**		
Central Erie	**0.29**	**4.07**	**3.33**	**0.46**	**8.15**	**0.54**		
Eastern Erie	**0.19**	**2.67**	**2.19**	**1.99**	**7.03**	**0.49**		
Ontario	**0.05**	**0.66**	**0.54**	**0.49**	**1.73**	**1.73**	**4.64**	**6.37**

4. Conclusions/recommendations

Although our model is parsimonious, it provides a long-term perspective that nicely complements the other models employed in this study. In addition, it provides a direct link to earlier attempts to set phosphorus loading for the Great Lakes system.

5. References

Barbiero, R.P., Rockwell, D.C., Warren, G.J., Tuchman, M.L. 2006. Changes in spring phytoplankton communities and nutrient dynamics in the eastern basin of Lake Erie since the invasion of *Dreissena* spp. *Can. J. Fish. Aquat. Sci*. 63(7):1549-1563.

Barbiero, R.P., Tuchman, M.L. 2004. Long-term Dreissenid impacts on water clarity in Lake Erie. *J. Great Lakes Res*. 30(4):557–565.

Beletsky, D., Saylor, J.H., and Schwab, D.J. 1999. Mean circulation in the Great Lakes. *J. Great Lakes Res*. 25(1):78–93.

Bierman, Jr., V.J., 1980. A comparison of models developed for phosphorus management in the Great Lakes. In: Loehr, C., Martin, C.S., Rast, W. (Eds.), *Phosphorus management strategies for lakes*. Ann Arbor Science Publishers, Ann Arbor, pp. 235–255.

Chapra, S.C. 1975. Comment on 'An empirical method of estimating the retention of phosphorus in lakes,' by W. B. Kirchner and P. J. Dillon. *Water Resources Res*. 11:1033.

Chapra, S.C. 1977. Total phosphorus model for the Great Lakes. *J. Environ. Engin. Div., ASCE*, 103:147-161.

Chapra, S.C. 1979. Applying phosphorus loading models to embayments. *Limnol. Oceanogr*., 24:163-168.

Chapra, S.C. 1980. Simulation of recent and projected total phosphorus trends in Lake Ontario, *J. Great Lakes Res*., 6:101-112, 1980.

Chapra, S.C. 1997. *Surface water-quality modeling*. McGraw-Hill, New York.

Chapra, S.C. 2003. Engineering water quality models and TMDLs. *J. Water Resour. Plann. Manage.*, 129(4):247-256.

Chapra, S.C. 2011. *Applied numerical methods with MATLAB for engineering and science, 3rd Ed*., WCB/McGraw-Hill, New York.

Chapra, S.C., Canale, R.P. 1991. Long-term phenomenological model of phosphorus and oxygen in stratified lakes, *Water Research*. 25(6):707–715.

Chapra, S.C., Dobson, H.F.H. 1981. Quantification of the Lake Trophic Typologies of Naumann (surface quality) and Thienemann (oxygen) with special reference to the Great Lakes, J. Great Lakes Res., 7(2):182-193.

Chapra, S.C., Dolan, D.M. 2012. Great Lakes total phosphorus revisited: 2. Mass balance modeling. J. Great Lakes Res. 38(4): 741–754.

Chapra, S.C., Dove, A., Rockwell, D. 2009. Great Lakes chloride trends: long-term mass balance and loading analysis. *J. Great Lakes Res*. 35(2):272-284.

Chapra, S.C., Dove, A., Warren, G.J. 2012. Long-term trends of Great Lakes major ion chemistry. *J. Great Lakes Res.* (in press).

Chapra, S.C., Robertson, A. 1977. Great Lakes eutrophication: The effect of point source control of total phosphorus. *Science*, 196:1448-1450.

Chapra, S.C., Sonzogni, W.C. 1979. Great Lakes total phosphorus budget for the mid-1970's, *J. Water Poll. Control Fed*., 51:2524-2533.

Croley II, T.E., Hunter, T.S., 1994. Great Lakes monthly hydrologic data, GLERL Technical Memorandum 83. Great Lakes Environmental Research Laboratory, NOAA, Ann Arbor, MI.

DePinto, J.V., Lam, D., Auer, M.T., Burns, N., Chapra, S.C., Charlton, M., Dolan, D.M., Kreis, R., Howell, T., Scavia, D. 2007. Examination of the status of the goals of Annex 3 of the Great Lakes Water Quality Agreement. Annex 3 Technical Sub-group of the RWG D. (http://www.epa.ohio.gov/portals/35/lakeerie/ptaskforce/Annex%203%20Technical%20Sub-group%20report-final%20_120706_.pdf)

Dillon, P.J., Rigler, F.H. 1975. A simple method for predicting the capacity of a lake for development based on lake trophic status. *J. Fish. Res. Board Can*. 31(9):1519-1531.

Dolan, D.M., Chapra, S.C. 2012. Great Lakes total phosphorus revisited: 1. Loadings. J. Great Lakes Res. 38(4): 730–740.

Dolan, D.M., Chapra, S.C.. Maccoux, M.J., Schmitt Marquez, H. 2011. Great Lakes total phosphorus models and loads: A fifteen year update. Final Report. EPA Grant No. GL 00E58501. EPA-GLNPO, Chicago, IL.

Dove, A. 2009. Long-term trends in major ions and nutrients in Lake Ontario. Aquatic Ecosystem Health & Management, 12(3):281–295.

Effler, S.W., Boone, S.R., Siegfried, C.A., Walrath, L., Ashby, S.L. 1997. Mobilization of ammonia and phosphorus by zebra mussels (*Dreissena polymorpha*) in the Seneca River, New York. Chapter 12 in " Zebra mussels and aquatic nuisance species" edited by D'Itri, F.M., CRC Press LLC, Boca Raton, FL, pp. 187-207.

Effler, S.W., Brooks, C.M., Whitehead, K., Wagner, B., Doerr, S.M., Perkins, M., Siegfried, C.A., Walrath, L., and Canale, R.P. 1996. Impact of zebra mussel invasion on river water quality. *Water Environ. Res*. 68:205–214.

Ghedotti, M.J., Smihula, J.C., Smith, G.R. 1995. Zebra mussel predation by round gobies in the laboratory. *J. Great Lakes Res.* 21(4):665–669.

GLERL. 2011. Great Lakes monthly hydrologic data. Great Lakes Environmental Research Laboratory, NOAA, Ann Arbor, MI. ftp://ftp.glerl.noaa.gov/publications/tech_reports/glerl-083/UpdatedFiles/, updated files accessed November 8, 2008.

Great Lakes Water Quality Board, 1974. Great Lakes Water Quality: 1973 Annual Report to the International Joint Commission. International Joint Commission, Great Lakes Regional Office. Windsor, Ontario.

Great Lakes Water Quality Board, 1975. Great Lakes Water Quality, Third Annual Report to the International Joint Commission. International Joint Commission, Great Lakes Regional Office. Windsor, Ontario.

Great Lakes Water Quality Board, 1976. Great Lakes Water Quality, Fourth Annual Report, Appendix B, Annual Report of the Surveillance Subcommittee. International Joint Commission, Great Lakes Regional Office. Windsor, Ontario.

Great Lakes Water Quality Board, 1978a. Great Lakes Water Quality, Sixth Annual Report, Appendix B, Annual Report of the Surveillance Subcommittee. International Joint Commission, Great Lakes Regional Office. Windsor, Ontario.

Great Lakes Water Quality Board, 1978b. Great Lakes Water Quality 1976, Sixth Annual Report, Appendix C, Remedial Programs Subcommittee Report. International Joint Commission, Great Lakes Regional Office. Windsor, Ontario.

Great Lakes Water Quality Board, 1979. Great Lakes Water Quality, Seventh Annual Report, Appendix B, Annual Report of the Surveillance Subcommittee. International Joint Commission, Great Lakes Regional Office. Windsor, Ontario.

Great Lakes Water Quality Board, 1987. Great Lakes Water Quality, Annual Report of the Surveillance Subcommittee. International Joint Commission, Great Lakes Regional Office. Windsor, Ontario.

Great Lakes Water Quality Board,1977a. Great Lakes Water Quality, Fifth Annual Report, Appendix B, Annual Report of the Surveillance Subcommittee. International Joint Commission, Great Lakes Regional Office. Windsor, Ontario.

Great Lakes Water Quality Board,1977b. Great Lakes Water Quality, Fifth Annual Report, Appendix C, Annual Report of the Remedial Programs Subcommittee. International Joint Commission, Great Lakes Regional Office. Windsor, Ontario.

Griffiths, R.W., Schloesser, D.W., Leach, J.H., Kovalak, W.P. 1991. Distribution and dispersal of the zebra mussel (Dreissena polymorpha) in the Great Lakes region. *Can. J. Fish. Aquat. Sci*. 48:1381–1388.

Hebert, P. D., B. W. Muncaster, G. L. Mackie. 1989. Ecological and genetic studies on *Dreissena polymorpha* (Pallas): a new mollusc in the Great Lakes. *Can. J. Fish. Aquat. Sci*. 46:1587-1591.

Hecky, R.E., Smith, R.E.H., Barton, D.R., Guildford, S.J., Taylor, W.D., Charlton, M.N., Howell, T., 2004. The nearshore phosphorus shunt: A consequence of ecosystem engineering by dreissenids in the Laurentian Great Lakes. *Can. J. Fish. Aquat. Sci*. 61, 1285–1293.

Homa, E.S., Chapra, S.C. 2011. Modeling the impacts of calcite precipitation on the epilimnion of an ultraoligotrophic, hard-water lake. *Ecol. Model*. 222(1):76–90.

International Joint Commission. 1978. Great Lakes Water Quality Agreement of 1978, with Annexes and Terms of Reference, Between the United States and Canada, Signed at Ottawa, November 22, 1978. International Joint Commission. Windsor, Ontario. (http://www.ijc.org/en/activities/consultations/glwqa/agreement.php).

Lesht, B.M., Fontaine III, T.D., Dolan, D.M. 1991. Great Lakes total phosphorus model: post audit and regionalized sensitivity analysis. *J. Great Lakes Res*. 17(1):3-17.

Mills, E.L., Dermott, R.,M., Roseman, E.F., Dustin, D., Mellina, E., Conn, D.B., Spidle, A.P., 1993. Colonization, ecology and population structure of the "quagga" mussel (Bivalvia: *Dreissenidae*) in the lower Great Lakes. *Can J. Fish. Aquat. Sci*. 50:2305–2314.

Murthy, C.R. 1976. Horizontal diffusion characteristics in Lake Ontario. *J. Physical Oceanography*, 6(1):76-84.

Neilson, M., L'Italien, S., Glumac, V., Williams, D., Bertram, P. 1995. Nutrients: Trends and System Response. State of the Lakes Ecosystem Conference (SOLEC) Background Paper. Environment Canada and U.S. Environmental Protection Agency.

Nicholls, K.H. 2001. CUSUM phytoplankton and chlorophyll functions illustrate the apparent onset of dreissenid mussel impacts in Lake Ontario. *J. Great Lakes Res*. 27(4):393–401.

Nicholls, K.H., Hopkins, G.J. 1993. Recent changes in Lake Erie (North Shore) phytoplankton: Cumulative impacts of phosphorus loading reductions and the zebra mussel introduction. *J. Great Lakes Res*. 19(4):637-647.

Okubo, A. 1971. Oceanic diffusion diagrams. *Deep-Sea Research*, 18:789-802.

Petrie, S.A., Knapton, R.W. 1999. Rapid increase and subsequent decline of zebra and quagga mussels in Long Point Bay, Lake Erie: Possible influence of waterfowl predation. *J. Great Lakes Res*. 25(4):772–782

Quinn, F.H. 1992. Hydraulic residence times for the Laurentian Great Lakes. *J. Great Lakes Res*. 18(1):22-28.

Rathke, D. E., McCrae, G. 1989. Appendix B, Volume III, Report of the Great Lakes Water Quality Board. International Joint Commission, Windsor, Ontario.

Ray, W.J., Corkum, L.D. 1997. Predation of zebra mussels by round gobies, *Neogobius melanostomus*. *Environ. Biol. Fish.* 50:267–273

Schmitt Marquez, H.S., 2010. Nutrient Loading in the Upper Great Lakes System: Chloride and Total Phosphorus Estimates in Lakes Superior, Michigan and Huron, 1994-2008. M.S. thesis University of Wisconsin-Green Bay, WI.

Thomann, R.V., Mueller, J.A. 1987. *Principles of surface water quality modeling and control*. Harper & Row. New York.

Vanderploeg, H.A., Liebig, J.R., Nalepa, T.F., Fahnenstiel, G.L., Pothoven, S.A., 2010. *Dreissena* and the disappearance of the spring phytoplankton bloom in Lake Michigan. *J. Great Lakes Res*. 36 (Suppl 3):50–59.

Waples, J.T., Klump, J.V. 2002. Biophysical effects of a decadal shift in summer wind direction over the Laurentian Great Lakes. *Geophysical Res. Letters*, 29(8): 10.1029/2001GL014564.

APPENDIX B-4: 1-Dimensional Central Basin Hypoxia Model

1. Model Description

Overview and Conceptual Model

The 1-Dimensional hypoxia model represents the offshore waters of the central basin (approximately 24 m depth) of Lake Erie, linking an external thermal model with a fairly simple eutrophication model. The thermal model provides temperature and vertical mixing profiles on an hourly basis (Rucinski et al., 2010) for 48 vertical layers (each 0.5m thick). The eutrophication portion of the linked model incorporates phosphorus and carbon loading from both the western and central basins of Lake Erie, internal phosphorus cycling, carbon cycling (in the form of algal biomass and detritus), algal growth and decay, zooplankton grazing, oxygen consumption and production processes, and sediment interactions (Figure B4-1).

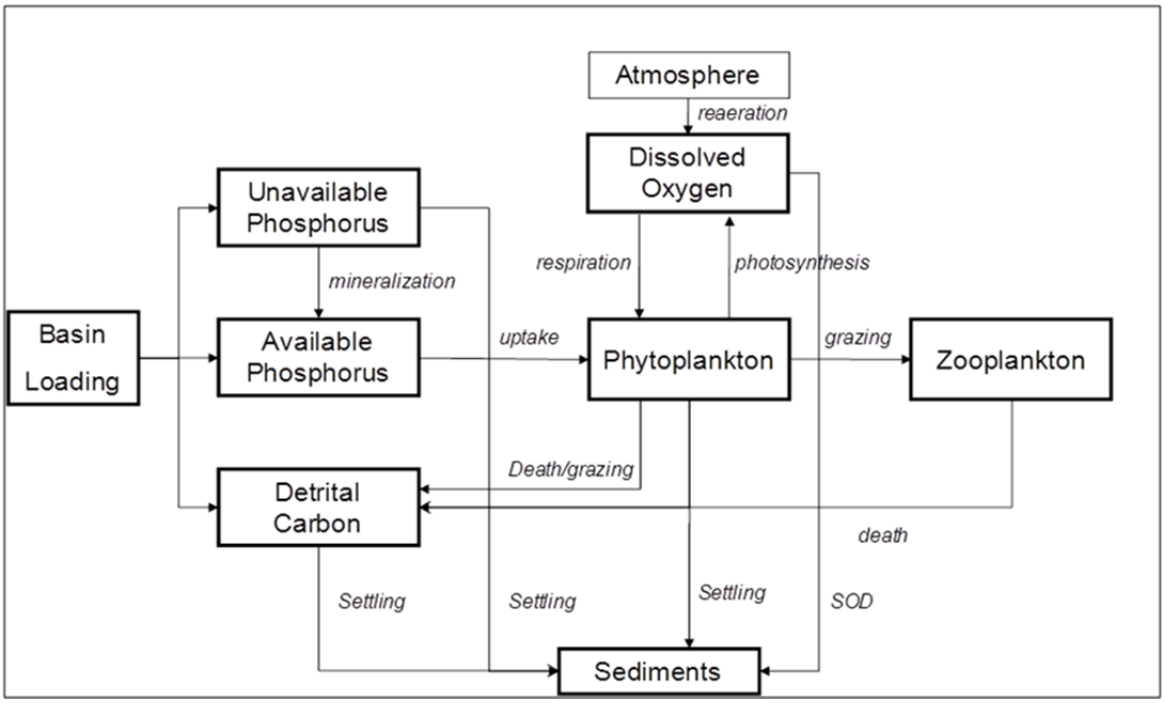

Figure B4-1: Conceptual diagram of eutrophication portion of the 1D Central Basin Hypoxia Model.

The model has been corroborated with in-lake data for dissolved oxygen (DO), total phosphorus (TP) and chlorophyll a (chl-a) (Rucinski et al., 2014). The model can produce a range of water quality responses for a given load to Lake Erie as a function of a range of observed or hypothesized physical forcing conditions that might affect the duration, magnitude and depth of stratification. As such, the model is applied to thermal profiles representing hydrometeorological conditions from 1987-2005. Response curves for several DO metrics (hypolimnion oxygen demand, hypoxia days, hypoxic area, bottom DO) vs annual TP and dissolved reactive phosphorus (DRP) loads were developed previously using the 1997 loading time-series (Rucinski et al., 2014). While no new calibration efforts are taken for the Annex 4 ensemble modeling effort (i.e., the model uses the existing published model parameterization), the application of the model updates and expands on the previous efforts, using the baseline common

loading year of 2008. Additionally, load-response curves for central basin chl-a are generated in this application.

Structure, Inputs, State Variables, Annex 4 Indicators modeled

Both the thermal and eutrophication models operate on the same spatial scale wit 48 half-meter thick layers, with an hourly temporal scale. The 1-D thermal model is based on the Princeton Ocean Model (Blumberg and Mellor, 1987) and was applied previously for Lake Michigan (Chen et al., 2002) and Lake Erie (Rucinski et al., 2010). It uses the Mellor-Yamada turbulence closure scheme to parameterize vertical mixing (Mellor and Yamada, 1982). The thermal model is driven by hourly meteorological observations from the Cleveland, Ohio airport with overland-overlake correction described in Beletsky and Schwab (2001).

Calibration and confirmation of the thermal model is fully described in Rucinski et al. (2010). Briefly, calibration was accomplished using temperature data from 1994, representative of central basin open water conditions, and confirmed with data collected in 2005. Maximum model error (represented as RMSE) varied with depth, and found to be 1.9 ^{o}C and 3.4 ^{o}C for 1994 and 2005, respectively. Both years exhibited maximum errors near thermocline depth. While some model errors can be attributed to either inaccuracies in forcing functions or model physics (e.g. vertical mixing parameterization), others can be attributed to 3D effects that are not represented in a 1D model, such as internal wave propagation, horizontal and vertical advection and diffusion. In particular, mid-lake thermocline conditions can be impacted by vertical velocities (upwelling or downwelling) generated by wind stress curl (Beletsky et. al., 2012). The thermal and eutrophication models are linked by first simulating the thermal structure of the model domain, and then passing the hourly outputs from the hydrodynamic model (i.e., temperature and vertical mixing coefficients) to the eutrophication model.

The eutrophication model incorporates external phosphorus and carbon loading; internal phosphorus and carbon cycling; algal growth, death, and sinking; zooplankton grazing, oxygen consumption and production; and sediment interactions (Figure B4-1). Stoichiometry among the state variables follows Redfield (1934). Algal growth rate is based on uptake of available (dissolved reactive) phosphorus following the Michaelis-Menten relationship, light limitation as a function of a constant extinction coefficient with self-shading from algal biomass, and water temperature. Algal photosynthesis and respiration are temperature-dependent 1st order rates, as are settling terms and mineralization of unavailable (organic) to available phosphorus. Sediment oxygen demand is a 0th order areal flux. The differential equations describing these processes (Table B4-1) are solved using an Euler integration scheme. There are dozens of input parameters required to be specified in these equations; a full list or which as well as literature ranges, are presented in the calibration/corroboration section (Table B4-2).

Model output is used to develop load-response curves for both hypoxia and chlorophyll-a metrics, as part of the Annex 4 ensemble modeling effort. Dissolved oxygen ($mg \cdot L^{-1}$) and chl-a concentrations ($mg \cdot L^{-1}$) are output as daily averages for each model layer. The daily averages are then aggregated in to various seasonal metrics (e.g., hypolimnion DO, summer average chl-a, etc) and related to the loading magnitude to develop the load-response curves.

Table B4-1. Eutrophication Model.

Phytoplankton

$$\frac{\partial Pc_n}{\partial t} = Pg_n - \mathrm{Pr}_n - Pvs_n + Pvs2_n + Diff_u + Diff_L - Out$$

Where: Pc_n = Phytoplankton carbon in model segment n
Pg_n = phytoplankton growth in model segment n
Pr_n = phytoplankton respiration in model segment n
Pvs_n = settling across the interface between segment n_{+1} and segment n
$Pvs2_n$ = settling across the interface between segment n_{-1} and segment n
$Diff_u$ = Turbulent dispersion across the interface between segment n_{-1} and segment n
$Diff_L$ = Turbulent dispersion across the interface between segment n_{+1} and segment n
Out = advection from model segment n to eastern basin

Available Phosphorus

$$\frac{\partial AP_n}{\partial t} = Wap_n - Pvs_n + Pvs2_n + Diff_u + Diff_L + AP_{rec,n} + MinP_n - Out$$

Where: UP_n = Available phosphorus in model segment n
Wap_n = Available phosphorus load in model segment n
$UP_{rec,n}$ = Recycled available phosphorus via zooplankton grazing and phytoplankton and zooplankton death in segment n
$MinP_n$ Mineralization of unavailable to available P in segment n

Unavailable Phosphorus

$$\frac{\partial UP_n}{\partial t} = Wup_n - Pvs_n + Pvs2_n + Diff_u + Diff_L + UP_{rec,n} - MinP_n - Out$$

Where: UP_n = Unavailable phosphorus in model segment n
Wup_n = Unavailable phosphorus load in model segment n
$UP_{rec,n}$ = Recycled unavailable phosphorus via zooplankton grazing and phytoplankton and zooplankton death in segment n
$MinP_n$ Mineralization of unavailable to available P in segment n

Zooplankton

$$\frac{\partial Zoo_n}{\partial t} = Zg_n - Zd_n - Zr_n - Out$$

Where: Zoo_n = Zooplankton carbon in model segment n
Zg_n = Zooplankton growth in model segment n
Zr_n = Zooplankton respiration in model segment n
Zd_n = Zooplankton death in model segment n

Organic Carbon

$$\frac{\partial OC_n}{\partial t} = Woc_n - Pvs_n + Pvs2_n + Diff_u + Diff_L - Oxid_n + \mathrm{Pr}_n + Zd_n + Zr_n - Out$$

Where: OC_n = Organic carbon in model segment n
Woc_n = Organic carbon load in model segment n
$Oxid_n$ = oxidation of organic carbon in segment n

Dissolved Oxygen

$$\frac{\partial DO_n}{\partial t} = \mathrm{Re}ar_n + Pg_n - \mathrm{Pr}_n + Diff_u + Diff_L - Oxid_n - SOD - Out$$

Where: DO_n = Dissolved oxygen in model segment n
$\mathrm{Re}ar$ = reparation at the surface
SOD = Sediment oxygen demand in the bottom layer

2. Model Input and Evaluation Data

Model Input Data

Model input data consist of initialization (i.e., initial conditions) data, western and central basin daily loading, and meteorological data.

Initialization data are required for each state variable at the beginning of each year's simulation (1987-2005); generally in early April when ice cover has diminished. These data, in the form of TP, DRP, total organic carbon (TOC), DO, chl-a, and zooplankton biomass, were obtained from several sources: EPA's online database (GLENDA), EPA's Great Lakes National Program Office (GLNPO), Environment Canada's Water Science & Technology Branch (ECWSTB), and the International Field Years on Lake Erie Program (IFYLE, 2006).

Long-term TP loads are from Dolan (1993) and Dolan and McGunagle (2005), and DRP loads (available P in the model) are from Richards (2006) and Richards and Baker (2002). It was required to manipulate some of the TP loading data, to convert it into daily basin total loads. The description of the required manipulation of the loading data is fully described in Rucinski et al. (2014). In summary, all loads to the western basin were routed to the central basin after accounting for a constant net apparent settling loss of 10 $m \cdot yr^{-1}$ based on an estimate of basin specific net apparent settling rates for phosphorus via a post-audit of The Great Lakes Total Phosphorus Model (Lesht et al., 1991). Dolan (1993) and Dolan and McGunagle (2005) provide western and central basin annual total loading values, while Richards (2006) and Richards and Baker (2002) provide daily loads of both TP and DRP for the 6 major tributaries in these two basins (Maumee, Raisin, Sandusky, Vermillion, Cuyahoga, and Grand). The annual loads from (1993) and Dolan and McGunagle (2005) were then decomposed to daily loads, using the ratio of annual loads from the 6 major tributaries to the annual loads from the basins. Note that the eastern basin loading is ignored in this analysis.

Atmospheric data needed to drive the thermal sub-model and components of the algal growth equations, were obtained from the NOAA National Climatic Data Center. These data include solar radiation, cloud cover, air temperature, wind speed and direction, air pressure and relative humidity.

Model Calibration/Confirmation Data

Model corroboration data were obtained from the same group of sources as the initialization data: EPA's online database (GLENDA), EPA's Great Lakes National Program Office (GLNPO), Environment Canada's Water Science & Technology Branch (ECWSTB), and the International Field Years on Lake Erie Program (IFYLE, 2006). In-lake data were averaged for central basin stations with an average depth of at least 20 m.

The base light extinction coefficient (0.3 m^{-1}) was estimated from extensive data on photosynthetic active radiation at varying depths in the central basin (GLNPO). Measured sediment oxygen demand (SOD) has not varied significantly over the analysis period, so for model testing an average value of 0.75 $gO2 \cdot m^{-2} \cdot d^{-1}$ (Matisoff and Neeson, 2005; Schloesser et al., 2005; Snodgrass, 1987; Snodgrass and Fay, 1987) was used, corrected for temperature deviations from 20 ^{o}C.

3. Calibration/Confirmation

Approach

Model performance was assessed by comparing output to state variable observations while ultimately applying the same parameter values to the entire 19 year data set (1987-2005). Model coefficients were determined via an iterative calibration/corroboration process, focusing on DO and chl-a observations, and to a lesser extent on DRP and zooplankton biomass because data for those constituents were less available. While particular emphasis was placed on calibrating to the 1994 and 2005 observations because those years had the most observations, additional modest adjustments were used in the corroboration with other years in the 1987-2005 dataset. While data were collected much less frequently in some years, the length of the record serves as an adequate corroboration dataset. For comparisons, both model output and observations were aggregated into mixed layer averages, representing the epilimnion, metalimnion, and hypolimnion based on the temperature profiles from the thermal model. The metalimnion was estimated as the zone where the temperature gradient was at least 2°C per meter. Because stratification in the thermal model varies, the depth of the bottom of the metalimnion (i.e., top of the hypolimnion) changes both seasonally and annually as a consequence of meteorological inputs. Table B4-2 lists the coefficient values, as well as calculated rates based on data (SOD, light extinction). Parameters in bold italics are ones that were adjusted.

Results

Results for DO (Figure B4-2), DRP (Figure B4-3), and chl-a (Figure B4-4) show best correspondence in years where the calibration was most focused (1994, 2005). The model-data comparison for DO agrees quite well in the full corroboration data set. The model captures the expected temporal trends in DO and chl-a (where data are available), however, chl-a data are only available during spring and fall cruises for the vast majority of years, and therefore the data fail to capture phytoplankton dynamics during the summer. The temporal trends in DRP are difficult to delineate because those data were only available for the late summer in most years. However, as expected the values reach very low concentrations coinciding with increased phytoplankton and zooplankton abundance. Comparison with vertically averaged zooplankton (Figure B4-5) was only possible for 2005, and the model estimates captured the temporal trend reasonably well during the stratified period. The vertical trends in DO are also captured well. The modeled yielded less than 17% relative error in summer dissolved oxygen concentration, and less than 25% relative error in chlorophyll-a concentration.

Table B4-2. 1D Model Parameter Set.

Variable Group	Parameter	Value	Units	Literature Range
Phosphorus	Phosphorus Half-Saturation	0.001	mg/L	0.001[a]
Phosphorus	Phosphorus:Carbon Ratio	0.01		0.01 - 0.05[a]
Phosphorus	***Mineralization Rate***	0.03	1/day	0.03[b]
Phosphorus	temperature coefficient	1.08		1.08[a,b]
Phosphorus	***Phosphorus settling rate***	0.06	m/d	
Light	Physical Light Extinction	0.3	1/m	
Light	Self Shading	0.3	(L/mgC)/m	0.2 - 0.7[a]
Light	Photo period	0.5	day	0.3 - 0.7[a]
Light	Saturating Light Intensity	350	ly/day	200 - 500[a]
Phyotplankton	***Max Growth Rate***	2.7	1/day	2.0 - 3.0[a]
Phyotplankton	temperature coefficient	1.08		1.06 - 1.08[a]
Phyotplankton	Optimal Growth Temp	22	C	
Phyotplankton	Respiration Rate	0.1	1/day	0.075-0.125[a]
Phyotplankton	temperature coefficient	1.08		1.05 - 1.08[a]
Phyotplankton	Settling Rate	0.05	m/day	0.01 - 0.1[a]
Phyotplankton	temperature coefficient	1.028		1.02 - 1.028[a]
Phyotplankton	Carbon:Chlorophyll ratio	40		20 - 50[a]
Zooplankton	***Grazing Rate***	2	(L/mgC)/day	
Zooplankton	Respiration Rate	0.03	1/day	
Zooplankton	temperature coefficient	1.04		
Zooplankton	Grazing efficiency	0.6		0.6[b]
Zooplankton	***Death rate***	0.05	1/day	
Zooplankton	temperature coefficient	1.08		1.08[b]
Oxygen	Surface Transfer Coeff.	0.2	m/d	
Oxygen	temperature coefficient	1.024		1.02 - 1.028[a]
Oxygen	Oxygen: Carbon Ratio	2.67		2.67[a,b]
Oxygen	Oxygen:Phosphorus Ratio	267		
Oxygen	SOD	0.75	g/m2/d	0.2 - 4.0[a]
Carbon	Oxygen Half Saturation	0.4	mgO2/L	0.5[a]
Carbon	***Oxidation Rate***	0.2	1/day	0.1[b]
Carbon	temperature coefficient	1.08		1.08[a]
Carbon	***Detritus settling rate***	0.05	m/d	

[a]Wool et al. 2002; [b]DiToro and Connely 1980

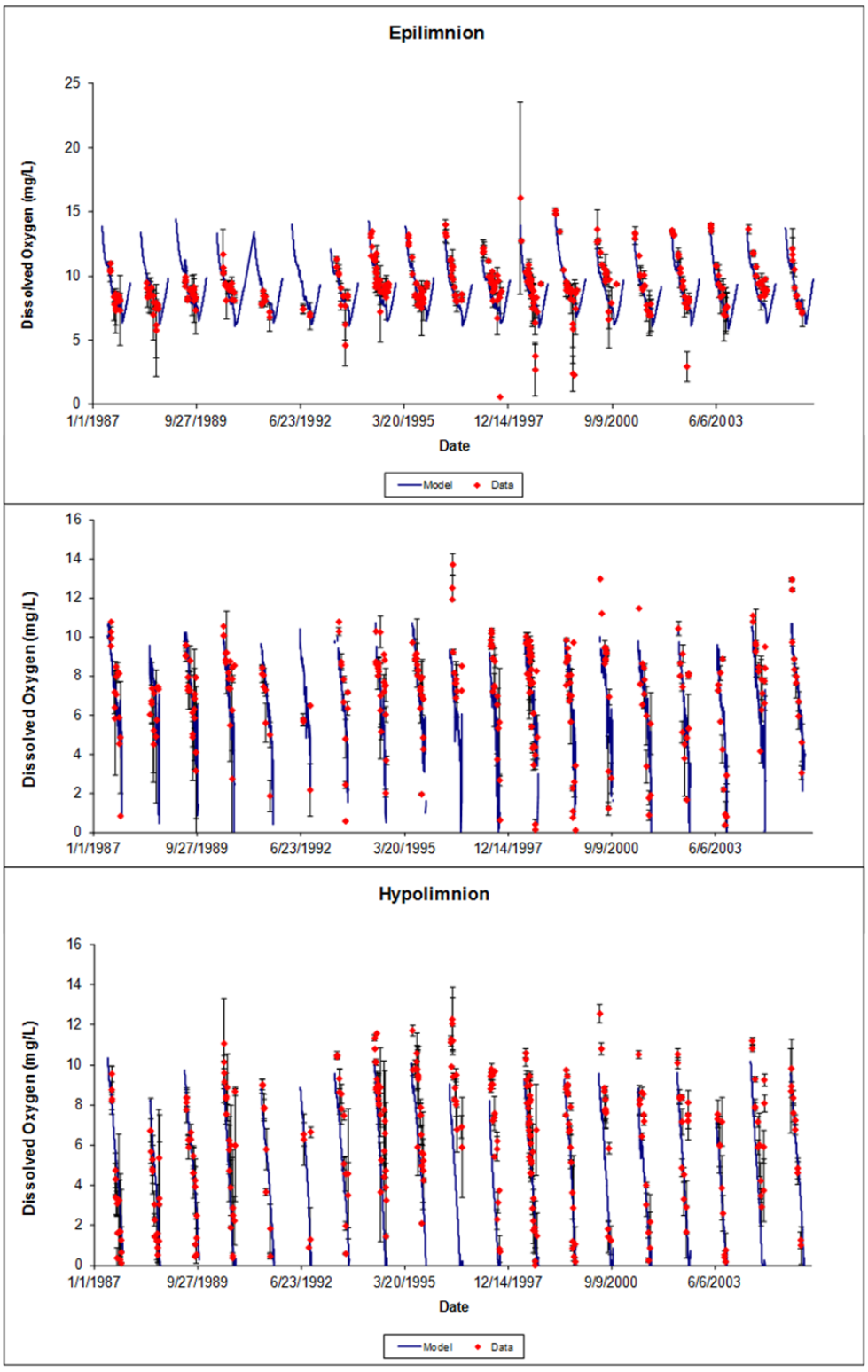

Figure B4-2: Comparison of model (line) and data (points) for mixed-layer averages of dissolved oxygen 1987-2005.

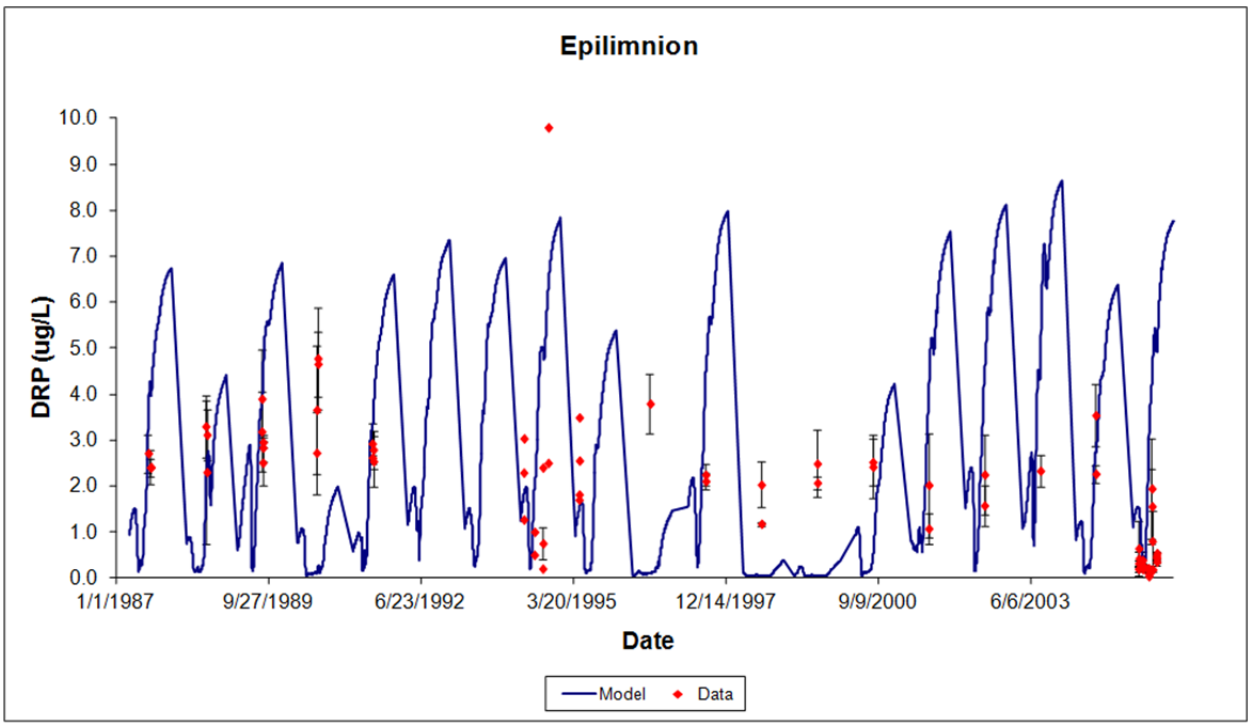

Figure B4-3: Comparison of model (line) and data (points) for epilimnion mixed-layer average of dissolved reactive phosphorus 1987-2005.

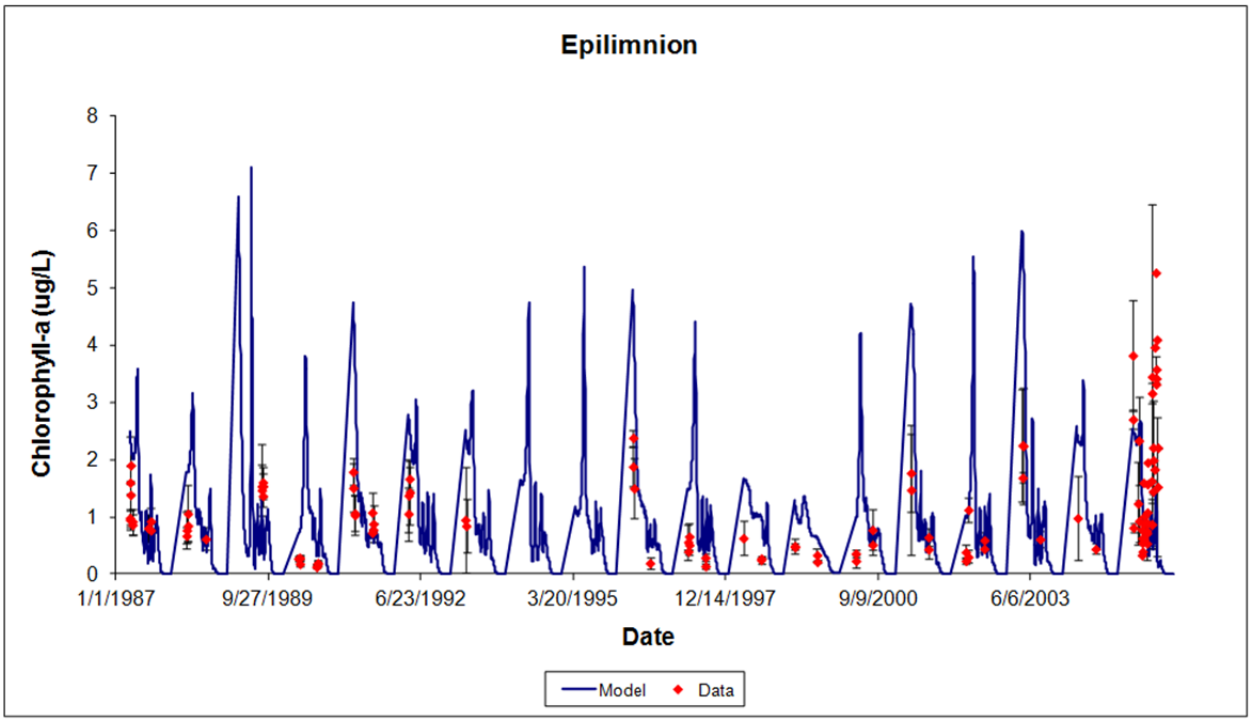

Figure B4-4: Comparison of model (line) and data (points) for epilimnion mixed-layer average of chlorophyll-a 1987-2005.

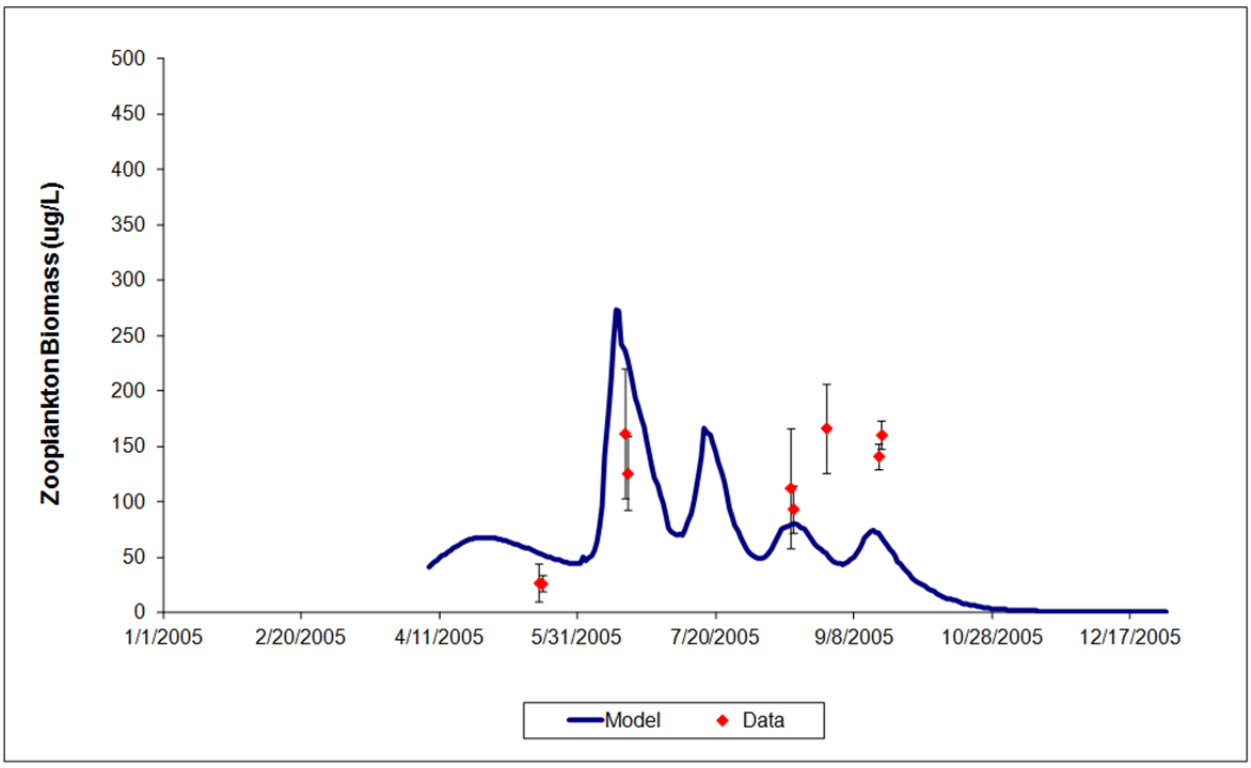

Figure B4-5: Comparison of model (line) and data (points) for epilimnion mixed-layer average of zooplankton 2005.

As a another corroboration test, model output was used from the layers located within the daily evolving hypolimnion, and a relationship between bottom water dissolved DO and hypoxic area ($A= 9.3\exp(-DO^2/7.09)$ developed by Zhou et al. (2013) was used to compare modeled areal extent to those estimated from a geostatistical analysis of the observations (Zhou et al., 2013). It is important to note that hypoxic area derived from geostatistical analysis of observations from individual cruises (Zhou et al., 2013) varies considerably within a year, even when cruises were only a few weeks apart (Figure B4-6). A comparison between modeled and observed summer hypoxic area, averaged over the timeframe of the observations in each year, shows the model also captures the inter-annual dynamics of this key management-focused metric. The Zhou et al. (2013) equation is carried forward to convert the 1-dimensional model output into an areal extent of hypoxia, for comparison with other models in the Annex 4 ensemble.

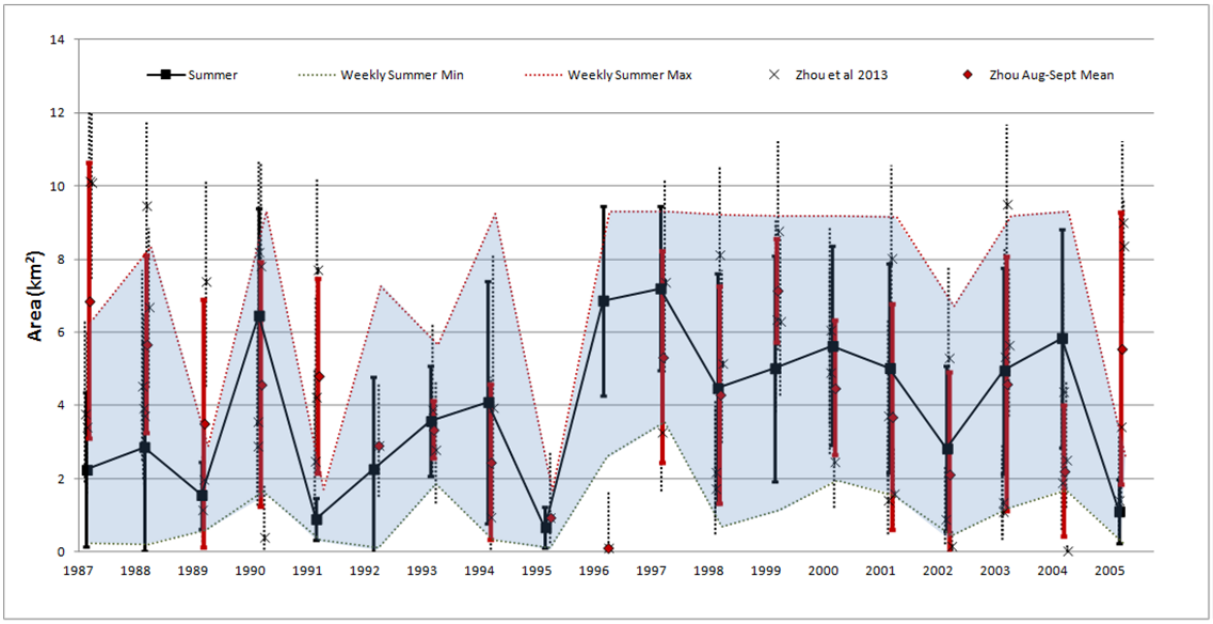

Figure B4-6: Light symbols with dotted error bars are 95% confidence intervals for individual cruises (Zhou et al., 2013). The shaded region represents modeled 7-day minimum and maximum for Aug-Sept. Red symbols and error bars are monthly means and standard deviation of the individual cruise estimates. Dark black line and bars represent model Aug-Sept means and standard deviation.

While the model is relatively simple, containing only six state variables, there are over thirty parameters that can be adjusted during calibration. The vast majority of these parameter values are within ranges used in similar models of large lakes, from the literature, and from EPA model guidelines (Table B4-2). However, in such under-determined models (Anderson, 2005; Friedrichs et al., 2006), it is possible to match state variable observations with more than one set of rate coefficients, such that over-estimation of one rate process is compensated by under-estimation of another. For this reason and to further confirm model performance, the calibrated model results were also compared to sedimentation, primary production, and oxygen depletion rates. The June-September mean primary production rates calculated by the model (18.7 - 92.7 $mgC \cdot m^{-3} \cdot d^{-1}$) are within the range of values measured during the growing season (Table B4-3). There are fewer published measurements of sedimentation rates in Lake Erie, particularly in recent decades. However, the model average of 1.59 $g(dw) \cdot m^{-2} \cdot d^{-1}$ is consistent within the 0.2-71.2 $g(dw) \cdot m^{-2} \cdot d^{-1}$ range measured in Lake Erie by Charlton and Lean (1987) and the 1.47-2.2 $g(dw) \cdot m^{-2} \cdot d^{-1}$ range measured in offshore Lake Ontario by Rosa (1985).

Table B4-3. Published Primary Production Rates in Lake Erie.

Reference	Minimum Production ($mgC \cdot m^{-3} \cdot d^{-1}$)	Maximum Production ($mgC \cdot m^{-3} \cdot d^{-1}$)
Ostrom et al. 2005a	11.5	395.5
Ostrom et al. 2005b	76.8	230.4
Depew et al. 2006	37.0	85.1
Smith et al. 2005	50.2	81.9
Model estimates	**18.7**	**92.7**

4. Model Application

In an earlier analysis that aggregated all oxygen consumption into water column and sediment demands, Rucinski et al. (2010) found that SOD represented on average 63% of the total hypolimnetic oxygen demand. In the present model, SOD also represents a substantial fraction of the overall demand. For example, in a simple model test, after removing all external phosphorus load, a 67% reduction of SOD is still required to eliminate hypoxia.

Because SOD is dependent upon settled organic matter, primarily from phytoplankton production driven by nutrient loads, it is logical to assume that reduced loads would eventually lead to reduced SOD. So, it was necessary to develop estimates of SOD changes in response to projected changes in phosphorus loads. To account for this, a relationship developed by Borsuk et al. (2001) between SOD and carbon deposition was used:

$$SOD = a\left(\frac{L_c}{1+kL_c h}\right)^b$$

where L_c is deposited organic carbon, h is the thickness of hypolimnion, and a, b, and k are model coefficients. Although their study focused mostly on large estuaries, it was possible to calculate values for a, b, and k via a least-squares regression such that the equation reproduced the average observed SOD for rates of organic carbon deposition simulated by the eutrophication model across the range of loads from the 19-year data set (Figure B4-7). This provides a reasonable representation of the relationship between carbon sedimentation and SOD; however to adjust SOD in the load-reduction scenarios, it is required to know how SOD would vary with nutrient load. To address this, current model was run with a wide range of loads to generate a relationship between load and carbon deposition and then, by way of the modified Borsuk equation, created a TP-SOD relationship (Figure B4-8):

$$SOD = \left(\frac{SOD_{\max}\ TP_{load}}{K_{SOD} + TP_{load}}\right)$$

where $SOD_{\max}$ is Maximum sediment oxygen demand , TP_{load} is the annual total phosphorus load, and K_{SOD} represents a half-saturation constant. This approximation assumes that SOD reaches a new steady state with nutrient loading. The values for SOD_{max} and K_{SOD}, obtained by regression, are 0.98 g·m^{-2}·d^{-1} and 3847 tonnes·$year^{-1}$, respectively. With this ability to adjust SOD based on loads, the model was used to investigate the response of several water quality metrics as a function of load and inter-annual variability in physical drivers.

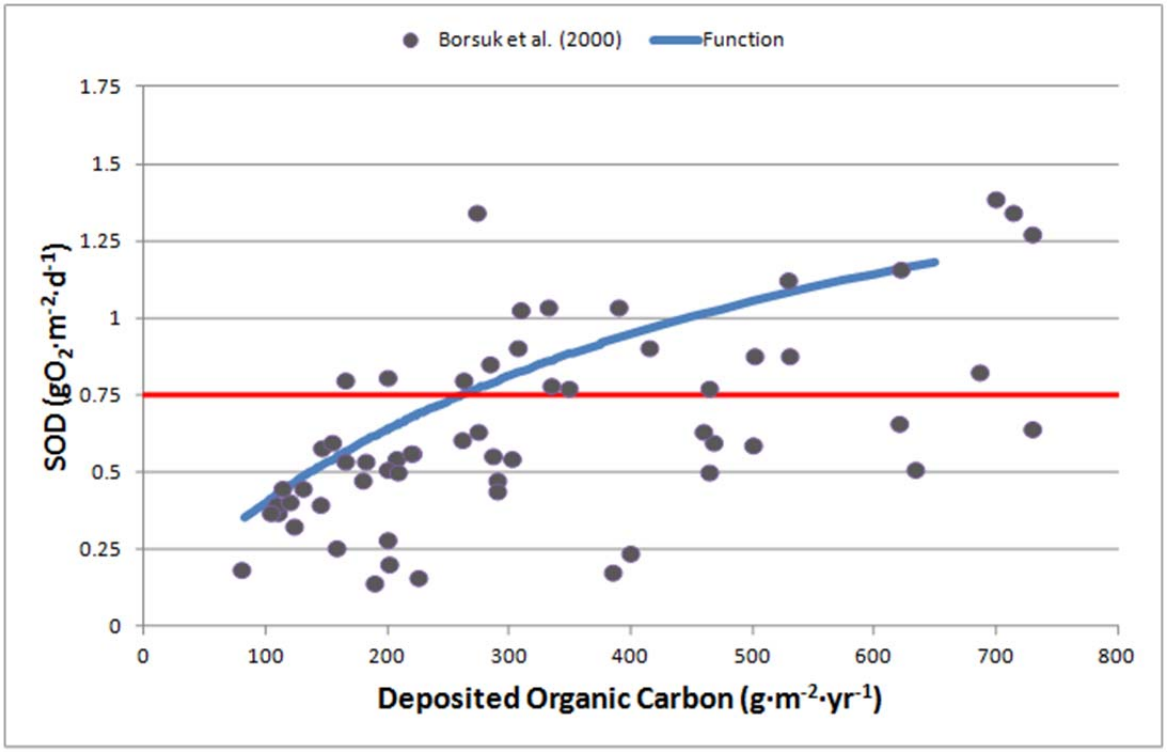

Figure B4-7: Comparison of model calculated SOD and sampled estuaries in Borsuk et al. 2001. Average of published Lake Erie SOD values is shown as solid red line. Solid blue line shows the obtained function relating SOD to deposited carbon. Black circles show the values published in Borsuk et al. 2001 for other systems.

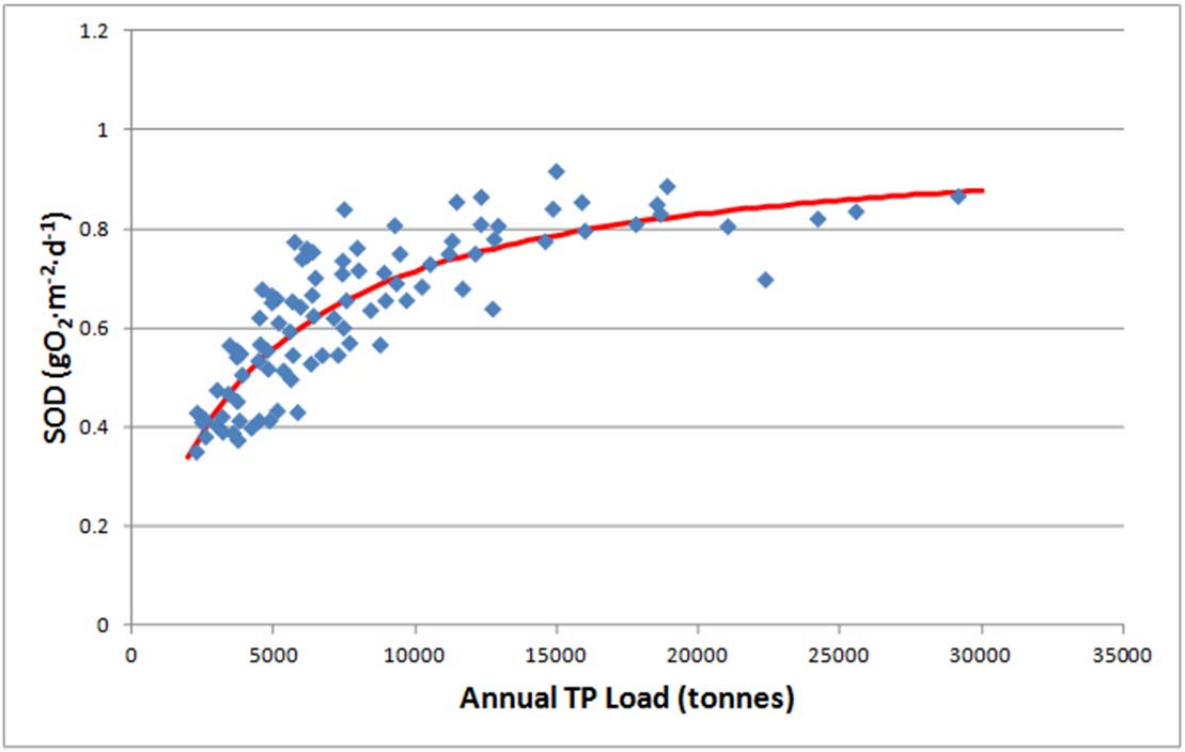

Figure B4-8: Relationship between annual total phosphorus load and model calculated SOD. Model estimated values shown as blue diamonds. Regression curve shown as red line.

Load-response Curves

Process Description. Using the corroborated 1D hypoxia model, along with the described relationship between steady-state TP load and sediment oxygen demand, it is then possible to explore the system's response to altered loads and inter-annual variability in physical drivers. This was accomplished by scaling the 2008 load time-series by six different factors (0%, 25%, 50%, 75%, 100%, 125%) and running the model with temperature and mixing patterns from each of the 19 years (1987-2005). The 2008 loading time series was used as the base case as the total annual TP load for the year was approximately equal to the current GLWQA target of 11,000 MT. Daily tributary inputs for total phosphorus and dissolved reactive phosphorus were provided by Dave Dolan for twenty six major tributaries across the Lake Erie basin. Tributary loads where aggregated for those falling within the western and central basins of the lake. The only difference between the simulations was the input loads; all other model input parameters and forcing functions remained constant. It should be noted that the change in loads for each model run resulted in a change in the steady-state SOD, as described previously.

Simulating the different hydrometeorological regimes produces response envelopes represented by the mean and standard deviation of the 19 cases. This approach allows development of response curves for the central tendency in system response, but also emphasize that the meteorological conditions in a given year can produce significant deviation from the mean. That is, while one can estimate the projected impact of a load reduction on average, the actual hypoxia metric might deviate substantially in any given year based on the timing and magnitude of stratification.

Response curves were generated for hypoxic extent (1000 km^2), bottom water dissolved oxygen ($mg \cdot L^{-1}$), number of hypoxic days, and chlorophyll-a ($\mu g \cdot L$) as a function of annual TP load. Hypoxic extent and bottom water dissolved oxygen are both averaged over the August-September period of each thermal simulation year (1987-2005). The number of hypoxic days is calculated over the entire stratified period, which typically lasts from mid-May to early October. Summer chl-a is calculated from June-Aug for each simulation year. It should be noted that the loads used in these curves represent total western and central basin loads. Eastern basin loads are assumed to not influence the central basin significantly.

Results and Interpretation. Using the relationship of Zhou et al. (2013), the areal extent of hypoxia is calculated from bottom water DO, and averaged over the August-September period, corresponding to the typical period of prolonged hypoxia. These model-calculated values are related to the six TP loading scenarios to produce the response curve shown in Figure B4-9. The mean values (blue diamonds) approximate an inverse parabolic function, however the trend is fairly linear in this range of TP loading rates. Rucinski et al. (2014) developed equivalent plots using the 1997 loading time-series (although with scaling factors ranging to 200%) showing a similar trend at the lower loading scales and approaching an asymptote at loads near 20,000 MT. The vertical error bars show +/- 1 st.dev from the mean, which is representative of the variation from the 19 different thermal regimes (i.e., the mean corresponds to the central tendency for a given load, while hydrometeorology determines the deviation from the mean).

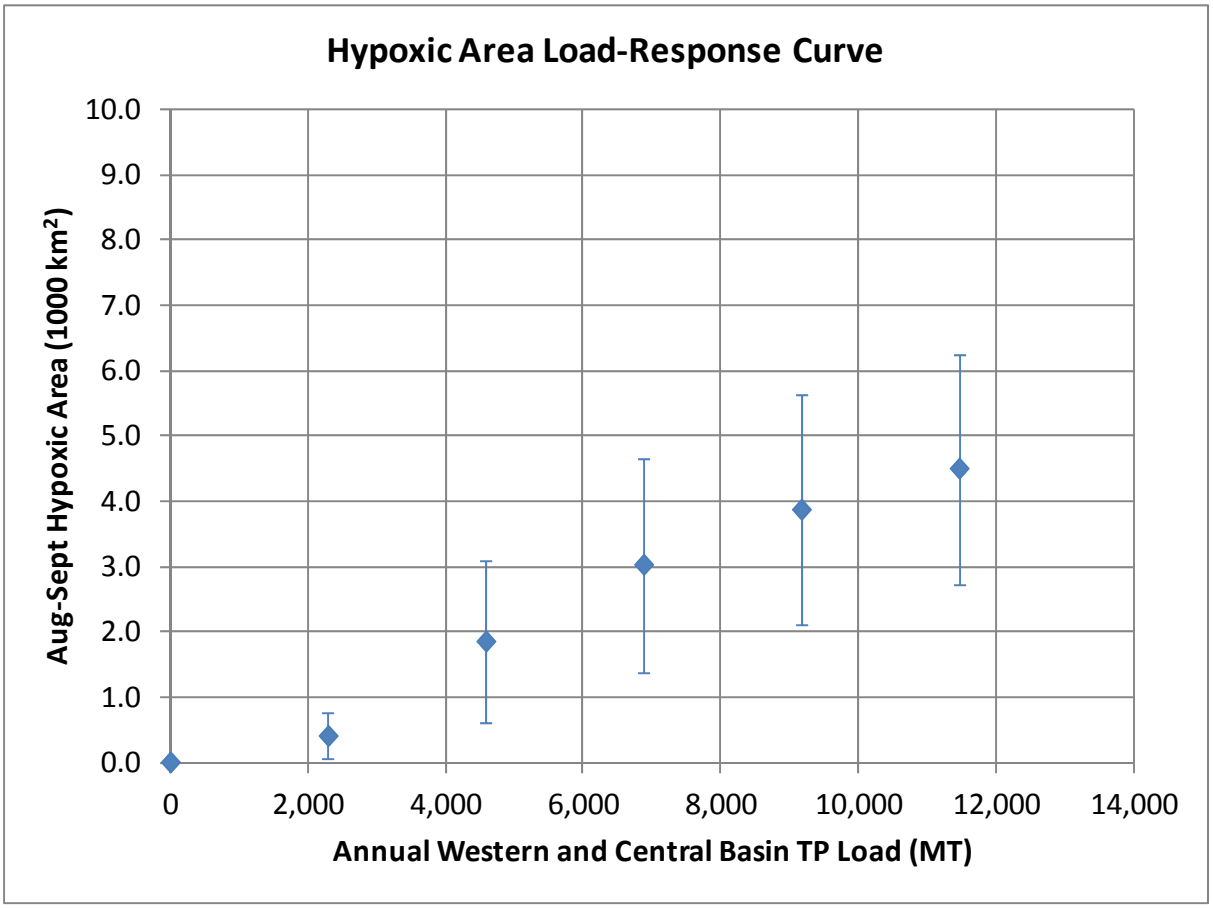

Figure B4-9: Aug-Sept average hypoxic area load-response curve. Mean of 1987-2005 model estimates values shown as blue diamonds. Standard deviation of 1987-2005 values shown as vertical error bars.

Figure B4-10 shows a companion load-response curve for summer average (August-September) bottom water dissolved oxygen. As expected, the hypolimnetic DO shows a negative exponential trend, compared to annual total phosphorus load. Again, the means of the 1987-2005 thermal regimes are shown as points, while the vertical error bars show +/- 1 st.dev of the values.

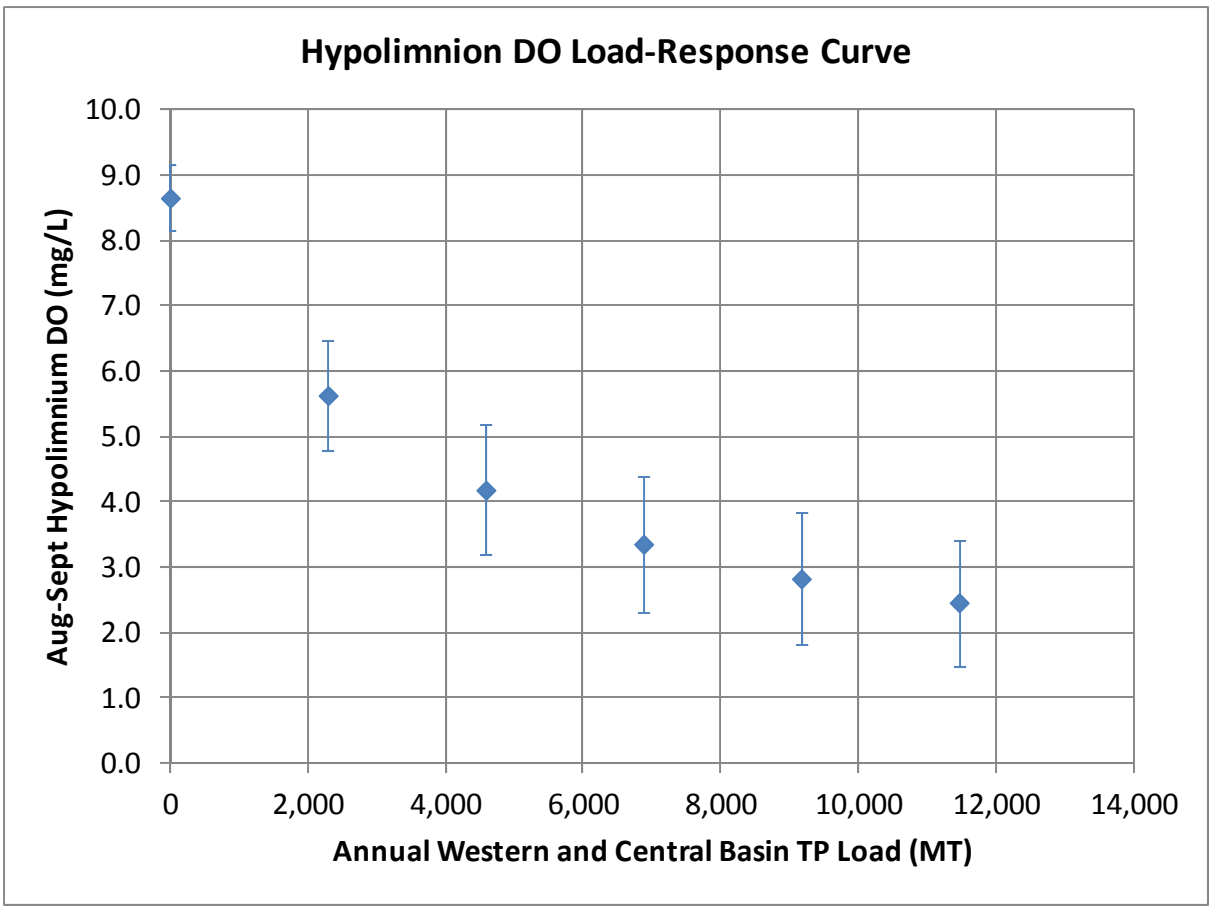

Figure B4-10: Aug-Sept average bottom water dissolved oxygen load-response curve. Mean of 1987-2005 model estimates values shown as blue diamonds. Standard deviation of 1987-2005 values shown as vertical error bars.

Similar to the load-response curve for hypoxic area (Figure B4-9), the number of hypoxic days (days where hypoxic area exceeds the area of the bottom model layer, approximate 750 km^2) shows an inverse parabolic relationship to annual TP load (Figure B4-11). Note that the number of hypoxic days is calculated for the entire duration of stratification, which varies in each of the 19 thermal regimes, but typically lasts from mid-May to early-October.

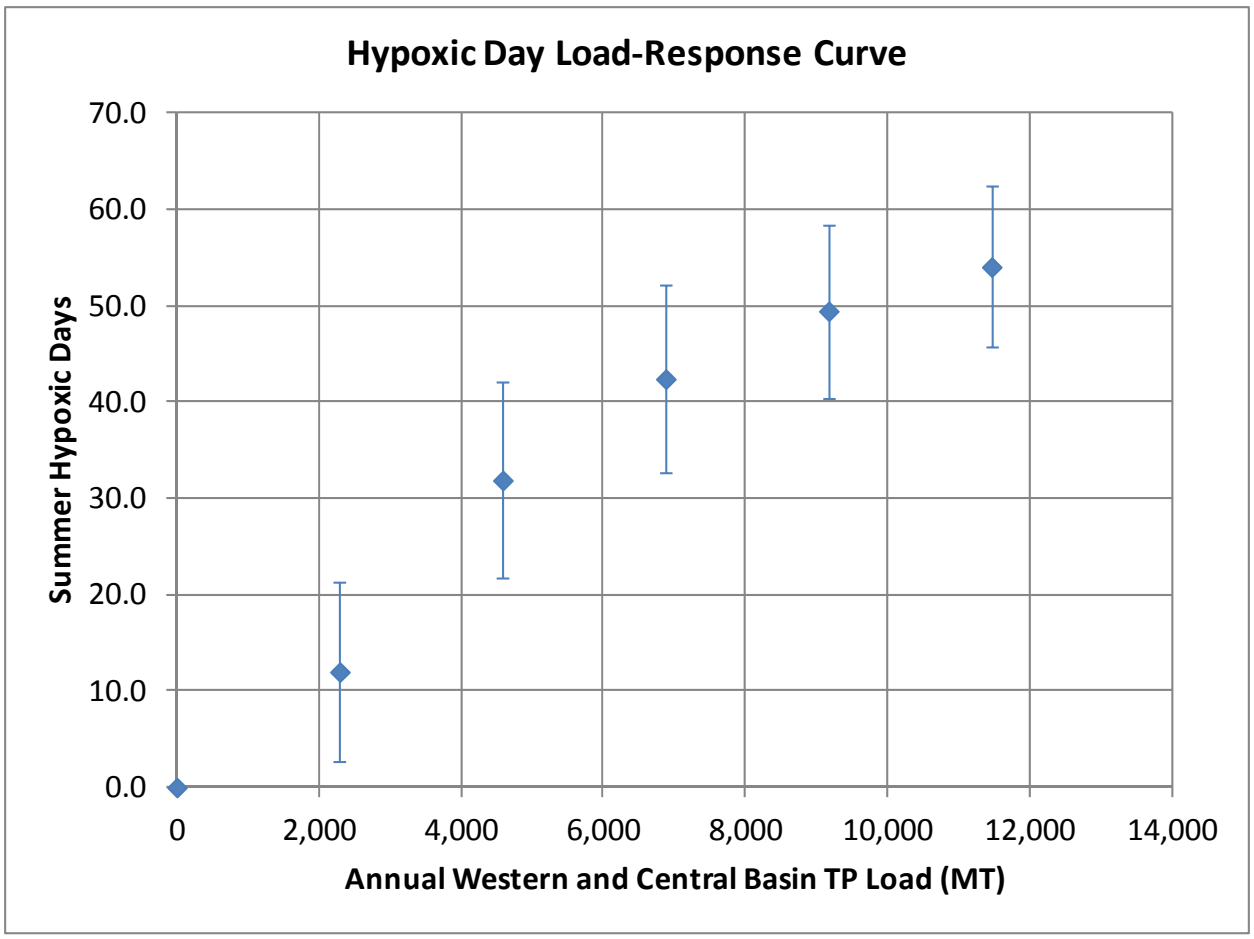

Figure B4-11: Number of hypoxic days load-response curve. Mean of 1987-2005 model estimates values shown as blue diamonds. Standard deviation of 1987-2005 values shown as vertical error bars.

Conversely, the load-response curve for chl-a shows an exponential relationship with total annual TP load (Figure B4-12). Note that at the lower end of the loading scale, the initialization conditions of the model appear to be driving the magnitude, resulting in a minimum of around 1.4 $\mu g \cdot L^{-1}$. The mean summer average chl-a (June-August) are shown as points, while the vertical error bars show +/- 1 st.dev of the values across the 1987-2005 thermal regimes.

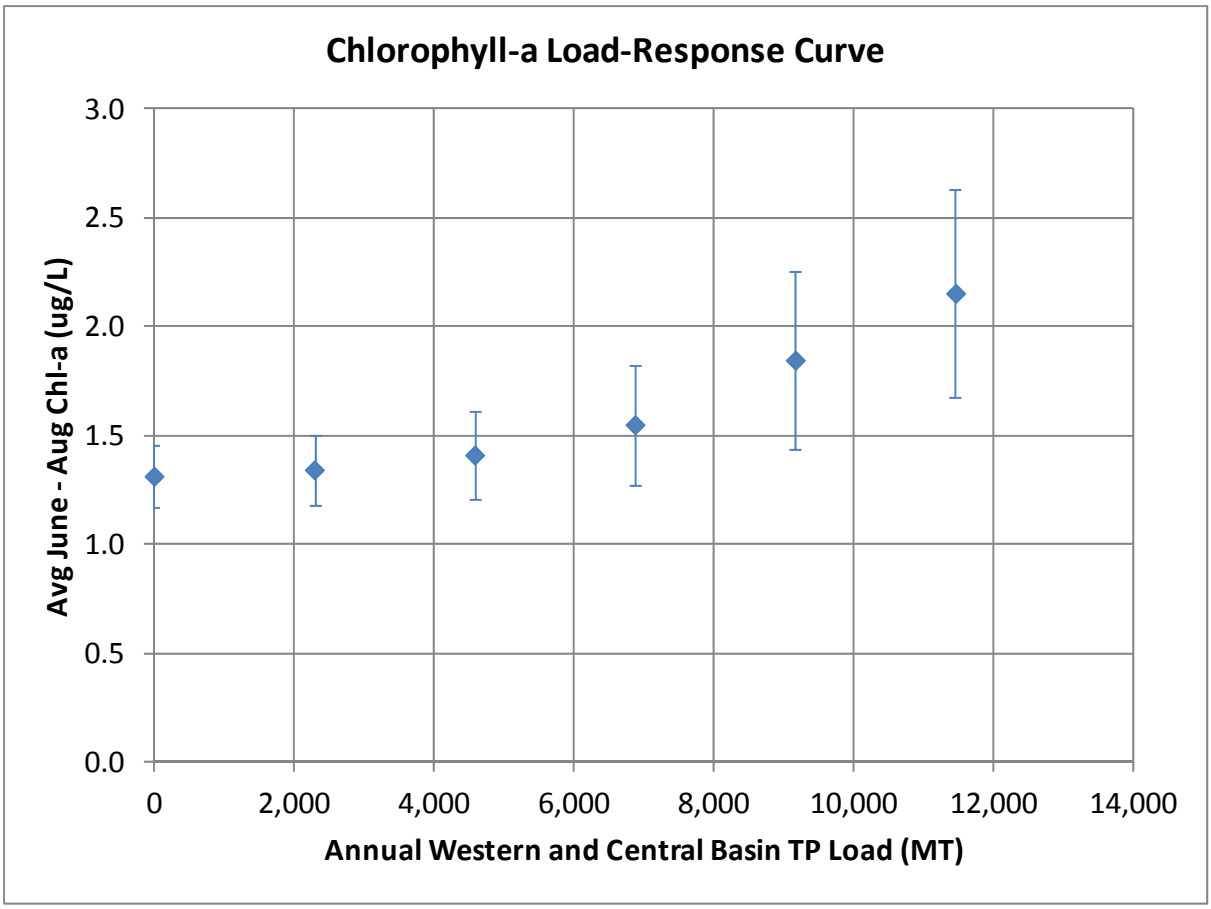

Figure B4-12: Chlorophyll-a load-response curve. Mean of 1987-2005 model estimates values shown as blue diamonds. Standard deviation of 1987-2005 values shown as vertical error bars.

Figure B4-13 shows the time-evolution of the hypoxic area estimated by the model. The blue line represents the mean of all 19 thermal regimes, while the vertical error bars again represent +/-1 st.dev. The time-series demonstrates that hypoxia can begin as early as mid-July, although significant magnitude usually occurs in early August. Hypoxia persists in the model until fall turnover, when oxygen in the bottom waters is replenished via mixing. Figure B4-14 shows a companion time-series, comparing the different loading scenarios. The reduction in hypoxia per load reduction is relatively small near the baseline loading conditions (blue line); but it increases towards the smaller loads (i.e., consistent with the inverse parabolic shape of the response curve in Figure B4-9).

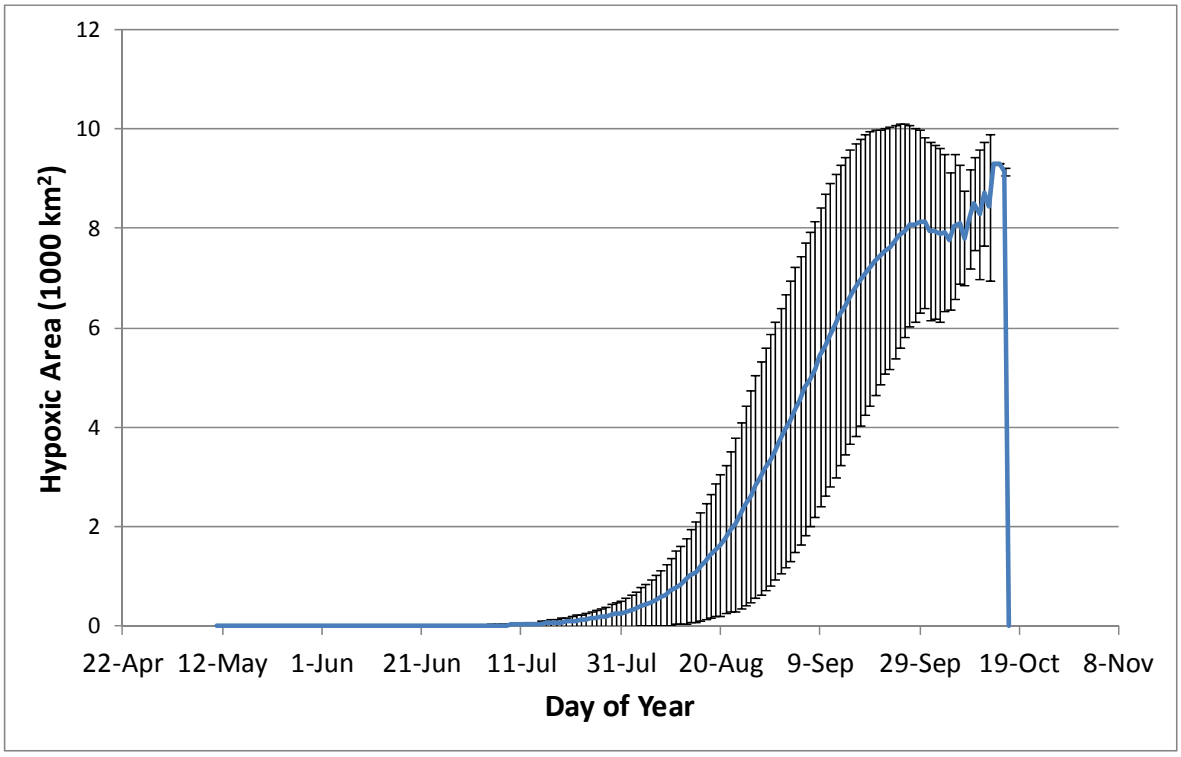

Figure B4-13: Temporal evolution of hypoxic extent. Mean of 1987-2005 model estimates values shown as blue line. Standard deviation of 1987-2005 values shown as vertical error bars.

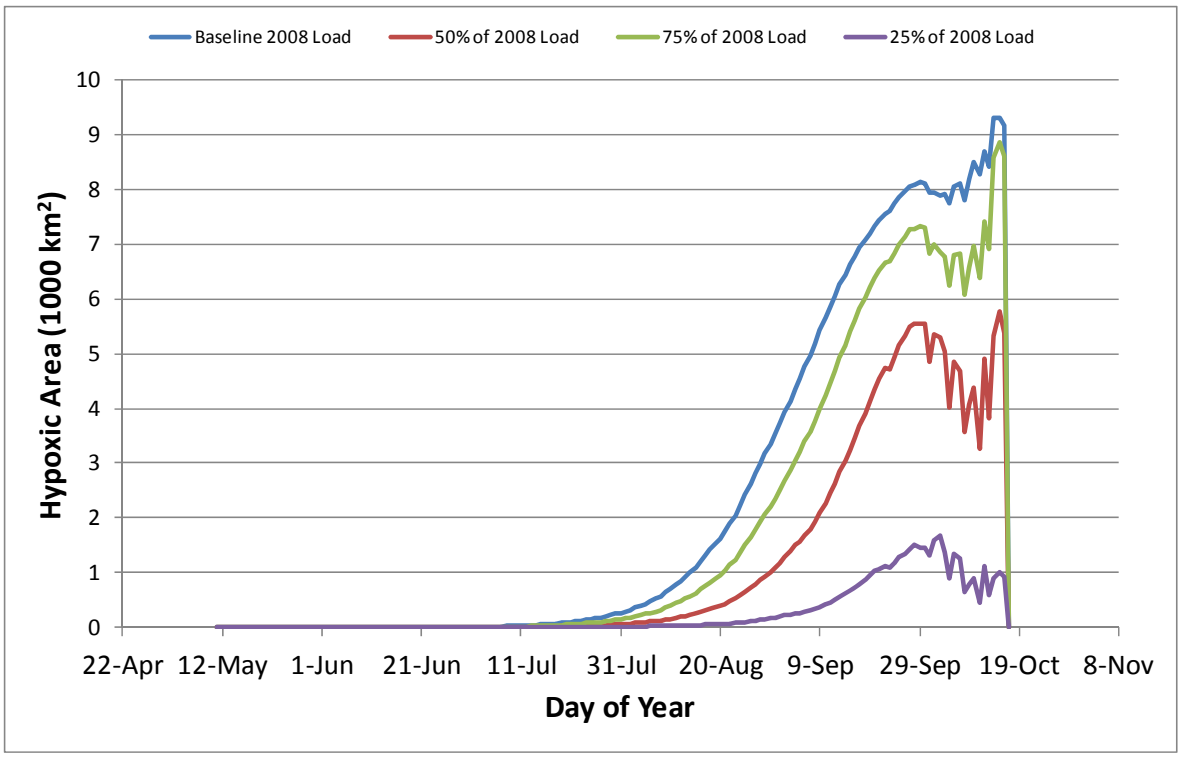

Figure B4-14: Temporal evolution of hypoxic extent bot different loading scenarios. Mean of 1987-2005 model estimates values shown as solid lines.

Uncertainty and Sensitivity Analysis

The original configuration of the model described above (and presented in Rucinski et al., 2014), is driven by basin-specific nutrient loads, as provided by Dave Dolan. The model accounts for attenuation of the loads from the Western Basin during transport to the Central Basin using a net apparent settling loss rate of 10 $m \cdot yr^{-1}$ (Lesht et al., 1991). One approach to address potential uncertainty and sensitivity to this method is to use loads entering the Central Basin from the Western Basin as calculated by LimnoTech's Western Lake Erie Ecosystem Model (WLEEM). WLEEM provides daily aggregates of the mass flux crossing the Western-Central basin boundary. The model was therefore modified to use these estimated fluxes from the Western Basin, in place of using the net apparent attenuation loss. Load-response curves for hypoxic area, hypolimnetic DO, number of hypoxic days, and chl-a were developed using the WLEEM-linked version of the model, in the same manner as the curves developed with the original model framework. Both versions of the curves are plotted for comparison in Figures B4-15 through B4-18.

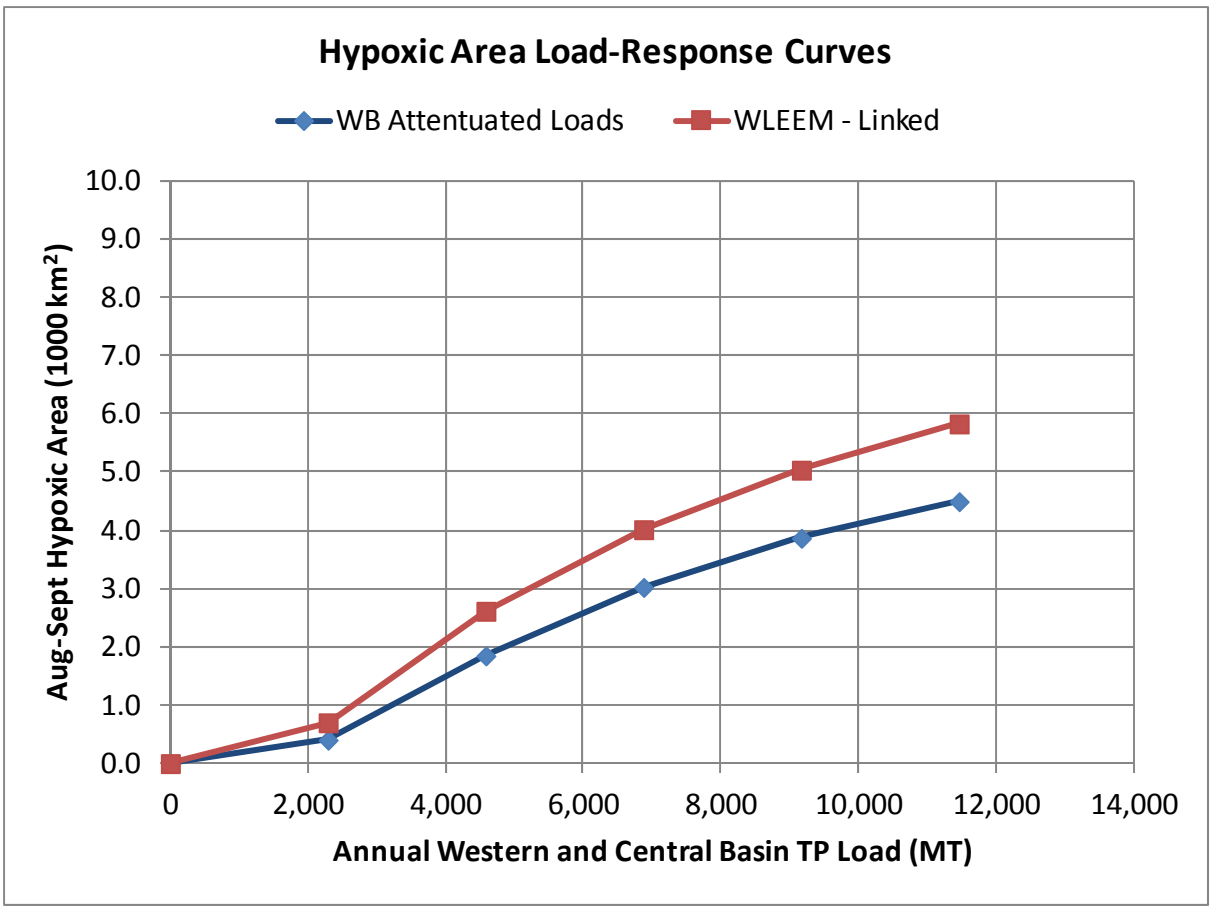

Figure B4-15: Comparison the hypoxic area load-response curves obtained from original model configuration (blue), and using loads from WLEEM (red).

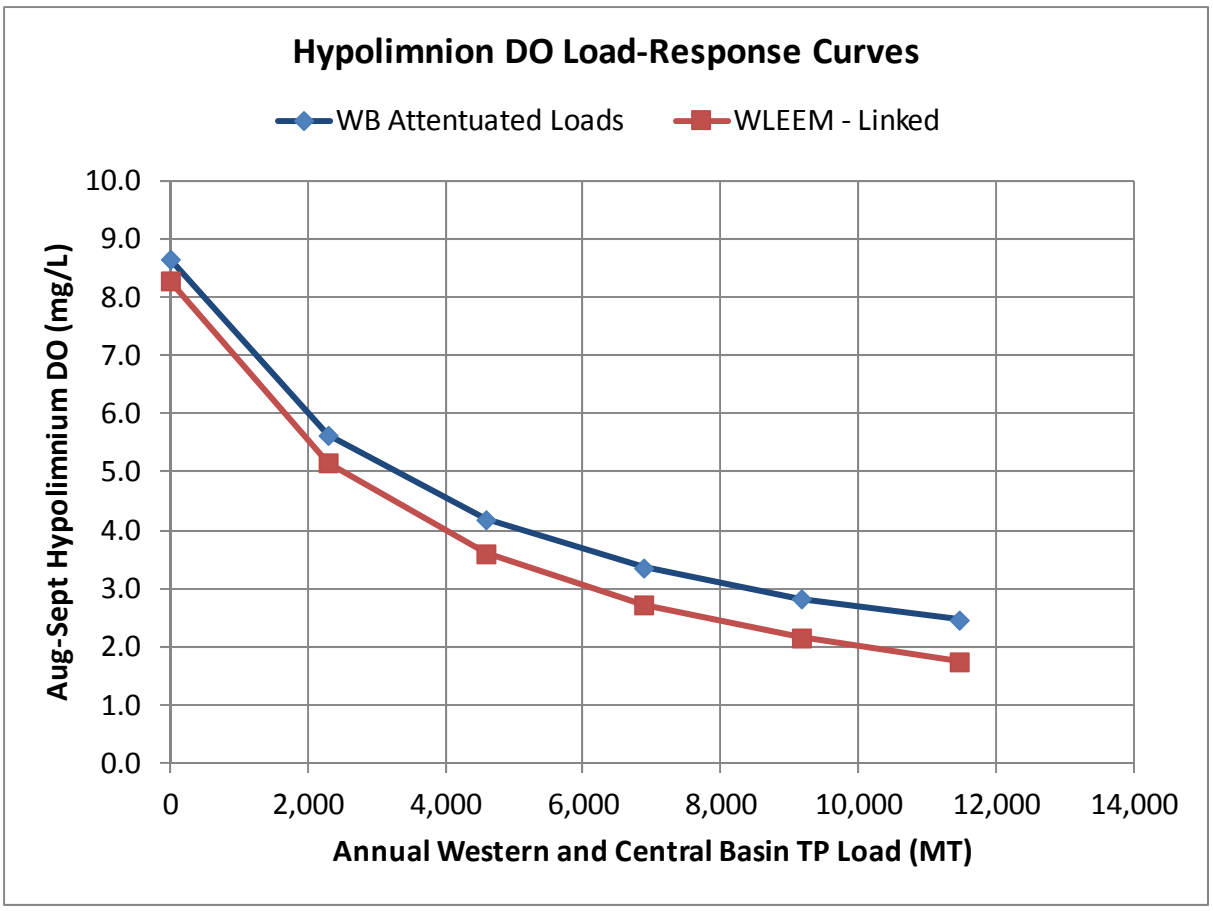

Figure B4-16: Comparison the hypolimnetic DO load-response curves obtained from original model configuration (blue), and using loads from WLEEM (red).

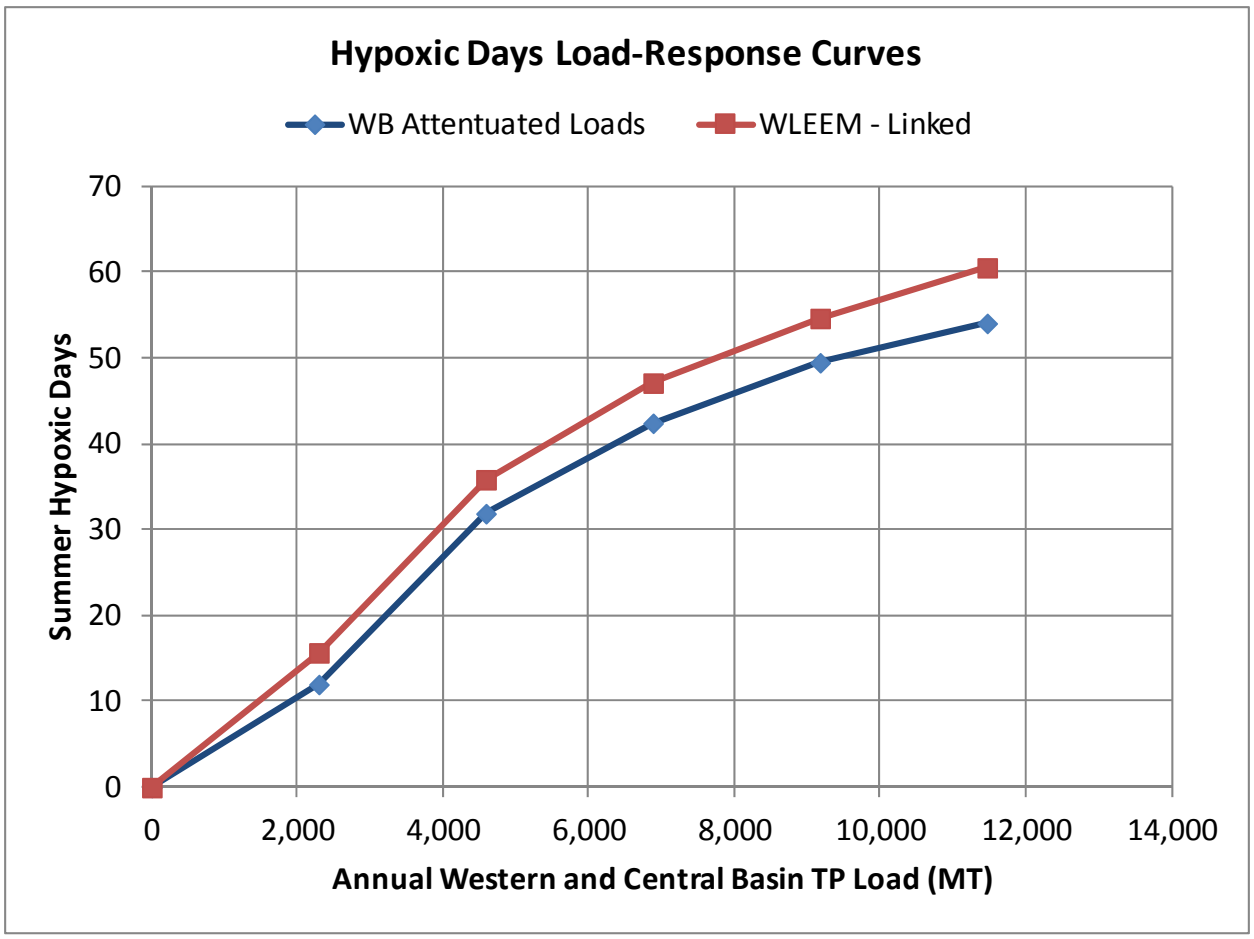

Figure B4-17: Comparison the hypoxic day load-response curves obtained from original model configuration (blue), and using loads from WLEEM (red).

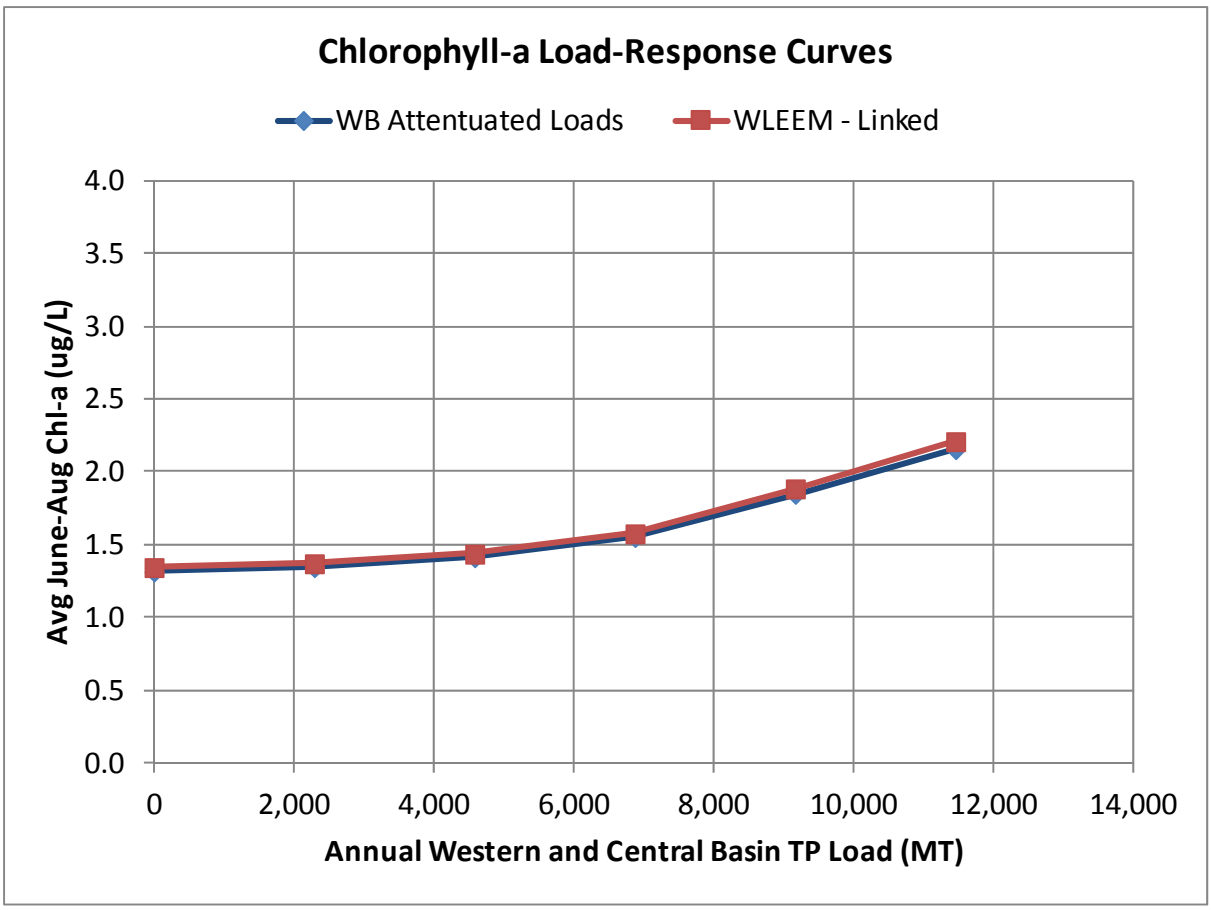

Figure B4-18: Comparison the chlorophyll-a load-response curves obtained from original model configuration (blue), and using loads from WLEEM (red).

The comparison of the load-response curves in Figures B4-15 through B4-18 show a similar trend for each water quality metric: the response is very similar for both versions of the model at lower loading rates, while they diverge more significantly at higher loading rates. The WLEEM-linked model tends to produce higher levels of hypoxia and lower bottom water DO. Both chl-a curves are very similar, again likely do to constraints of the initialization conditions in the model. However, the curves follow the same general trend and produce fairly similar values of the water quality metrics for current loads and reductions.

It is important to note that both versions of the model used the same calibrated/corroborated parameter set from the original version of the model with the western basin loads attenuated at a constant rate. Therefore, it is expected that the differences in loads entering from the Western Basin would produce a difference in response. However, another difference in the model versions is the flow that is transported to the Central Basin. WLEEM incorporates a full 3-dimensional hydrodynamic model, which allows circulation and retention in the Western Basin. The original version of the model simply assumed that the sum of the flow from the Western Basin tributaries entered the Central Basin, following the observed hydrograph. The differences in flow time-series are likely the cause of a significant portion of the differences between the values estimated by the two model versions, as

changes in flow affects the net export components of the differential equations shown in Table B4-1. The differences in flow entering the Central Basin from the Western Basin are shown in Figure B4-19.

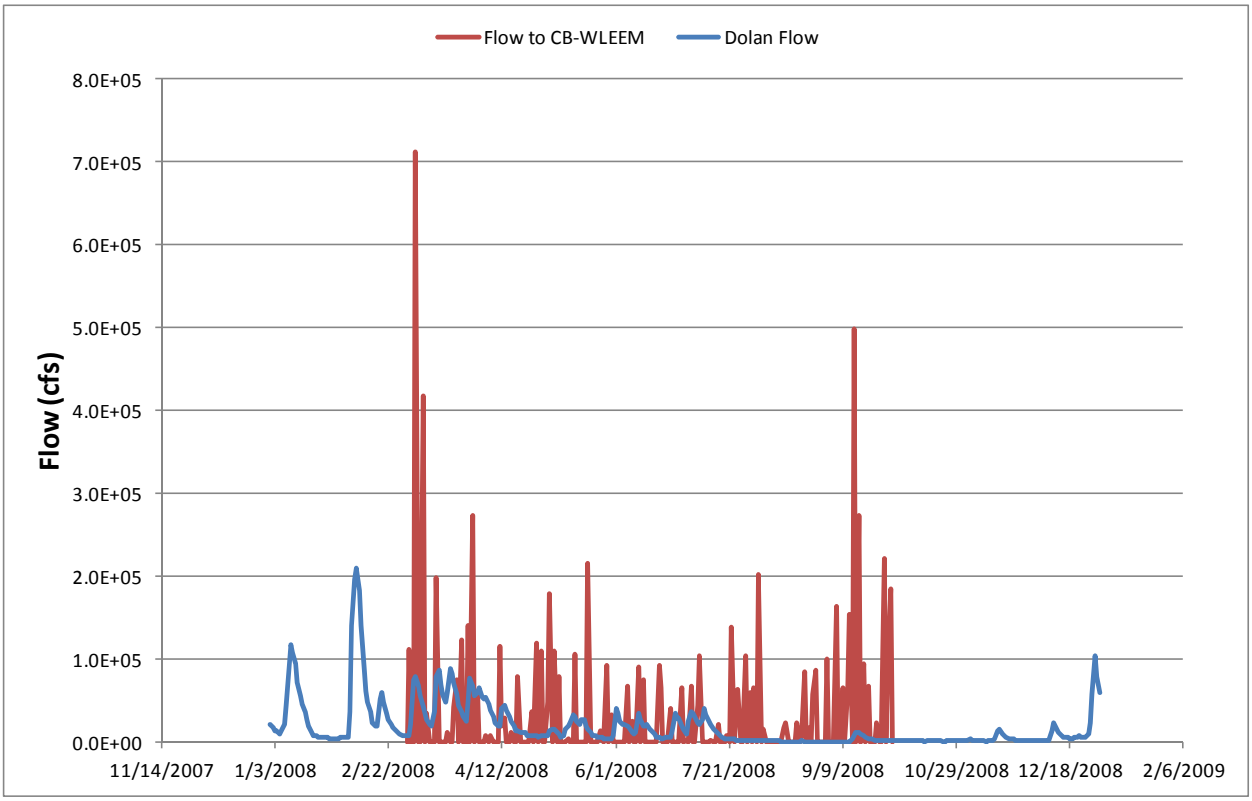

Figure B4-19: Comparison of the flow from the western basin to the central basin using Dolan estimates (blue), and WLEEM hydrodynamics (red).

While the version of the model that uses WLEEM estimated loads produces somewhat different values than the calibrated version, it can provide opportunities to investigate targeted load reductions in specific tributaries. For example, WLEEM can simulate the fate and transport of nutrients in the Western Basin given load reductions in only one tributary, such as Maumee or Detroit Rivers. This can potentially be valuable to determine where to focus management practices, but it is not possible using the original calibrated version as the model treats all Western Basin loads equivalently.

5. Conclusions and Recommendations

The 1D Central Basin Hypoxia model has been calibrated and corroborated to in-lake data over a 19 year (1987-2005) period, during which hydrometeorological conditions vary greatly. Applying the calibrated model to the 2008 loading time-series and simulating the response under the 19 different thermal regimes produces an envelope of expected lake response, for a given total phosphorus load. Scaling the 2008 loading time-series generates response curves (Figures B4-10 through B4-13) that can help guide management decisions on target load reductions. For example, if managers wished to reduce the hypoxic area in the Central Basin to approximately 2,000 km^2, a total maximum western and central basin load of approximately 4800 MT would be required, representing approximately 48% reduction

from the baseline 2008 loads. While this would be an average expected value give the load reduction, as illustrated by the error bars in Figure 10, climate and meteorology will also determine the level of hypoxia. Very warm years with early or prolonged stratification or a very deep thermocline would produce greater than average hypoxia for a given load. Conversely, a shallow thermocline or enhanced mixing from wind events could produce lower than average hypoxia.

6. References

Anderson, T. R. 2005. Plankton functional type modelling: running before we can walk? Journal of Plankton Research, 27, (11), 1073-1081

Beletsky, D., Schwab, D.J., 2001. Modeling circulation and thermal structure in Lake Michigan: Annual cycle and interannual variability. J. Geophys. Res. 106, 19745–19771.

Beletsky, D., N. Hawley, Y.R. Rao, H. A. Vanderploeg, R. Beletsky, D. J. Schwab and S.A. Ruberg. 2012. Summer thermal structure and anticyclonic circulation of Lake Erie, Geophysical Research Letters 39:L06605

Blumberg, A. F., Mellor, G. L. 1987. A description of a three-dimensional coastal ocean circulation model. In Three-Dimensional Shelf Models, Coastal and Estuarine Sciences, ed. N. S. Heaps, pp. 1-16. American Geophys. Union.

Borsuk, M., Higdon, D., Stow, C. and Reckhow, K. 2001. A Bayesian hierarchical model to predict benthic oxygen demand from organic matter loading in estuaries and coastal zones. Ecological Modelling 143:165–181.

Burns, N. M., Rockwell, D. M., Bertram, P. E., Dolan, D. M., and Ciborowski, J. J. H. 2005. Trends in Temperature, Secchi Depth, and Dissolved Oxygen Depletion Rates in the Central Basin of Lake Erie, 1983-2002. Journal of Great Lakes Research 31:35-49.

Charlton, M.N., Lean, D.R.S. 1987. Sedimentation, Resuspension, and Oxygen Depletion in Lake Erie (1979), Journal of Great Lakes Research. 13(4):709-723

Chen, C., R. Ji, D.J. Schwab, D. Beletsky, G.L. Fahnenstiel, T.H. Johengen, H.A. Vanderploeg, B.J. Eadie, M. Bundy, W. Gardner, and J. Cotner. 2002. A model study of the coupled biological and physical dynamics in Lake Michigan. Ecological Modeling, 152, 145-168

Depew, D.C., Guildford, S.J, Smith, R.E.H. 2006. Nearshore–offshore comparison of chlorophyll a and phytoplankton production in the dreissenid-colonized eastern basin of Lake Erie. Canadian Journal of Fisheries and Aquatic Sciences, 63:1115-1129

DiToro, D. M. and Connolly, J. P.,1980. Mathematical models of water quality in large lakes, Part 2: Lake Erie, EPA-600/3-80-065 Report, Duluth, MN,

Dolan, D. M. 1993. Point source loadings of phosphorus to Lake Erie: 1986-1990. Journal of Great Lakes Research 19:212-223.

Dolan, D.M., and McGunagle, K.P., 2005. Lake Erie total phosphorus loading analysis and update: 1996–2002. J. Great Lakes Res. 31 (Suppl. 2), 11–22

ECWSTB (Environment Canada, Water Science & Technology Branch) ftp:// charon.cciw.ca (accessed June 2007)

IFYLE 2006. NOAA Great Lakes Environmental Research Laboratory: International Field Years on Lake Erie (IFYLE). http://www.glerl.noaa.gov/ifyle/ 11/12/2006.GLNPO (Great Lake National Program Office. http://cdx.epa.gov/ (accessed February 2007).

Friedrichs, M.A.M., Hood, R.R., Wiggert, J.D., 2006. Ecosystem model complexity versus physical forcing: quantification of their relative impact with assimilated Arabian Sea data. Deep-Sea Research II 53, 576–600.

GLWQA 1978. Great Lakes Water Quality Agreement.

Lesht, B.M., Fontaine, T.D., Dolan, D.M., 1991. Great Lakes total phosphorus model: post-audit and regionalized sensitivity analysis. Journal of Great Lakes Research 17 (1), 3–17.

Mellor, G. L., and T. Yamada, Development of a turbulence closure model for geophysical fluid problems, Rev. Geophys., 20, 851–875, 1982.

Ostrom, N.E., Russ, M.E., Field, A., Piwinski, L., Twiss, M.R., Carrick, H.J. 2005a. Ratios of Community Respiration to Photosynthesis and Rates of Primary Production in Lake Erie Via Oxygen Isotope Techniques, Journal of Great Lakes Research, Volume 31, Supplement 2. 138-153

Ostrom, N.E., Carrick, H.J., Twiss, M.R., Piwinski, L. 2005b. Evaluation of primary production in Lake Erie by multiple proxies. Oecologia 144: 115–124

Redfield A.C., 1934. On the proportions of organic derivations in sea water and their relation to the composition of plankton. In James Johnstone Memorial Volume. (ed. R.J. Daniel). pp. 177-192.

Richards, R. P. 2006. Trends in sediment and nutrients in major Lake Erie tributaries, 1975-2004. In Lake Erie Lakewide Management Plan 2006 Update pp. 22.

Richards, R. P. and Baker, D. B. 2002. Trends in water quality in LEASEQ rivers and streams, 1975-1995. Journal of Environmental Quality 31:90-96.

Rosa, F. 1985. Sedimentation and Sediment Resuspension in Lake Ontario, Journal of Great Lakes Research 11(1): 13-25

Rosa, F. and Burns, N. M. 1987. Lake Erie Central Basin Oxygen Depletion Changes from 1929-1980. Journal of Great Lakes Research 13:684-696.

Rucinski, D. K., D. Beletsky, J.V. DePinto, D.J. Schwab, and D. Scavia. 2010. A simple 1-dimensional, climate based dissolved oxygen model for the central basin of Lake Erie. Journal of Great Lakes Research, 36:465-476.

Rucinski, D.K., D. Scavia, J.V. DePinto, D. Beletsky. 2014. Modeling Lake Erie's hypoxia response to nutrient loads and meteorological variability. Journal of Great Lakes Research. (in press).

Schloesser, D. W., Stickle, R. G., and Bridgeman, T. B. 2005. Potential Oxygen Demand of Sediments from Lake Erie. Journal of Great Lakes Research 31:272-283.

Snodgrass, W. J. 1987. Analysis Of Models And Measurements For Sediment Oxygen Demand In Lake Erie. Journal of Great Lakes Research 13:738-756.

Snodgrass, W. J. and Fay, L. A. 1987. Values of sediment oxygen demand measured in the central basin of Lake Erie, 1979. Journal of Great Lakes Research 13:724-730.

Smith, R.E.H., Hiriart-Baer, V.P., Higgins, S.N., Guildford, S.J., and Charlton, M.N. 2005 Planktonic Primary Production in the Offshore Waters of Dreissenid-infested Lake Erie in 1997. Journal of Great Lakes Research, Volume 31, Supplement 2. 50-61.

Wool, T.A., Ambrose, R.B., Martin, J. L, and Coormer, E.A. 2002 Water Qaulity Analysios Simulation Progrma (WASP). Version 6.0

Zhou, Y., Obenour, D.R., Scavia, D., Johengen, T.H. and Michalak, A.M., 2013. Spatial and Temporal Trends in Lake Erie Hypoxia, 1987-2007. Environ Sci Technol. 47, 899-905.

APPENDIX B-5: Ecological Model of Lake Erie (EcoLE)

Hongyan Zhang, Cooperative Institute for Limnology and Ecosystems Research, University of Michigan

Acknowledgement

Thanks to Ms. Xin Xu at University of Michigan for compiling input data and simulation model runs.

1. Model description

Overview

EcoLE (Ecological Model of Lake Erie) was based on the two-dimensional hydrodynamic and water quality model CE-QUAL-W2 (version 2.0), which is constructed to simulate relatively long and narrow waterbodies exhibiting longitudinal and vertical water quality gradients (Cole and Buchak, 1995, Zhang et al., 2008). Hundreds of studies have applied CE-QUAL-W2 to water bodies of various kinds (rivers, reservoirs, lakes and estuaries) all over the world. Boegmen (1999) applied this model to simulate hydrodynamics of Lake Erie (Boegman et al., 2001), and used this model to assess the impacts of dreissenids and nutrient loads on the algal biomass in the western basin (Boegman et al., 2008a, Boegman et al., 2008b). Zhang et al. (2008) divided the phytoplankton into three algal groups: non-diatom edible algae, non-diatom inedible algae, and diatoms; they also added in zooplankton (cladocerans and copepod) submodels. This model was use to evaluate the dreissenid impacts on different algal groups and the phosphorus dynamics (Zhang et al., 2008, Zhang et al., 2011), and to assess the importance of weather and sampling intensity on monitoring hypoxia (Conroy et al., 2011).

Structure/forcing functions/state variables/key relationship/conceptual model

The physical model. EcoLE divided Lake Erie into as many as 65 vertical layers at 1 m intervals and 222 longitudinal segments from west to east (Figure B5-1). The depths of segments were assigned relative to the Great Lakes Datum (GLD) of 1985. A unique width was specified for each cell. The model has six variables for hydrodynamic simulations: free water surface elevation, pressure, horizontal velocity, vertical velocity, constituent concentration, and density. The relations among these variables are expressed by six equations: the horizontal momentum equation, the constituent transport equation, the free water surface elevation equation, the hydrostatic-pressure equation, the continuity equation, and the equation of state (Table B5-1).

The chemical-biological model. This model includes 28 water quality variables, with flexibility to including more variables (Figure B5-2): a conservative tracer, suspended solid, coliform, dissolved solids, labile dissolved organic matter (DOM), refractory DOM, non-diatom edible algae, non-diatom inedible algae, diatoms, labile particulate organic matter (POM), soluble reactive phosphorus (SRP), ammonium, nitrate+nitite, dissolved oxygen, sediment, inorganic carbon, alkalinity, pH, carbon dioxide, bicarbonate, carbonate, iron, chemical/biological oxygen demand (CBOD), and cladocerans and four copepod variables (copepod eggs, nauplii, copepodites and copepods). Two dreissenid mussel processes are included in the EcoLE model, i.e., grazing on phytoplankton and excretion of N and P nutrients. Mussel population was forced depth-dependent densities. Table B5-1 includes the equations for state variables we are most interested. See CE-QUAL-W2 user manual (Cole and Buchak, 1995) and Zhang's dissertation (Zhang, 2006) for all equations that govern the dynamics of these state variables.

Conceptual model. Flow charts (Figures B5-2 and B5-3) summarize the over structure of the EcoLE. Specifically, Figure B5-3 (left panel) shows the simulation steps of initialization, hydrodynamic sources/sinks, hydrodynamic calculation, temporal balance terms and temperature, constituent transport and balance, layer-segment addition and subtraction, and updating variables for next time step and output results at the end of simulation. Figure B5-3 (right panel) shows the detail of constituent transport and balance terms, including updating kinetics, call subroutines, external sources/sinks, and temporal balance. Figure B5-2 shows the connections among chemical and biological state variables, which were presented as the subroutines in the EcoLE.

External Forcings .The model is driven by the weather conditions (air temperature, wind, cloud cover, precipitation), and tributary input (flow, temperature, constituent loads).

2. Data used for model input and evaluation (calibration, confirmation)

Model input included meteorological data and tributary inputs. The meteorological data were retrieved from http://rda.ucar.edu/datasets/ds093.1/#!access NCEP Climate Forecast System Reanalysis (CFSR) Selected Hourly Time-Series Products. Calculated surface temperature, dew-point temperature, cloud cover, wind magnitude and direction for the same locations as meteorological stations previously used in the model. Tributaries considered in this modeling activity include Maumee River, Raisin River, Detroit River, Portage River, Sandusky River, Huron River (OH), Black River, Cuyahoga River, Grand River (ON), and Cattaraugus River that have annual TP loads greater than 160 MT. Tributary flows and constituent loads of TP, SRP, NO2+NO3 were from the EcoFore project database of years 2007 and 2008. Model initial data were from the EcoFore project database, including DO, Chla, SRP. Calibration data were also from the EcoFore project database of 2008 including water temperature, DO and Chl a. Monthly averaged bottom DO from EPA hypoxia monitory program (http://www.epa.gov/grtlakes/monitoring/d_o/index.html) were also used to compare model DO predictions.

3. Calibration and confirmation approach and results

Due to the difference in meteorological data sources between 2008 and 1997-1999 (calibration and confirmation years), we found that a couple of parameters needed to be adjusted for a good simulation on water temperature. One is a coefficient in the cloud cover function. We increase this value from 0.0017 to 0.007 for central basin and 0.012 for western basin. The other one is to increase the mixing parameter in the central basin. The model prediction agreed well with the vertical distribution of the water temperature in the central basin (Figure B5-4).

Comparisons of chlorophyll a between model simulation and observations showed that model predictions agreed very well with observations in segments 31,32,37 and 41, but predicted higher Chl a in the segments 14 and 21. We increased the maximum sediment DO demand (SODmax) for a better DO simulation in the central basin. We increase the SOD max from 0.27 to 0.84 and decrease the half-saturation coefficient from 1.4 to 0.9. The model predictions match well with the vertical DO profile for most segments in the central basin (Figure B5-5). The modeled monthly bottom DO also matched well

with the EPA monthly bottom DO (Figure B5-6). This also indicates that the 10 EPA sampling stations sufficiently represented spatial distribution of bottom DO conditions in the central basin.

4. Application Results

Consistent with other model simulation scenarios, we also varied the TP loads as 0, 25, 50, 75, 100 and 125% of the 2008 TP load, and varied the SRP loads as 0, 25, 50, 75, 100 and 125% of the 2008 SRP load. We keep all model parameters and forcings the same, except for TP or SRP loads, and the SODmax (Table B5-2, Rucinski et al., 2014) that are varied in different P loading scenarios.

Load-Response curves

Chlorophyll a. For each load scenario, we output the biomass of non-diatom edible algae (NDEA) and diatom in the western basin at noon for each day. The response curve was between P loads and basin-wide averaged total biomass of NDEA and diatoms from June 1 to August 31, 2008 (Figures B5-8 and B5-9). The minimum and maximum of daily western basin-wide Chl a between June 1 and August 31 were also reported.

Bottom DO. For each load scenario, we output DO distribution in the central basin at noon for each day. We calculated two parameters for the bottom DO response curve, one is average bottom DO between August 1 to September 30, 2008 over the segments that corresponding to the 10 EPA monitoring stations (Figures B5-10 and B5-11), the other parameter is similar but averaged bottom layers of 1-3 meters above the sediment (Figure B5-12 and B5-13, hereafter refer to hypolimnetic DO). The minimum and maximum of daily bottom DO between August 1 and September 30 were also reported.

Hypoxic area. Using bottom DO values generated above and the relationship developed by Zhou et al. (Zhou et al., 2013), we converted the bottom DO into hypoxic area in the central basin for different P loading scenarios (Figures B5-14 through B5-17). The minimum and maximum of daily hypoxic area between August 1 and September 30 were also reported.

Diagnosis/interpretation

The Chl a response curve in the western basin showed that Chl a decreased with reduction in TP or SRP loads, while a 2-order polynomial relationship fit the best between Chl a and TP loads of SRP scenarios. Chl a is very sensitive to the reduction in SRP.

The response curves of bottom DO or hypolimnetic DO were very similar, except that hypolimnetic DO values were higher, especially with high P loads. Bottom DO and hypolimnetic DO were less sensitive to reduction in SRP loads than in TP loads.

Hypoxic areas were estimated based on DO values and Zhou et al's (2013) relationship. Model predicted hypoxic areas ranged from 0-6608 km^2 for different load scenarios. Depending on the approach to estimate DO values, TP loads needed to decrease more than 50% in order to keep the hypoxic area under 2000 km^2. Reduction in SRP load only cannot reach a goal of hypoxic area < 2000 km^2.

Uncertainty/sensitivity assessment

Our simulation showed large range with values in Chl a with high P loads, which indicated high uncertainty in predicting algal biomass with increased P loads. The difference between hypoxic area calculated from bottom DO and from hypolimnetic DO indicated that clear definitions of the metrics are needed.

5. Conclusions/recommendations

The model has been used in many studies on Lake Erie water qualities. It catches well the characteristics of chemical and biological processes. The model showed good simulations for 2008 data. The response curves showed that reduction in either SRP or TP would be effective to decrease algal biomass in the western basin. However, hypoxia only responded to changes in TP loads.

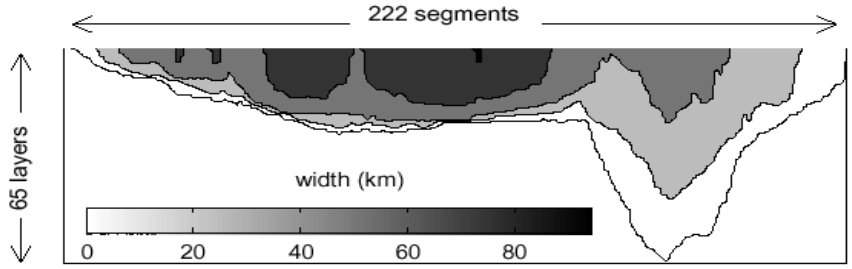

Figure B5-1: EcoLE's longitudinal-vertical resolution plane (longitudinal cross-section), showing width contours of 20 km intervals (from Boegman, 1999).

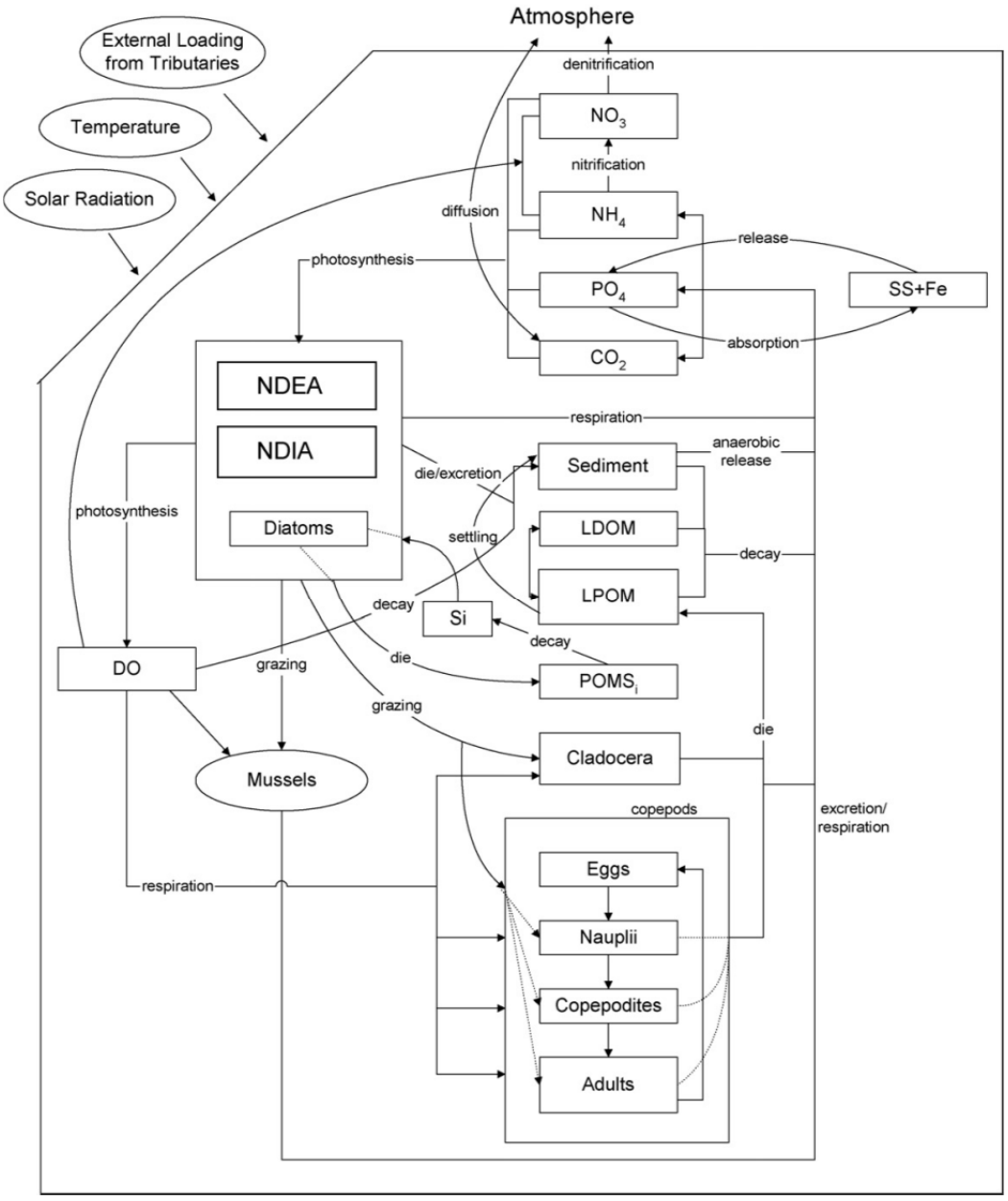

Figure B5-2: Model structure of the chemical and biological components of EcoLE (from Zhang et al., 2008, Fig 2.)

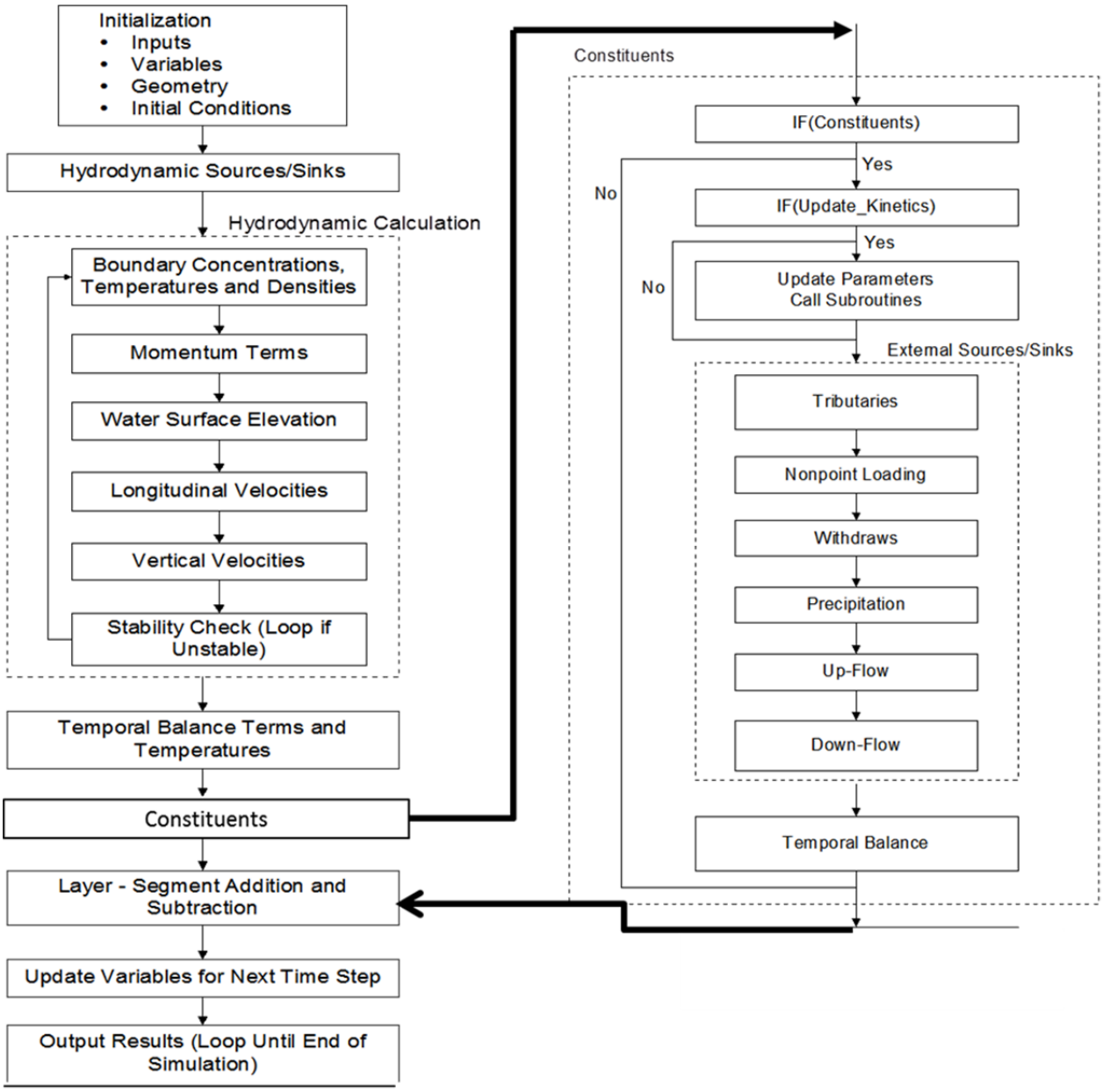

Figure B5-3: Flowchart of the model EcoLE (left panel), and detailed flowchart of the constituents (right panel), modified from Boegman (1999).

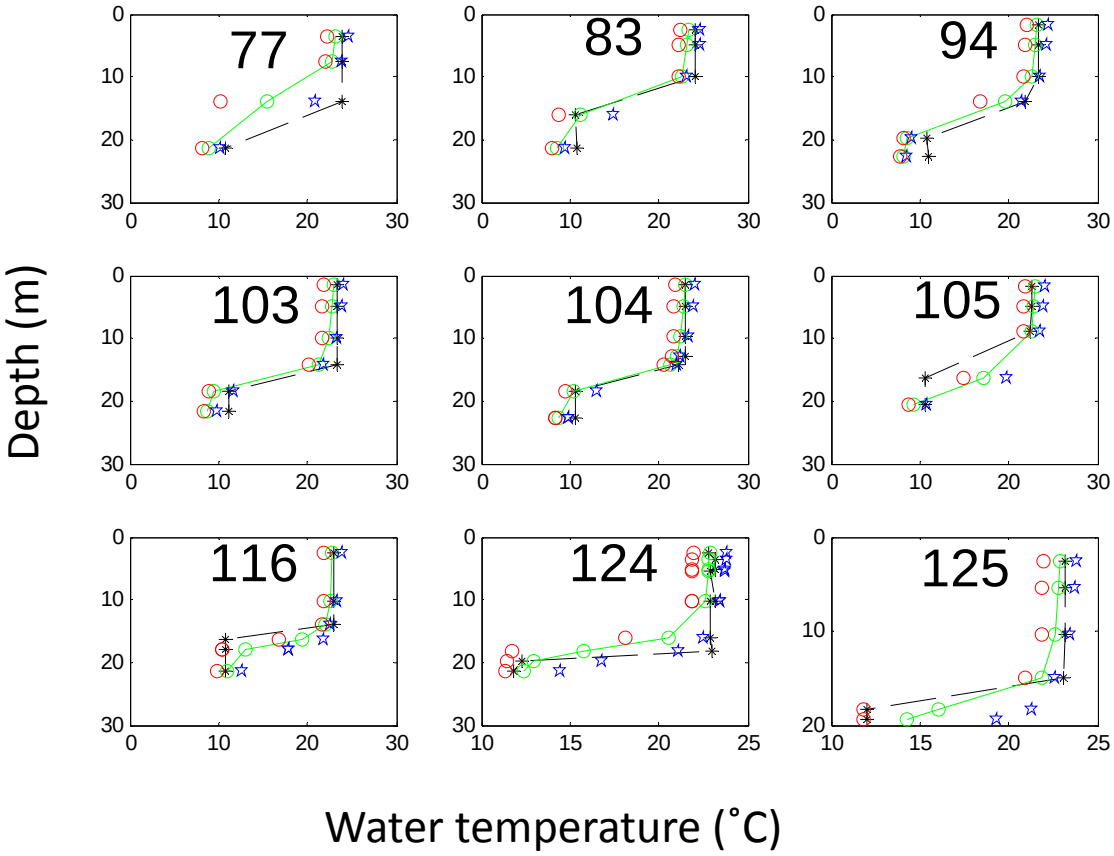

Figure B5-4: Comparison of water temperature between modeled and observations. Black lines are observations. Green lines are modeled water temperature that averaged between ± 10 days of the sampling dates. The red circles indicate the minimum water temperature predicted within the 20-day window. The blue stars indicate the maximum water temperature predicted within the 20-day window. The title numbers indicate the model segments.

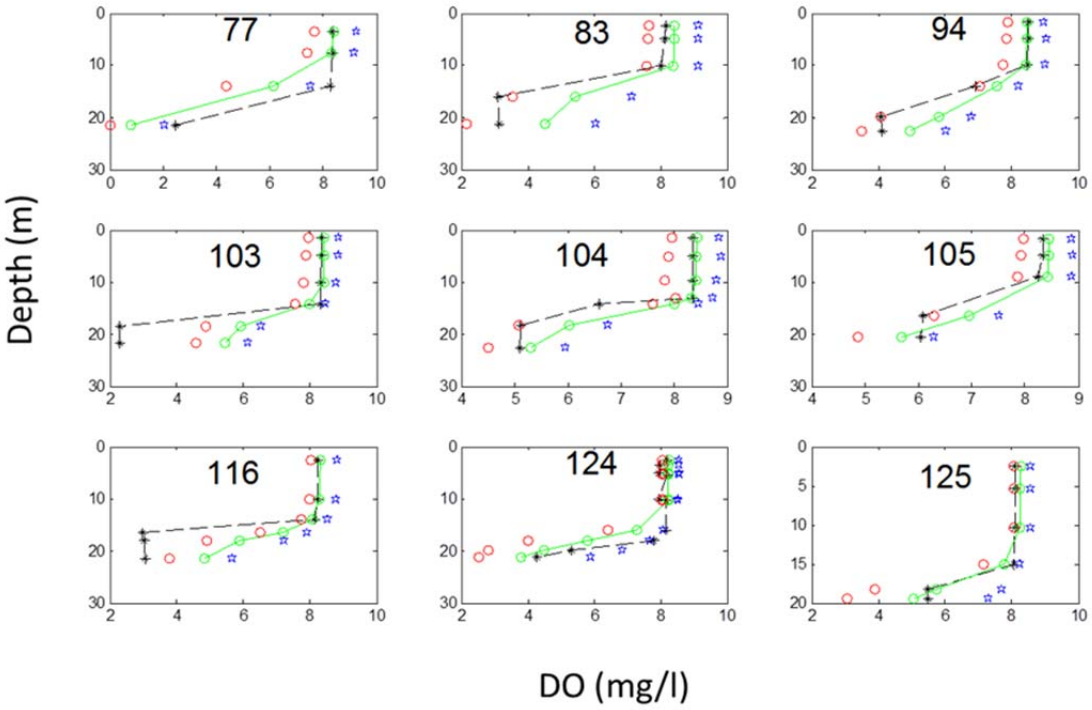

Figure B5-5: Comparison of DO between modeled and observations. Black lines are observations. Green lines are modeled DO that averaged between ± 10 days of the sampling dates. The red circles indicate the minimum DO predicted within the 20-day window. The blue stars indicate the maximum DO predicted within the 20-day window. The title numbers indicate the model segments.

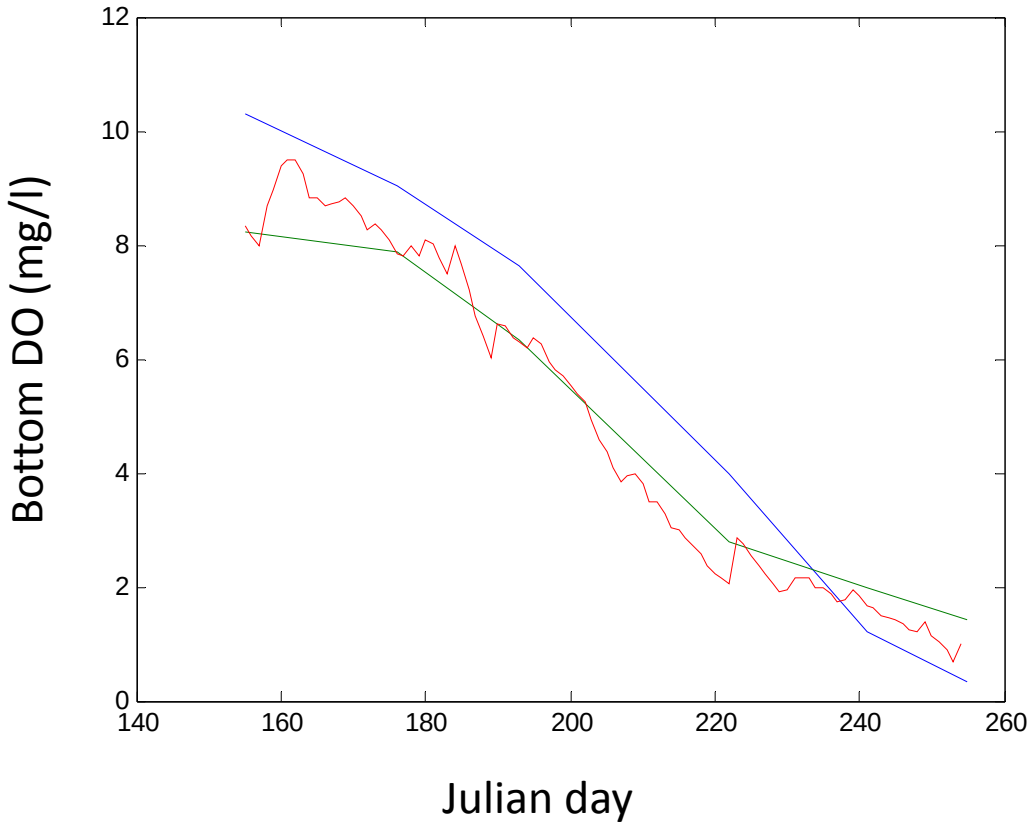

Figure B5-6: Comparison of bottom DO between EPA monitoring data (blue line) and the model predictions. Green line indicates the bottom DO averaged among the 10 EPA sampling stations, while the red line indicates the bottom DO averaged over the central basin.

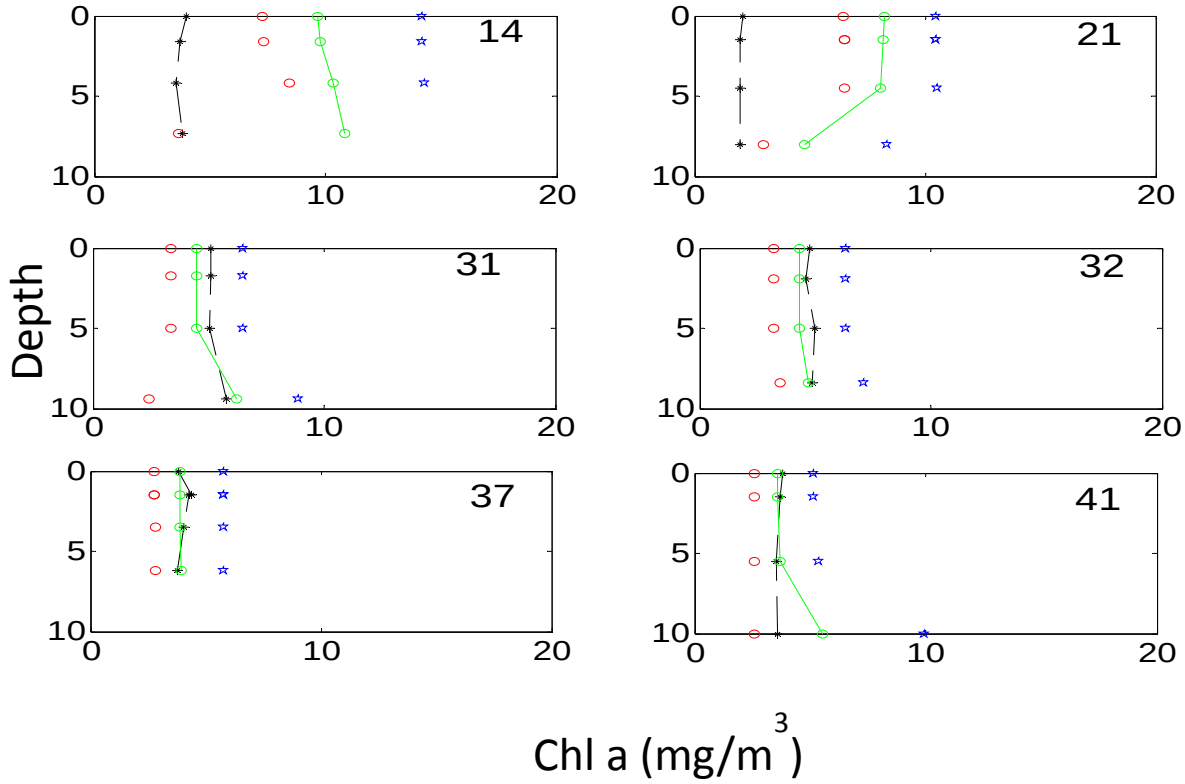

Figure B5-7: Comparisons of Chlorophyll a in the western basin between model simulations and observations. Black lines indicate the observation in August. Green lines are modeled Chl a that averaged between ± 10 days of the sampling dates. The red circles indicate the minimum Chl a predicted within the 20-day window. The blue stars indicate the maximum Chl a predicted within the 20-day window. The title numbers indicate the model segments.

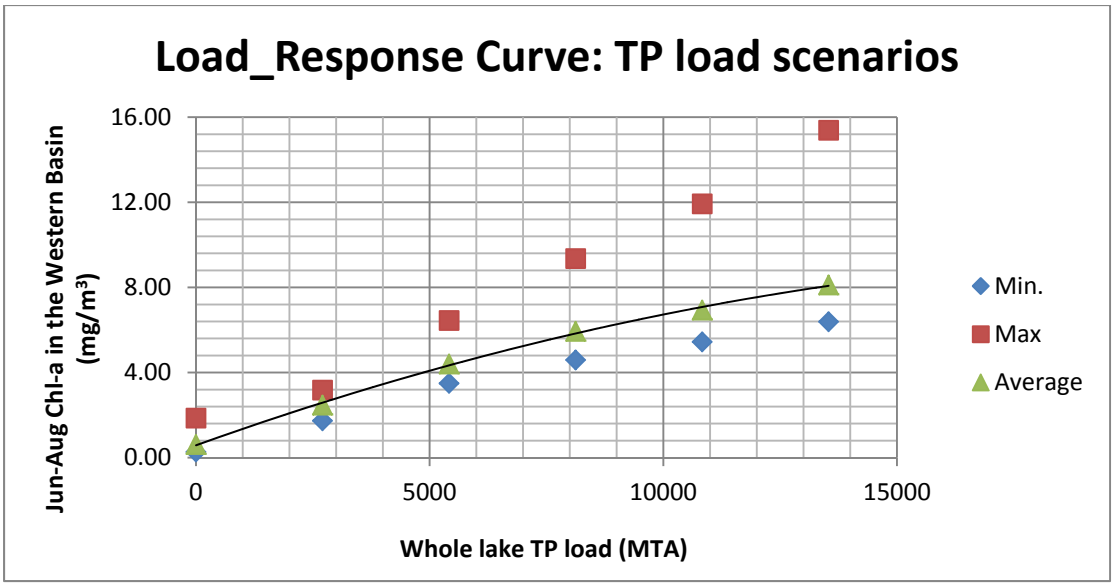

Figure B5-8: Changes in western basin-wide Chlorophyll a (averaged between June 1 to August 31 in the western basin) among different TP loading scenarios. Blue indicates the minimum daily Chl a, red indicates the maximum and green indicates the average over the period.

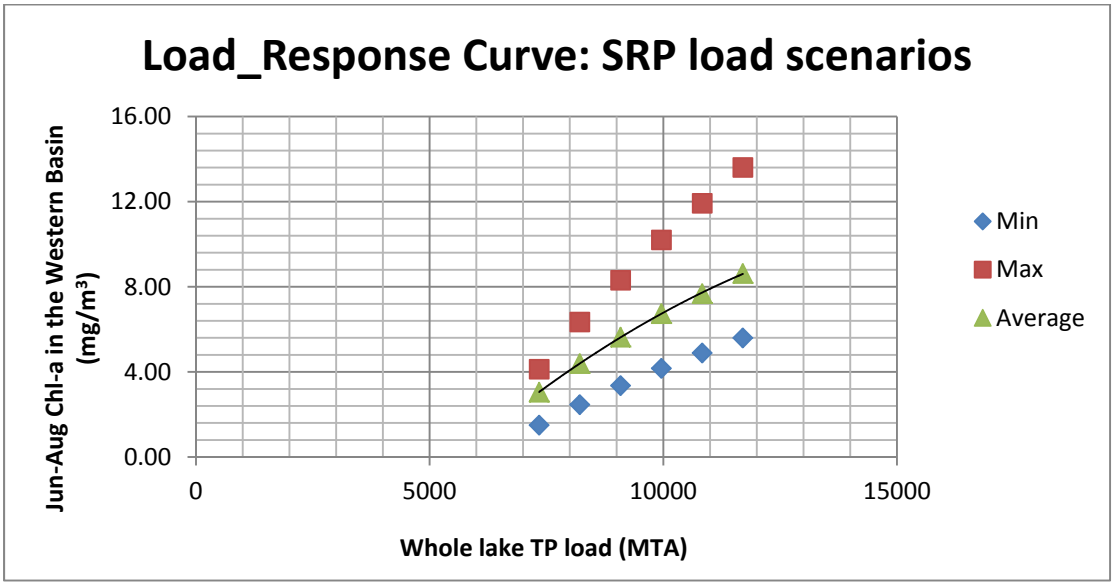

Figure B5-9: Changes in western basin-wide Chlorophyll a (averaged between June 1 to August 31 in the western basin) among different SRP loading scenarios. Blue indicates the minimum daily Chl a, red indicates the maximum and green indicates the average over the period.

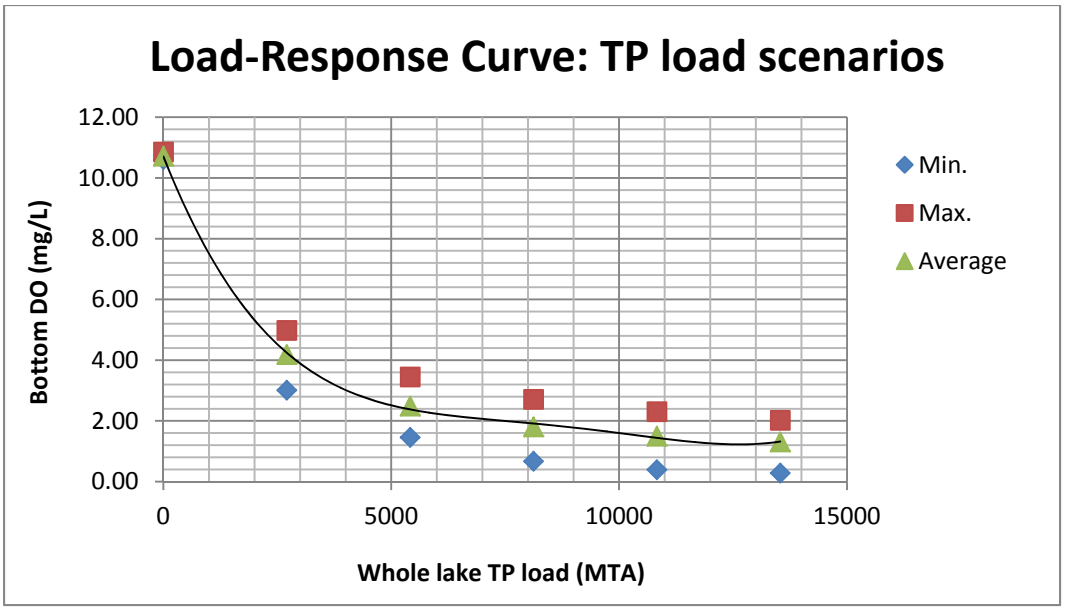

Figure B5-10: Changes in bottom DO (averaged between August 1 and September 30 in the central basin) among different TP loading scenarios. Blue indicates the minimum daily bottom DO, red indicates the maximum and green indicates the average over the period.

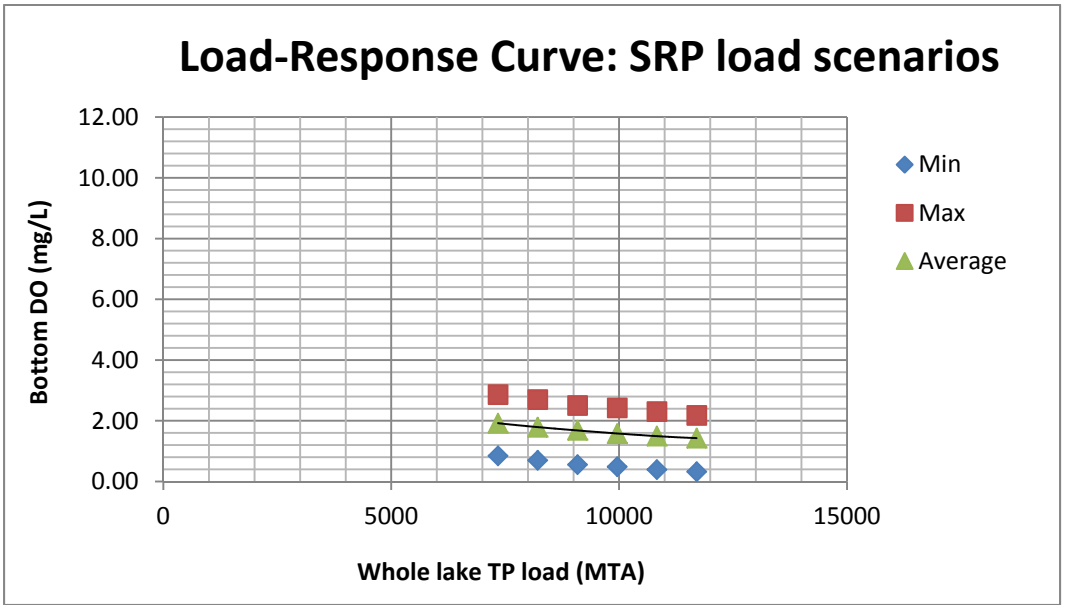

Figure B5-11: Changes in bottom DO (averaged between August 1 and September 30 in the central basin) among different SRP loading scenarios. Blue indicates the minimum daily bottom DO, red indicates the maximum and green indicates the average over the period.

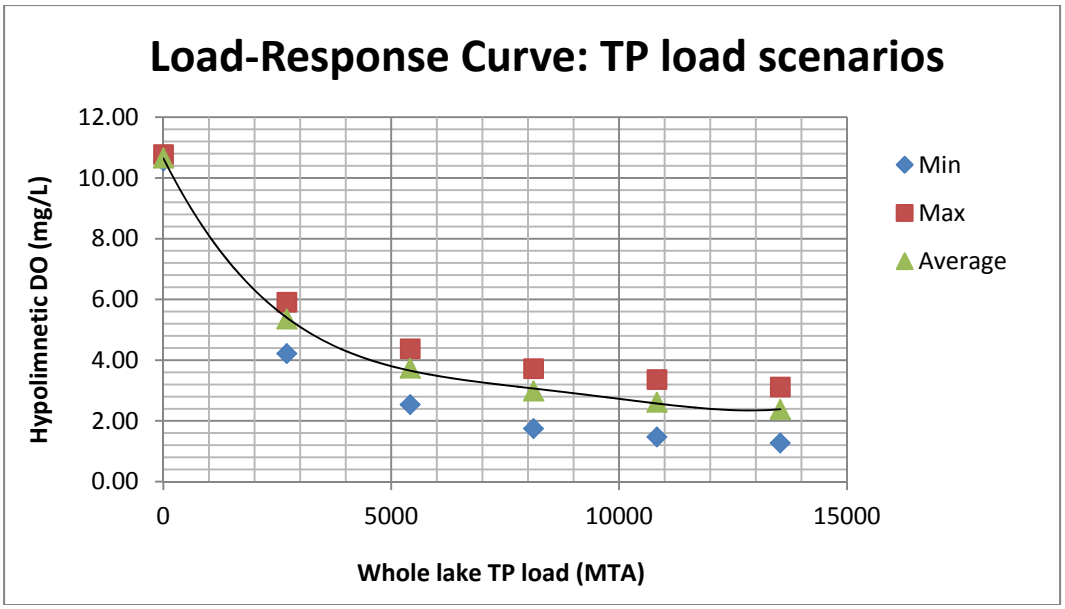

Figure B5-12:. Changes in hypolimnetic DO (averaged between August 1 and September 30 and over bottom layers of 1-3 m above sediment in the central basin) among different TP loading scenarios. Blue indicates the minimum daily hypolimnetic DO, red indicates the maximum and green indicates the average over the period.

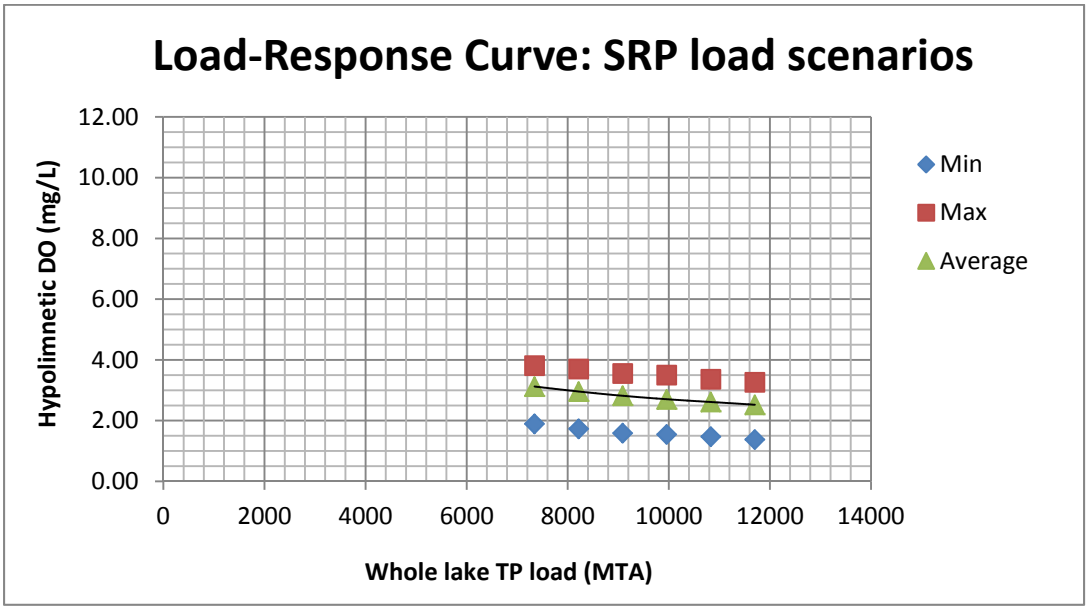

Figure B5-13: Changes in hypolimnetic DO (averaged between August 1 and September 30 and over bottom layers of 1-3 m above sediment in the central basin) among different SRP loading scenarios. Blue indicates the minimum daily hypolimnetic DO, red indicates the maximum and green indicates the average over the period.

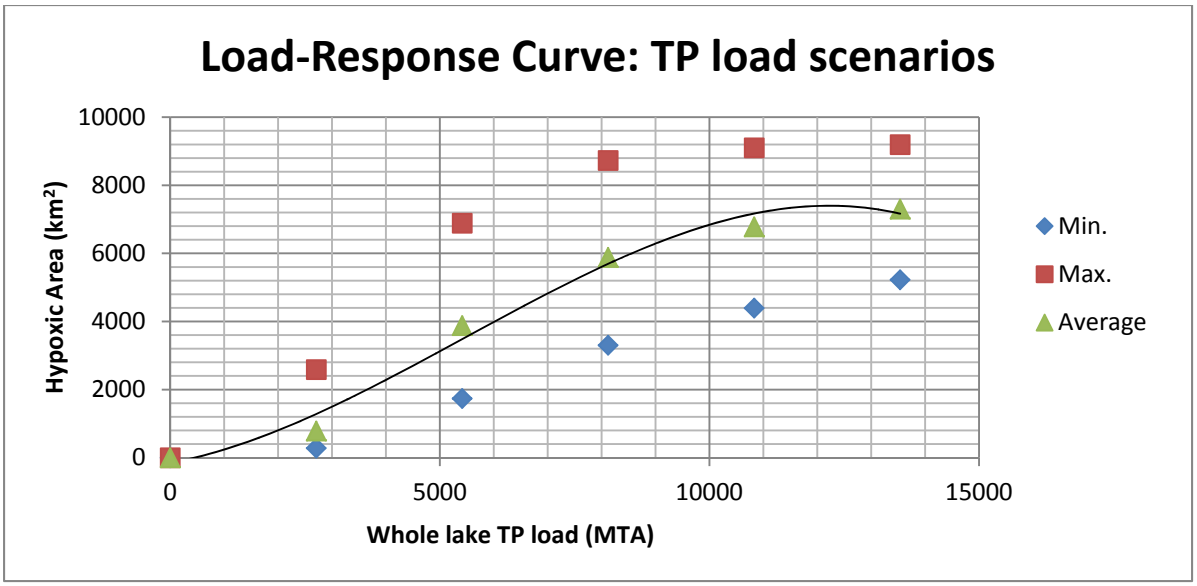

Figure B5-14: Changes in hypoxic area in the central basin among different TP loading scenarios. Hypoxic areas were calculated based on the bottom DO values (see Figure B5-10). Blue indicates the minimum daily hypoxic area, red indicates the maximum and green indicates the average over the period.

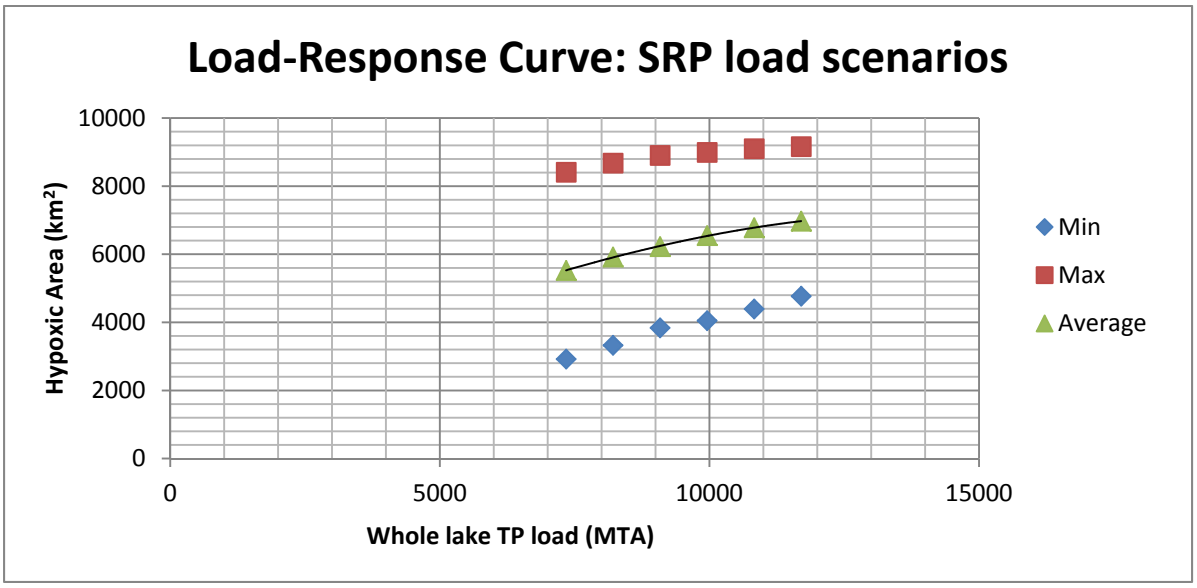

Figure B5-15: Changes in hypoxic area in the central basin among different SRP loading scenarios. Hypoxic areas were calculated based on the bottom DO values (see Figure B5-11). Blue indicates the minimum daily hypoxic area, red indicates the maximum and green indicates the average over the period.

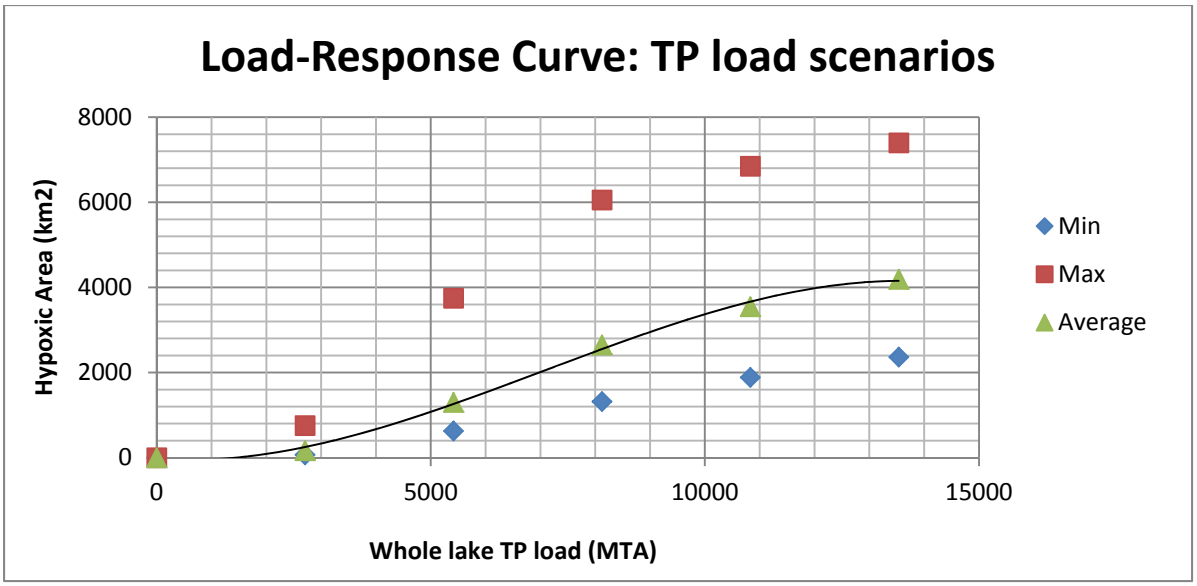

Figure B5-16: Changes in hypoxic area in the central basin among different TP loading scenarios. Hypoxic areas were calculated based on the averaged DO values of bottom 1-3 m water above sediment (see Figure B5-12). Blue indicates the minimum daily hypoxic area, red indicates the maximum and green indicate the average over the period.

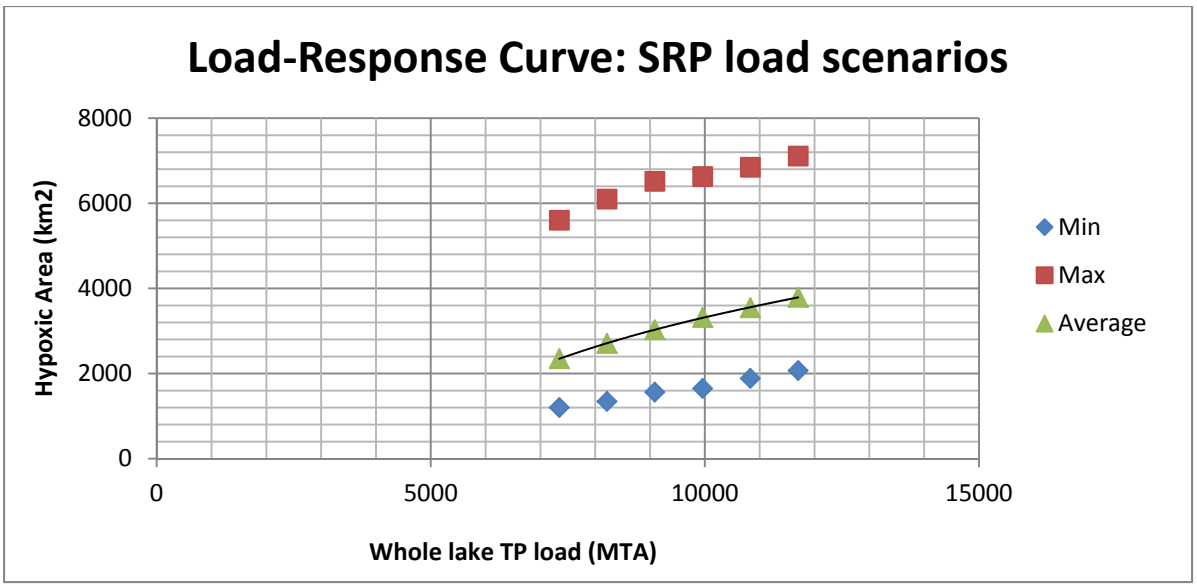

Figure B5-17: Changes in hypoxic area in the central basin among different SRP loading scenarios. Hypoxic areas were calculated based on the averaged DO values of bottom 1-3 m water above sediment (see Figure B5-13). Blue indicates the minimum daily hypoxic area, red indicates the maximum and green indicate the average over the period.

Table B5-1. A list of equations used in the EcoLE model developed in this study. a, equations from Cole and Buchak (1995); b, modified from Cole and Buchak (1995); c, modified from Scavia et al. (1988); d, from Fennel and Neumann (2003); e, this study; f, from Conroy et al. (2005b). From Zhang's (2006) Table 2.1.

Hydrodynamic equations[a]:

Horizontal momentum

$$\frac{\partial UB}{\partial t}+\frac{\partial UUB}{\partial x}+\frac{\partial WUB}{\partial z}=\frac{1}{\rho}\frac{\partial BP}{\partial X}+\frac{\partial\left(BA_x\frac{\partial U}{\partial x}\right)}{\partial x}+\frac{\partial B\tau_x}{\partial z},$$

$$\tau_x=-A_z\frac{\partial U}{\partial z}+\tau_{wx}e^{-2kz}$$

Constituent Transport

$$\frac{\partial B\Phi}{\partial t}+\underbrace{\frac{\partial UB\Phi}{\partial x}+\frac{\partial WB\Phi}{\partial z}}_{advection(x,z)}-\underbrace{\frac{\partial\left(BD_x\frac{\partial\Phi}{\partial x}\right)}{\partial x}-\frac{\partial\left(BD_z\frac{\partial\Phi}{\partial z}\right)}{\partial z}}_{diffusion(x,z)}=q_\Phi B-S_\Phi B$$

Free Water Surface Elevation

$$\frac{\partial B_\eta\eta}{\partial t}=\frac{\partial}{\partial x}\int_\eta^h UBdz-\int_\eta^h qBdz$$

Hydrostatic Pressure

$$\frac{\partial P}{\partial z}=\rho g$$

Continuity

$$\frac{\partial UB}{\partial x}+\frac{\partial WB}{\partial z}=qB$$

Equation of State

$$\rho=f\left(T_w,\Phi_{TDS},\Phi_{SS}\right)$$

Heat budget equation:

$$H_n=H_s+H_a+H_e+H_c-(H_{sr}+H_{ar}+H_{br})$$

Continued

Table B5-1, Continued

where,

U : longitudinal, laterally averaged velocity, m sec^{-1}

B : waterbody width, m

t : time, sec

x : longitudinal Cartesian coordinate: x is along the lake centerline at the water surface, positive to the right.

z : vertical Cartesian coordinate: z is positive downward

W : vertical, laterally averaged velocity, m sec^{-1}

ρ : density, kg m^{-3}

P : pressure, N m^{-2}

A_x : longitudinal momentum dispersion coefficient

τ_x : shear stress per unit mass resulting from the vertical gradient of the horizontal velocity.

τ_{wx} : surface shear due to wind along the x-axis of the model

A_z : the vertical eddy viscosity.

Φ : laterally averaged constituent concentration

D_x : longitudinal temperature and constituent dispersion coefficient

D_z : vertical temperature and constituent dispersion coefficient

q_Φ : lateral inflow or outflow mass flow rate of constituent per unit volume

S_Φ : kinetics source/sink term for constituent concentrations

B_η : time and spatially varying surface width, m

η : free water surface location

h : total depth

q : lateral boundary inflow or outflow, m^3 sec^{-1}

g : acceleration due to gravity, m sec^{-2}

$f(T, \Phi_{TDS,}, \Phi_{ss})$: density function dependent upon temperature, total dissolved solids or salinity, and suspended solids

H_n : net rate of heat exchange across the water surface

H_s : incident short wave solar radiation

H_a : incident long wave radiation

H_e : evaporative heat loss

H_c : heat conduction

H_{sr}: reflected short wave radiation

H_{ar}: reflected long wave radiation

H_{br}: back radiation from the water surface

T_s : water surface temperature

T_a : air temperature

Continued

Table B5-1, Continued

Equations of non-living constituents[b]

Inorganic suspended solids (Φ_{ss})

$$\frac{\partial \Phi_{ss}}{\partial t} = -\frac{\omega_{ss}}{\Delta z}\Phi_{ss}$$

Labile DOM (Φ_{ldom})

$$\frac{\partial \Phi_{ldom}}{\partial t} = \sum_j (K_{je}\Phi_j + (1-P_m)K_{jm}\Phi_j) - \gamma_{om}K_{ldom}\Phi_{ldom}$$

j: refers to non-diatom edible algae, non-diatom inedible algae and diatoms

Detritus (Φ_{lpom})

$$\frac{\partial \Phi_{lpom}}{\partial t} = \sum_j P_m K_{jm}\Phi_j - K_{lpom}\gamma_{om}\Phi_{lpom} - \frac{\omega_{lpom}}{\Delta z}\Phi_{lpom} + f_{Clpom}$$

Diatom detritus (Φ_{Dpom})

$$\frac{\partial \Phi_{Dpom}}{\partial t} = P_m K_{Dm}\Phi_D - K_{Dpom}\gamma_{om}\Phi_{Dpom} - \frac{\omega_{Dpom}}{\Delta z}\Phi_{Dpom} + f_{CDpom}$$

D: diatoms

Phosphorus (Φ_P)

$$\frac{\partial \Phi_P}{\partial t} = \sum_j (K_{jr} - K_{jg})\delta_P\Phi_j + K_{ldom}\delta_P\gamma_{om}\Phi_{ldom} + K_{lpom}\delta_P\gamma_{om}\Phi_{lpom}$$

$$+ K_{Dpom}\delta_P\gamma_{om}\Phi_{Dpom} + \frac{S_P A_s}{\Delta V} + f_{mP} + f_{CP}$$

Ammonium-Nitrogen (Φ_{NH4})

$$\frac{\partial \Phi_{NH4}}{\partial t} = \sum_j (K_{jr}\Phi_j\delta_N - K_{jg}\Phi_j\delta_N P_{NH4}) + K_{ldom}\delta_N\gamma_{om}\Phi_{ldom} + K_{lpom}\delta_N\gamma_{om}\Phi_{lpom}$$

$$+ K_{Dpom}\delta_N\gamma_{om}\Phi_{Dpom} + \frac{(S_{od}\delta_N/\delta_{om} + S_{NH4})A_s}{\Delta V} + K_{NO3}\gamma_{NO3}\Phi_{NO3} - K_{NH4}\gamma_{NH4}\Phi_{NH4} + f_{mNH4} + f_{CNH4}$$

Continued

Table B5-1, Continued

Nitrate-Nitrogen (Φ_{NO3})

$$\frac{\partial \Phi_{NO3}}{\partial t} = K_{NH4}\gamma_{NH4}\Phi_{NH4} - K_{NO3}\gamma_{NO3}\Phi_{NO3} - \sum_i (K_{ig}\Phi_i\delta_N(1-P_{NH4}))$$

Silicon (Φ_{Si})

$$\frac{\partial \Phi_{Si}}{\partial t} = K_{Dpom}\gamma_{om}\delta_{Si}\Phi_{Dpom} + \frac{(S_{od}\delta_{Si}/\delta_{om} + S_{Si})A_s}{\Delta V} - K_{Dg}\delta_{Si}\Phi_D$$

Dissolved Oxygen (Φ_{DO})

$$\frac{\partial \Phi_{DO}}{\partial t} = \sum_j (K_{jg} - K_{jr})\delta_{om}\Phi_j - K_{NH4}\delta_{NH4}\gamma_{NH4}\Phi_{NH4} - K_{lpom}\delta_{om}\gamma_{om}\Phi_{lpom}$$

$$- K_{Dpom}\delta_{om}\gamma_{om}\Phi_{Dpom} - \frac{S_{od}/\delta_{om}A_s}{\Delta V} - K_{ldom}\gamma_{om}\delta_{om}\Phi_{ldom} - A_{kt}E_o(\Phi'_{DO} - \Phi_{DO}) - f_{mO} - f_{CO}$$

where, Φ_i = concentration of variable i, g m^{-3}

Δz = model cell thickness, m

P_m = proportional of dead algae contributed to particulate organic matter.

K_i = kinetic rates, sec^{-1}

γ_i = temperature rate multipliers

δ_i = stoichiometric coefficients

A_s = sediment area, m^2

ω_i = sinking rates, m sec^{-1}

ΔV = model cell volume, m^3

S_i = sediment release rates, g m^{-2} sec^{-1}

f_{Ci} =impact of crustacean activities on variable i, g m^{-3} sec^{-1}

f_{mi} = impact of mussels activities on variable i, g m^{-3} sec^{-1}

P_{NH4} = ammonium preference factor

$$S_{od} = S_{od\max}\frac{\Phi_{DO}}{\Phi_{DO} + O_h}\theta^{(T-20)}$$

$S_{od\max}$: maximum sediment oxygen demand at 20°C, g O_2 m^{-2} d^{-1},

O_h : oxygen concentration half-saturation constant, g O_2 m^{-3}.

Equations of phytoplankton[b]

Diatoms (Φ_D):

$$\frac{\partial \Phi_D}{\partial t} = K_{Dg}\Phi_D - K_{Dr}\Phi_D - K_{De}\Phi_D - K_{Dm}\Phi_D - \frac{\omega_D}{\Delta z}\Phi_D - f_{mD} - f_{CD}$$

Continued

Table B5-1, Continued

Non-diatom edible algae (Φ_{NDEA}):

$$\frac{\partial \Phi_{NDEA}}{\partial t} = K_{NDEAg}\Phi_{NDEA} - K_{NDEAr}\Phi_{NDEA} - K_{NDEAe}\Phi_{NDEA} - K_{NDEAm}\Phi_{NDEA}$$

$$- \frac{\omega_{NDEA}}{\Delta z}\Phi_{NDEA} - f_{mNDEA} - f_{CNDEA}$$

Non-diatom inedible algae (Φ_{NDIA}):

$$\frac{\partial \Phi_{NDIA}}{\partial t} = K_{NDIAg}\Phi_{NDIA} - K_{NDIAr}\Phi_{NDIA} - K_{NDIAe}\Phi_{NDIA} - K_{NDIAm}\Phi_{NDIAm} - \frac{\omega_{NDIA}}{\Delta z}\Phi_{NDIA}$$ **Auxiliary functions:**

Growth rates:

$$K_{ig} = \gamma_{ir}\gamma_{if}\lambda_{i\min}K_{ig\max}$$

Dark respiration rates:

$$K_{ir} = \gamma_{ir}K_{ir\max}$$

Photorespiration rates:

$$K_{ie} = \gamma_{ir}\gamma_{if}\lambda_{i1}K_{ie\max}$$

Mortality rates:

$$K_{im} = \gamma_{ir}\gamma_{if}K_{im\max}$$

Limiting factor (light):

$$\lambda_{i1} = \frac{I}{I_{is}}e^{(-\frac{I}{I_{is}}+1)}$$

Limiting factor (phosphorus or nitrogen):

$$\lambda_{ij} = \frac{\Phi_j}{P_{ij} + \Phi_j}$$

Ammonium preference factor:

$$P_{NH4} = \Phi_{NH4}\frac{\Phi_{NOx}}{(K_{NH4} + \Phi_{NH4})(K_{NH4} + \Phi_{NOx})} + \Phi_{NH4}\frac{K_{NH4}}{(\Phi_{NH4} + \Phi_{NOx})(K_{NH4} + \Phi_{NOx})}$$

where *i* = diatoms, non-diatom edible algae or non-diatom inedible algae

γ_r = temperature rate multiplier for rising limb of curve

γ_f = temperature rate multiplier for falling limb of curve

$\lambda_{\min}$ = multiplier for limiting growth factor (minimum of light, phosphorus and nitrogen)

I_s = saturating light intensity at maximum photosynthetic rate, W m^{-2}

Continued

Table B5-1, Continued

$K_{g\max}$ = maximum algal growth rate, s^{-1}

K_{rmax} =maximum dark respiration rate, sec^{-1}

$K_{e\max}$ = maximum excretion rate constant, sec^{-1}

K_{mmax} = maximum mortality rate, sec^{-1}

I = available light, W m^{-2}

Φ_j = phosphorus or nitrate+ammonium concentration or silicon, g m^{-3}

P_j = half-saturation coefficients for phosphorus or nitrate+ammonium, or silicon, g m^{-3}

K_{NH4} = ammonia preference half-saturation coefficient, g m^{-3}, 0.01

Equations of Cladocerans[c]

$$\frac{dZ}{dt} = (Ag - r - s)Z - P$$

where, A is assimilation rate

g is ingestion rate

$$g = g_{\max}\frac{F}{K+F}$$

g_{max} is the maximal weight-specific ingestion rate.

K is the half-saturation constant.

F is the weighted combination of algae and detritus.

r is respiration loss, which consists of a basic value and a portion that proportional to the food function. i.e. $r = (r_1 + r_2\frac{F}{K+F})\theta^{(T-20)}$

s is the loss of starvation, $s = s_0 \min(1,1-\frac{g}{g_s})$,

P is the predation loss. $P = p_0(\frac{Z}{Z_h+Z})Z$

Equations of Copepods[d]

Populations:

$$\frac{dZ_e}{dt} = T_{ae}Z_a - T_{en}Z_e - \mu_e Z_e$$

$$\frac{dZ_n}{dt} = T_{en}Z_e + (g_n - l_n - \mu_n)Z_n - T_{nc}Z_n$$

Continued

Table B5-1, Continued

$$\frac{dZ_c}{dt} = T_{nc}Z_n + (g_c - l_c - \mu_c)Z_c - T_{ca}Z_c$$

$$\frac{dZ_a}{dt} = T_{ca}Z_c + (g_a - l_a - \mu_a)Z_a - T_{ae}Z_a$$

Auxiliary functions:

Ingestion rate:

$$g_i = \beta_0 e^{(\alpha T)}(1 - e^{(-I_i^2 F^2)})\, f(m_i, X_i)$$

Reproduction:

$$T_{ae} = (\frac{1}{2})0.3 g_a$$

Hatching rate:

$$T_{en} = h\theta(T - T_0)\exp(a(T - T_0))$$

Transfer rates to the next stage:

$$T_{i,i+1} = g_i\, f(< m_i >, m_i)$$

Food function:

$$F = \Phi_G + 0.5 * \Phi_D + 0.2 * \Phi_{dt}$$

Fermi function:

$$f(x, y) = \frac{1}{1 + \exp(\frac{20}{y}(x - y))}$$

where, Z_i = total biomass of stage i.

μ_i = mortality rate per day

l_i = egestion rates per day, a portion of ingestion,

m_i = individual weight of stage i

X_i = critical individual weight

$<m_i>$ = molting weight

Activity functions of mussels and crustacean zooplankters[e]

Detritus:

$$f_{Cdt} = ((1 - A)g\frac{\Phi_{NDEA} + 0.5 * \Phi_D}{K + F} - Ag\frac{0.5 * \Phi_{lpom}}{K + F})Z_{cladoceran} + \sum_i^{copepod}(l_i - g_i\frac{0.2 * \Phi_{lpom}}{K + F})Z_i$$

Continued

Table B5-1, Continued

Excretion of crustaceans:

$$f_{CP} = \delta_{P-clad} rm_{cladoceran} + \sum_{i}^{copepod} \delta_{P-cop} rm_i$$

$$f_{CNH4} = \delta_N rZ_{cladoceran} + \sum_{i}^{copepod} \delta_N rm_i$$

Excretion of dreissenid mussels[f] (ZMP, QMP, MNH4):

$$\log_{10}(ZMP) = 0.505[\log_{10}(W_{zm})] - 1.172$$

$$\log_{10}(QMP) = 0.297[\log_{10}(W_{qm})] - 1.195$$

$$\log_{10}(MNH_4) = 0.379[\log_{10}(W_m)] + 0.021$$

$$f_{zmP} = W_{zm} N_{zm} ZMP$$

$$f_{qmP} = W_{qm} N_{qm} QMP$$

$$f_{mNH4} = W_m N_m MNH_4$$

Oxygen consumption:

$$f_{CO} = \delta_{om} rZ_{cladoceran} + \sum_{i}^{copepod} \delta_{om} rm_i$$

$$f_{mO} = \varepsilon_O W_{mussel} N_{mussel}$$

where,

δ_i = stoichiometric equivalent between nutrient and dry weight biomass.

ε_O = oxygen consumption rate of mussels, g $g^{-1}s^{-1}$

W_{mussel}= individual dry weight of mussels, g.

N_{mussel}= density of mussels, # m^{-3}, areal density divided by depth of the water

Table B5-2. SODmax values used in EcoLE for different load scenarios, which was scaled up and down using Rucinski et al's (2014) relationship between SOD and TP loads

P scenario	Rucinski's ($g/m^2/d$)	EcoLE used ($g/m^2/d$)
Baseline	0.723	0.84
TP00	0	0
TP25	0.405	0.470
TP50	0.573	0.666
TP75	0.665	0.773
TP125	0.763	0.886
SRP00	0.643	0.747
SRP25	0.667	0.775
SRP50	0.689	0.800
SRP75	0.707	0.821
SRP125	0.738	0.857

6. References

Boegman, L. 1999. Application on a two-dimensional hydrodynamic and water quality model to Lake Erie. University of Toronto, Toronto, Canada.

Boegman, L., M. R. Loewen, D. A. Culver, P. F. Hamblin, and M. N. Charlton. 2008a. Spatial-dynamic modeling of algal biomass in Lake Erie: Relative impacts of dreissenid mussels and nutrient loads. Journal of Environmental Engineering-Asce **134**:456-468.

Boegman, L., M. R. Loewen, P. F. Hamblin, and D. A. Culver. 2001. Application of a two-dimensional hydrodynamic reservoir model to Lake Erie. Can. J. Fish. Aquat. Sci. **58**:858-869.

Boegman, L., M. R. Loewen, P. F. Hamblin, and D. A. Culver. 2008b. Vertical mixing and weak stratification over zebra mussel colonies in western Lake Erie. Limnol. Oceanogr **53**:1093-1110.

Cole, T. M., and E. M. Buchak. 1995. CE-QUAL-W2: a two dimensional, laterally averaged, hydrodynamic and water quality model, version 2.0: User manual. US Army Corps of Engineers, Washington, DC.

Conroy, J. D., L. Boegman, H. Y. Zhang, W. J. Edwards, and D. A. Culver. 2011. "Dead Zone" dynamics in Lake Erie: the importance of weather and sampling intensity for calculated hypolimnetic oxygen depletion rates. Aquatic Sciences **73**:289-304.

Rucinski, D. K., J. V. DePinto, D. Scavia, and D. Beletsky. 2014. Modeling Lake Erie's hypoxia response to nutrient loads and physical variability. Journal of Great Lakes Research.

Zhang, H. 2006. Ecological modeling of the lower trophic levels of Lake Erie. The Ohio State University, Columbus, OH, USA.

Zhang, H., D. A. Culver, and L. Boegman. 2008. A two-dimensional ecological model of Lake Erie: Application to estimate dreissenid impacts on large lake plankton populations. Ecological Modelling **214**:219-241.

Zhang, H., D. A. Culver, and L. Boegman. 2011. Dreissenids in Lake Erie: an algal filter or a fertilizer? Aquatic Invasions **6**:175-194.

Zhou, Y. T., D. R. Obenour, D. Scavia, T. H. Johengen, and A. M. Michalak. 2013. Spatial and Temporal Trends in Lake Erie Hypoxia, 1987-2007. Environmental Science & Technology **47**:899-905.

APPENDIX B-6: Lake Erie Nine-Box Model

Craig McCrimmon, Luis Leon, and Ram Yerubandi, S&T/WHERD/Integrated Modelling
Environment Canada

Acknowledgements
The authors thank Environment Canada Star database cruise leaders (Bourbonniere, Marvin, Watson, Wilhelm, and Yerubandi) for the 2008 cruise temperature, DO, TP and SRP data.

1. Model Description

Overview

The NWRI 9-box model (Lam et al., 1983, Lam et al., 1987) divides Lake Erie into nine boxes consisting of the west, central and eastern basins in the horizontal and three thermal stratification layers in the vertical dimension. For simplicity, it is assumed that the west basin is fully mixed. Figure B6-1 shows a schematic of the major physical processes parameterized in the model and Figure B6-2 shows the biochemical sub-model. The physical processes (Figure B6-1) used in the model include the hydraulic flows, i.e. the Detroit River inflow, the Niagara outflow, the inter-basin transport, vertical entrainment processes due to thermal stratification, water level changes, turbulent diffusion and water temperature. The variables (Figure B6-2) used in the model are: soluble reactive phosphorus (SRP), organic phosphorus (OP), and dissolved oxygen (DO). The total phosphorus (TP) can be calculated as TP = SRP + OP, and the particulate phosphorus can be obtained from the empirical formula (Lam et al., 1987). During the scenario runs of this study, the model did not produce reasonable results for the -100% TP load scenario. The original model was never tested for such a scenario with such small phosphorous concentrations. The cause of the problem was related to the calculation of PP as a function of OP which was originally "hard coded" in the model as PP = OP – 0.005 (mg/L). This relationship requires a minimum OP of 0.005 mg/L so is not applicable for the small OP concentrations we get during low load scenarios. Data was extracted from the Environment Canada StarDatabase and it was found the relationship for low OP concentrations can be approximated as PP=0.7 * OP (R^2=0.68), which does not require a minimum OP concentration. The biological and chemical processes include the uptake and respiration of nutrient/planktons, the settling of particulate phosphorus, the aeration of surface waters, the anoxic regeneration of phosphorus from sediment, and the physical resuspension of phosphorus due to wind-wave actions. The model includes the factors of water temperature, nutrients and light attenuation in photosynthesis, but it does not separate the phytoplankton into different subspecies. For a detailed discussion of these processes, the reader is referred to Lam et al. (1987). Model inputs and outputs are daily and extend from day 1 to 365 for the selected year.

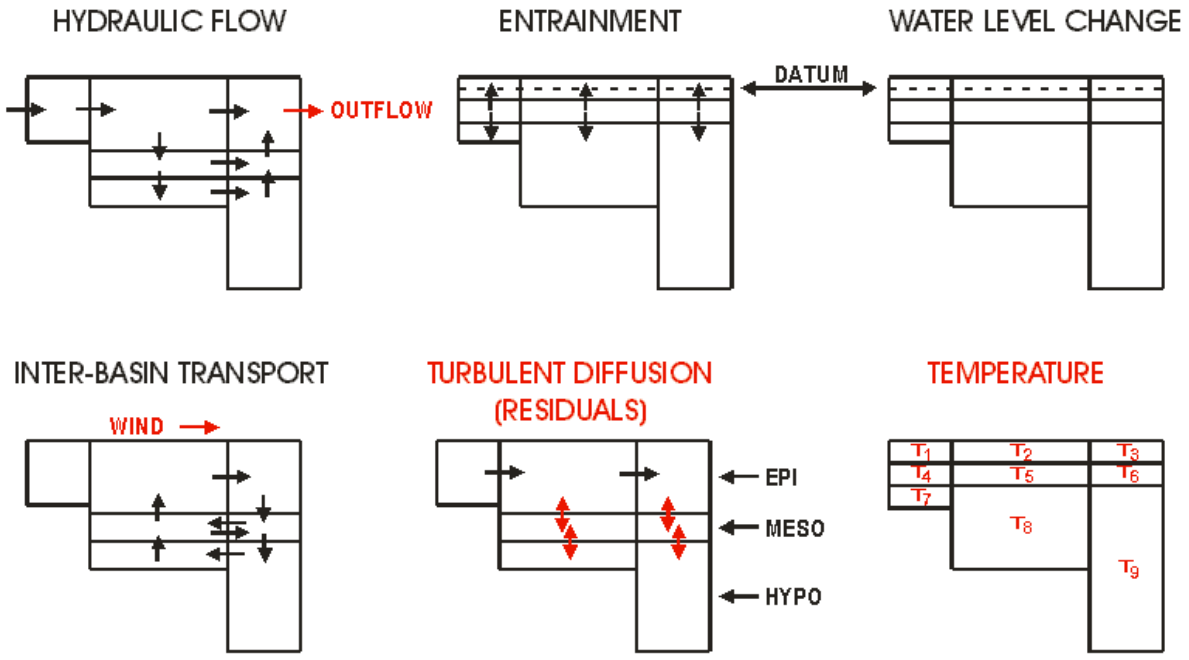

Figure B6-1: Schematic of the major physical processes parameterized in the NWRI nine-box model of Lake Erie (Lam et. al., 1987)

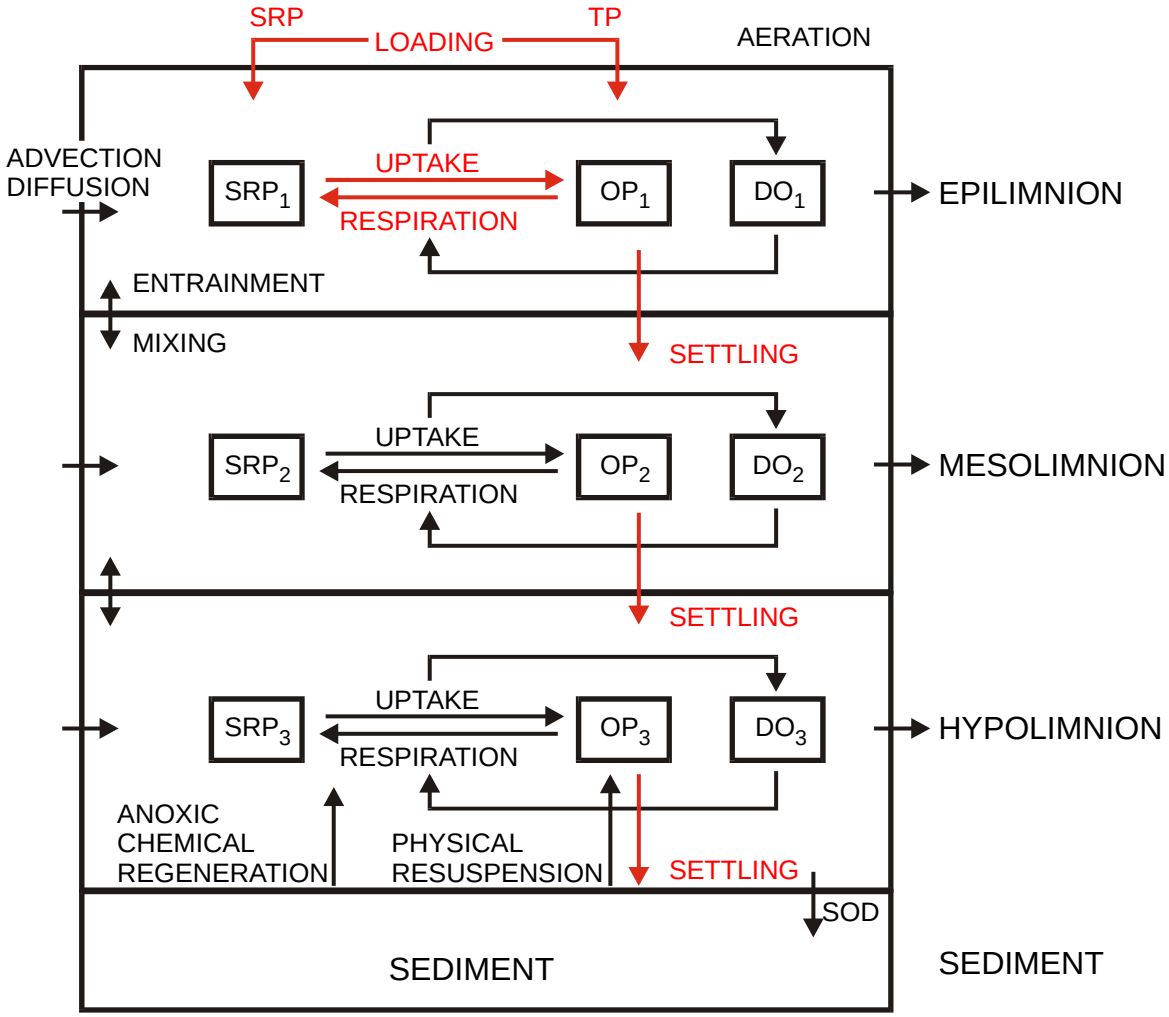

Figure B6-2: Schematic of the NWRI nine-box plankton–nutrient–dissolved oxygen sub-model (Lam et. al., 1987) showing processes in a vertical water-sediment column: Soluble Reactive Phosphorus (SRP), Organic Phosphorus (OP), Dissolved Oxygen (DO), Total Phosphorus (TP) and Sediment Oxygen Demand (SOD)

The model has been verified and validated over 16 years of data (1967-82) (Lam et al., 1987). Possible short comings of the model are that most of previous work was for years before zebra mussels which could affect processes such as settling, resuspension, and production ratios. Also, the model is based on basin averages so it is not possible to analyze differences between near-shore and off-shore.

2. Data – Input and Evaluation

The sources of input data included the following:

- Daily OP and SRP external loads: Detroit River used the CAEDYM input file; west, central and east basins used Node values.

- Daily box temperatures, vertical diffusion between layers, thermocline depths were computed using the observed temperature profile loggers (Yerubandi)

- Daily box light factors were calculated using thermocline depths (see above), average vertical extinction and daily solar radiation (Lake Erie met. buoy, Yerubandi)

- Daily wind speed: met. buoy (Yerubandi)

- Daily lake average water level: observed monthly average (NOAA)

- Daily Detroit and Niagara river flow rates: CAEDYM input files

- Initial box concentrations (January 1):

    - First run: TP and SRP basin averages from the earliest cruise (Feb. 14, 2008 from EC StarDatabase), DO assumed at saturation using water temperatures.

    - The full effects of loading changes could not be seen with a one year simulation since the time of residence for Lake Erie is almost 3 years. To better capture the effects of loading changes for each loading scenario, the 9-box model was essentially run for three years for 2008: the end of first year concentrations were used as the initial concentrations for the second year run etc. It was found that after the third year the concentrations initial / final concentrations reach equilibrium.

3. Calibration / Evaluation

Evaluation data for the base case 2008 included DO, TP, and SRP box averages and maximum/minimum (for each layer and basin) computed for each GLENDA and Environment Canada StarDatabase cruise. For the Annex4 2008 simulations, the initial thought was to maintain the nine-box model parameter coefficients mostly unchanged from previous Lake Erie modeling (Lam et al., 1983, 1987, 2007) including the SOD rate for the whole hypolimnion box (0.15 g/m2/d). The only calibration made for this study was increasing the bottom layer settling rate from 0.4 to 0.5 m/d to better match the east basin bottom layer. This change is in line with recommendations to account for *Dreissena* (Lam et al., 2007).

4. Application Results

Load Response Curves

Load Response curves were developed using the following steps:

- Adjusting the SRP and TP daily loads for the Detroit River, and W, C, and E basins. The scenarios include the base case, +25%, -25%, -50%, -75%, and -100% load.

- Adjusting SOD. The base case maintains the original SOD of 0.15 g/m2/d. The -100% TP loading scenario (zero load) set SOD = 0. $g/m^2/d$. The SOD rates for the other load scenarios were adjusted using linear interpolation/extrapolation between the base case (loading 10,750 MTA with SOD 0.15 g/m2/d) and the -100% TP loading case (loading of 0 MTA and SOD 0.0 g/m2/d). The resulting values are shown in Table B6-1.

- Extract model results: August average and August-September averages concentrations were both extracted for DO for the central basin bottom layer, and for TP and SRP for the west basin,

and central and east basin top and bottom layers. Results were copied to an excel spreadsheet and response curves were plotted.

The following plots were produced using the 9-box model for the different loading scenarios. The 9-box model allows for input loads for SRP and TP, where TP is the sum of OP and SRP, and include loads for the Detroit River, and west (W), central (C) and east (E) basins. The base case loadings were determined using node values from the Annex 4 CTools files:

- 052913_EcoForeNodes_CY2008_TP_DMD_Final.xlsx
- 052813_EcoForeNodes_CY2008_DRP_DMD_Final.xlsx

The "TP Load Scenarios" include percent changes to SRP and TP.
The "SRP Load Scenarios" include only percent changes to SRP load, and do not include changes to OP. TP load is adjusted to account for the change in SRP. The range of TP load for these scenarios will be narrower than the "TP Load Scenarios" since only SRP is changed.
The scenarios include the base case, +25%, -25%, -50%, -75%, and -100%.
The 9-box model input coefficients were mostly unchanged from previous work, i.e. Lam et al. 1987, including the SOD rate of 0.15 (DO g/m2/d) for the base case. The only calibration modification was to change the settling rate for the bottom layer from 0.4 to 0.5 m/d to better simulate bottom layer TP.
The SOD rates for each load scenario were adjusted using linear interpolation/extrapolation between the base case (loading 10,750 MTA with SOD 0.15 g/m2/d) and the -100% TP loading case (loading of 0 MTA and SOD 0.0 g/m2/d). The resulting values are shown Table B6-1.

Table B6-1: 9-box Scenario SOD rates

TP Scenario	SOD (g/m2/d)	SRP Only Scenario	SOD (g/m2/d)
TP+25% (increase SRP and OP)	0.188	SRP+25%	0.162
base case	0.150	base case	0.150
TP-25% (decrease SRP and OP)	0.113	SRP-25%	0.138
TP-50% (decrease SRP and OP)	0.075	SRP-50%	0.126
TP-75% (decrease SRP and OP)	0.038	SRP-75%	0.114
TP-100% (decrease SRP and OP)	0.0	SRP-100%	0.102

The full effects of loading changes could not be seen with a one year simulation, as expected, since the time of residence for Lake Erie is almost 3 years. To better capture the effects of loading changes for each loading scenario, the 9-box model was run for 2008 repeatedly until equilibrium was reached: the end of first year concentrations were used as the initial concentrations for the second year run, and the end of the second run was used as the initial conditions of the third run. After the second year some parameters last day concentrations were still more than 5% different than the previous years, i.e. had not reached steady state: typically the DO is steady state as well as P in W basin, but the P was up to 4% different in C basin and 8% in E basin and for the -100% load scenario the P in C basin was 16% and E basin was 23% different. The third year run resulted in steady state conditions for all scenarios and used for scenario developments.

The following plots are the 2008 base case showing 9-box simulation, overlapping all 3 year runs, and observed values. Note for most plots the 2nd and 3rd year runs (black and red lines, respectively) are mostly the same. The observations average, maximum and minimum are included for comparison with the first year run (blue lines).Typically the equilibrium TP and SRP are much lower than the first year run, in the early months but similar later in the summer and fall.

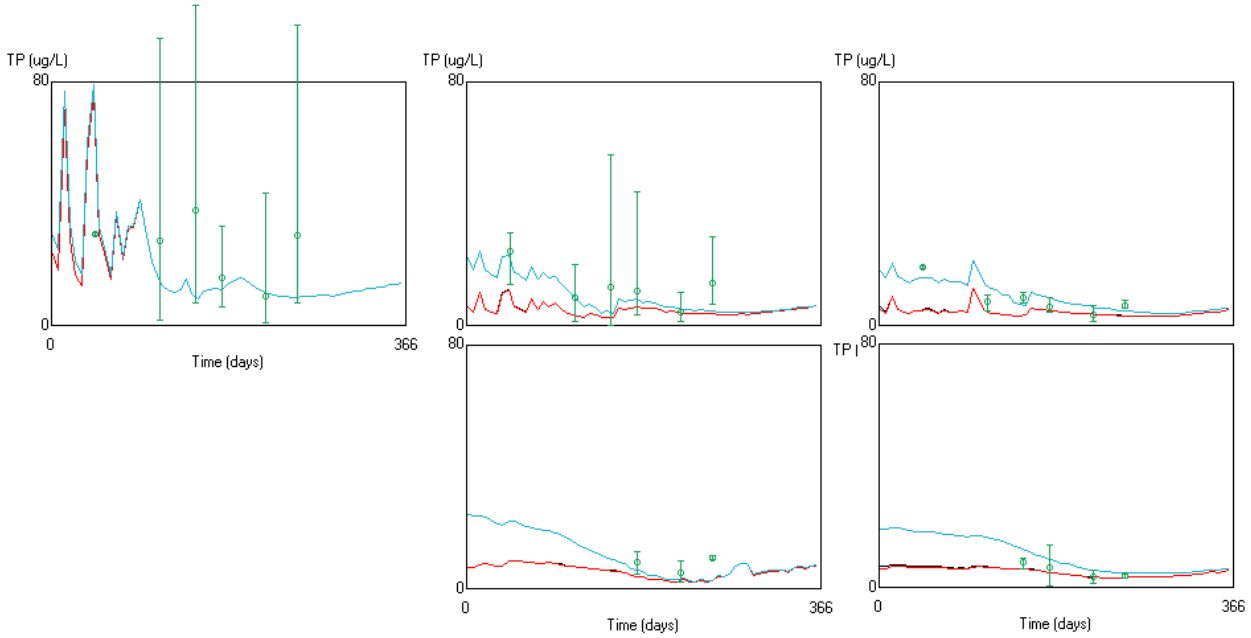

Figure B6-3: TP concentration time series 9-box model (1st year = blue, 2nd year = black, 3rd year = red) (average and max/min range bars, green) for west (left), central (middle) and east (right) basins, top and bottom layers

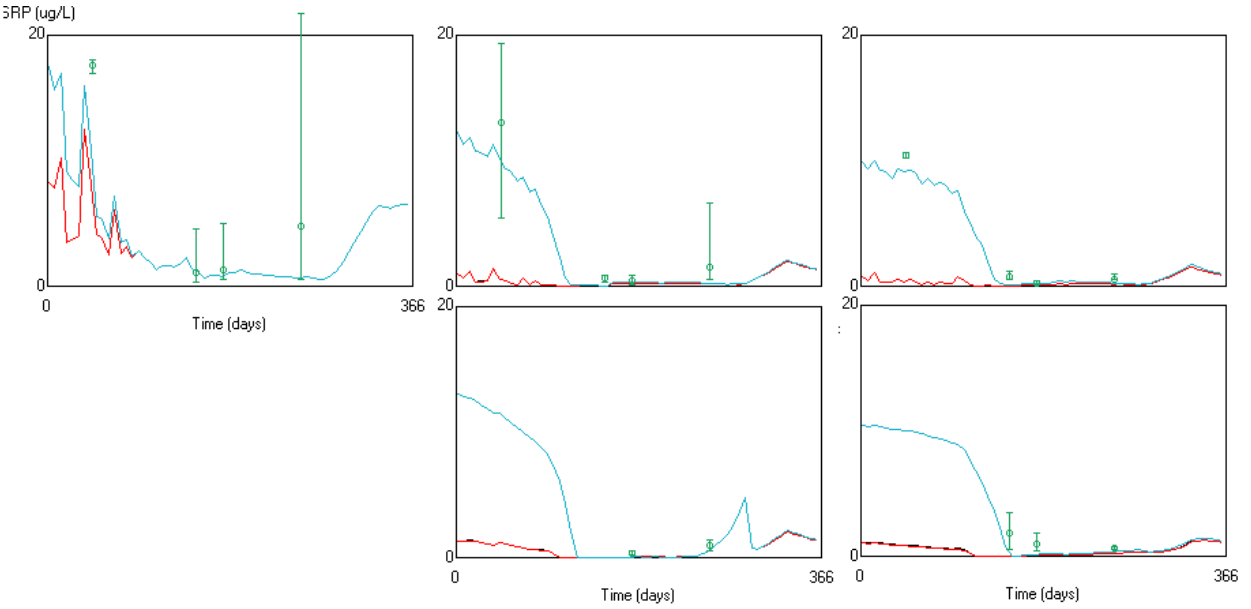

Figure B6-4: SRP concentration time series 9-box model (1st year = blue, 2nd year = black, 3rd year = red) (average and max/min range bars, green) for west (left), central (middle) and east (right) basins, top and bottom layers

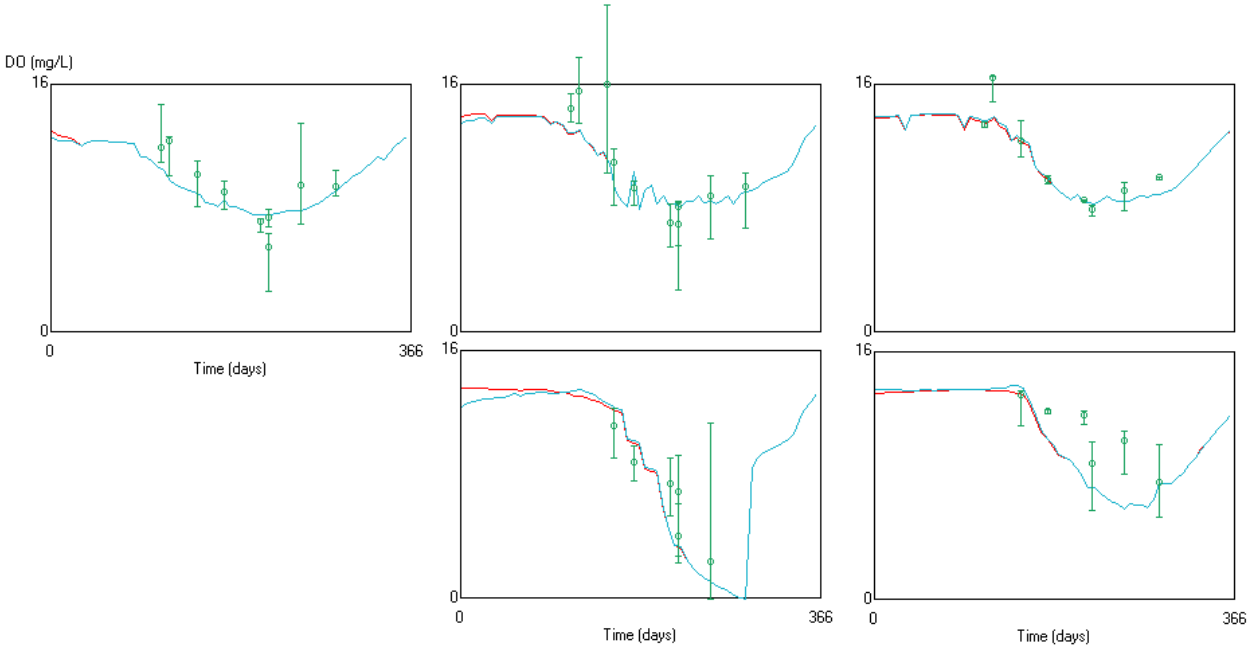

Figure B6-5: 2008 DO concentration time series 9-box model (1st year = blue, 2nd year = black, 3rd year = red) (average and max/min range bars, green) for west (left), central (middle) and east (right) basins, top and bottom layers

The following plots are provided below for each load scenario:

- Hypoxic area in the central basin
- Number of days with DO < 2 ppm in the central basin bottom layer
- DO concentration in the central basin bottom layer
- TP and SRP concentrations in:
    - west basin
    - central basin top and bottom layers
    - east basin top and bottom layers
    - Note thermocline layer is not shown as it is typically a thin layer of only a couple meters and data is not always available.

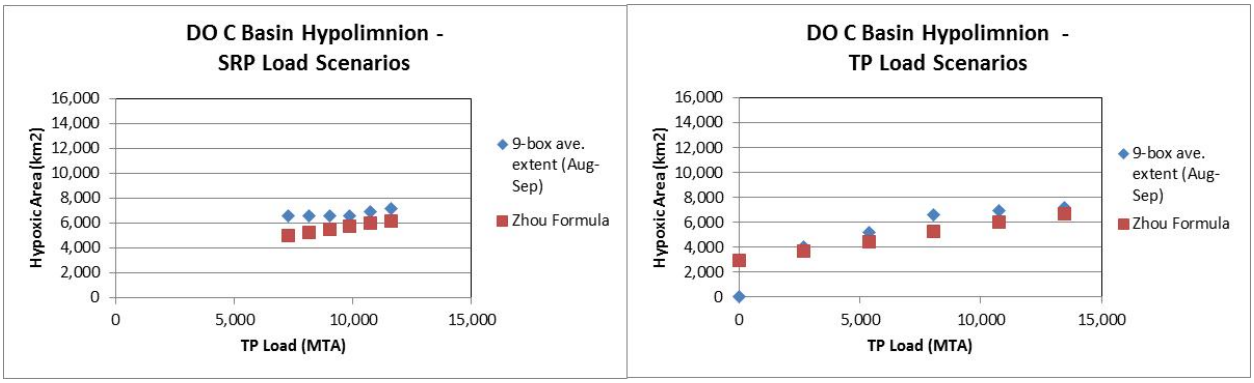

Figure B6-6: Average hypoxic area for central basin bottom layer for SRP (left) and TP (right) load scenarios. Zhou Formula values calculated using Zhou et al. (2013) method: HypoxicExtent=9.3 exp(-DOave^2/7.09) where DOave was taken as the average DO bottom concentration for August-September.

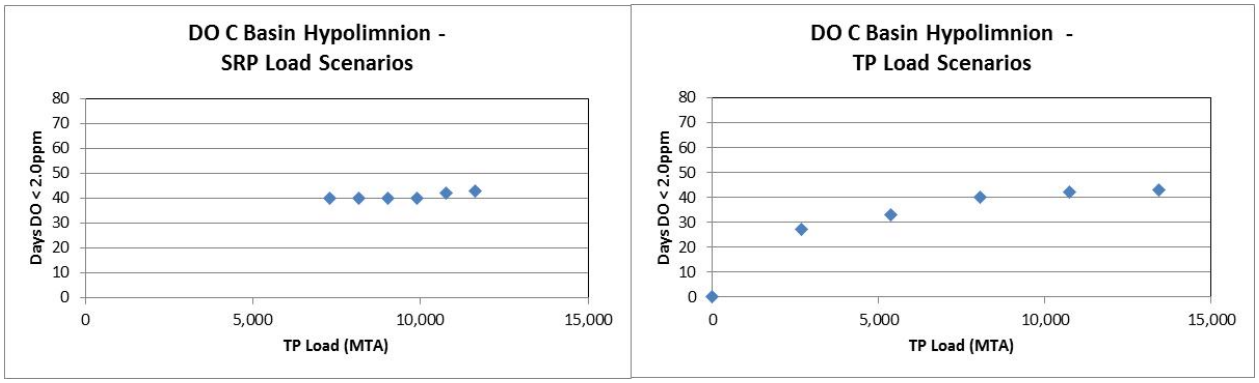

Figure B6-7: Number of hypoxic days in the central basin hypolimnion for SRP (left) and TP (right) load scenarios

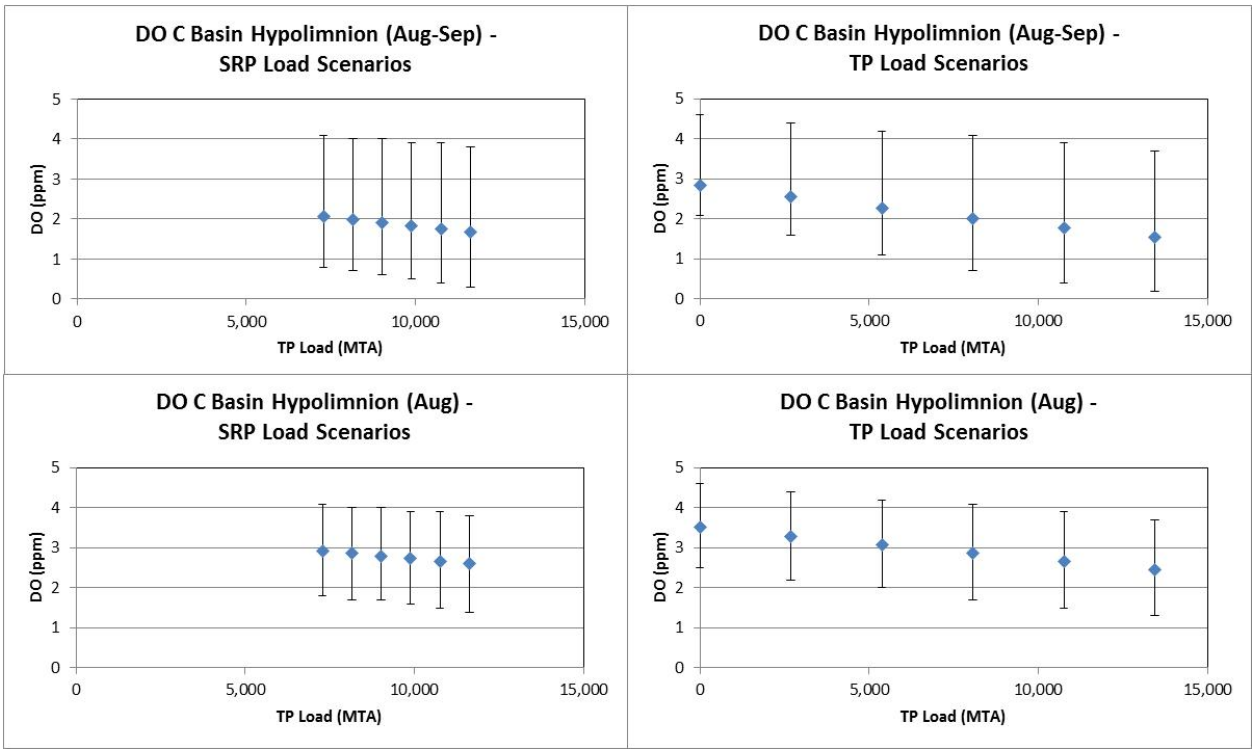

Figure B6-8: Central basin bottom layer average DO concentration with max/min range bars for SRP (left) and TP (right) load scenarios (upper: Aug.-Sep. average; lower: Aug. average)

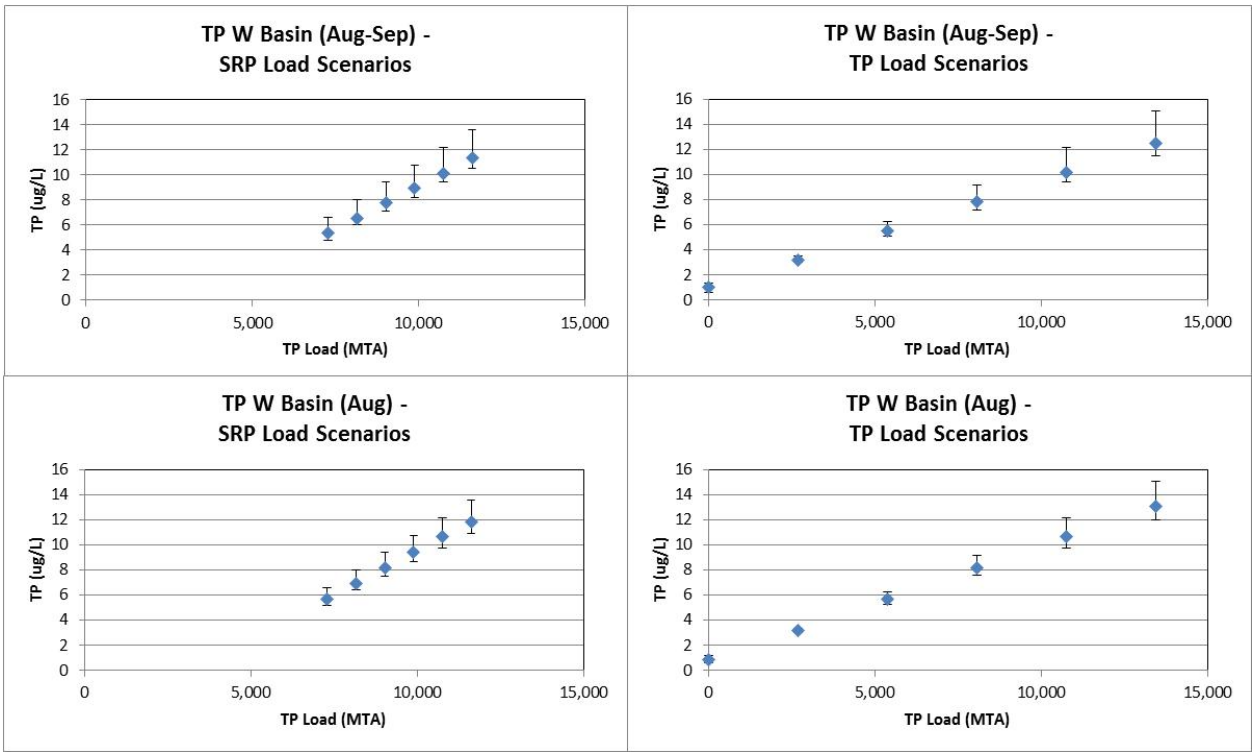

Figure B6-9: West basin average TP concentration with max/min range bars for SRP (left) and TP (right) load scenarios (upper: Aug.-Sep. average; lower: Aug. average)

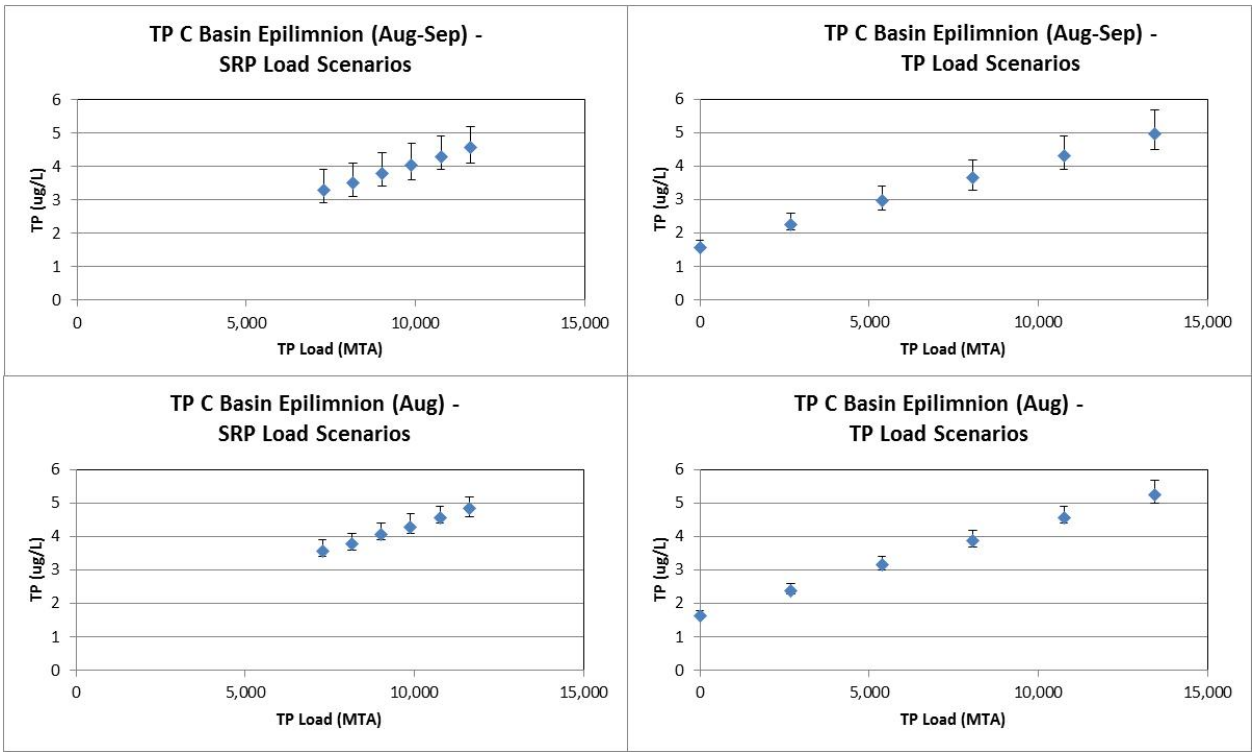

Figure B6-10: Central basin top layer average TP concentration with max/min range bars for SRP (left) and TP (right) load scenarios (upper: Aug.-Sep. average; lower: Aug. average)

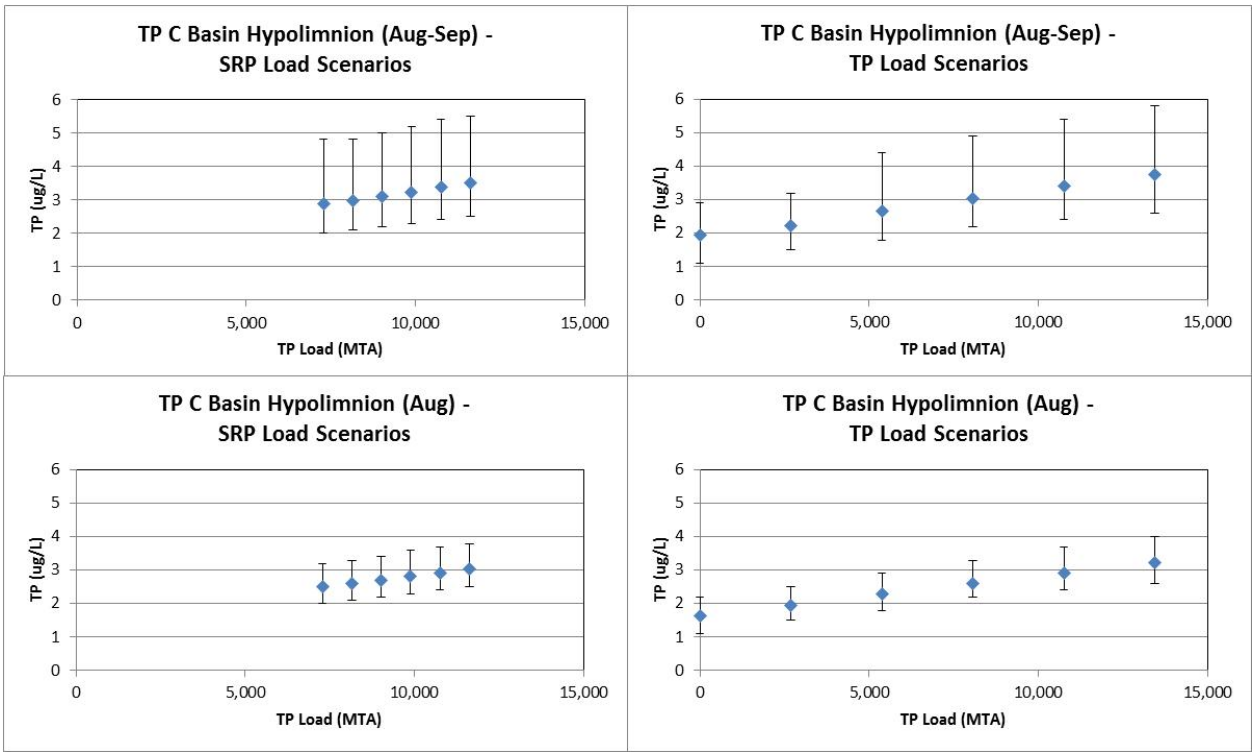

Figure B6-11: Central basin bottom layer average TP concentration with max/min range bars for SRP (left) and TP (right) load scenarios (upper: Aug.-Sep. average; lower: Aug. average)

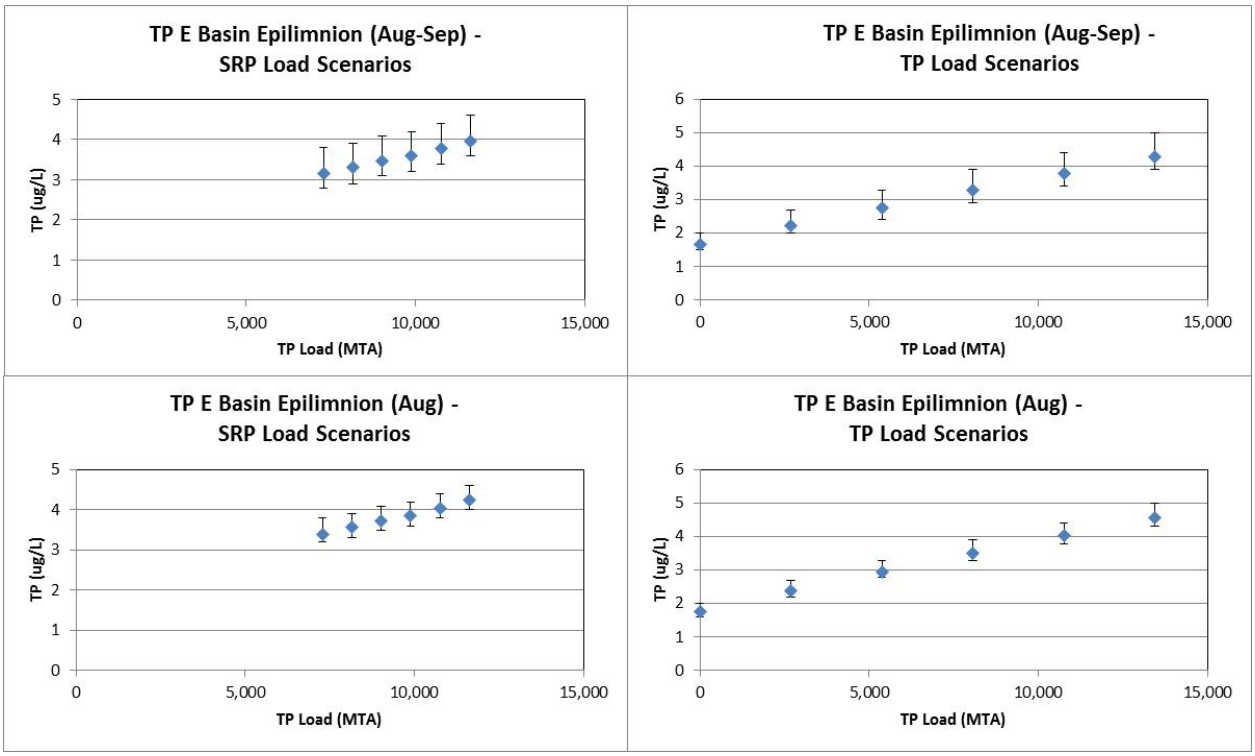

Figure B6-12: East basin top layer average TP concentration with max/min range bars for SRP (left) and TP (right) load scenarios (upper: Aug.-Sep. average; lower: Aug. average)

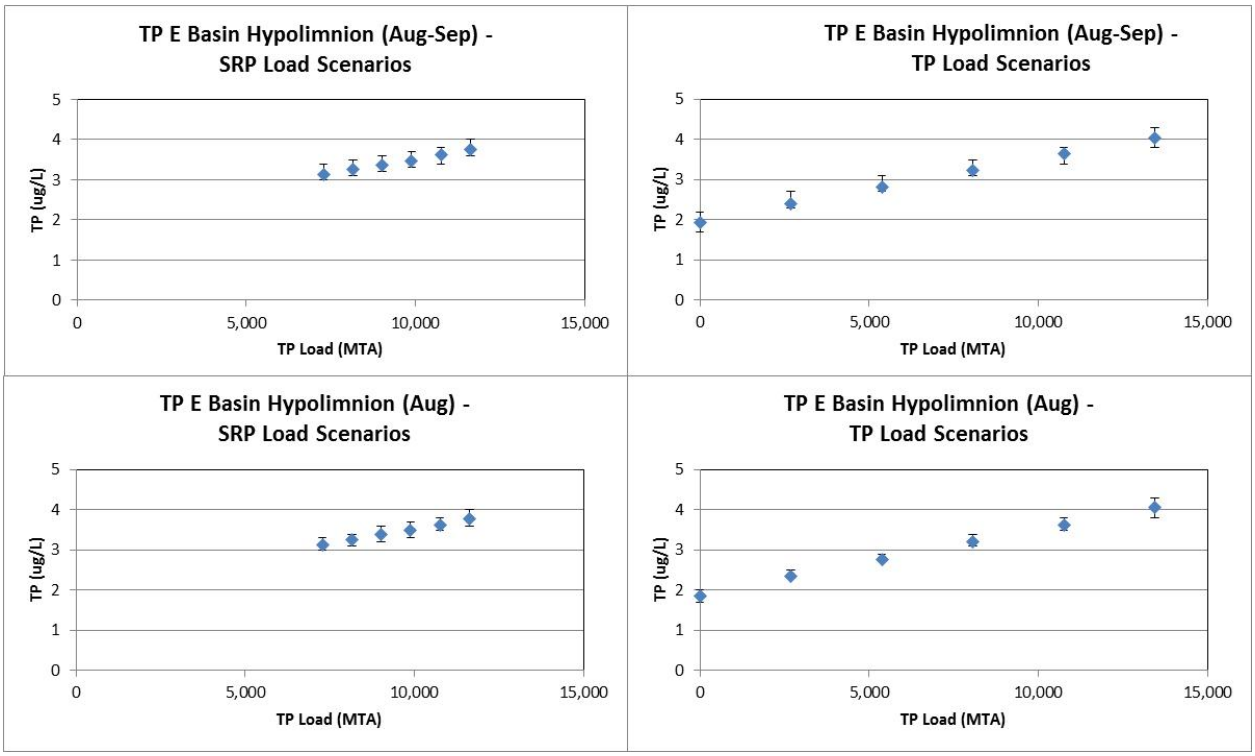

Figure B6-13: East basin bottom layer average TP concentration with max/min range bars for SRP (left) and TP (right) load scenarios (upper: Aug.-Sep. average; lower: Aug. average)

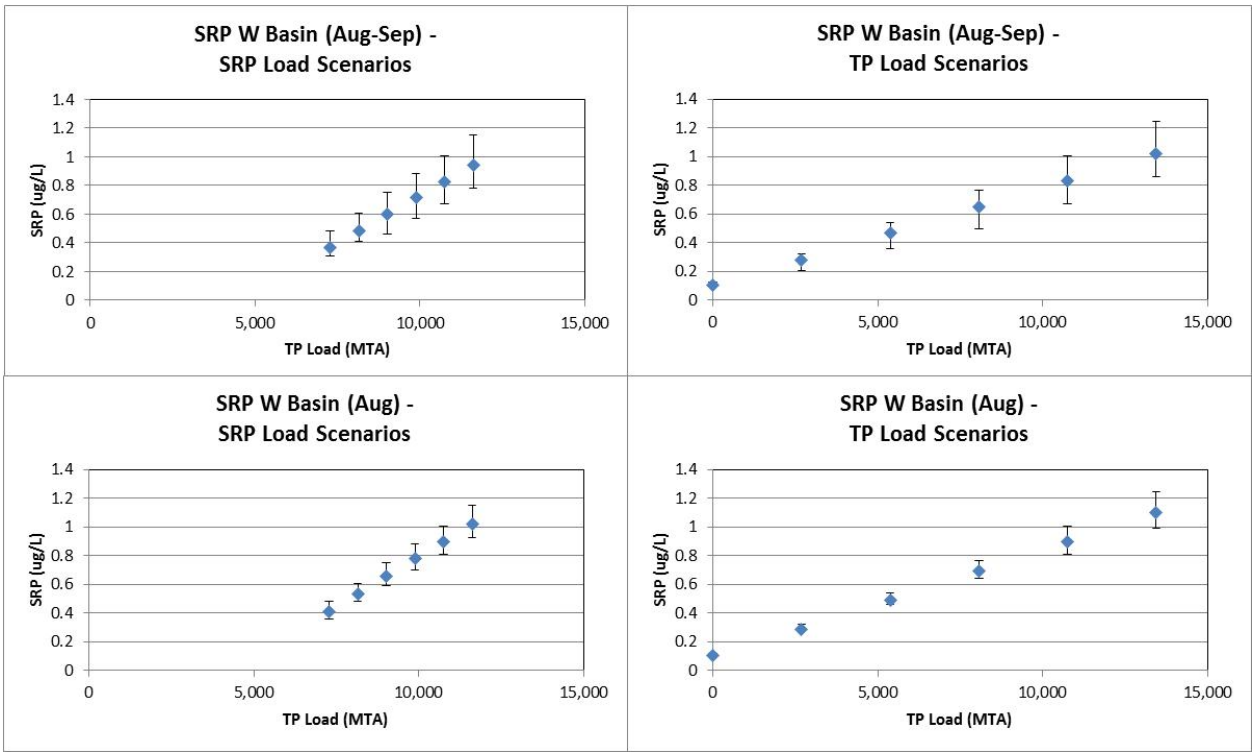

Figure B6-14: West basin average SRP concentration with max/min range bars for SRP (left) and TP (right) load scenarios (upper: Aug.-Sep. average; lower: Aug. average)

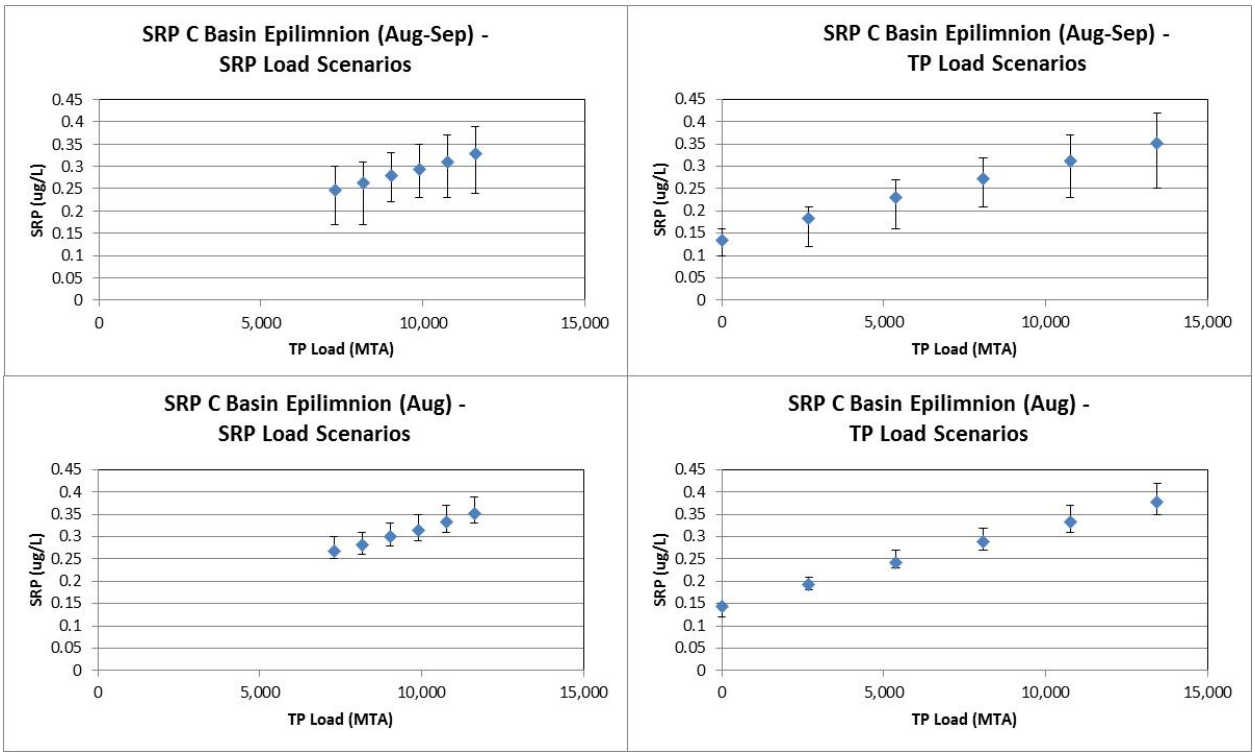

Figure B6-15: Central basin top layer average SRP concentration with max/min range bars for SRP (left) and TP (right) load scenarios (upper: Aug.-Sep. average; lower: Aug. average)

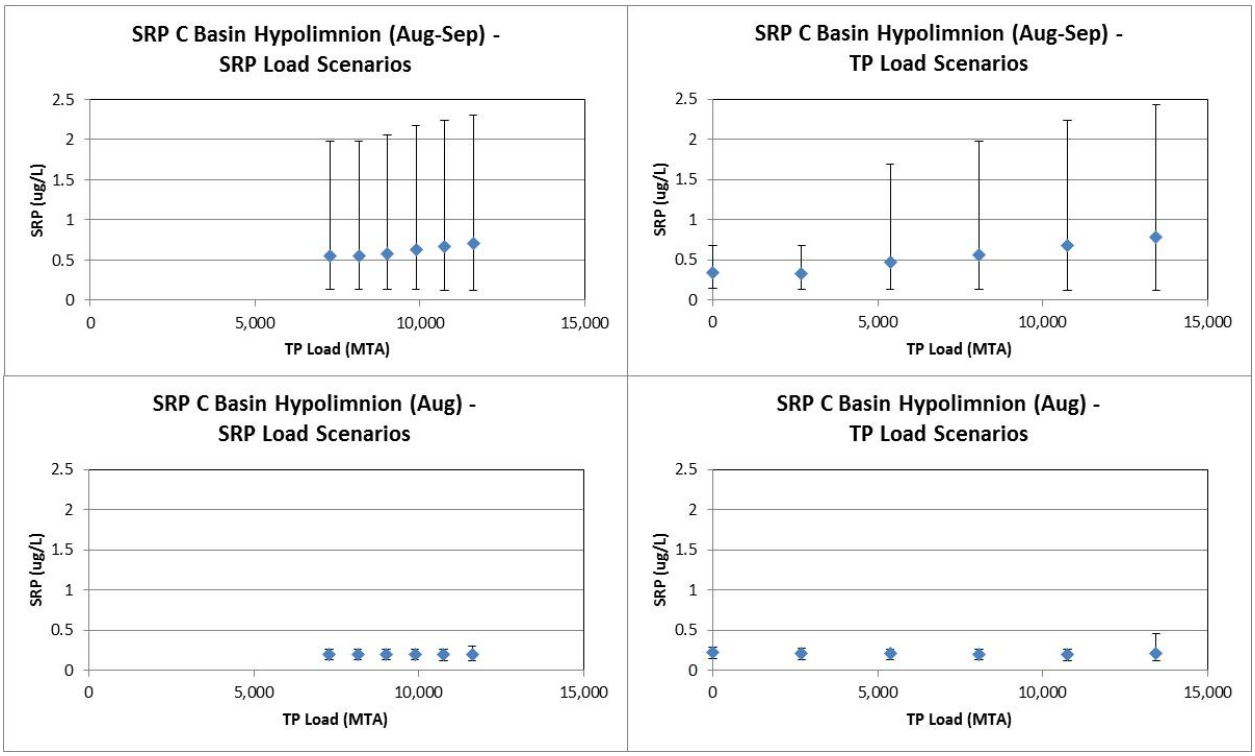

Figure B6-16: Central basin bottom layer average SRP concentration with max/min range bars for SRP (left) and TP (right) load scenarios (upper: Aug.-Sep. average; lower: Aug. average)

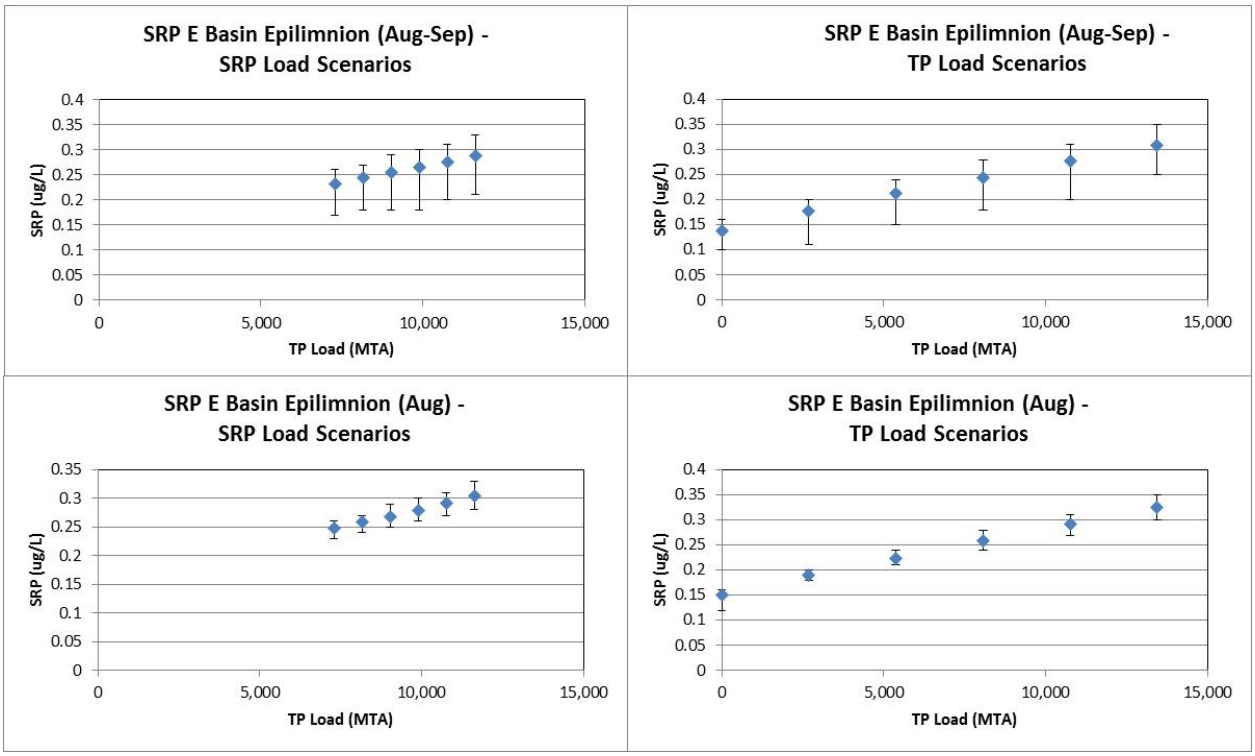

Figure B6-17: East basin top layer average SRP concentration with max/min range bars for SRP (left) and TP (right) load scenarios (upper: Aug.-Sep. average; lower: Aug. average)

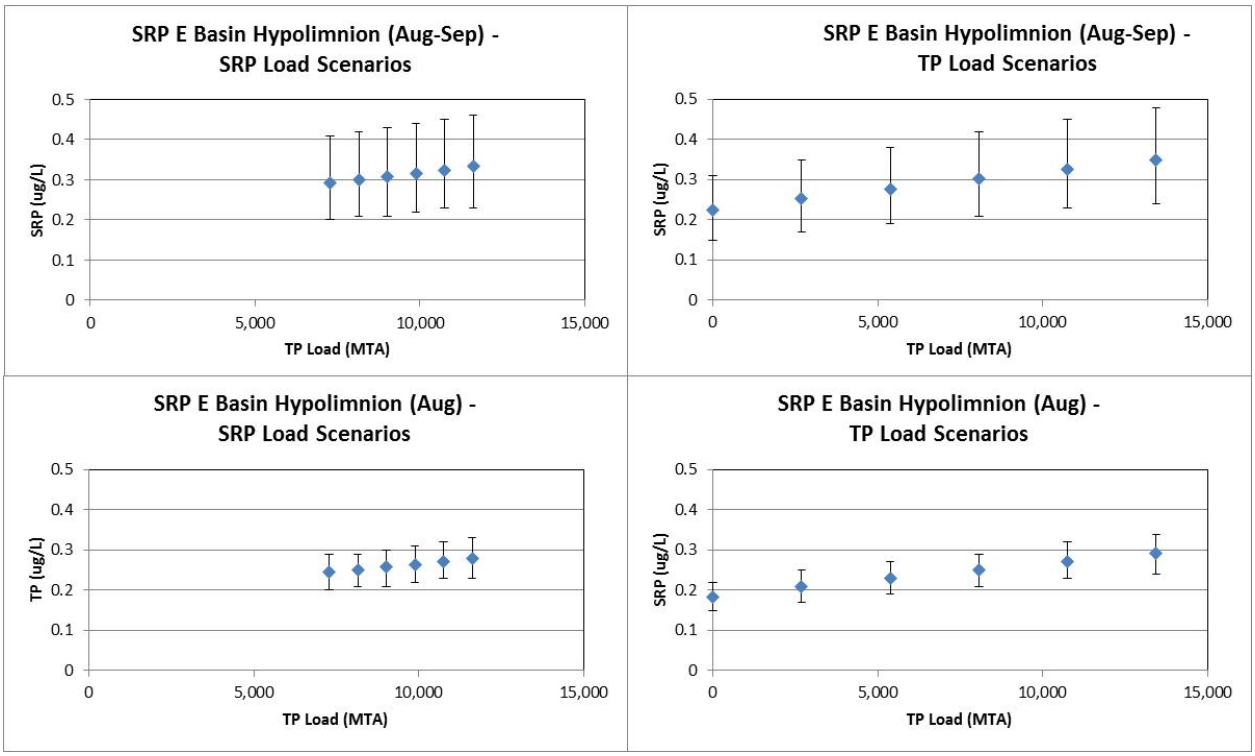

Figure B6-18: East basin bottom layer average SRP concentration with max/min range bars for SRP (left) and TP (right) load scenarios (upper: Aug.-Sep. average; lower: Aug. average)

Sensitivity

Model sensitivity has been addressed previously, for other years, in Lam et al. (2007). The same sensitivity cases were run for 2008 and yielded similar results. The following plots show the sensitivity of simulated DO, TP and SRP, to nine different model inputs, for the west basin (Figure B6-19) central basin bottom layer (Figure B6-20), and east basin top layer (Figure B6-21). The normalized gradient average deviation is taken over the whole year for the 2008 base case and shows the average percent difference for runs with +20% and -20% of the input parameters. DO is most sensitive to water temperature in the top layer and vertical diffusion in the bottom layer. In the west basin, TP and SRP are both sensitive to loading. TP is also sensitive to settling rate and wind speed (re-suspension) in all basins. SRP is also sensitive to the uptake rate in all basins.

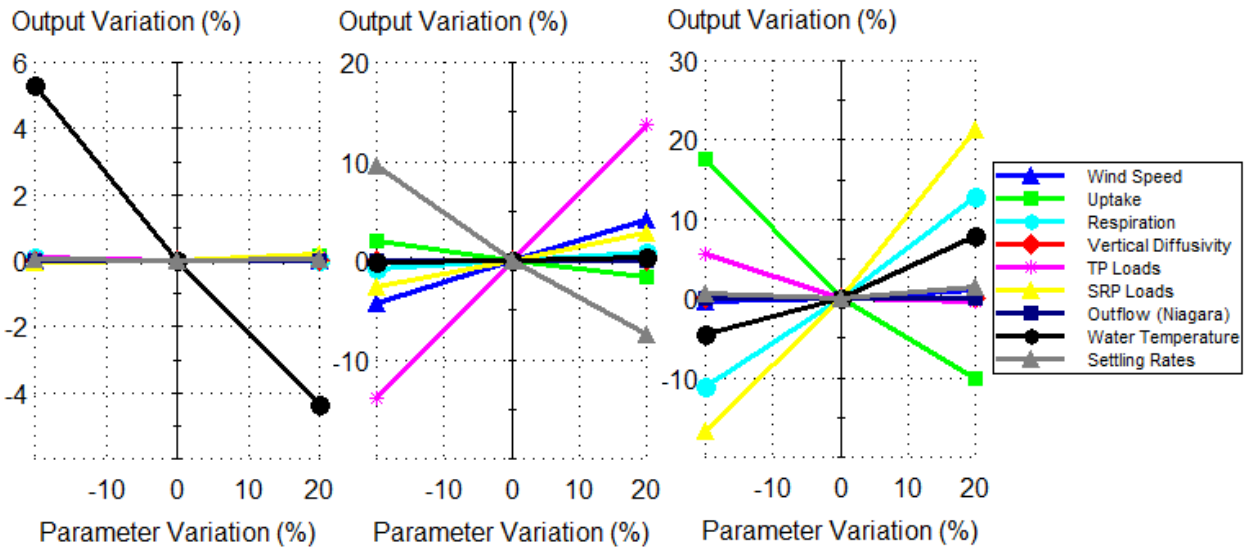

Figure B6-19: West basin top layer normalized gradients (average deviation) sensitivity for DO, TP and SRP with inputs +/- 20%

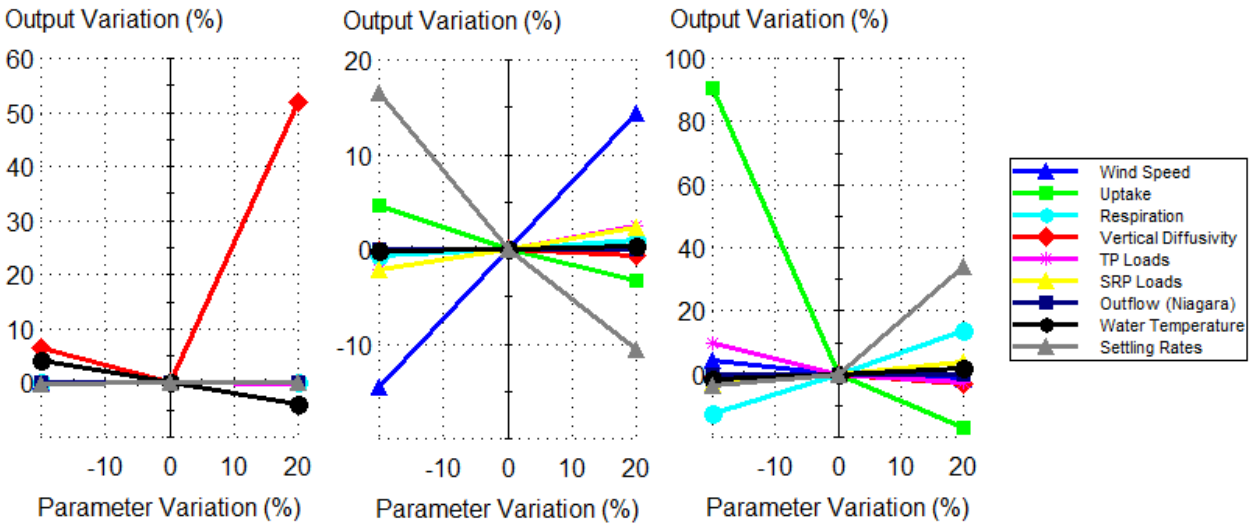

Figure B6-20: Central basin bottom layer normalized gradients (average deviation) sensitivity for DO, TP and SRP with inputs +/- 20%

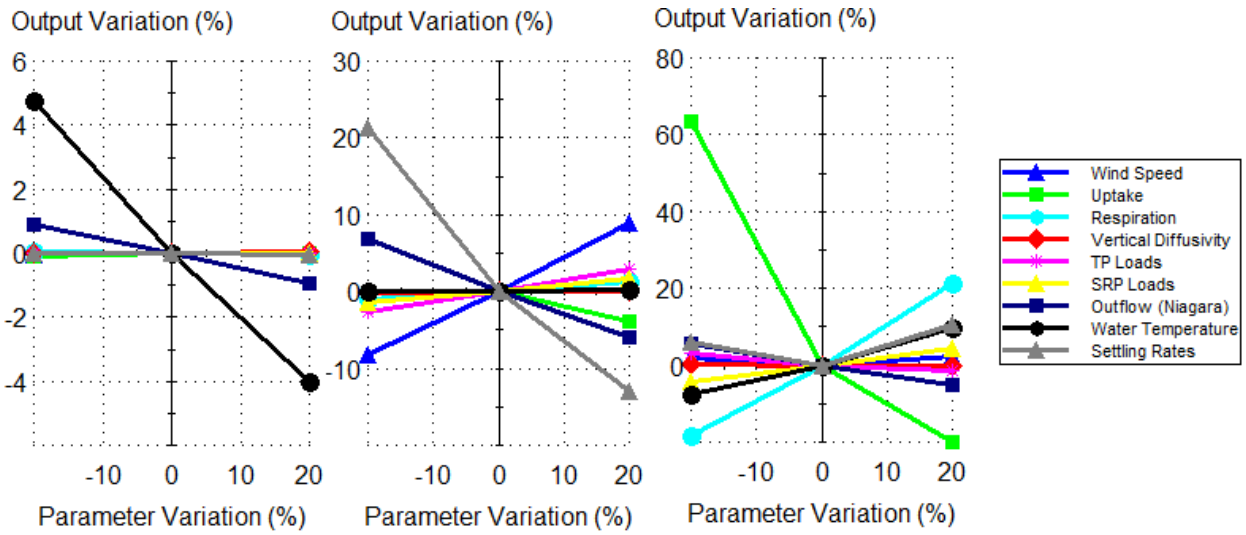

Figure B6-21: East basin top layer normalized gradients (average deviation) sensitivity for DO, TP and SRP with inputs +/- 20%

Time series of each parameter and hypothetical concentrations when adjusting more sensitive parameters +20% and – 20% are shown in Figure B6-22 to Figure B6-24. The results are similar to previous sensitivity results (Lam et al., 2007). Figure B6-22 shows that increasing vertical diffusion would increase the end of summer low DO in the central basin bottom layer. Figure B6-23 shows generally TP will increase over the whole year with lower settling rates and increase with higher settling rates. Figure B6-24 shows that SRP increases with lower uptake and increases with higher uptake and the magnitude of these differences is more noticeable during the winter months.

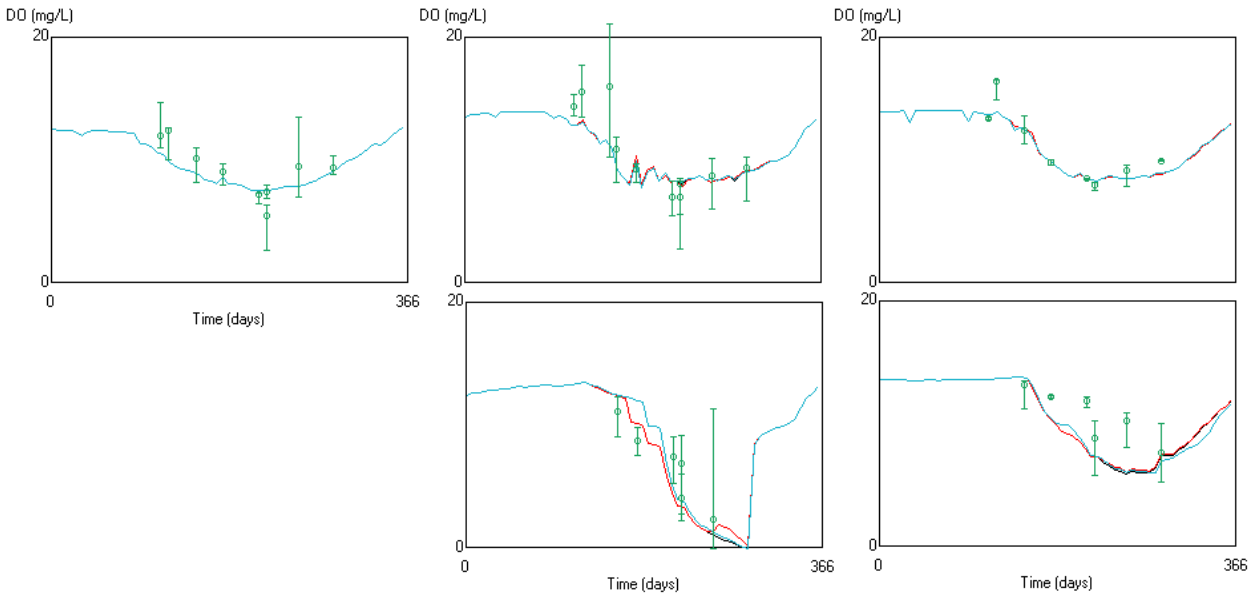

Figure B6-22: DO time series concentrations (base run black line, vertical diffusion +20% (blue line) and -20% (red line)) for east, central and west basins, top and bottom layers.

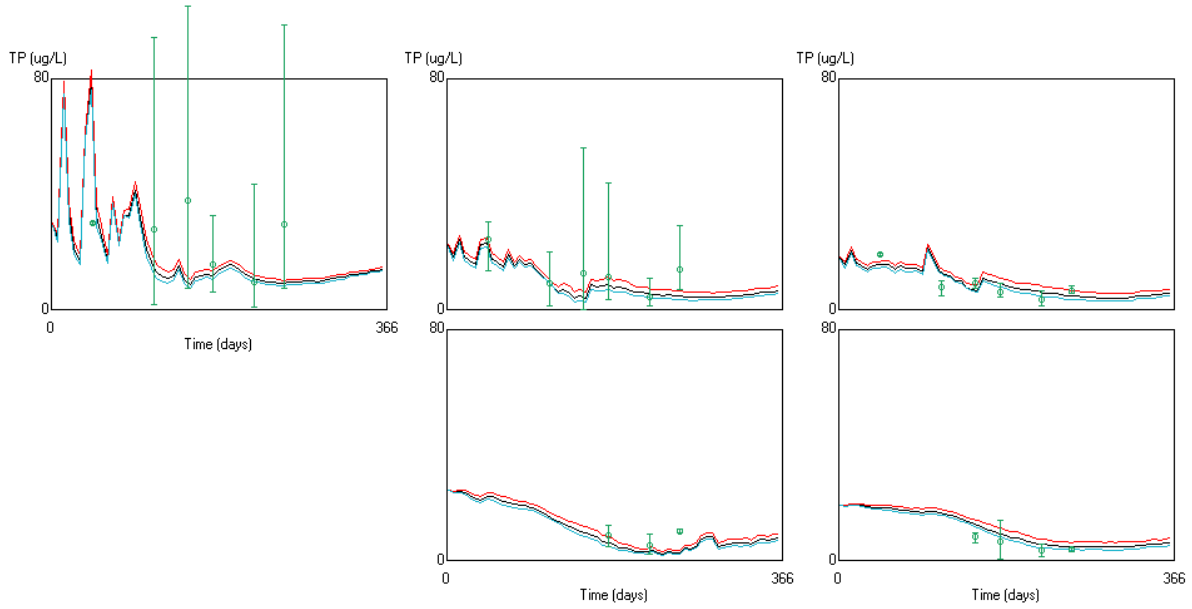

Figure B6-23: TP time series concentrations (base run black line, settling +20% (blue line) and -20% (red line)) for east, central and west basins, top and bottom layers.

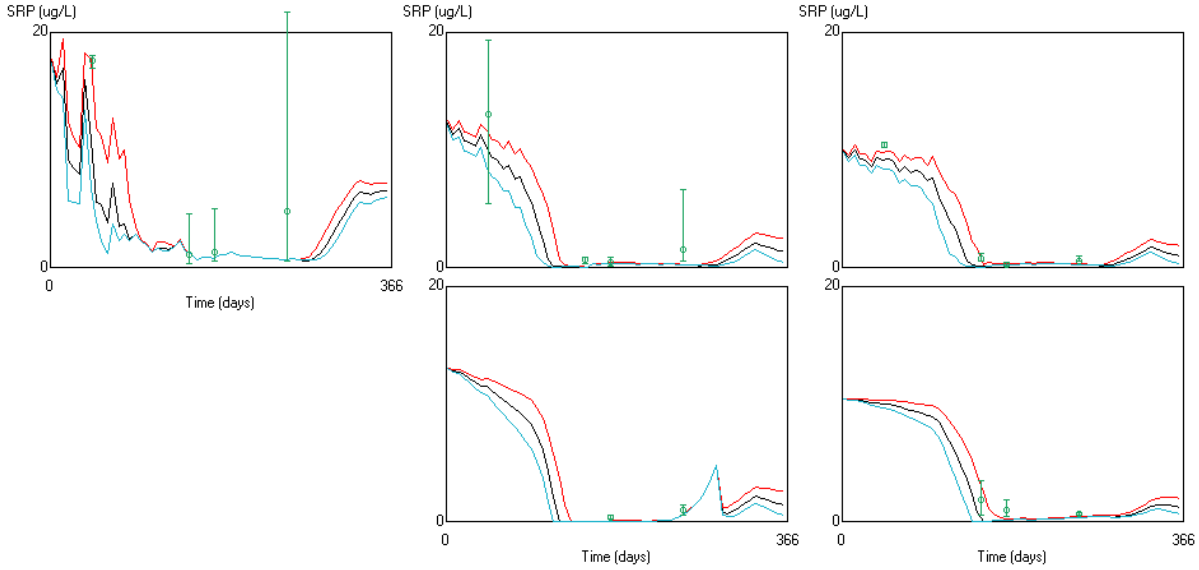

Figure B6-24: SRP time series concentrations (base run black line, uptake +20% (blue line) and -20% (red line)) for east, central and west basins, top and bottom layers.

During the scenario runs of this study, the model did not produce reasonable results for the -100% TP load scenario. The original model was never tested for such a scenario with such small phosphorous concentrations. The cause of the problem was related to the calculation of PP as a function of OP which was originally "hard coded" in the model as PP = OP – 0.005 (mg/L). This relationship requires a minimum OP of 0.005 mg/L so is not applicable for the small OP concentrations we get during low load scenarios. Data was extracted from the Environment Canada StarDatabase and it was found the relationship for low OP concentrations can be approximated as PP=0.7 * OP (R^2=0.68), which does not require a minimum OP concentration.

5. References

Lam, D.C.L., Schertzer, W.M. and Fraser, A.S. 1987. A post-audit analysis of the NWRI nine-box water quality model for Lake Erie. J. Great Lakes Res. 13: 782-800.

Lam, D.C.L., Schertzer, W.M. and A.S. Fraser. 1993. Simulation of Lake Erie water quality responses to loading and weather variations. 1983. Burlington, Ont.: Environment Canada, Scientific series / Inland Waters Directorate; no. 134

Lam, D.C.L., W.M. Schertzer and R.C. McCrimmon, 2002, Modelling changes in phosphorus and dissolved oxygen pre- and post-zebra mussel arrival in Lake Erie. NWRI Contribution No. 02-198, Environment Canada, Burlington, ON, Canada.

Lam, D.C.L., Schertzer, W.M., McCrimmon, R.C., Charlton, M. and Millard, S. 2007. Modelling Phosphorus and Dissolved Oxygen Conditions Pre- and Post-Dreissena Arrival in Lake Erie. In: Munawar, M., and Heath, R. (ed), Checking the Pulse of Lake Erie, World Monograph Series, Aquatic Ecosystem Health and Management Society.

Zhou, Y., Obenour, D.R., Scavia, D., Johengen, T.H., Michalak, A.M., 2013. Spatial and temporal trends in Lake Erie hypoxia, 1987–2007. Environ. Sci. Technol. 47, 899–905.

APPENDIX B-7: Western Lake Erie Ecosystem Model (WLEEM)

Joseph V. DePinto, Edward Verhamme, Derek Schlea, and Todd Redder, LimnoTech, Ann Arbor, MI

1. Model Description

Overview and Conceptual Model

The Western Lake Erie Ecosystem Model (WLEEM) has been developed as a 3D fine-scale, process-based, linked hydrodynamic-sediment transport-advanced eutrophication model to provide a quantitative relationship between loadings of water, sediments, and nutrients to the Western Basin of Lake Erie from all sources and its response in terms of turbidity/sedimentation and total and functional group phytoplankton biomass. It was developed over the last four years by LimnoTech (funding: USACE-Buffalo District and NSF) specifically to address the types of questions posed by this project. WLEEM is a time-dependent, 3-D model that computes temporal and spatial profiles of water, sediment, nutrients, and plankton and benthos dynamics as a function of loadings from all major and minor watersheds, the Detroit River, and hydro- meteorological forcing functions. The model consists of two linked public domain models, Environmental Fluid Dynamics Code (EFDC) (TetraTech, 2007) and a modified version of RCA (HydroQual, 2004). LimnoTech has also coupled EFDC with a wind-wave model (SWAN) (Delft University of Technology, 2006) to facilitate simulation of wind-driven sediment resuspension as a source of internal sediment and P loading in the western basin. The LimnoTech-customized RCA includes the capability to model up to five phytoplankton functional groups; the effects of Dreissenids on nutrient cycling, particle fate and transport, algal production, and water clarity; and a benthic algal functional group based on the Auer GL *Cladophora* Model (GLCM) (Auer et al., 2010; Bierman et al., 2005; DePinto et al., 2009; LimnoTech, 2010; LimnoTech, 2013). This improved RCA framework is called the Advanced Aquatic Ecosystem Model (A2EM).

WLEEM operates on a daily time scale and can produce time series outputs and spatial distributions of either total chlorophyll and/or cyanobacteria biomass as a function of loading. Therefore, it can produce load-response plots for several potential endpoints of interest in the Western Basin. It will also produce mass balances for the Western Basin for any one of its ~30 states variables; therefore, it can compute the daily loading of Western Basin nutrients and oxygen-demanding materials to the Central Basin as a function of loads to the Western Basin. This will provide valuable information on how load reductions to the Western Basin will impact hypoxia development in the Central Basin.

Figure B7-1 is a presentation of the model domain and the surface model grid superimposed on the Western Basin model bathymetry. The model domain is bounded by a line connecting Pointe Peele with Marblehead.

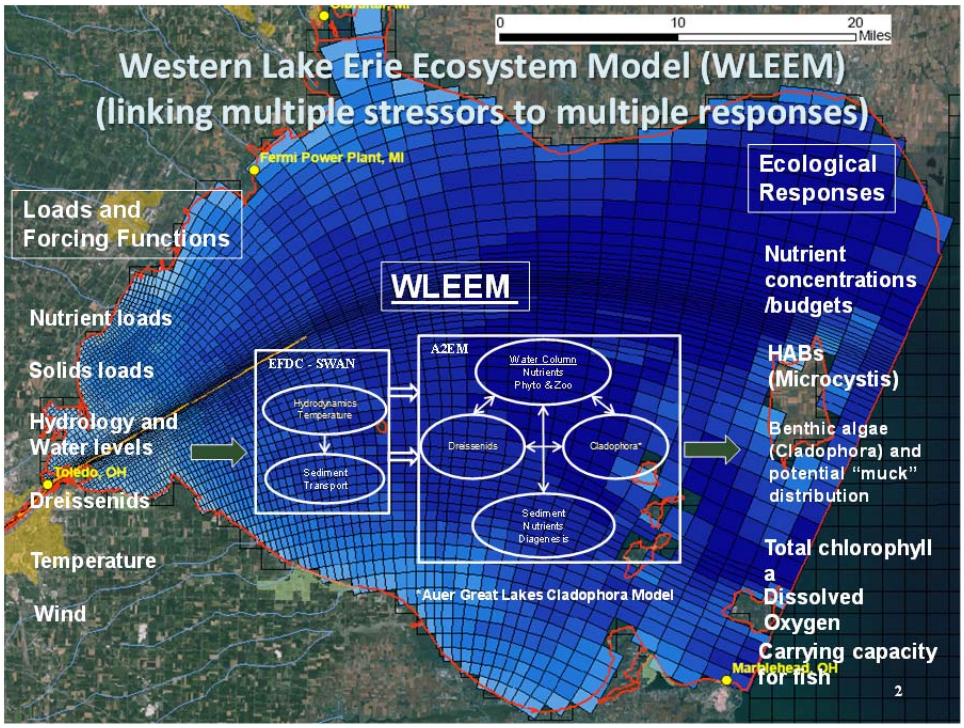

Figure B7-1: Depiction of WLEEM inputs and outputs superimposed on the model grid and bathymetry.

The WLEEM utilizes the following model components:

- *Simulating Waves Nearshore* (SWAN) for the wind-wave sub-model;
- *Environmental Fluid Dynamics Code* (EFDC) for the hydrodynamic sub-model;
- *Sandia National Laboratory* (SNL) algorithms for the sediment transport sub-model; and
- Advanced Aquatic Ecosystem Model (A2EM).

Figure B7-2 illustrates how the wind/wave model, hydrodynamic model, sediment transport, and water quality model all interact together.

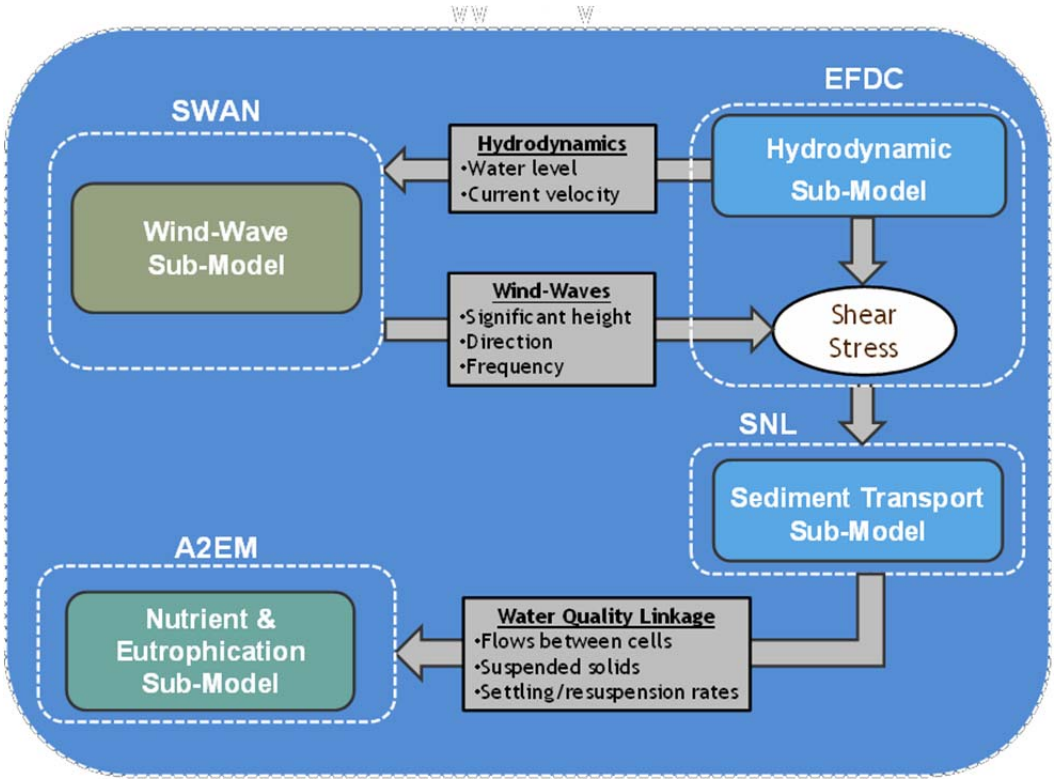

Figure B7-2: Illustration of linkage and data flow between model components of WLEEM.

WLEEM was initially calibrated to 2005 data and recalibrated/corroborated by application to the 2008 and 2011-2013 field data, with an emphasis on cyanobacteria biomass data from Bridgeman at the University of Toledo.

Model Structure

EFDC is a state-of-the-art finite difference model that can be used to simulate hydrodynamic and sediment transport behavior in one, two, or three dimensions in riverine, lacustrine, and estuarine environments (TetraTech 2007a, 2007b). EFDC was developed by John Hamrick at the Virginia Institute of Marine Science in the 1980s and 1990s, and the model is currently maintained under support from the United States Environmental Protection Agency (EPA). The model has been applied to hundreds of water bodies, including Chesapeake Bay and the Housatonic River. Recently, LimnoTech has successfully applied EFDC to a number of sites in the Great Lakes, including Saginaw Bay, Saginaw River, and the Tittabawassee River. The EFDC model is both public domain and open source, meaning that the model can be used free of charge, and the original source code can be modified to tailor the model to the specific needs of a particular application. As a result, EFDC provides a powerful and highly flexible framework for simulating hydrodynamic behavior and sediment transport dynamics for the WLEB.
The SWAN model is a numerical wave model for predicting wave conditions in coastal areas, lakes, and estuaries based on site-specific wind, depth, friction, and water velocity conditions (Young, 1999; Booij et al., 1999). The SWAN model is based on the wave action balance equation and is capable of simulating various wave propagation (movement) processes, as well as wave generation processes (e.g., by wind) and dissipation processes, such as dissipation by bottom friction. SWAN provides the flexibility

to simulate either steady-state or dynamic wave conditions. As part of the model development effort on this project, the SWAN model was linked to the EFDC hydrodynamic and sediment transport sub-models. The SWAN-EFDC linkage involved two steps: 1) water level/depth and current velocity results generated by the hydrodynamic sub-model were processed and input as forcing functions to the SWAN wind-wave simulations; and 2) SWAN results for wave characteristics (e.g., height, frequency) were fed as input forcing functions to the EFDC sediment transport sub-model to inform calculations of bottom shear stress.

The Sediment Transport Model (SEDTRAN) is a modified version of the original code developed and maintained by Sandia National Laboratory (James et al., 2005; Thanh et al., 2008). This version of the model incorporates a custom sediment transport sub-model based on the SEDZLJ model algorithms developed by Craig Jones and Wilbert Lick at the University of California – Santa Barbara (Jones and Lick, 2001). The SNL/SEDZLJ models are typically used along with site-specific data obtained using SedFlume, a custom-designed flume device that can be used to measure erosion rates and sediment properties for an intact sediment core. The integration of the SNL code into LimnoTech's in-house version of the Row-Column AESOP (RCA) model code and associated testing work was accomplished previously under a separate LimnoTech modeling project (LimnoTech, 2010).

SEDTRAN Model Configuration. The SNL-SEDTRAN sediment transport sub-model can be used to simulate sediment transport in one, two, or three dimensions. It provides a flexible set of options for simulating erosion, deposition, and bed armoring and handling for cohesive and non-cohesive sediment types (James et al., 2005; Thanh et al., 2008). Multiple cohesive and non-cohesive sediment size classes may be represented in a single model simulation. This section provides a summary of the transport processes, selection of sediment particle size classes, and bottom shear stress calculations for the WLEEM sediment transport model.
The transport processes represented in SEDTRAN for cohesive and non-cohesive sediments are illustrated in Figure 3 and include the following:

The transport processes represented in SEDTRAN for cohesive and non-cohesive sediments are illustrated in Figure B7-3 and include the following:

- Loading of sediments from upstream and watershed sources;
- Horizontal transport between adjacent model cells (based on velocity and flow magnitude and direction predicted by the hydrodynamic sub-model);
- Settling and deposition to the sediment bed from the water column;
- Erosion and resuspension of sediments from the bed to the water column;
- Transport of non-cohesive sediments as bedload or suspended load based on applied bottom shear stress and particle characteristics;
- Representation of the sediment bed as discrete layers (to permit tracking of changes in particle size distribution by depth); and
- Armoring of the sediment bed in nearshore areas and areas of hard substrate, including the use of an "active layer."

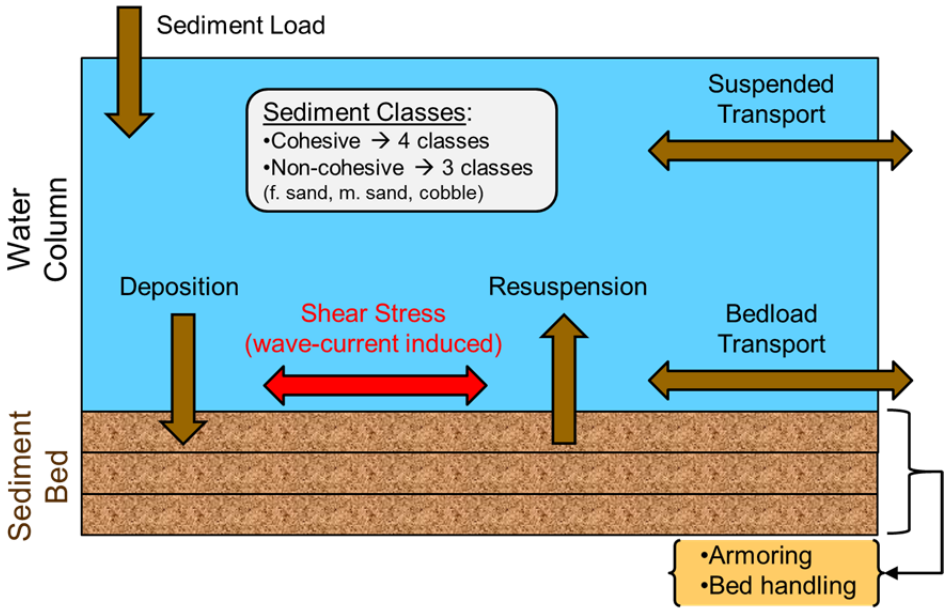

Figure B7-3: Sediment transport processes included in SEDTRAN.

The A2EM is a state-of-the-science aquatic ecosystem simulation model. The model framework was customized by LimnoTech from a publicly available version of the RCA model developed and documented by HydroQual, Inc. (HydroQual, 2004). The RCA model framework developed by HydroQual is capable of simulating water quality dynamics on a fine-scale, multi-dimensional computational grid based on linkage to an external hydrodynamic model application. The basic RCA framework includes a suite of state variables to represent carbon, nitrogen, phosphorus, oxygen, and phytoplankton dynamics. The framework includes a coupled sediment diagenesis sub-model that simulates the cycling of detrital material and nutrients in the surface sediments and subsequent impacts on near-bed sediment oxygen demand and release of dissolved nutrients, including dissolved inorganic phosphorus. The LimnoTech enhancements to this model include a custom linkage from the hydrodynamic model (EFDC) and the sediment transport model (SEDTRAN). This allows output from one model to be included as inputs to the next model in the simulation chain. LimnoTech has also added the capability to dynamically simulate zooplankton, benthic algae, dreissenid mussels, and further process refinement of inorganic and organic particulate phosphorus. A conceptualization of the phosphorus cycling included in A2EM is depicted in Figure 4.

The linked modeling framework comprised of EFDC, SWAN, SEDTRAN, and A2EM, collectively referred to as the WLEEM, provides a powerful and flexible tool for evaluating hydrodynamic, wind-wave, sediment transport, and nutrient and phytoplankton processes at a variety of temporal and spatial scales.

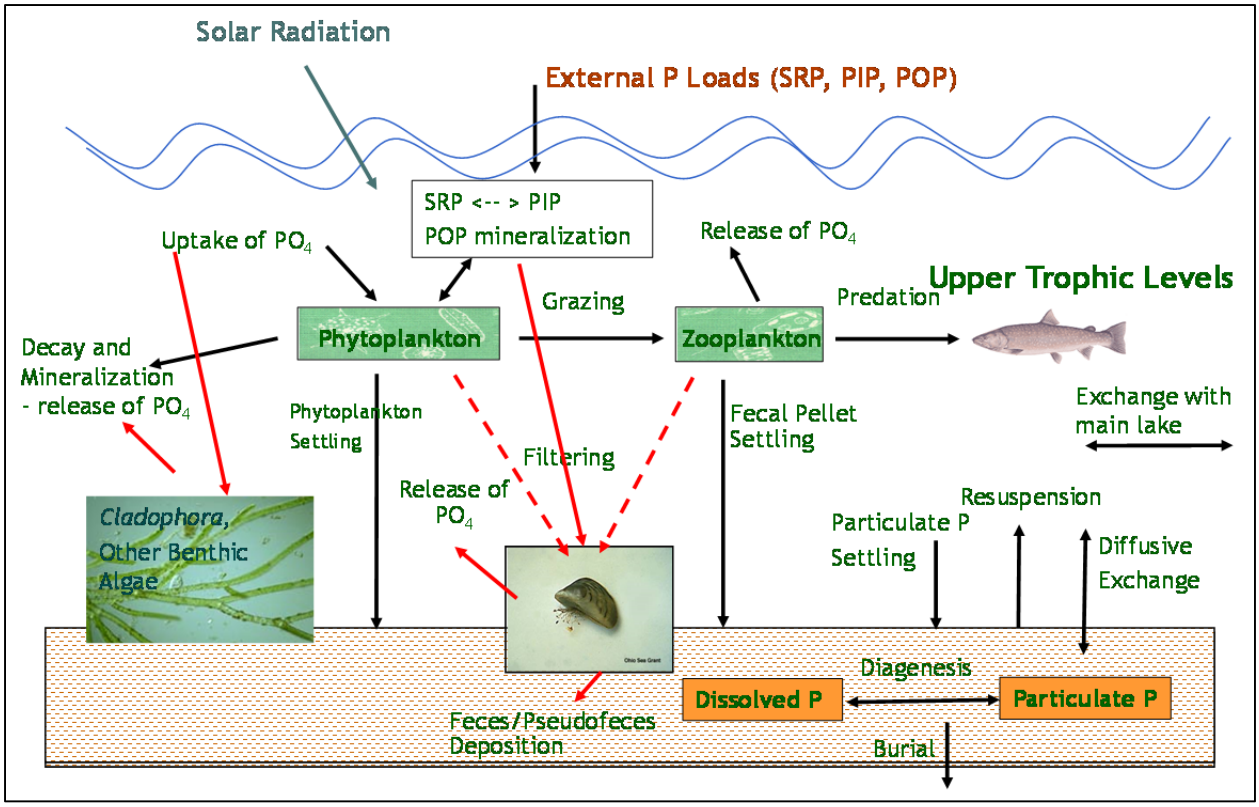

Figure B7-4: Phosphorus cycling included in WLEEM.

2. Model Input and Evaluation Data

Model Input Data

EFDC Boundary Conditions. Model boundary conditions provide a basis, or starting point, for calculations internal to the model. Four types of hydrodynamic forcings were applied as boundary conditions to the hydrodynamic model, including:

- A water level boundary condition in Lake Erie;
- Inflow boundary conditions for the Maumee River, the Detroit River, and other minor tributaries including flow rate and water temperature;
- Atmospheric forcings (e.g., wind and air temperature); and
- A water level boundary was applied at the interface of the central and western basins of Lake Erie. Data from NOAA station number 9063079 (Marblehead, Ohio) was used to describe hourly variations in water level at this location. This "boundary forcing" controls the depth of water and circulation patterns in the WLEB and also influences the strength of flow reversals in the lower Maumee River as changes in water levels drive the seiche activity experienced in the drowned river mouth and dredged channel of Toledo Harbor.

Tributary inflows to the system were represented in the model using available data (Section 3.3.2). Flow gauging datasets available from the United States Geological Survey (USGS) were used to develop daily flow time series for each tributary. In many cases, the USGS gauge dataset did not represent the entire drainage area of a given tributary; therefore, drainage area ratios were used to scale the daily measured flow time series to represent the entire watershed.

The model utilizes a spatially variable "wind forcing" that is consistent with the established whole lake model. Wind forcings were extracted from the Great Lakes Observing System (GLOS) point query website (GLOS 2013). This website allows a user to extract model inputs or model outputs at a specified location from the NOAA supported Great Lakes Coastal Forecasting System (GLCFS). Wind time series were extracted for 10 locations within the WLEEB model domain. A Thiessen polygon analysis was then performed on the model grid and the wind forcing locations so that each grid cell in the WLEEB model grid was attributed with weighting factors for the nearest of these 10 wind forcings. Additional information on the wind forcings and the GLCFS model can be found at the NOAA's website (NOAA 2013b).

SEDTRAN Boundary Conditions. Sediment transport boundary conditions describe the quantity and particle size distribution of suspended sediments entering the model domain from various sources. This section describes the sediment boundary conditions developed for the Maumee River and other tributary sources and point sources to Maumee Bay/WLEB that are represented in the WLEEM model. An extensive suspended solids dataset is available for the Maumee River at Waterville, Ohio, based on long-term research conducted by Heidelberg University's National Center for Water Quality Research (NCWQR).

Several other tributary inflows are represented in the WLEEM model in addition to the Maumee River, including the Detroit River, Swan Creek, Ottawa River, River Raisin, Huron River, Stony Creek, and Portage River/Cedar River. In addition, inflows are represented for the Toledo Bay View Wastewater Treatment Plant (WWTP) and Maumee River direct drainage contributions between Waterville, Ohio, and the mouth (see Table B7-1). Suspended sediment boundary conditions were developed for each of these flow sources. The boundary condition for the Detroit River was set at a constant value of 10 milligrams per liter (mg/L) based on a review of available data for this Great Lakes connecting channel. The Bay View WWTP was also assigned a constant concentration of 10 mg/L based on available data from the plant's discharge monitoring reports (DMRs).

Table B7-1. Suspended Sediment Boundary Conditions for Maumee Bay/WLEB Flow Sources

Flow Source Description	Flow-Based Regression[a]
Detroit River	$C_{TSS} = 10$
Swan Creek	$C_{TSS} = 0.085*Q + 30.52$
Ottawa River	$C_{TSS} = 0.13*Q + 24.81$
River Raisin	$C_{TSS} = 0.0415*Q + 10.60$
Portage River + Cedar River	$C_{TSS} = 0.0406*Q + 20.42$
Toledo Bay View WWTP	$C_{TSS} = 10$

Note:

[a.] C_{TSS} are in units of milligrams per liter and Q are in units of cubic feet per second.

Key:

C_{TSS} = Suspended solids concentrations

Q = flows

WWTP = wastewater treatment plant

Sufficient suspended sediment data were also available to develop a tributary-specific relationship between sediment concentration and flow rate for Swan Creek, Ottawa River, River Raisin, and Portage River. These regressions were applied to estimate suspended solids concentrations for the entire duration of model simulations.

The open boundary condition at the interface between the WLEB and the central Lake Erie basin is characterized with a constant concentration of 10 mg/L based on available monitoring data from the International Field Year in Lake Erie (IFYLE) datasets (Hawley et al., 2006).

A2EM Boundary Conditions. The A2EM model uses the same boundary locations as the hydrodynamic model, which includes the open boundary with the central basin of Lake Erie and tributary inflows from the Detroit, Maumee, and other minor tributaries. Daily estimated concentrations of nutrients, dissolved oxygen, and phytoplankton, are applied at every boundary location. The boundary conditions are described in more detail below.

Maumee River. Nutrient concentrations for the Maumee River were derived from measurements made by Heidelberg University at their monitoring station located in Waterville, Ohio. This station is approximately 20 miles upstream of the mouth of the Maumee River. Concentrations at this station are assumed to be representative of what enters Lake Erie on a daily basis. The frequency of sediment and nutrient sampling at this station is one or more samples per day. As a result, monitoring data was used directly to drive the model.

Detroit River. A regular monitoring program does exist for the lower Detroit River; however data from the Michigan Department of Environmental Quality have a five-year lag until they are released. The latest published report of observations released in February 2013 summarizes monitoring data through 2008 (MDEQ 2013). These observations were used to parameterize the concentrations of TP, TSS, and DRP that enter Lake Erie.

Lake Erie. Monitoring data from EPA- GLNPO's open-lake limnology program were utilized to set the open boundary concentration of nutrients. Monitoring data were downloaded from the Great Lakes Environmental Database (GLENDA; USEPA, 2013).

Other Tributaries. Concentrations of nutrients in other minor tributaries were based on of a limited review of existing data and engineering judgment based on of the nature of the watershed land uses.

A plot of the annual distribution of TP load between the major external tributary sources is shown in Figure B7-5 for 2008, 2011, 2012, and 2013. For comparison purposes the average annual flow rate and flow weighted mean TP concentration is shown in Figure B7-6. The TP load from the Detroit River is fairly constant, while the load from the Maumee River varies considerably from year to year. Although the Detroit and Maumee account for the majority of TP delivered to the Western Basin, the average flow from the Detroit River is significantly larger than that of the Maumee. This large flow imbalance highlights why the flow-weighted mean concentration of the Maumee River is over 400 µg-P/L.

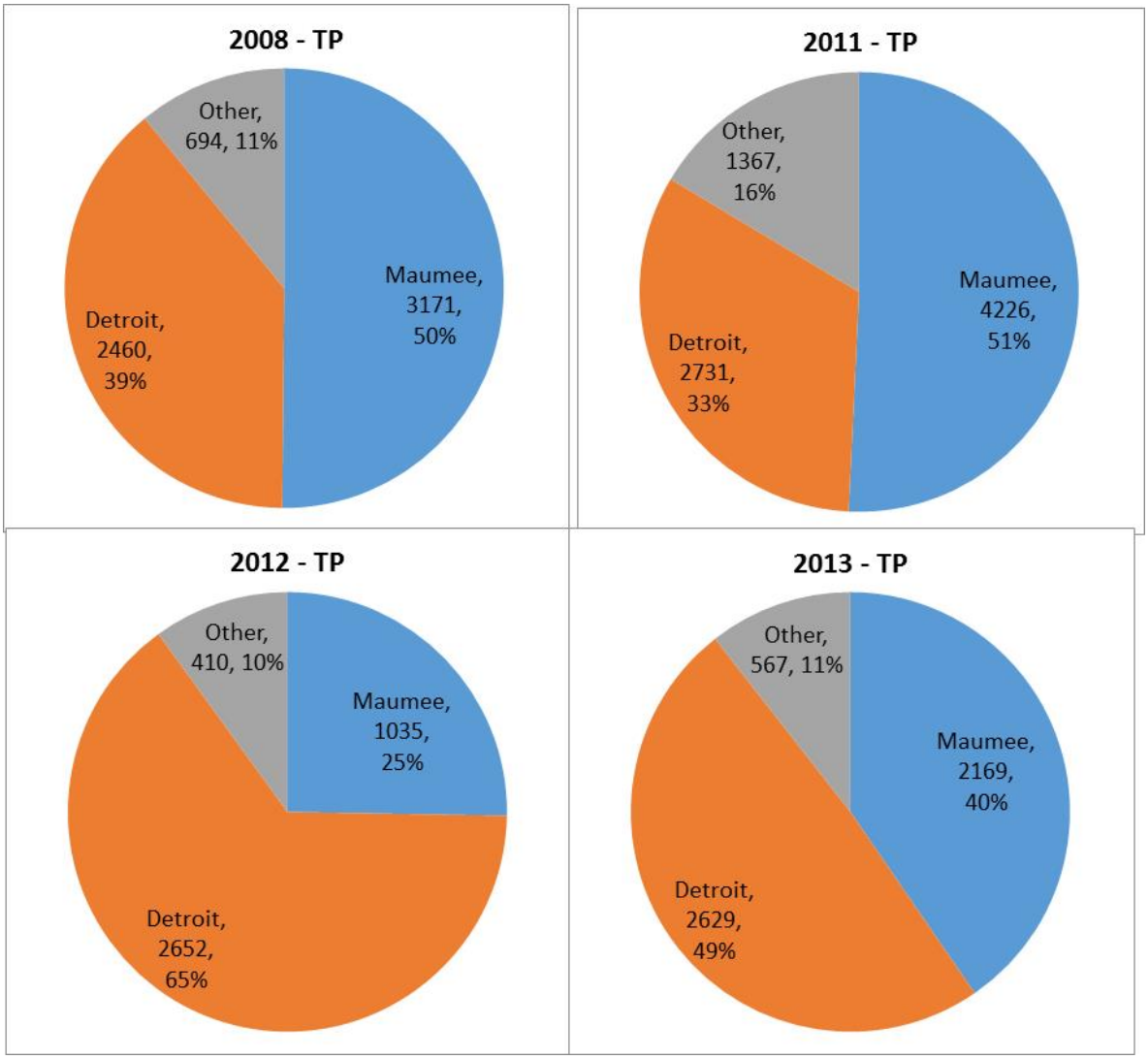

Figure B7-5: Annual average external TP load (metric tons) to the western basin from 2008, 2011, 2012, and 2013.

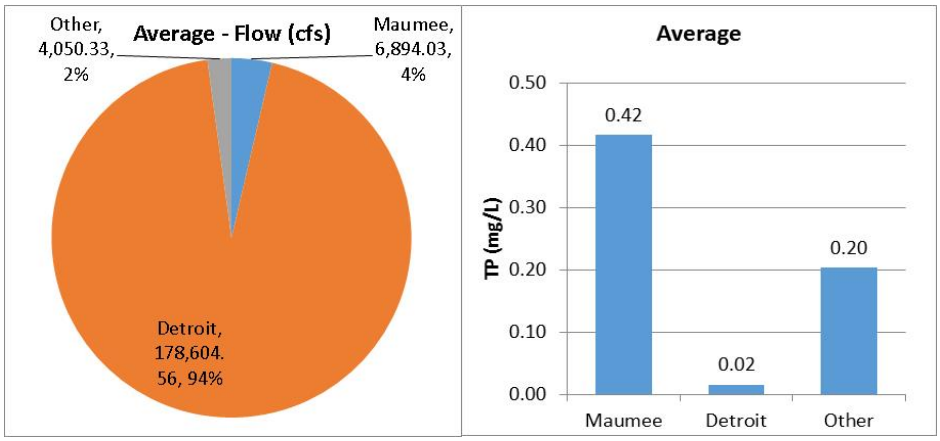

Figure B7-6: Average flow (left) and flow weighted mean TP concentration (right) to the western basin from 2008, 2011, 2012, and 2013.

Model Calibration/Confirmation Data

The primary dataset used for model calibration was from the University of Toledo. A brief description of that dataset is described below

University of Toledo. Data was collected by the University of Toledo from 2008, and 2011 to 2013 from Tom Bridgeman (Bridgeman 2014). Depth integrated samples were collected at the WLEB locations shown in Figure B7-7. The samples were analyzed for TSS, VSS, NH_3, chloride, sulfate, NO_2, NO_3, SiO_2, TP, SRP, total DP, fluoride, blue-green algal biovolume, and photosynthetic active radiation (PAR). Profile data using a water quality sonde were also collected, including temperature, dissolved oxygen, specific conductivity, pH, turbidity, and chlorophyll profiles. Biovolume was converted to biomass using the methods found in Bridgeman (2013).

3. Calibration/Confirmation

Approach

Calibration and confirmation of the model progressed from investigating model-data comparisons of physical parameters, to chemical parameters, and finally biological parameters. The physical model-data comparisons included surface water temperature model predictions to measured surface water temperatures. Chemical model-data comparisons were investigated for total phosphorus and soluble reactive phosphorus. Biological parameters that were calibrated include total chlorophyll a and cyanobacteria biomass.

Physical parameters. Water temperature calibration was achieved by ensuring that input atmospheric conditions were reasonable and accurate. Given the large surface area of the western basin, atmospheric conditions (air temperature and solar radiation) are two key model input time series that directly affect the simulated water temperature. Careful attention was made to extract appropriate time series forcings for these inputs from existing NOAA-GLERL interpolated data. Measurements of water temperature from the University of Toledo monitoring program were used to compare with the model for calibration and confirmation.

Chemical/Nutrient Parameters. Total phosphorus calibration focused heavily on ensuring appropriate time series concentrations were developed for tributaries with a low number of observations. These included the Detroit, Raisin, and Ottawa rivers. Western Lake Erie has a relatively low retention time (30

to 60 days), especially during high flow events and tributary boundary conditions highly influence the concentration of nutrients within the model domain. Additional attention was paid to understanding how particulate phosphorus settles within Western Lake Erie and how resuspension can increase TP concentrations in the water column. One additional point of calibration was ensuring sediment TP concentrations were set appropriately so that the relative contributions of resuspended sediments and pore water diffusive flux from the sediments on water column TP concentrations were reasonable. Grab samples of total phosphorus obtained from various sources were used as the basis for calibrating the model.

Soluble reactive phosphorus (SRP) calibration also focused on ensuring tributary concentrations were set appropriately for under-monitored tributaries and that sediment P concentrations are consistent with available observations. Additionally, SRP calibration was conducted coincident with phytoplankton calibration as the uptake of SRP by phytoplankton is the primary loss mechanism for SRP within the model domain.

Biological Parameters. Calibration of chlorophyll a and phytoplankton biomass focused on ensuring that each major algal group (blue-greens, diatoms, and greens) produced the appropriate measured biomass during its optimal time of the year. The chlorophyll a measurement provided a bulk estimate of the total algal biomass regardless of algal class in the water column, while blue-green biomass observations were specifically used to ensure that the model was capturing the size and magnitude of the harmful algal bloom (HAB). A table of the calibration values for each key model coefficient is presented below for each algal group. Calibration focused on altering the first four constants related to shaping the optimal temperature curve as well as the phosphorus half constant that governs nutrient limited growth. In addition, the base algal settling rate was adjusted to reflect current scientific understanding of the buoyancy of blue-green algae.

Table B7-2. Key phytoplankton functional group calibration coefficients used for WLEEM application.

Constant ID	Coefficient Description	Units	Blue-greens	Diatoms	Greens
TOPT*	Optimal growth temperature	deg C	25	15	22
K*C	Saturated phytoplankton growth rate at TOPT*	/day	2.2	1.6	1.8
K*BETA1	Temperature correction effect on growth rate below TOPT*	(deg C)-2	0.005	0.005	0.008
K*BETA2	Temperature correction effect on growth rate above TOPT*	(deg C)-2	0.002	0.008	0.012
IS*	Saturating algal light intensity	ly/day	300	150	150
KMN*	Half saturation constant for nitrogen	mg-N/L	0.010	0.020	0.020
KMP*	Half saturation constant for phosphorus	mg-P/L	0.002	0.001	0.001
KMS*	Half saturation constant for silica	mg-Si/L	0.002	0.002	0.002
CCHL*	Carbon to chlorophyll ratio	mg-C/mg-Chla	33	50	33
CRBP*1	Carbon to phosphorus ratio (Non P-limited)	mg-C/mg-P	40	40	40
CRBP*2	Carbon to phosphorus ratio (P-limited)	mg-C/mg-P	90	90	90
VSBAS*	Base algal settling rate	m/day	-0.5	0.25	0.1

The state variables mentioned above were compared with Western Basin observations using the same model coefficients for four different years (2008, 2011-13) that represent a wide range of hydrological, phosphorus loading, and other environmental forcing functions. The extent to which the model output is able to compare favorably with observations in the Western Basin for these state variables over time and space is viewed as a calibration/confirmation (sometimes referred to as “corroboration”) of WLEEM. Presented below are the results of that corroboration process.

Results

Calibration Period (2011-2013). Calibration comparisons for the model focused on comparisons of model prediction and monitoring data collected in 2011-2013 at the University of Toledo's stations MB18, 8M, and GR1 (Figure B7-7) for water temperature, TP, SRP, total chlorophyll a, and blue green algae biomass. These three station comparisons are focused on here because they represent a distance gradient from the mouth of the Maumee River. Figures 8 through 11 provide model-to-data comparisons of time series for the key state variables at each of these stations.

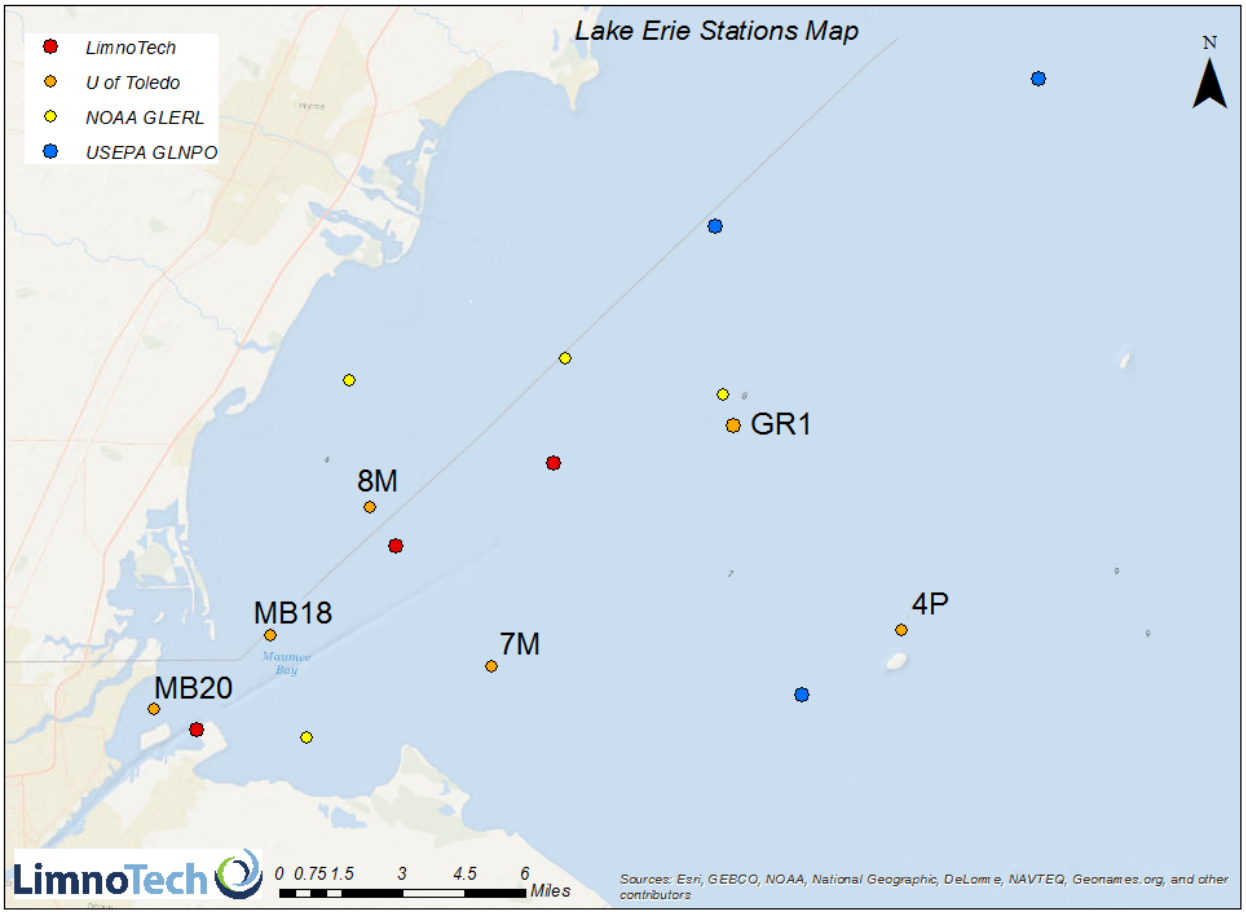

Figure B7-7: University of Toledo and other program monitoring stations in the Western Lake Erie Basin.

Figure B7-8 shows that the model (solid blue line shown with a label of "RCA (Baseline)") reproduces measured water temperature (points) very closely. Maximum water temperatures in 2011, 2012, and 2013 reach ~27°C, with the summer of 2013 being slightly cooler than the other two years. The model accurately captures decreases in water temperature in the late summer and early fall. In 2013, continuous water temperature data available from NOAA-GLERL station (RA-2) near GR1 show how the model captures the observed decline in temperature in mid-August.

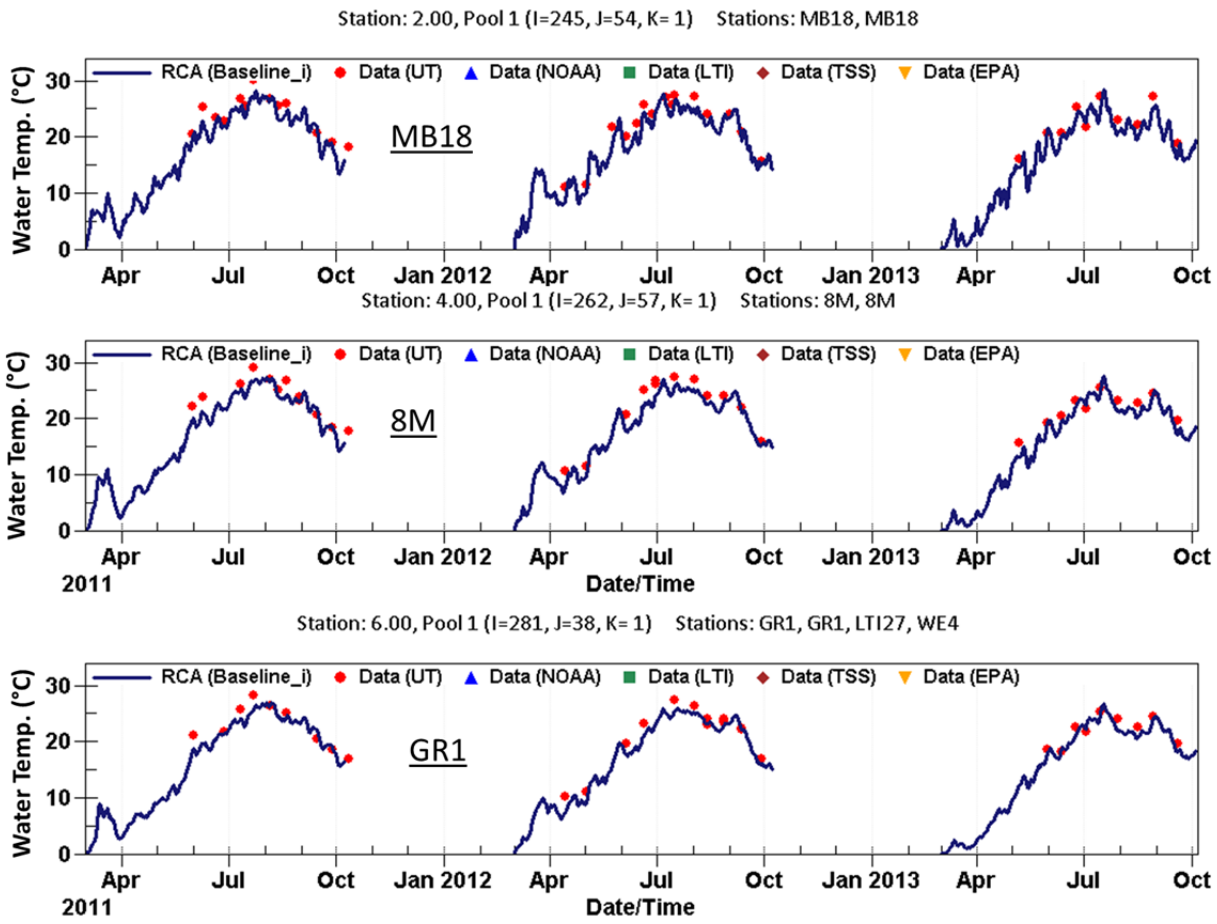

Figure B7-8: Water temperature (°C) model-data comparison at University of Toledo stations MB18 (top), 8M (middle), and GR1 (bottom) for 2011 to 2013 (Mar.-Oct.).

The water quality state variables evaluation focused on comparing model predictions and monitoring data for TP, SRP, and chlorophyll-a. Time series plots from 2011, 2012, and 2013 for these parameters are shown below for stations MB18, 8M, and GR1 (see Figures B7-9 through B7-11). Figure B7-9 shows the TP response to high flow spring loading events, with the response being attenuated (diluted) with distance from the Maumee River mouth. Note that 2013 experienced higher than usual July and August loading, which had as shown below an impact on the magnitude and duration of the *Microcystis* bloom. In Figure B7-10, it is evident that the SRP concentration behaves as expected, with high load driven spring concentrations followed by low summer concentrations as a result of biological uptake at that time. This behavior is also captured well by the model. Finally, Figure B7-11 shows the pattern of total chlorophyll a concentration for the system. There seems to be a small spring peak that the model indicates as diatom-dominated; but that occurs before sampling has begun. The higher late summer – fall chlorophyll a levels are dominated by cyanobacteria, which is simulated by the model and measured in the data.

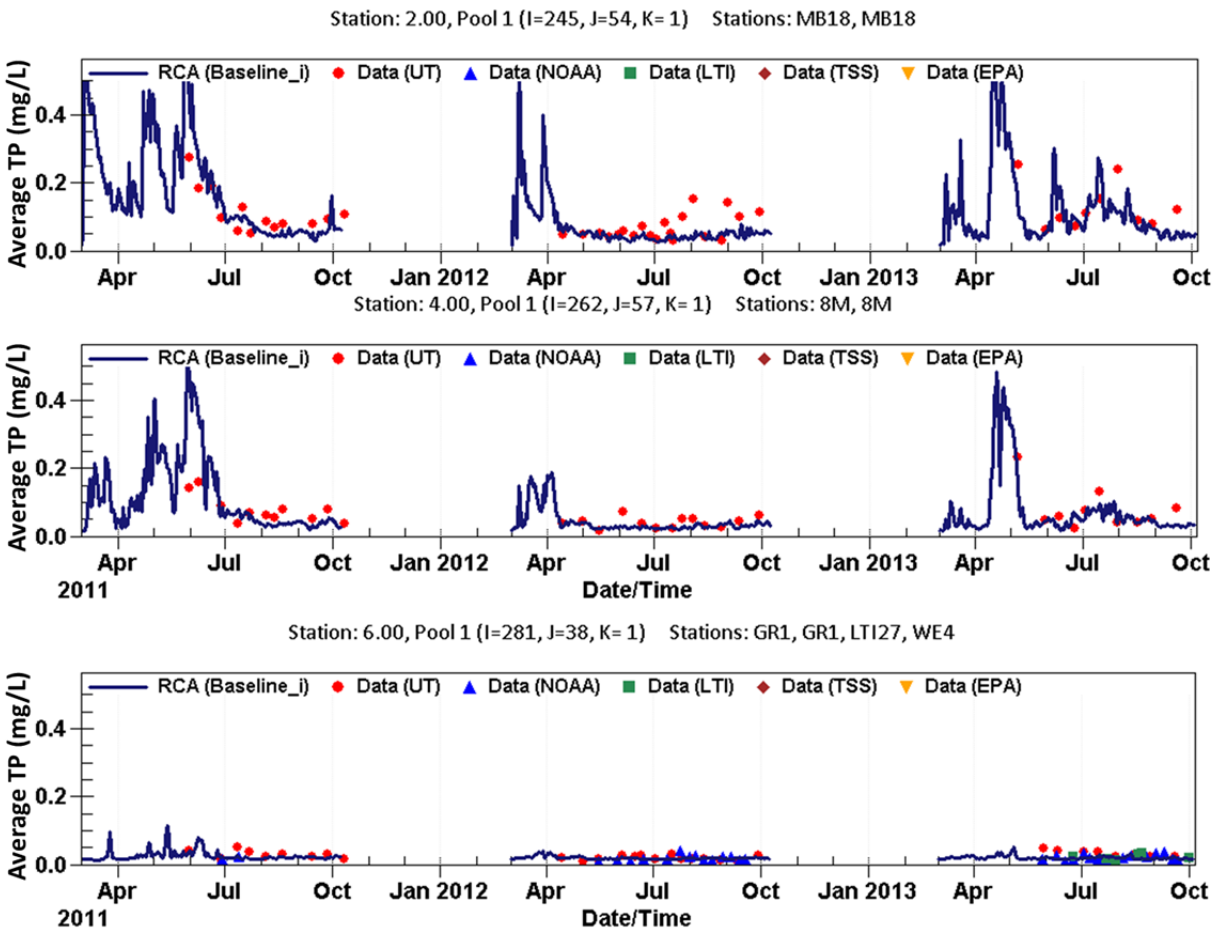

Figure B7-9: Total phosphorus (mg/L) model-data comparison at University of Toledo stations MB18 (top), 8M (middle), and GR1 (bottom) for 2011 to 2013 (Mar.-Oct.).

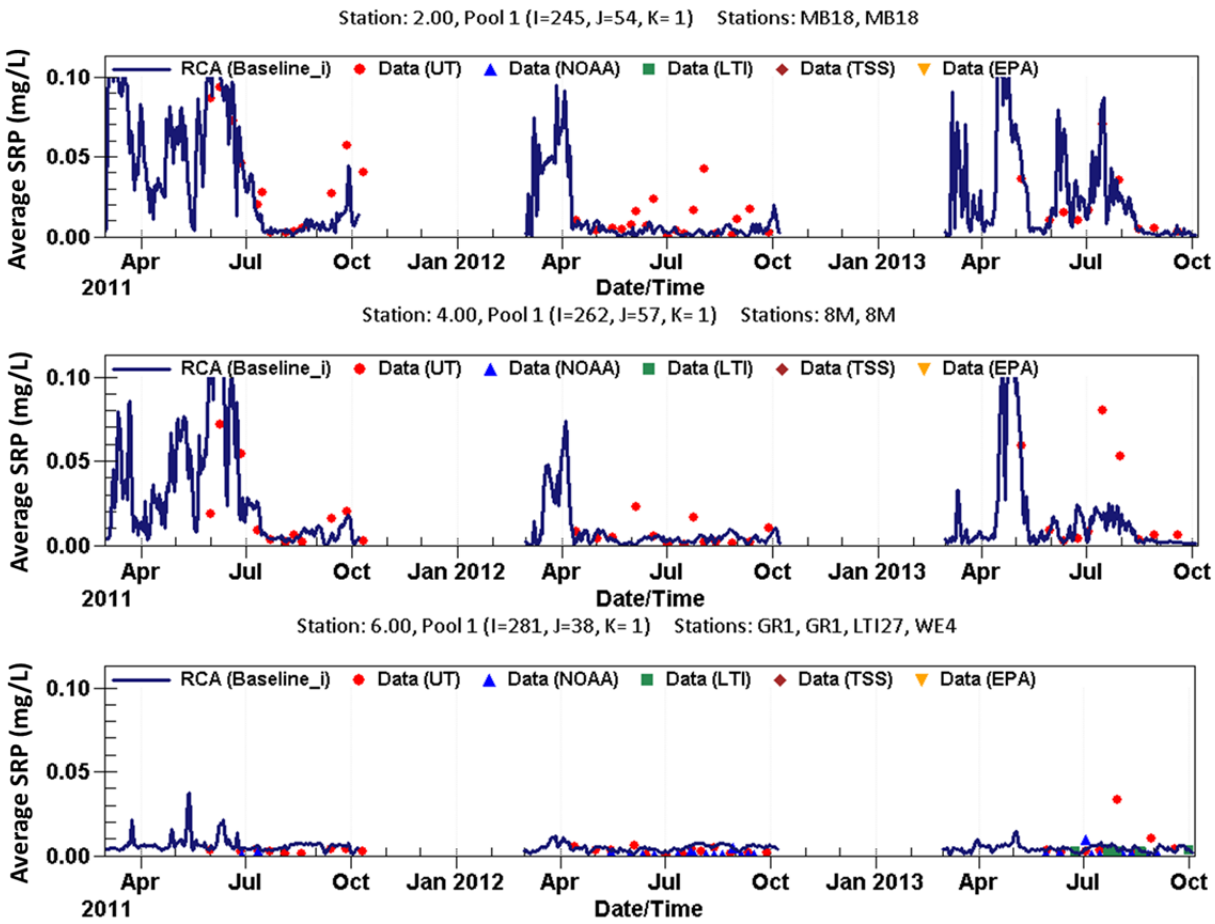

Figure B7-10: Soluble reactive phosphorus (mg/L) model-data comparison at University of Toledo stations MB18 (top), 8M (middle), and GR1 (bottom) for 2011 to 2013 (Mar.-Oct.).

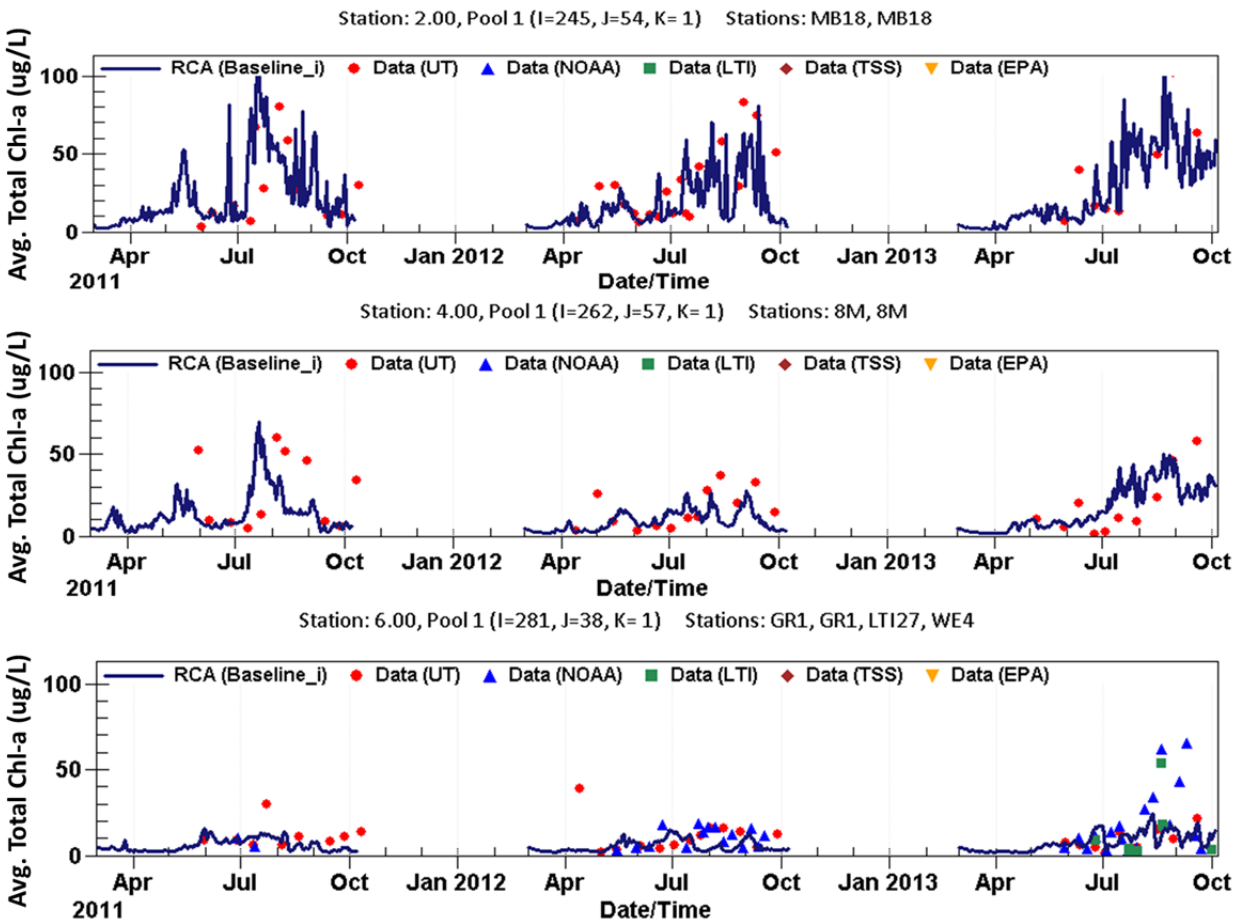

Figure B7-11: Chlorophyll (ug/L) model-data comparison at University of Toledo stations MB18 (top), 8M (middle), and GR1 (bottom) for 2011 to 2013 (Mar.-Oct.).

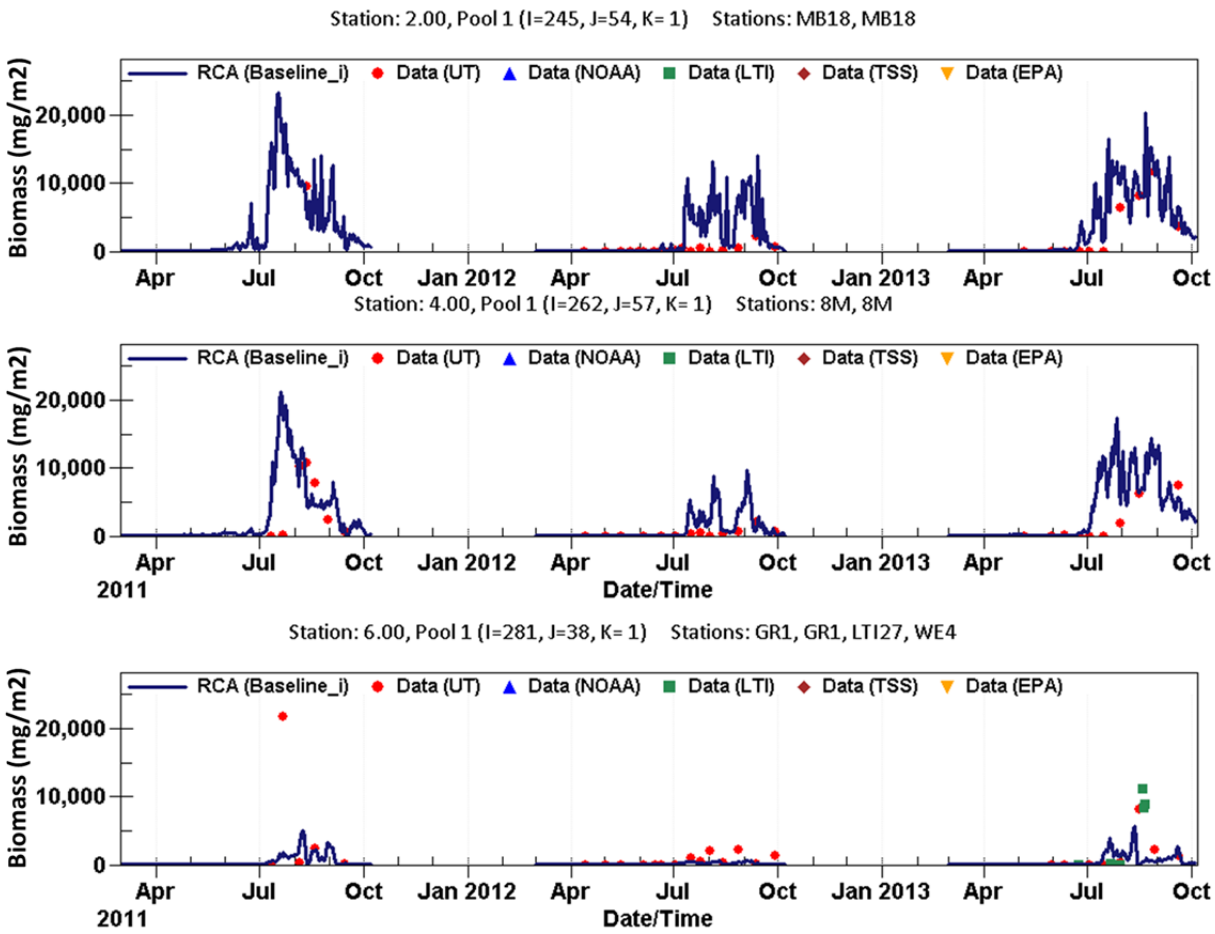

Figure B7-12: Cyanobacteria biomass (mg/m^2) model-data comparison at University of Toledo stations MB18 (top), 8M (middle), and GR1 (bottom) for 2011 to 2013 (Mar.-Oct.).

Finally, comparisons of model predicted HAB depth-averaged mass density at the same stations are shown in Figure B7-12. These comparisons show that WLEEM does a good job of capturing the relative differences in profiles among years; however, it over-predicts peak densities during the low spring load year (2012). This seems to occur because in that year our model underestimates the deposition of particulate phosphorus in the Maumee River between Waterville and the river mouth (a distance of about 20 miles), thus computing a spring particulate phosphorus load to Maumee Bay that is too large.

Confirmation Period (2008)

After calibration of the WLEEM was completed for the 2011-2013 time period, model confirmation was performed by executing the WLEEM for a separate time period without changing input coefficients and parameters. The model confirmation was completed using 2008 hydrologic conditions and environmental forcing functions. Monitoring data collected in 2008 at the same University of Toledo stations for water temperature, TP, SRP, total chlorophyll a, and blue-green algae biomass were used to evaluate model performance during this confirmation period. Figures B7-13 through B7-17 were used to compare WLEEM output and observed data.

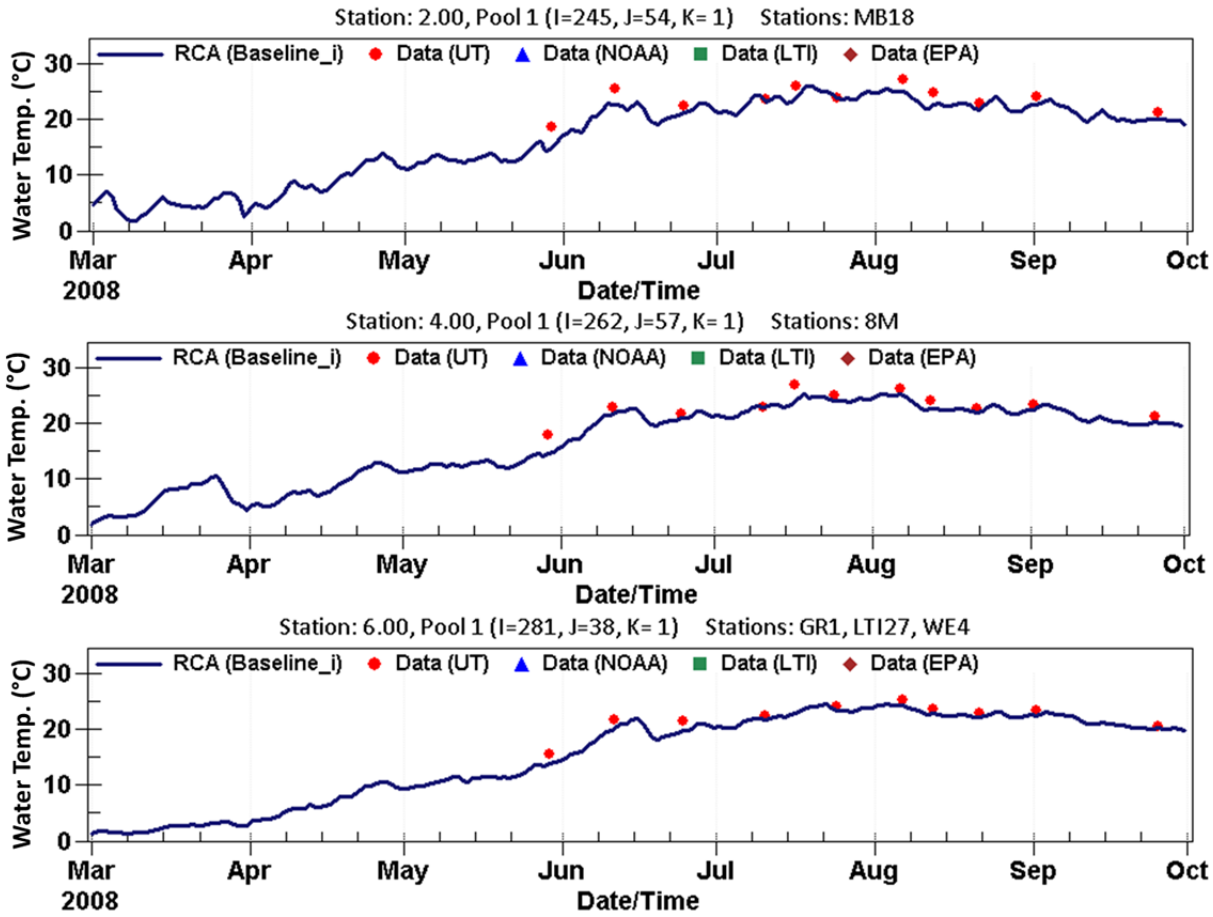

Figure B7-13: Water temperature (°C) model-data comparison at University of Toledo stations MB18 (top), 8M (middle), and GR1 (bottom) for 2008 (Mar.-Oct.).

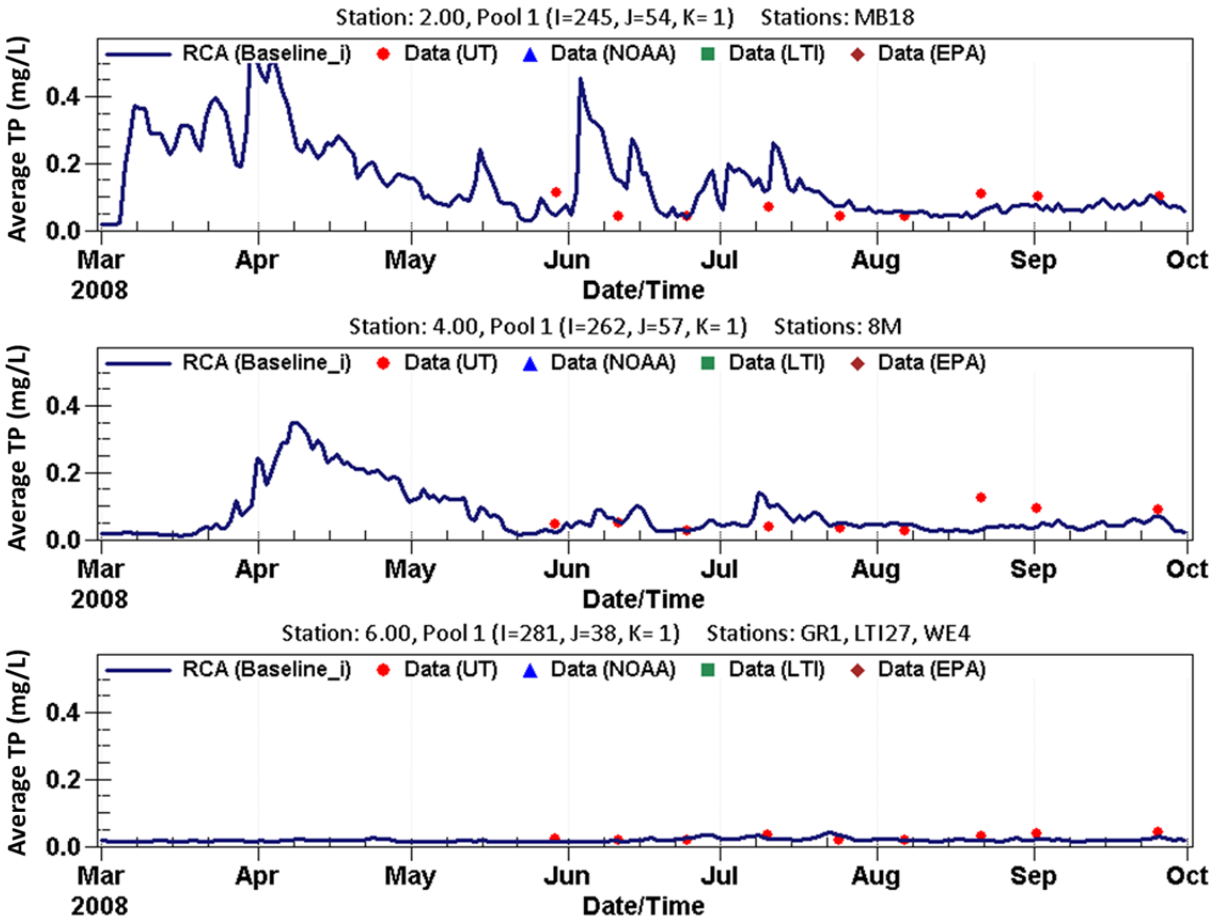

Figure B7-14: Total phosphorus (mg/L) model-data comparison at University of Toledo stations MB18 (top), 8M (middle), and GR1 (bottom) for 2008 (Mar.-Oct.).

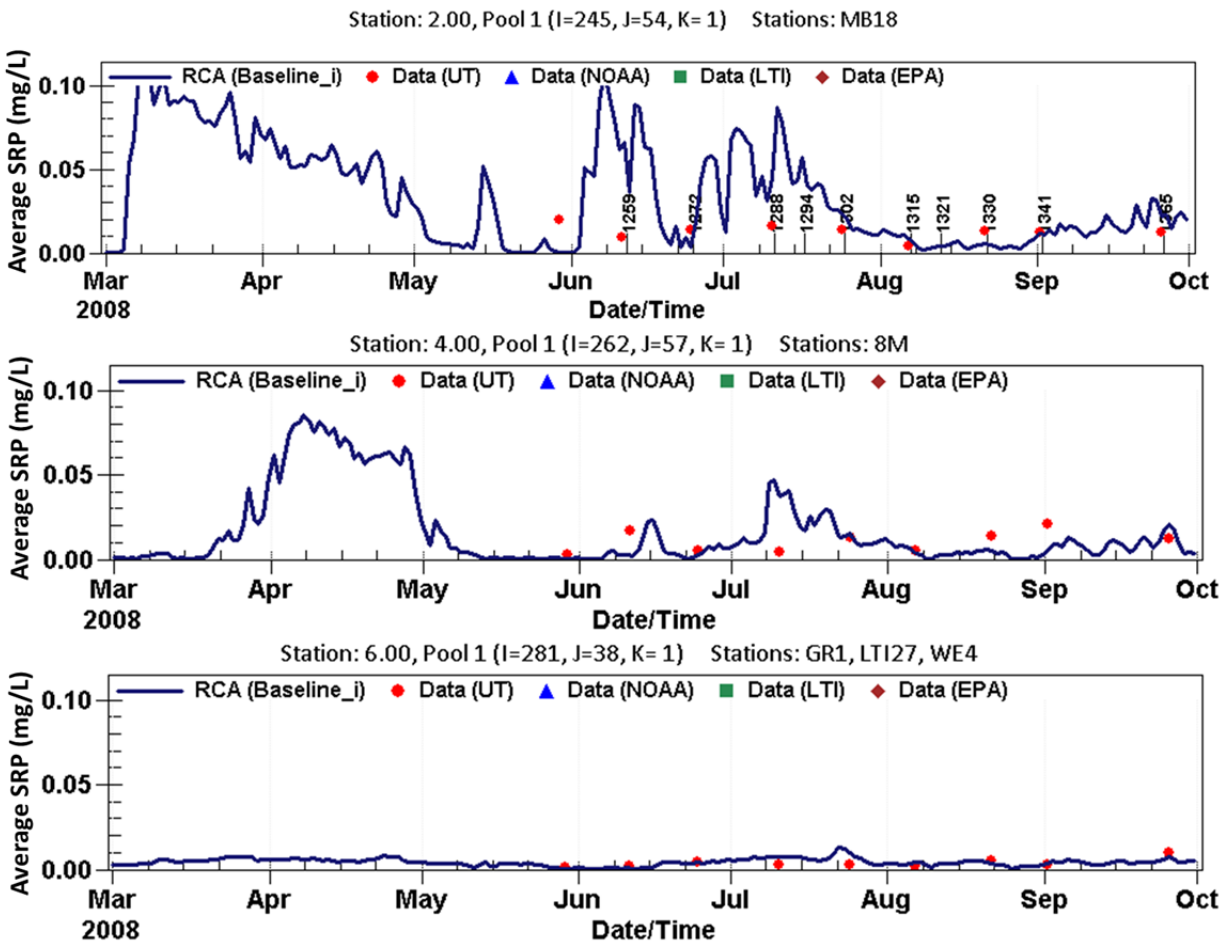

Figure B7-15: Soluble reactive phosphorus (mg/L) model-data comparison at University of Toledo stations MB18 (top), 8M (middle), and GR1 (bottom) for 2008 (Mar.-Oct.).

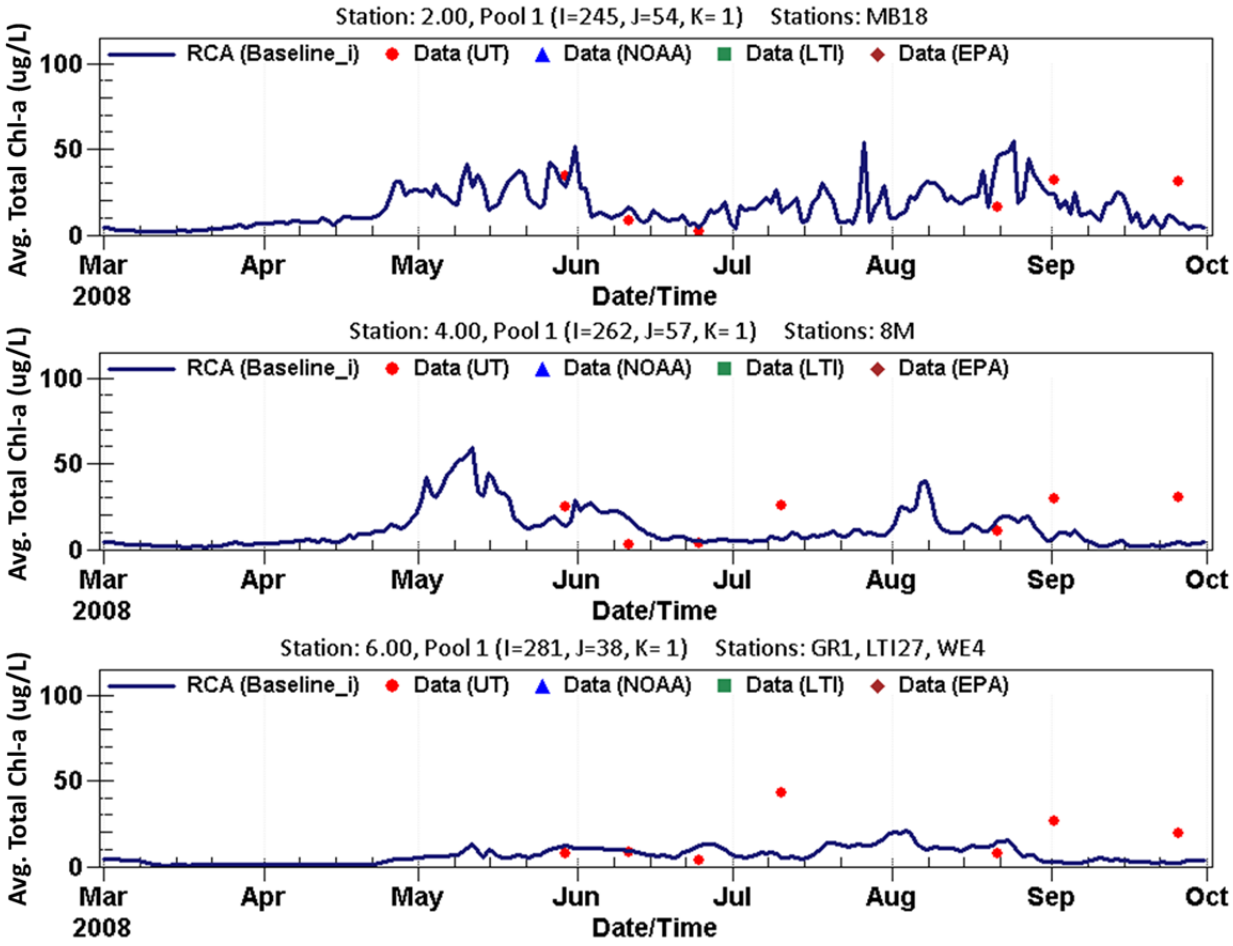

Figure B7-16: Total chlorophyll a (µg/L) model-data comparison at University of Toledo stations MB18 (top), 8M (middle), and GR1 (bottom) for 2008 (Mar.-Oct.).

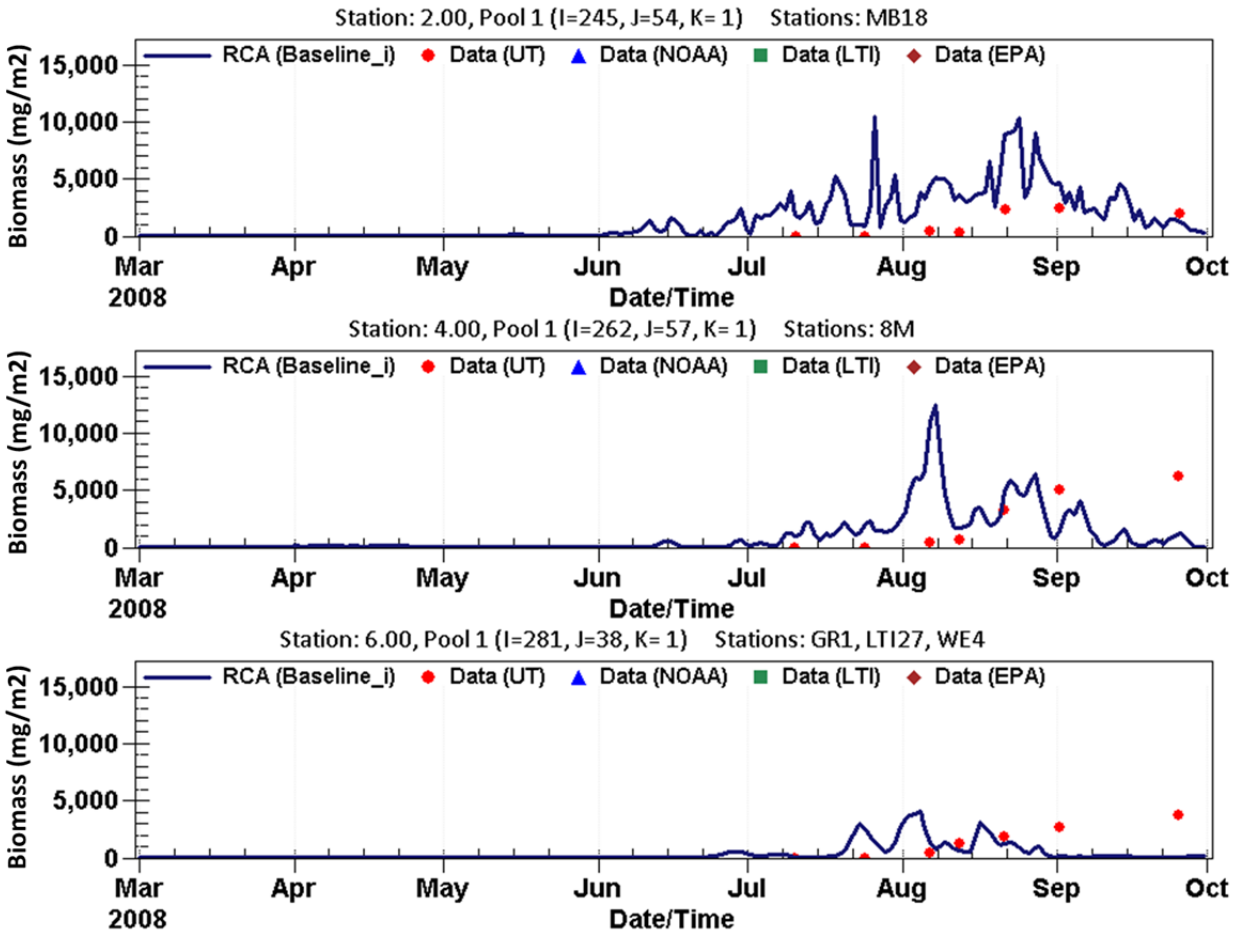

Figure B7-17: Cyanobacteria biomass (mg/m^2) model-data comparison at University of Toledo stations MB18 (top), 8M (middle), and GR1 (bottom) for 2008 (Mar.-Oct.).

The WLEEM comparison to 2008 data confirms that the model can simulate the key metrics of concern for a wide range of Western Basin forcing functions without adjusting any of its model coefficients. The 2008 comparison also shows that perhaps the change in particulate phosphorus load between Waterville and the mouth of the river is underestimated.

Annual Microcystis Biovolume. As an additional model confirmation test, an annual *Microcystis* biovolume was computed from WLEEM output to compare against estimates generated from University of Toledo monitoring data. The method used to estimate the annual biovolume followed the approach described in Bridgeman et al. (2013), which entailed calculating the area beneath the daily time series plots for a given station using the trapezoidal rule. The result of those computations were then averaged among the University of Toledo's 4P, 7M, 8M, and GR1 stations (Figure B7-7) to get the final annual estimate of HAB size. Figure B7-18 shows the 5-day rolling average *Microcystis* biovolume computed from WLEEM output compared with the bloom size time series data provided by Bridgeman. Bridgeman used this approach to produce a bar graph of measured bloom size for all years from 2002 -2013. Figure B7-19 compares the annual *Microcystis* biovolume computed by WLEEM against estimates computed

from data provided by Bridgeman. Comparisons were not available for 2009 and 2010, as the WLEEM has not been simulated for those periods.

These model-data comparisons corroborate the model's ability to capture inter-annual variability of HABs biomass across a wide range of conditions. This overall model skill assessment provides confidence in using the model to develop the desired load – response curves for the Western Basin of Lake Erie.

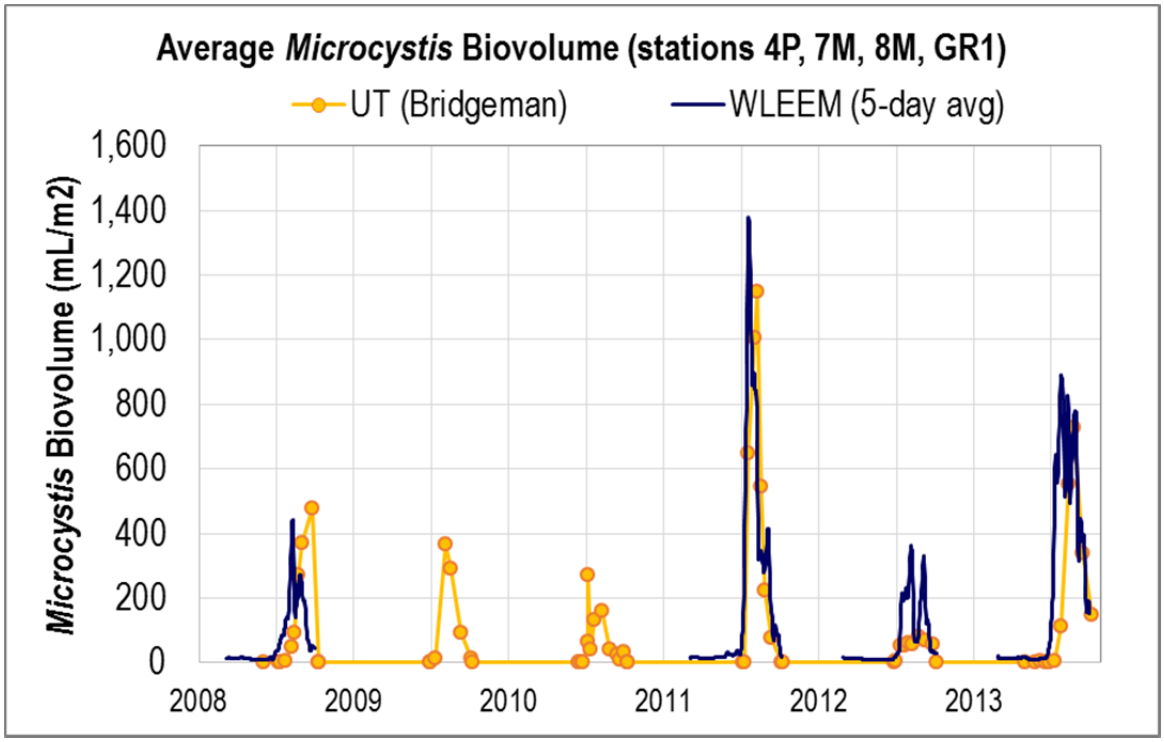

Figure B7-18: Average *Microcystis* biovolume (mL/m^2) model-data comparison at University of Toledo stations (4P, 7M, 8M, GR1) for 2008 – 2013.

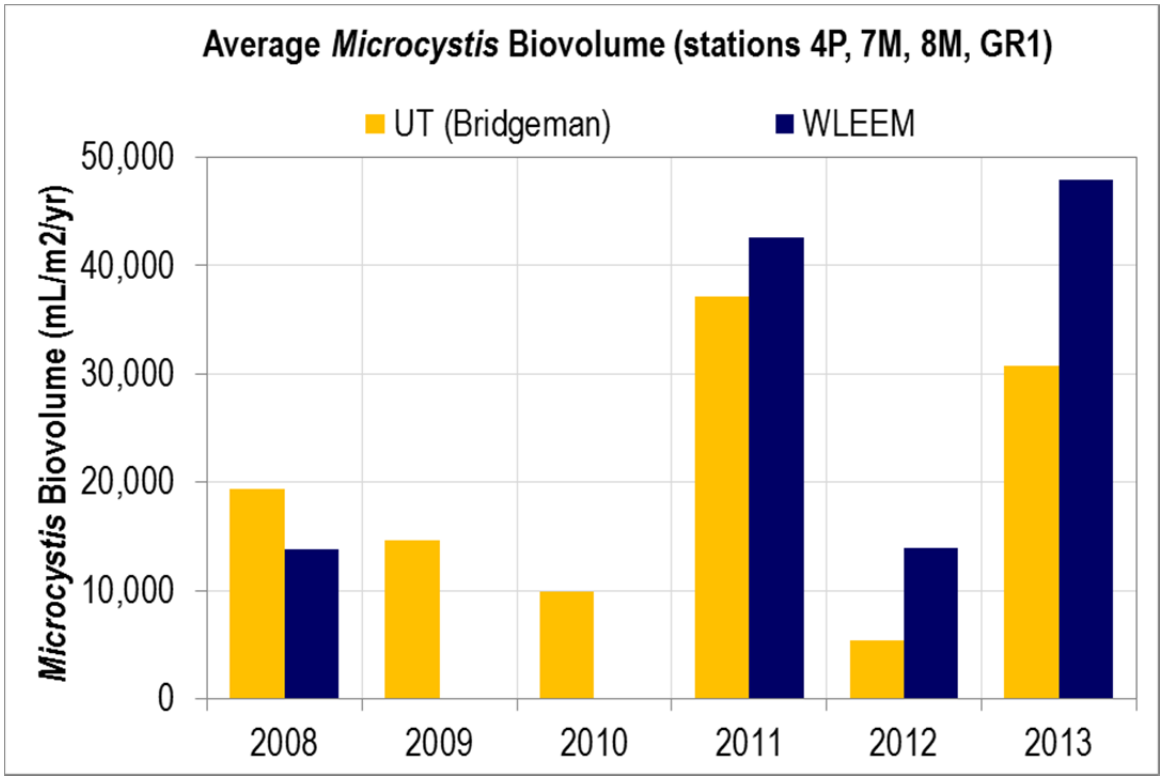

Figure B7-19: Average annual *Microcystis* biovolume (mL/m^2/yr) model-data comparison at University of Toledo stations (4P, 7M, 8M, GR1) for 2008 – 2013.

Statistical Evaluation and Uncertainty Analysis

A statistical evaluation of the model-data comparisons were developed for the purpose of: 1) quantifying the capability of the model to reproduce water quality and algal observations, and 2) providing the basis for evaluating the uncertainty of load-response curves developed based on model simulation results.

Although water quality models have been commonly applied in practice and presented in the literature, the WLEEM is unique in that it attempts to simulate both nutrients and algal functional groups within a very large coastal system. Although formal calibration targets have not been defined for the WLEEM, a useful point of reference is the calibration targets documented by Donigian et al. (2000, 2002) based on the application of the *Hydrologic Simulation Program – FORTRAN* (a watershed and riverine model). The general water quality targets defined by Donigian et al. are summarized in Table B7-3, with acceptable ranges of "percent difference" corresponding to categories of "Very Good", "Good", and "Fair". A comparison of the ranges in this table suggests that model accuracy is expected to be less for water quality (e.g., nutrient) parameters relative to physical parameters (e.g., water temperature). Although not indicated in Table B7-3, it follows that a model's capability to accurately reproduce chlorophyll a concentrations and *Microcystis* biomass will be less than it is for water quality/nutrient concentrations.

Table B7-3. General water quality calibration targets or tolerances (Donigian 2000, 2002).

Parameter	*% Difference Between Simulated and Recorded Values*		
	Very Good	*Good*	*Fair*
Water Temperature	< 7	8 - 12	13 - 18
Water Quality / Nutrients	< 15	15 - 25	25 - 35

CAVEATS: Relevant to monthly and annual values; storm peaks may differ more; Quality and detail of input and calibration data; Purpose of model application; Availability of alternative assessment procedures; Resource availability (i.e. time, money, personnel).

The development and calculation of representative metric(s) to support the evaluation of model-simulated water temperature, nutrients, and biological parameters is challenging for a fine-scale model like WLEEM being applied to a large aquatic ecosystem. The specification of a calibration metric is especially difficult for applications of models such as the WLEEM to large water bodies where monitoring data are only sporadically available at a limited number of locations. For example, even a small misrepresentation of the wind magnitude or direction in the WLEEM could affect the trajectory of the Maumee River plume and make a significant difference in the chlorophyll a concentration and/or *Microcystis* biomass being simulated at a particular location in the Western Basin on a given day. Monitoring data collected by the University of Toledo represent relatively infrequent snapshots of concentrations and *Microcystis* biovolume/biomass at single points in space, and therefore cannot be expected to capture all of the complex spatial and temporal variability within the Western Basin. Likewise, the hydrodynamic, sediment and nutrient transport, and algal processes represented in the model are only a simplification of reality, and it is not possible for the model to reproduce water quality conditions precisely at a given location at a specific time. Therefore, realistically both data representativeness and model insufficiencies (e.g., in terms of representing system processes) limit the capability of a model to reproduce observed concentrations and biovolume/biomass.

In recognition of the challenges described above, a unique metric was developed to quantify the WLEEM's performance in terms of reproducing available monitoring data. The metric established for represents the "median of the absolute station-specific average percent difference" for an individual water quality or biological state variable (referred to as the "median annual percent difference" below for brevity). All University of Toledo monitoring stations were included in the calculation of the metric. The steps outlined below were followed to compute the metric for water temperature, TP, SRP, and chlorophyll a concentration:

1. The relative percent difference (RPD) was calculated for each station for each day when sampling occurred at that station:

$$[RPD] = [(X_{model,i} - X_{data,i}) / (½*(X_{model,i} + X_{data,i}))] \quad (1)$$

where $X_{data,i}$ is the observed value and $X_{model,i}$ is the simulated value on day *i*.

2. The average of the daily RPD values was calculated for each station (MB20, MB18, 4P, 7M, 8M, and GR1) for each calendar year (i.e., 2008, 2011-13), and the absolute value was taken.
3. The median of the station-specific values calculated via step #2 was taken for each calendar year to serve as the final metric.

An alternative approach was used to develop a metric to quantify the WLEEM's performance in terms of predicting blue-green (*Microcystis*) biomass. This approach was based on the annual *Microcystis* biovolume estimated by Bridgeman and simulated by WLEEM, as shown in Figure B7-19. The steps followed in calculating this metric are as follows:

1. The annual average "observed" *Microcystis* biovolume (mL/m^2/yr) was calculated across the University of Toledo's 4P, 7M, 8M, and GR1 monitoring stations consistent with the approach followed by Bridgeman.
2. A comparable estimate of the "simulated" *Microcystis* biovolume (mL/m^2/yr) was estimated from daily WLEEM results for blue-green algae biomass.
3. The absolute values of the relative percent differences of the annual biovolume estimates were tabulated for each year.

A summary of model performance based on the metrics described above is provided in Figure B7- 20 and Table B7-4. The following observations can be made based on these results:

- In general, the model closely reproduces water temperature. When evaluated against the targets suggested by Donigian et al. (2000, 2002), the model rates as "very good" to "good" for each year.
- For TP, the "median annual percent difference" ranges from 9% to 31%, with a median value of 20% for the four years represented. Evaluating these results against the TP targets in Table 3 suggests that the model performance for TP is "Good" to "Fair".
- For SRP, the "median annual percent difference" ranges from 6% to 57%, with a median value of 26% for the four years represented. Evaluating these results against the SRP targets in Table 3 suggests that the model performance for SRP is generally "Fair" to "Good".
- For chlorophyll a concentration and blue-green (*Microcystis*) algae biovolume, "median annual percent difference" results generally fall within the range of 20-44%. As noted above, specific benchmarks for chlorophyll a and *Microcystis* biovolume/biomass have not been identified at this time. However, generally comparing these results to the water quality / nutrient metrics and taking into account the additional challenges and environmental variability involved with biological parameters suggests that the model performs satisfactorily for most years.
- The one exception to the above evaluation is blue-green algae biovolume in year 2012. As discussed above in the calibration discussion and shown in Figure B7-18, the model currently overpredicts blue-green during this year. It should be noted again that 2012 was a year with exceptionally low flow and TP and SRP loadings during the spring months. Given these conditions it is possible that the TP and SRP loads for 2012 are currently overstated, as there is limited information to estimate phosphorus deposition, uptake, and retention that would occur between the Waterville monitoring location (~20 miles upstream) and the mouth of the Maumee River.

The outcome of the statistical evaluation described above suggests that the overall performance of the model is acceptable with respect to simulation of water temperature, TP, SRP, chlorophyll a, and *Microcystis* biomass. Furthermore, the "median annual percent difference" results provided in Figure

B7-20 and Table B7-4 can be used as an indicator of model uncertainty with respect to simulating these water quality and biological variables for the load-response curves.

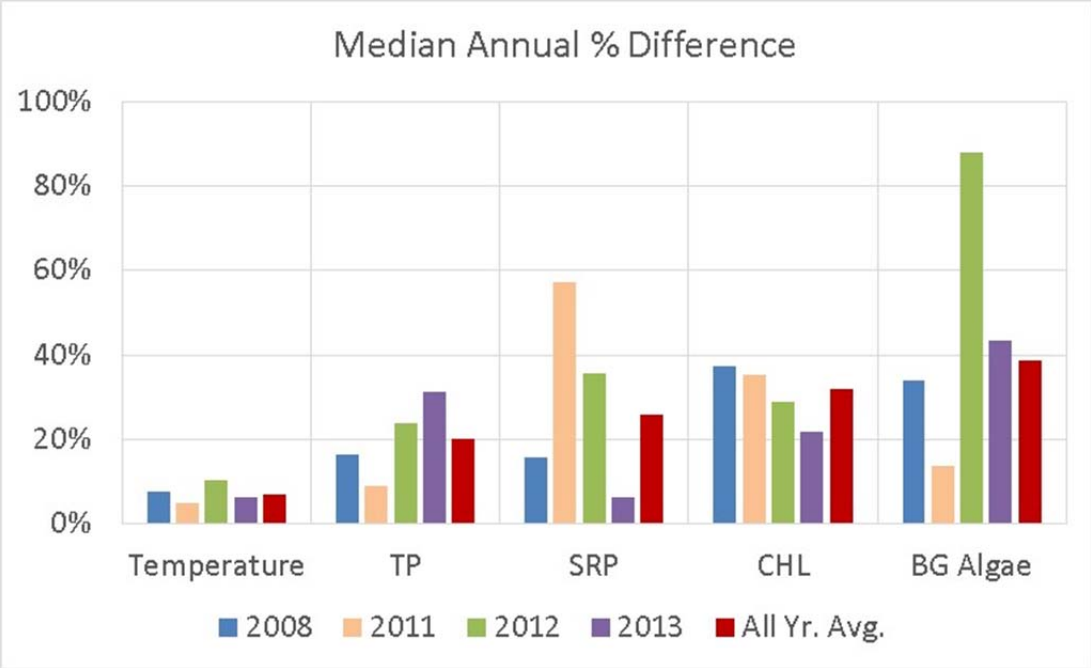

Figure B7-20: "Median annual percent difference" metric results by year and variable across all University of Toledo monitoring stations.

Table B7-4. "Median annual percent difference" metric results by year and variable across all University of Toledo monitoring stations.

Year	Temperature	TP	SRP	CHL	BG Algae
2008	8%	16%	16%	37%	34%
2011	5%	9%	57%	35%	14%
2012	10%	24%	36%	29%	88%
2013	6%	31%	6%	22%	44%
Median of Annual Results	**7%**	**20%**	**26%**	**32%**	**39%**

4. Model Application

Load-Response Curves

Process Description. Following completion of the calibration and confirmation efforts, the WLEEM was used to evaluate the response of several endpoints as a function of phosphorus loading to the WLEB. The process to develop the load-response curves presented in this section involved executing multiple simulations where the only difference from the baseline simulation was a scaling of the daily external phosphorus loads (by adjusting source concentration, but not flow) relative to a given baseline scenario. All other model input parameters, forcing functions (hydrology, temperature, wind, solar radiation, etc.), and external loads (sediment, nitrogen, etc.) were exactly the same as the baseline simulation. Four

baseline simulations were considered to introduce variability in environmental conditions and forcing functions; the 2008, 2011, 2012, and 2013 seasons which were used for the model calibration and evaluation process presented above. The independent variable on the load-response curves were presented as either the annual total phosphorus load to the WLEB from all sources for the conventional response indicators (TP, SRP, and total chlorophyll a; or both total annual load and the Spring (March-July and April-July) total phosphorus load from the Maumee River tributary only for the cyanobacteria response indicators. In summary, the following dependent variables (metrics) were evaluated for the entire WLEB as either a volume-weighted average concentration or total mass:

- July-September average TP concentration (mg/L)
- July-September average SRP concentration (mg/L)
- July-September average chlorophyll concentration (ug/L)
- July-September average cyanobacteria biomass (metric tons)
- Maximum 30-day rolling average cyanobacteria biomass (metric tons)

Results and Interpretation. Figures B7-21 and B7-22 examine the response of TP and SRP concentrations in the WLEB to a range of TP loading scenarios and environmental conditions. Annual TP loads were decreased by 50% and 75% for all tributaries to WLEB relative to the baseline for 2011, 2012, and 2013. The 2008 simulations also included reductions of 25% and 100%, and an increase of 25%. For both TP and SRP there is a strong linear relationship between the annual TP load to the WLEB and the July-September volume-weighted average concentrations. Varying hydrology for these four years can significantly affect the loading, but other environmental factors such as wind-driven circulation and temperature do not seem to cause great deviation from the linear relationships shown in these plots.

The results shown in Figure B7-21 suggest that an annual Western Basin TP load of 2500 metric tonnes would be required to achieve a July – September Western Basin concentration of 15 µg/L, the 1978 Annex 3 target TP concentration for the Western Basin. It should also be noted that the y-intercepts of the curves for both TP and SRP concentrations under the 100% TP load reduction scenario simulated for 2008 are greater than zero because flux of phosphorus from bed sediments by diffusion and resuspension contributes to the water column phosphorus concentrations.

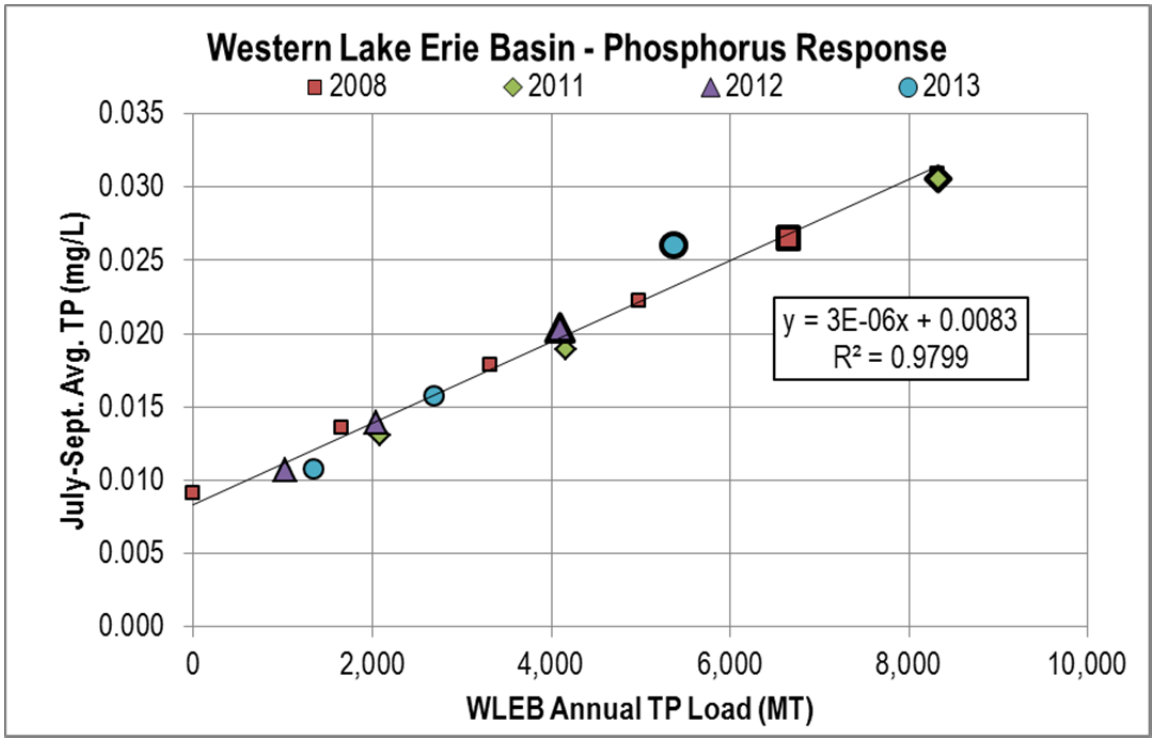

Figure B7-21: TP concentration response under various annual WLEB TP loading (from all external sources) scenarios and varying annual environmental conditions. Symbols for the baseline scenario for each year are larger and bolded.

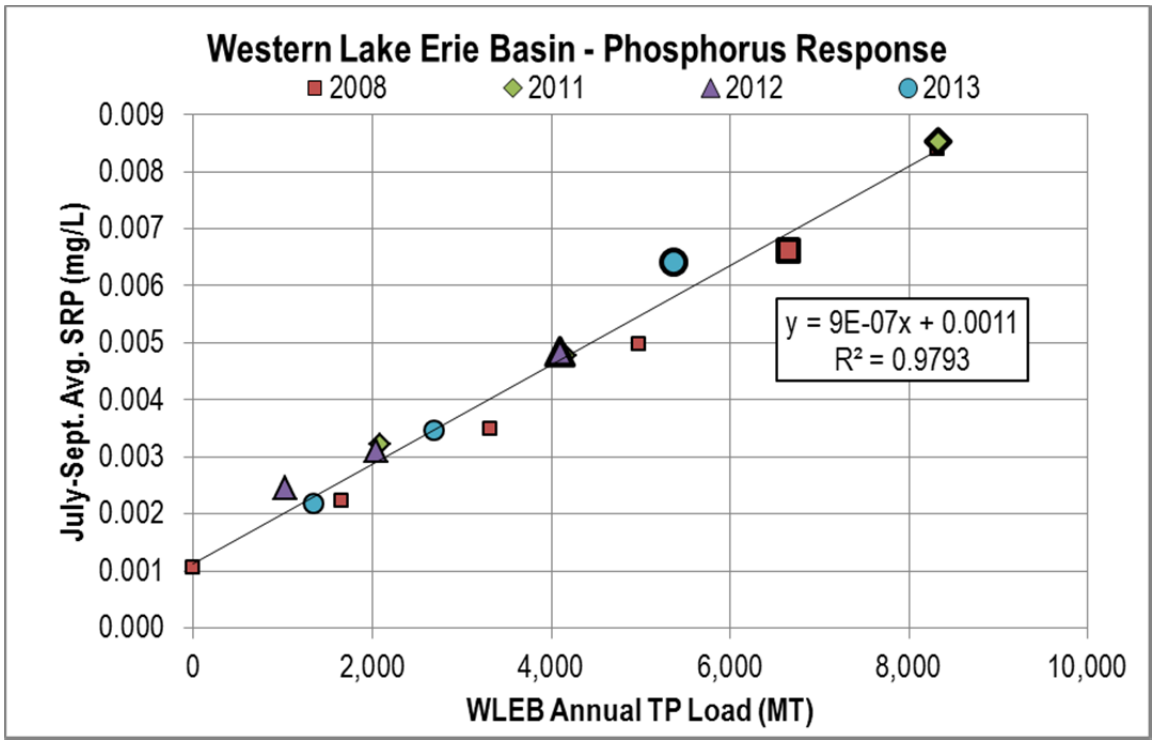

Figure B7-22: SRP concentration response under various annual WLEB TP loading (from all external sources) scenarios and varying annual environmental conditions. Symbols for the baseline scenario for each year are larger and bolded.

Figures B7-23 through B7-25 examine the response of total chlorophyll a concentrations and cyanobacteria biomass (July – September average basinwide biomass and peak 30-day average basinwide biomass) in the WLEB to the same annual WLEB TP loading scenarios. The responses are non-linear for both total chlorophyll a and cyanobacteria biomass, with chlorophyll a demonstrating a Michaelis-Menten inverse hyperbolic saturation response as typically observed for a chlorophyll a vs. phosphorus growth relationship. However, the cyanobacteria biomass plots are more exponential; suggesting that a larger response to a given TP load reduction is seen at higher baseline loads than at lower baseline loads. Again, this is expected since cyanobacteria have a higher available phosphorus concentration requirement for bloom formation than other phytoplankton groups.
All three of these relationships show more deviation from the regression line for a given set of environmental conditions than observed for the TP and SRP concentration curves. The scatter demonstrates both a greater uncertainty in predicting chlorophyll concentrations and cyanobacteria biomass, and a larger influence of variability in other forcing functions, such as water temperature, currents, and timing of nutrient loads, on biological growth from year-to-year.

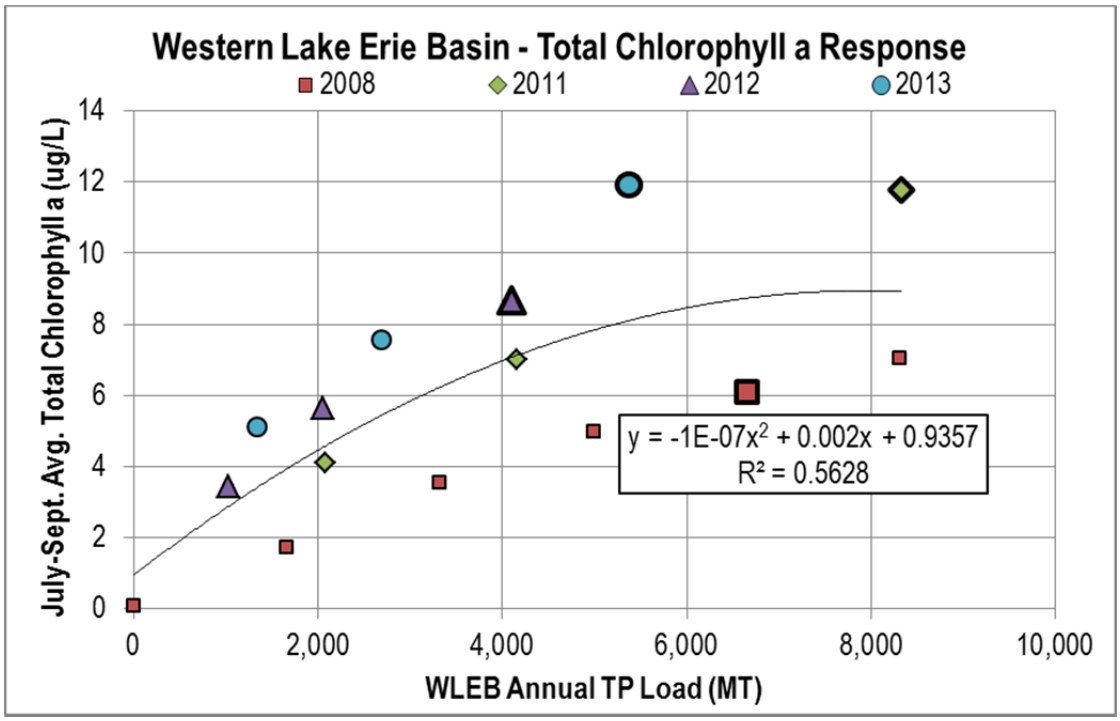

Figure B7-23: July – September average total chlorophyll a concentration response to a range of annual WLEB TP loading (from all external sources) scenarios and varying annual environmental conditions. Symbols for the baseline scenario for each year are larger and bolded.

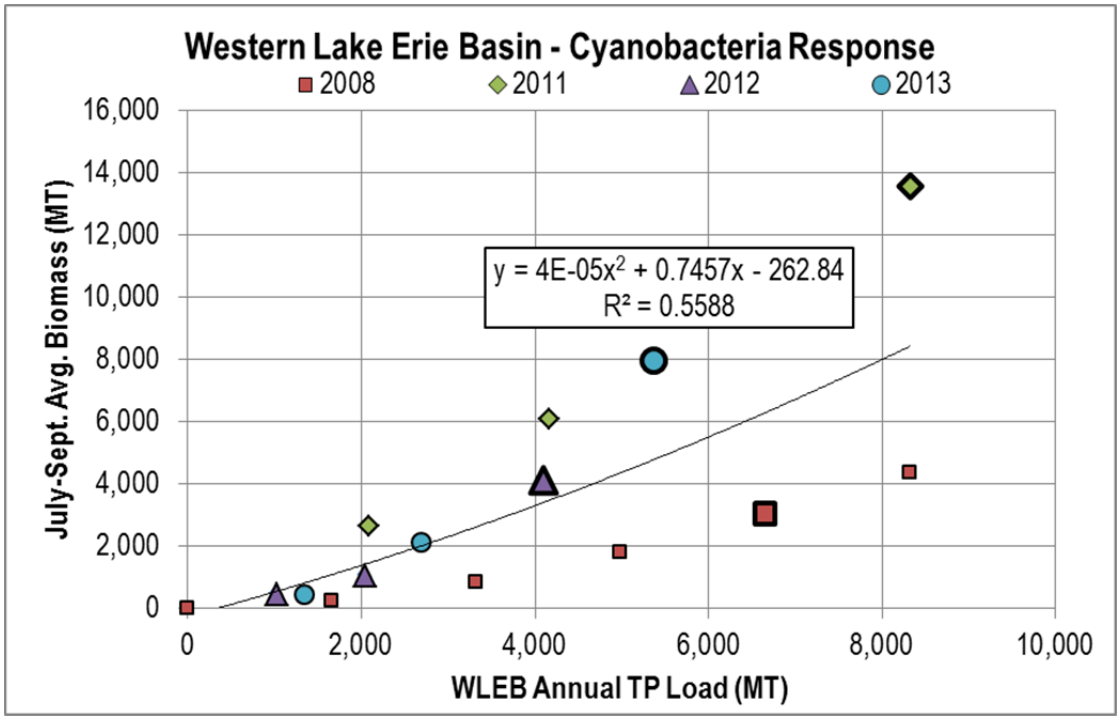

Figure B7-24: July – September average Cyanobacteria biomass response to a range of annual WLEB TP loading (from all external sources) scenarios and varying annual environmental conditions. Symbols for the baseline scenario for each year are larger and bolded.

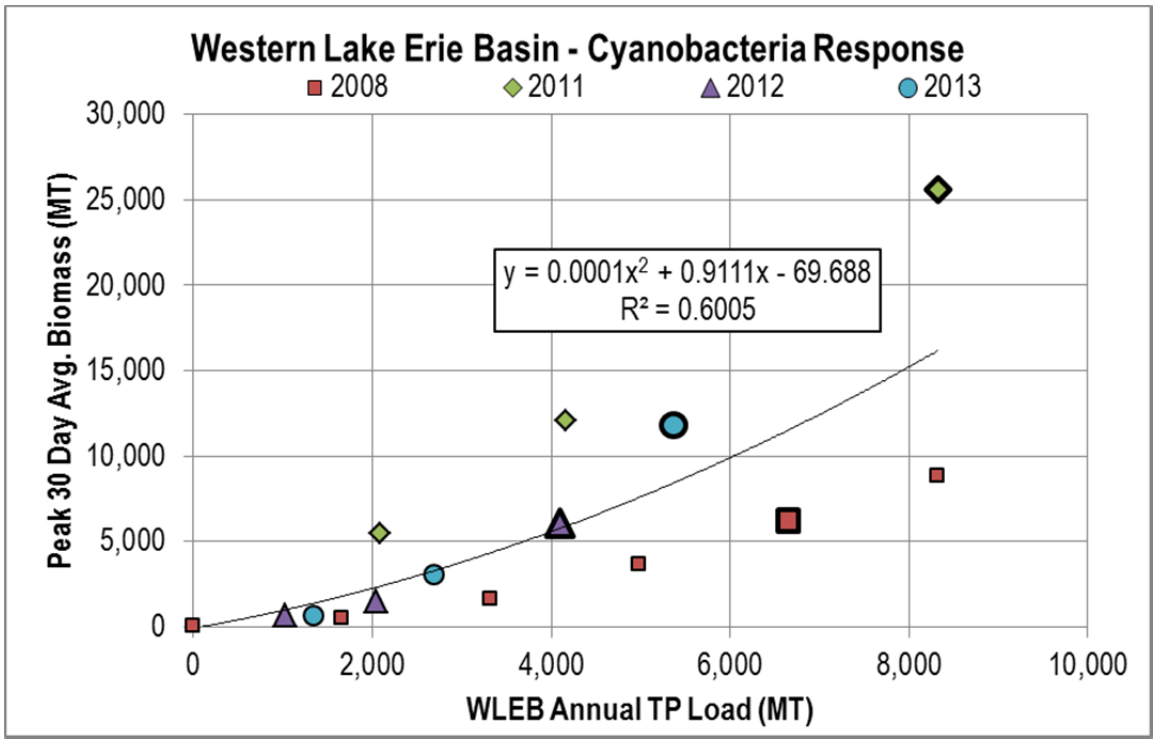

Figure B7-25: Peak 30-day average Cyanobacteria biomass response to a range of annual WLEB TP loading (from all external sources) scenarios and varying annual environmental conditions. Symbols for the baseline scenario for each year are larger and bolded.

Also, the Stumpf and Obenour empirical models are based on spring Maumee River loads. In order to compare better with this approach, we can plot the above cyanobacteria load-response curves using a comparable x-axis. Figures B7-26 and B7-27 examine the response of July-September average and peak 30-day average cyanobacteria basinwide biomass (metric tonnes) to spring-early summer (April-July) Maumee River TP loads, using the same annual WLEB load change scenarios as above. Compared to the previous cyanobacteria biomass response plots (Figures B7-24 and B7-25), there is a much stronger correlation between these independent and dependent variables. These relationships suggest annual variability in other forcing functions and non-spring phosphorus loads may not have as great an influence on cyanobacteria growth when only the spring Maumee River TP loads are used as the independent variable. Based on these results it would seem that the late summer cyanobacteria blooms are driven by April-July loads, which leads to a suggestion that the load-response relationships in Figures B7-26 and B7-27 should be used to derive a desired loading target for control of cyanobacteria blooms.

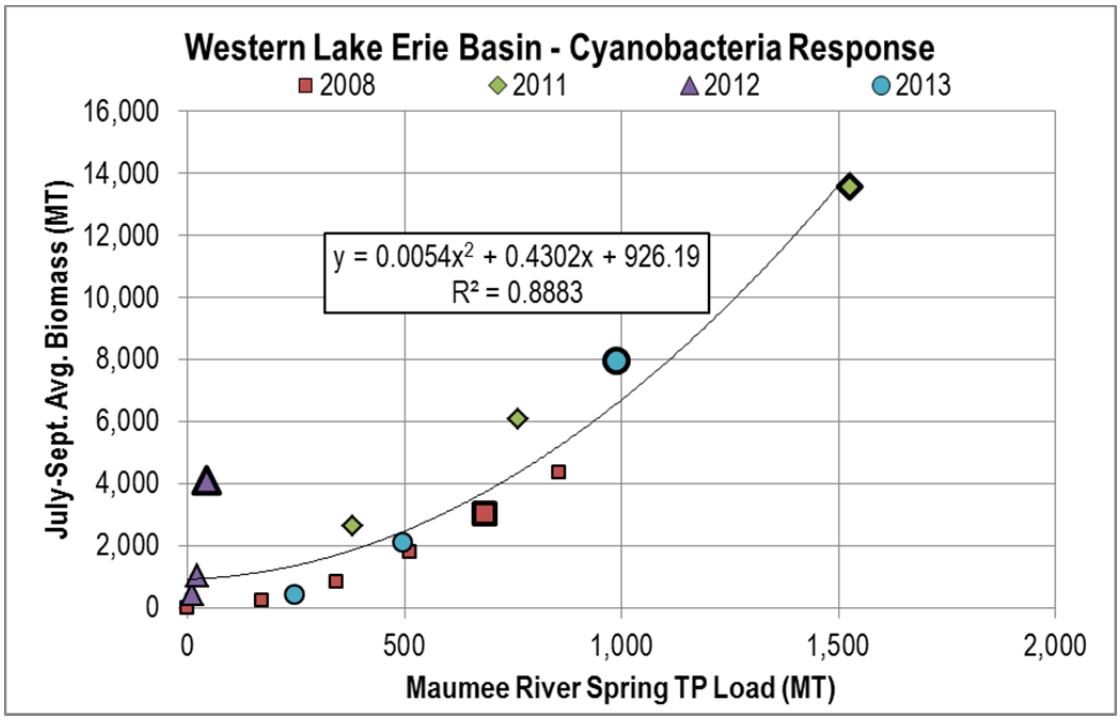

Figure B7-26: July – September average Cyanobacteria biomass response to a range of spring (April-July) Maumee River TP Loads and varying annual environmental conditions. Symbols for the baseline scenario for each year are larger and bolded.

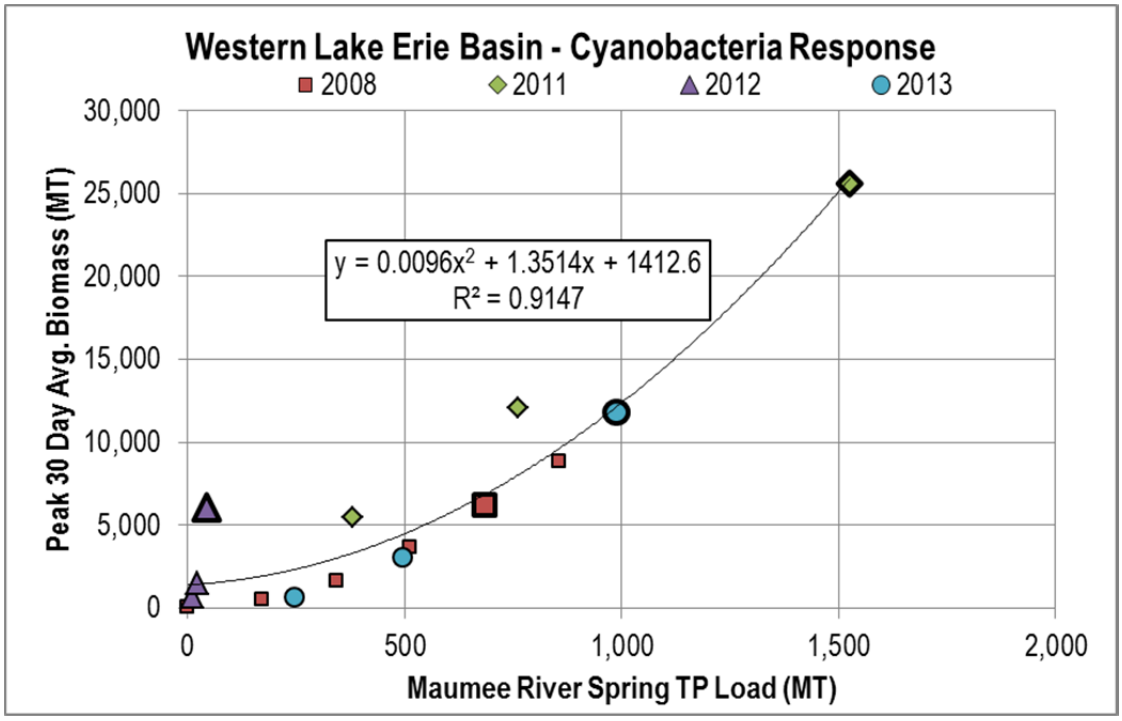

Figure B7-27: Peak 30-day average Cyanobacteria biomass response to a range of spring (April-July) Maumee River TP Loads and varying annual environmental conditions. Symbols for the baseline scenario for each year are larger and bolded.

An additional suite of simulations was conducted to examine the response of cyanobacteria biomass in the WLEB to scenarios where only Maumee River TP loads were reduced or increased. This load-response relationship has been used because, as discussed below, cyanobacteria blooms are very sensitive to Maumee River load and not as sensitive to the Detroit River load. Similar to the all tributaries scenarios, Maumee River TP loads were decreased by 50% and 75% relative to the baseline for 2011-2013, and the 2008 simulations included reductions of 25%, 50%, 75%, and 100%, and an increase of 25%. The results of these simulations are shown in Figures B7-28 and B7-29.

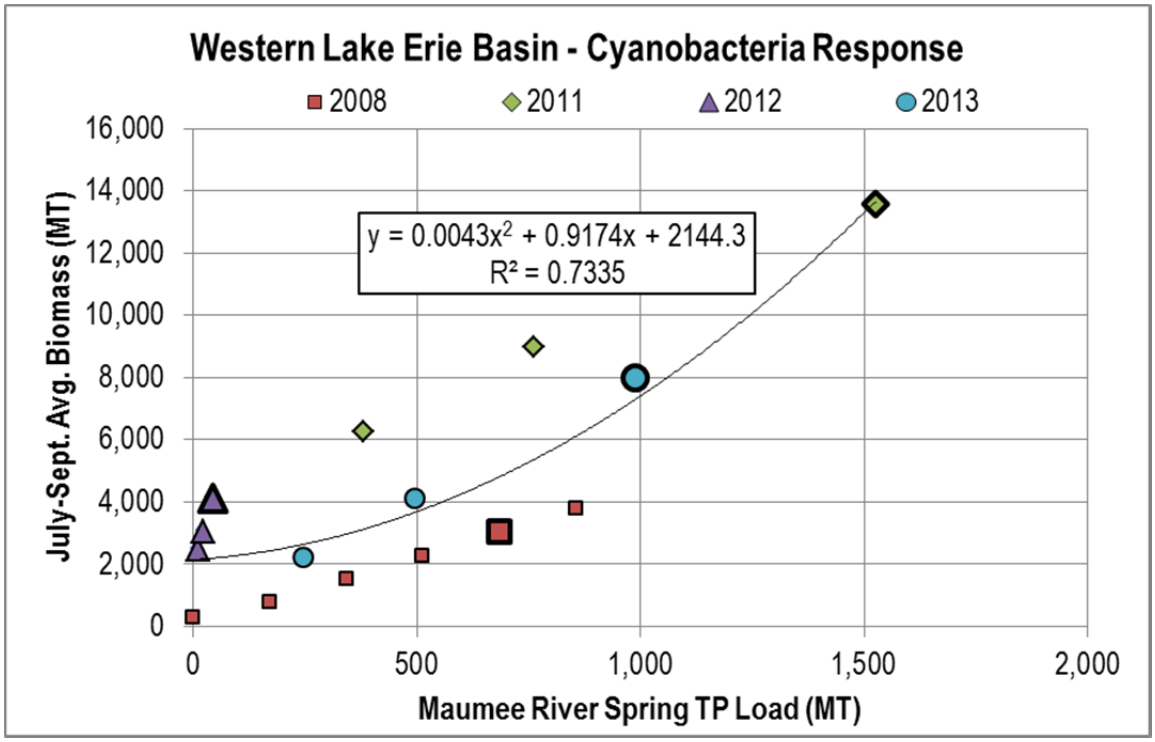

Figure B7-28: July – September average Cyanobacteria biomass response to adjustment of only annual Maumee River TP load but plotted against only spring (April-July) Maumee River TP Loads and varying annual environmental conditions. Symbols for the baseline scenario for each year are larger and bolded.

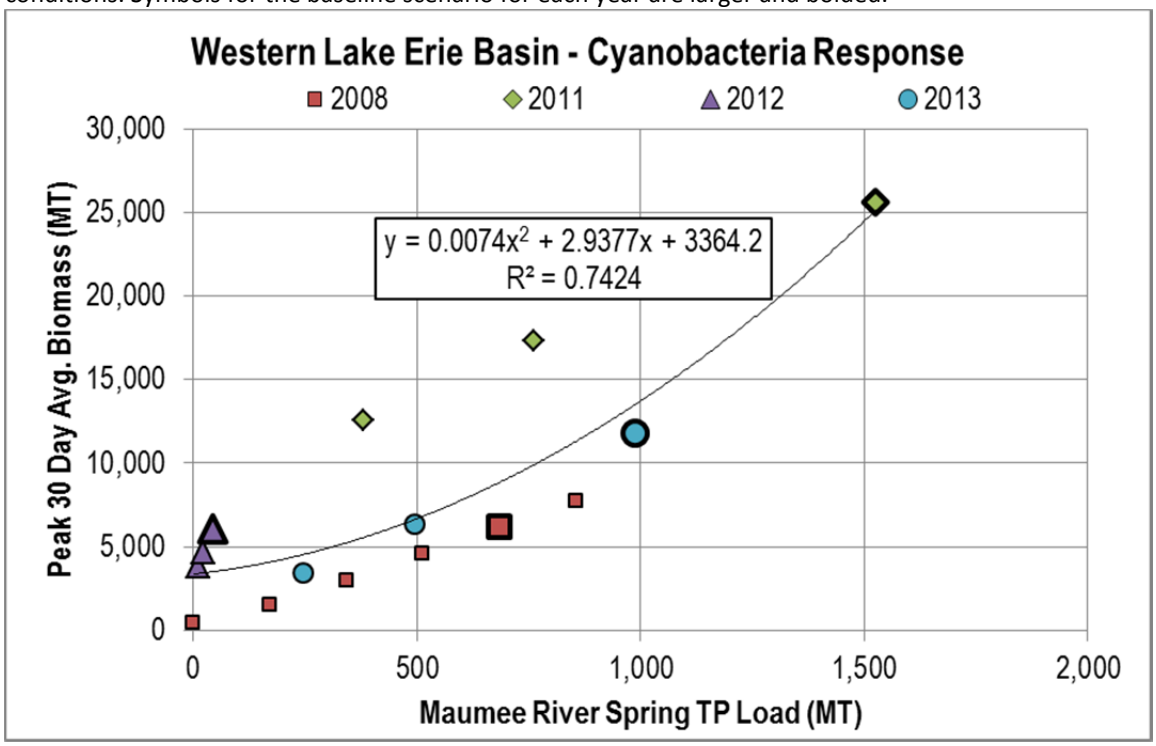

Figure B7-29: Peak 30-day average Cyanobacteria biomass response to adjustment of only annual Maumee River TP load but plotted against only spring (April-July) Maumee River TP Loads and varying annual environmental conditions. Symbols for the baseline scenario for each year are larger and bolded.

The importance of the Maumee River spring load versus other external loads to the WLEB is demonstrated by the similarity of Figures B7-28 and B7-29 (where only the annual Maumee River TP load was adjusted) with Figures B7-26 and B7-27 (where annual TP loads of all sources were adjusted). Although our modeling suggests that the April-July loads are most important in driving the late summer HABs, in order to better compare the WLEEM load-response relationships with the Stumpf and Obenour empirical models, we produce plots using the March – July load (Figures B7-30 and B7-31). These plots demonstrate that the high March, 2008 load moves the 2008 scenario loads to the right without significantly increasing the modeled biomass. Nevertheless, we suggest using the Figure B7-31 load-response curve to compare with the empirical models for determining a March-July load to achieve a given biomass threshold.

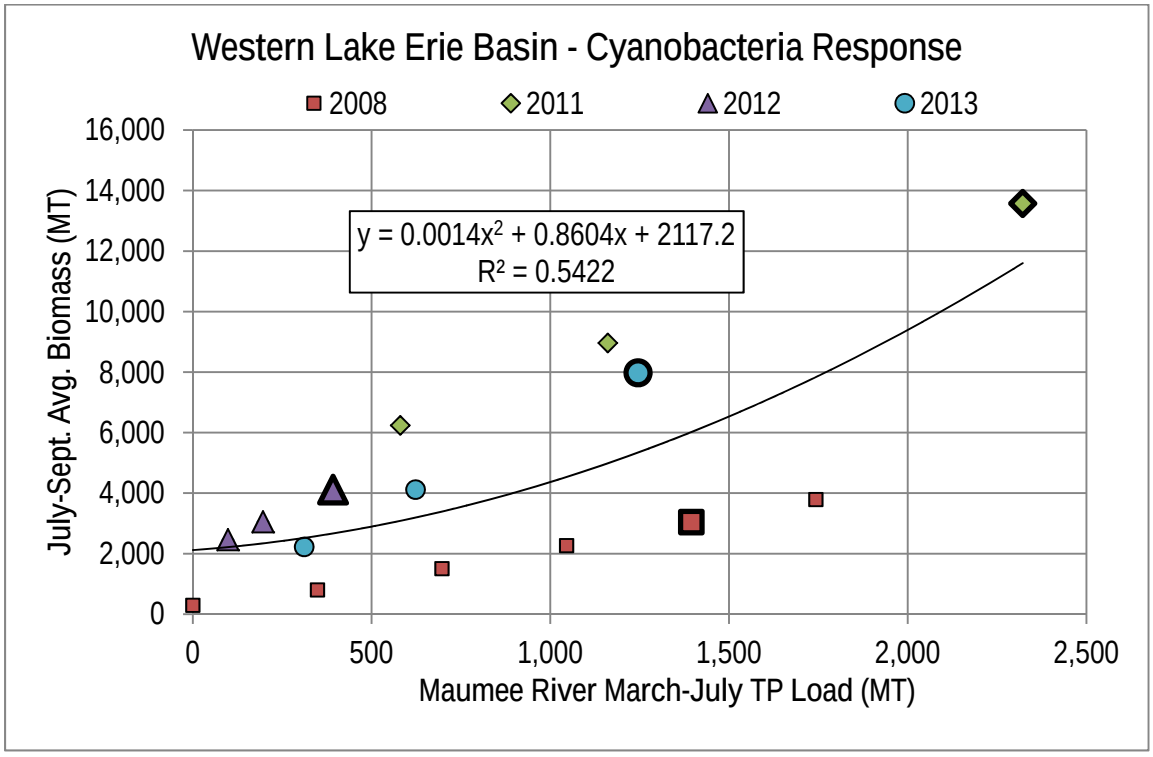

Figure B7-30: July – September average Cyanobacteria biomass response to adjustment of only annual Maumee River TP load but plotted against only spring (March-July) Maumee River TP Loads and varying annual environmental conditions. Symbols for the baseline scenario for each year are larger and bolded.

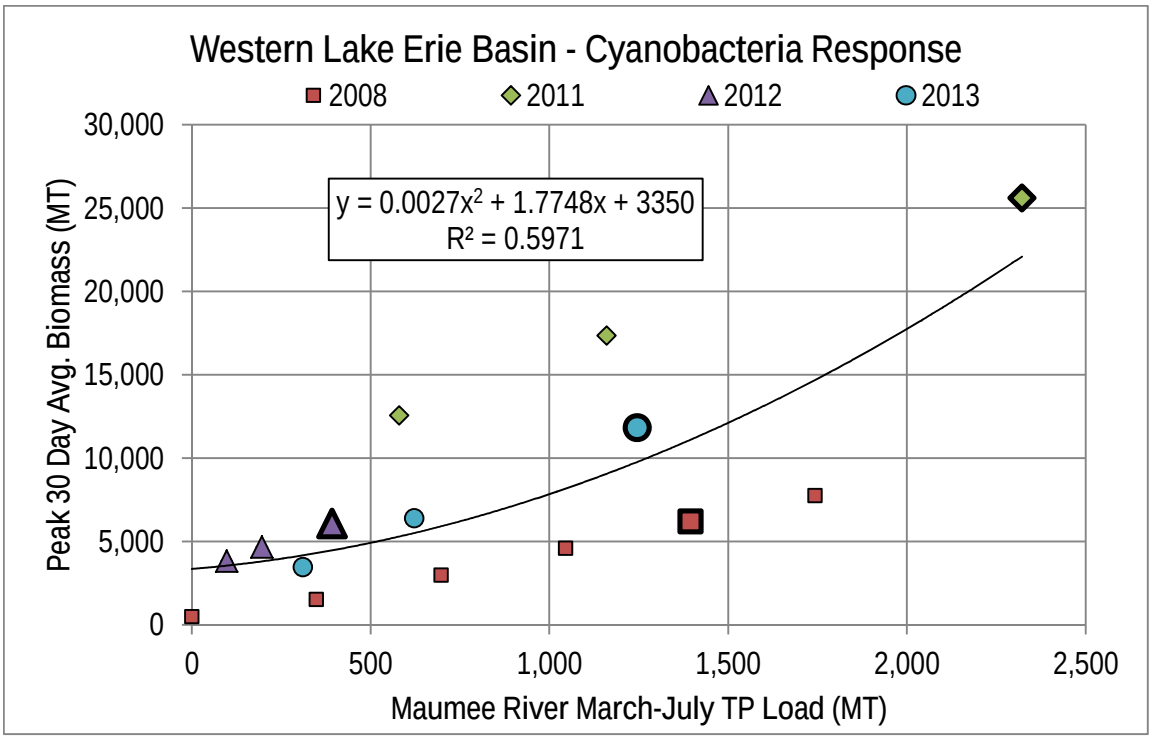

Figure B7-31: Peak 30-day average Cyanobacteria biomass response to adjustment of only annual Maumee River TP load but plotted against only spring (March-July) Maumee River TP Loads and varying annual environmental conditions. Symbols for the baseline scenario for each year are larger and bolded.

Load and Forcing Function Diagnostics

Load Source Analysis

The WLEEM was used to further investigate the response of the TP, SRP, total chlorophyll a, and cyanobacteria endpoints to scenarios with reductions and increases in key load sources. This is because Annex 4 calls for the investigation of the importance of load reduction in SRP as well as TP and in specific tributaries versus all. 2008 was selected as the single baseline year from which to create these load diagnostic scenarios. In addition to the changes in TP loads from all tributaries and the Maumee River, which were also included in the analyses presented in the previous section, the Detroit River TP loads and the Maumee River SRP loads were independently reduced by 25%, 50%, 75%, and 100%, and increased by 25% under these load source diagnostic simulations.

Figures B7-32 through B7-34 examine the response of TP, SRP, and total chlorophyll a concentrations to the various phosphorus loading scenarios. In all plots, the Maumee River SRP load reduction curve does not show much variation from the all tributaries TP load reduction curve, and the range of its effect on the WLEB Annual TP loads on the x-axis is limited. This demonstrates how the Maumee River SRP load is a relatively small fraction of the overall WLEB TP load and has a small effect on the summer average concentration of these state variables in the WLEB as a whole. For each of the three metrics examined in Figures B7-32 through B7-34, the Detroit River TP load reduction scenario results in a greater reduction and the Maumee River TP load reduction scenario results in a lesser reduction in the dependent variable for a given WLEB annual TP load.

The WLEEM response to the different source load reductions can be explained by the nature of the different sources. The 2008 Detroit River flow volume delivered to the WLEB was approximately 25 times higher than the flow volume from the Maumee River, yet the TP load delivered by the Maumee River was greater than that of the Detroit River. As shown in Figure B7-6, this means average TP concentrations in the Maumee River were more than an order of magnitude higher than those of the Detroit River. Because the magnitude of the Detroit River flow was relatively so much higher, when its TP load was fractionally reduced during these simulations, it impacted TP and SRP concentrations in the WLEB more than a similar Maumee River TP load reduction scenario. Less phosphorus in the WLEB for a given load reduction then resulted in less total phytoplankton growth overall in the WLEB and lower total chlorophyll a concentrations under the Detroit River load reduction scenarios. This suggests that if the ultimate objective is to decrease July-September TP, SRP, or total chlorophyll a concentrations in the WLEB, then actions should be prioritized to reduce TP load from the Detroit River.

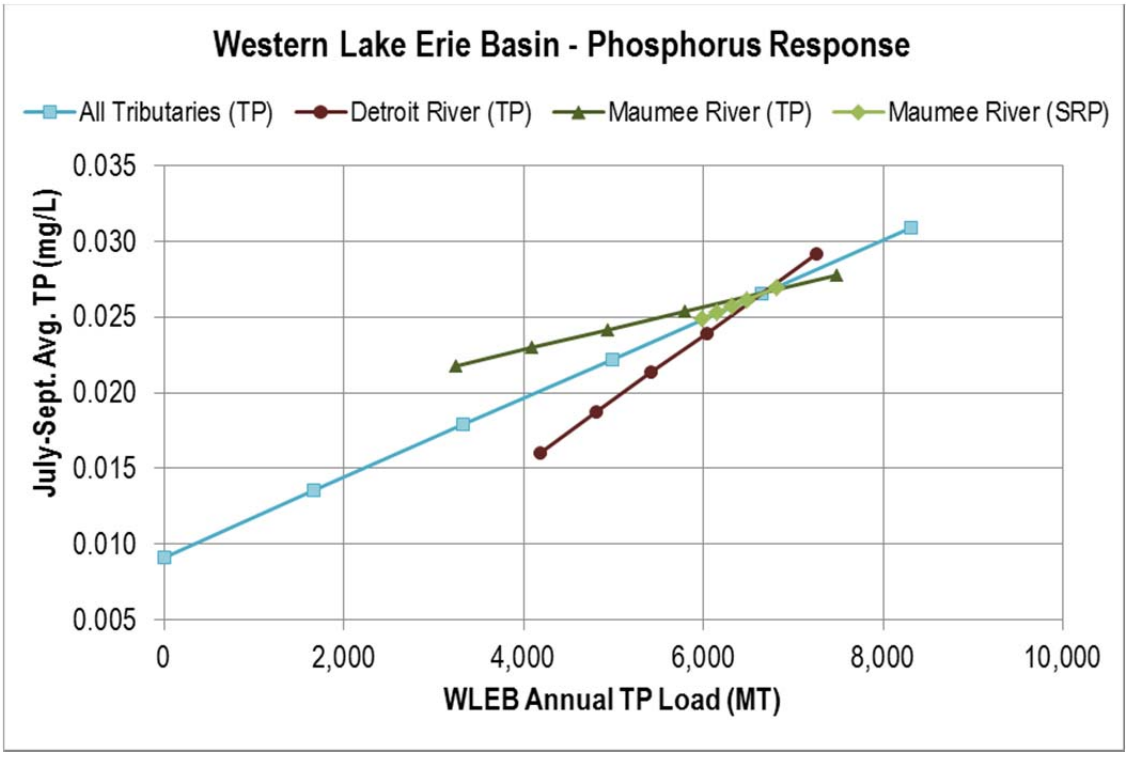

Figure B7-32: July – September average TP concentration response to alterations different phosphorus load sources under 2008 environmental conditions.

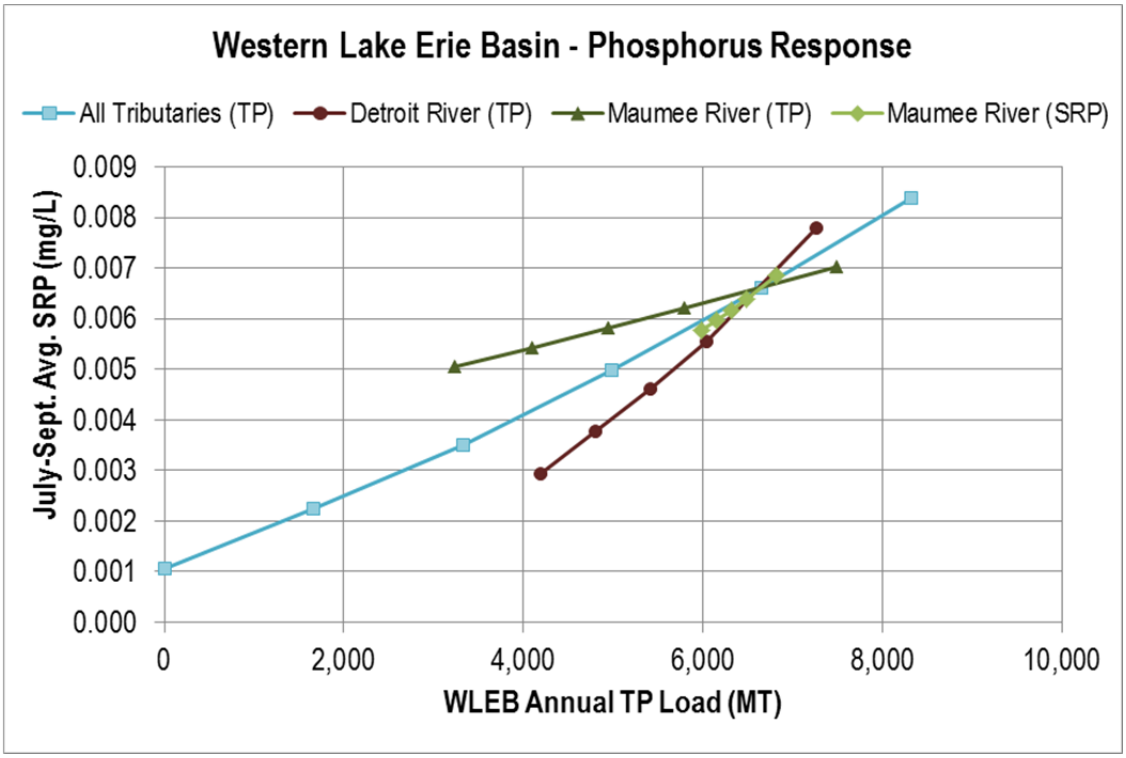

Figure B7-33: July – September average SRP concentration response to alterations of different phosphorus load sources under 2008 environmental conditions.

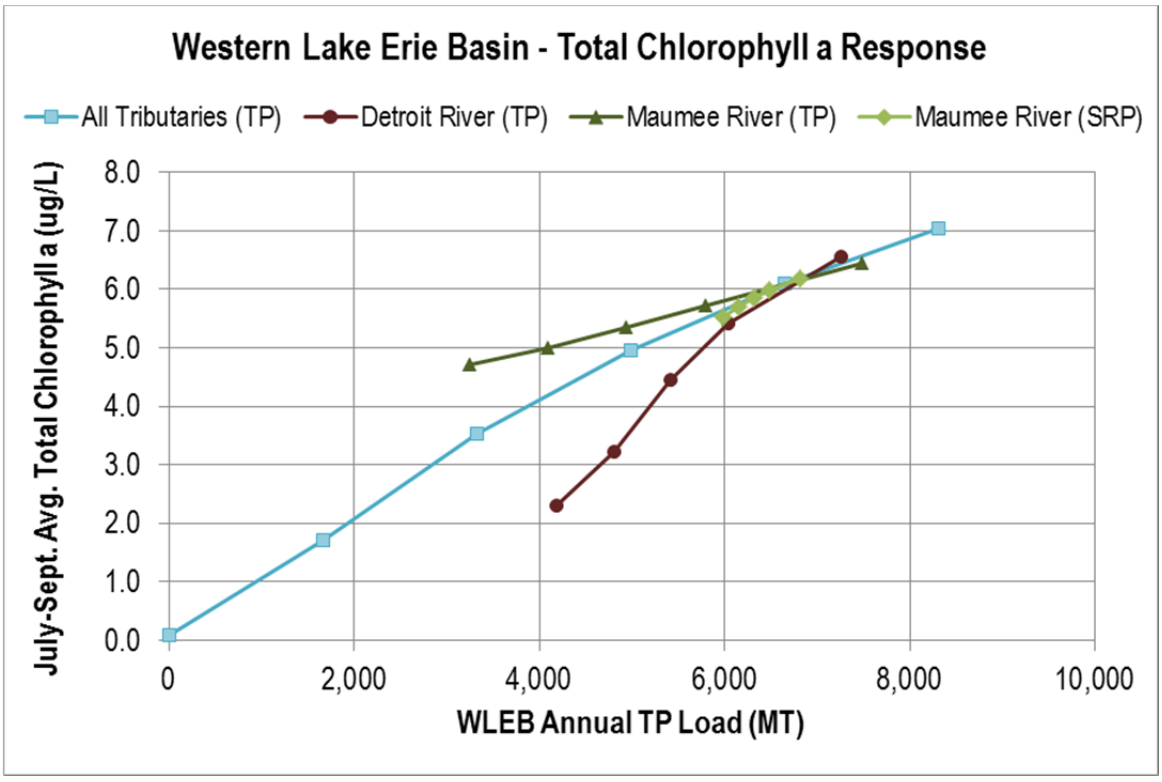

Figure B7-34: July – September average total chlorophyll a concentration response to alterations of different phosphorus load sources under 2008 annual environmental conditions.

Figures B7-35 and B7-36 examine the response of July-September average and peak 30-day average cyanobacteria biomass to the various phosphorus loading scenarios. Reductions in the Maumee River TP and SRP loads resulted in a steeper declines in WLEB cyanobacteria biomass relative to reductions in the other phosphorus load sources. Because the Maumee River delivers phosphorus at average concentrations more than ten times higher than those in the Detroit River, the WLEEM predicts the greatest cyanobacteria growth in areas of the WLEB under the influence of the Maumee River's flow and phosphorus load, including Maumee Bay and nearshore areas extending to the Catawba Island peninsula. The higher phosphorus concentrations give cyanobacteria a slight advantage over diatoms and greens, which have lower phosphorus half saturation constants as parameterized in the WLEEM. In addition to having higher phosphorus concentrations, these areas influenced by the Maumee River plume are also slightly warmer, shallower, and well-mixed, facilitating cyanobacteria growth throughout the water column. Therefore, while reducing the Detroit River TP load resulted in a lower WLEB average TP concentration (Figure B7-32), reducing the Maumee River TP load resulted in a greater cyanobacteria biomass reduction. Also, reducing the Maumee River SRP load resulted in an even steeper drop in cyanobacteria biomass as annual WLEB TP decreased (Figures B7-35 and B7-36); however, even with 100% removal of the Maumee River SRP load, levels of cyanobacteria biomass may remain at unacceptable levels.

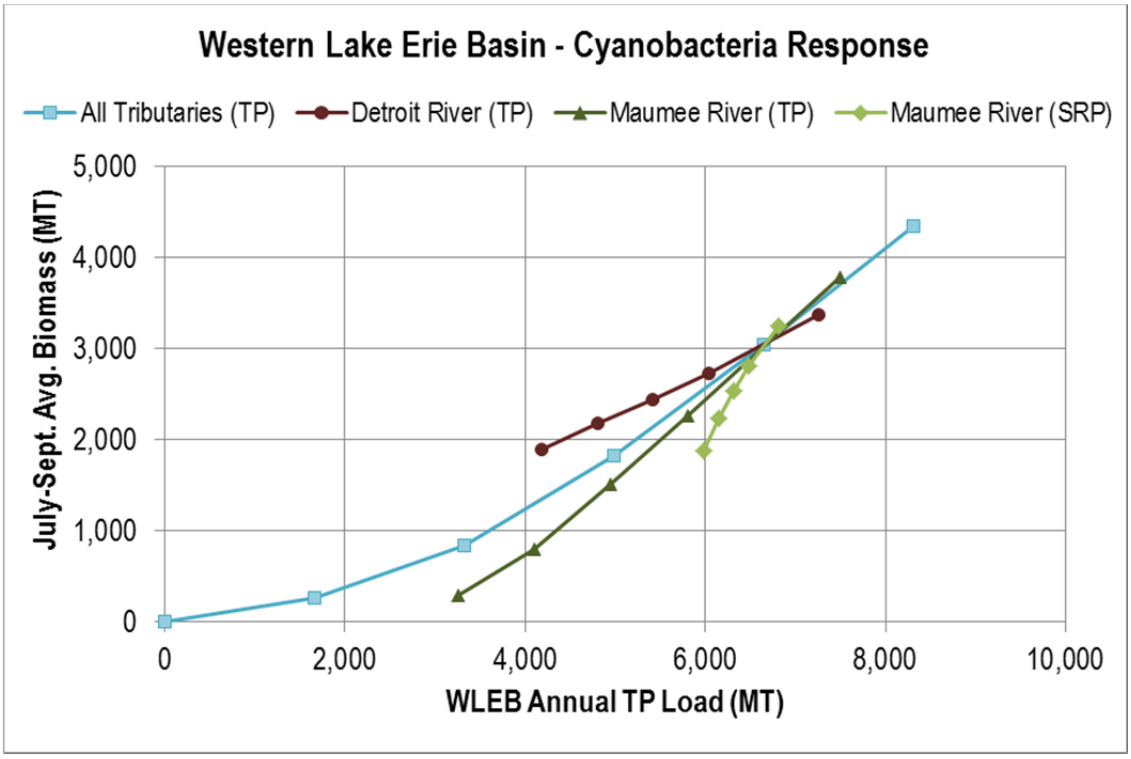

Figure B7-35: July – September average cyanobacteria biomass response to alterations of different phosphorus load sources under 2008 annual environmental conditions.

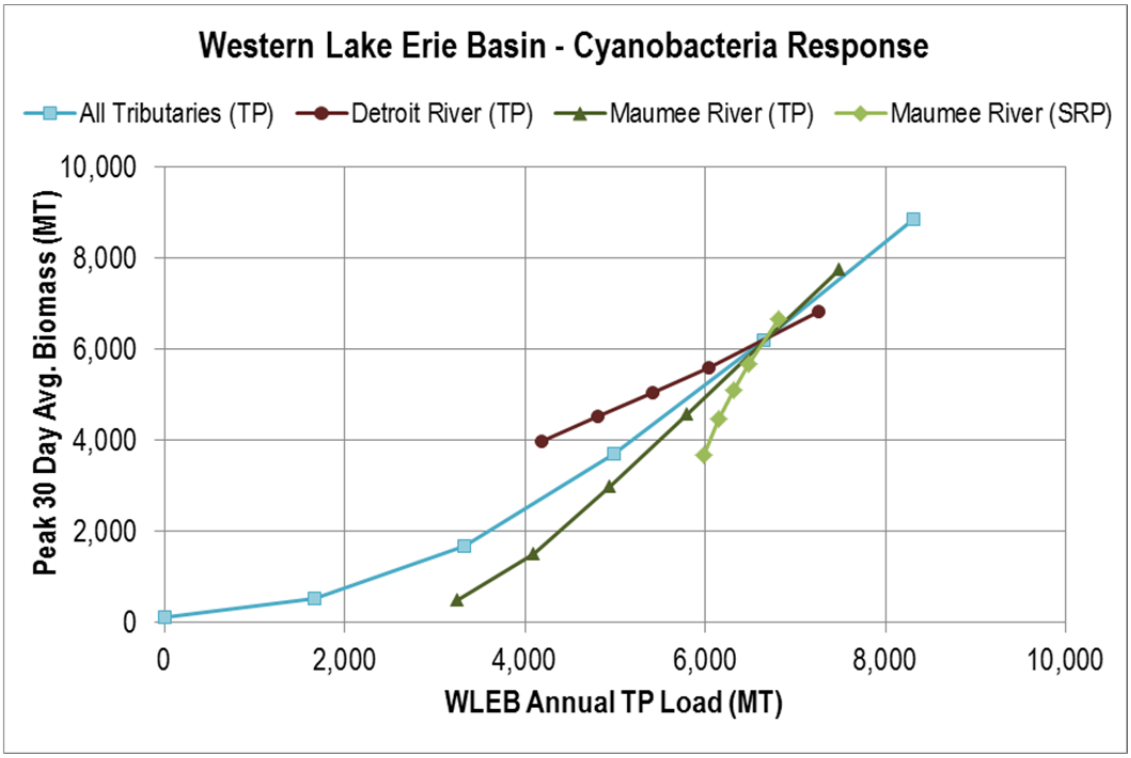

Figure B7-36: Peak 30-day average cyanobacteria biomass response to alterations of different phosphorus load sources under 2008 annual environmental conditions.

Climate Change Analysis

An investigation of the cyanobacteria biomass response to a two degree Celsius rise in ambient temperature was conducted using the WLEEM to demonstrate the effects of potential climate change. Figure B7-37 shows the cyanobacteria biomass result of this climate change simulation at the University of Toledo's 8M station. Production of cyanobacteria increased substantially relative to the baseline simulation with the two degree Celsius temperature rise, especially in the late June through early August period.

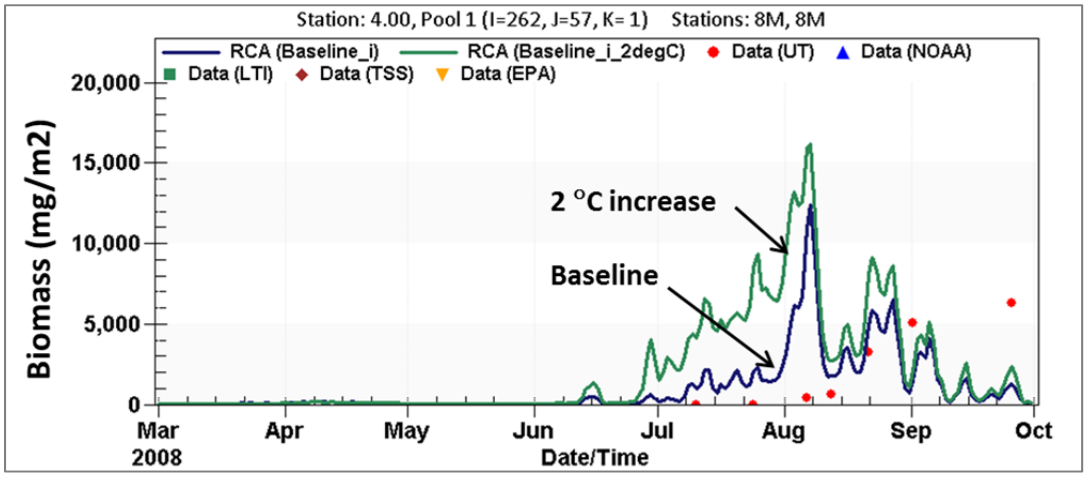

Figure B7-37: Cyanobacteria biomass sensitivity to a two degree Celsius increase in ambient temperature at the University of Toledo's 8M station for 2008 (Mar.-Oct.).

Sensitivity Analysis

Figure B7-38 below shows the change in model predicted biomass that would occur if the shape of the temperature limiting growth curve for blue-greens was shifted towards a lower growth rate at temperatures in the 22°C to 24°C range. This is the temperature range that dominates the system in July. This indicates that cyanobacteria can be very sensitive to changes in the parameterization of these constants, because there is a significant effect on temperature-limited growth rate.

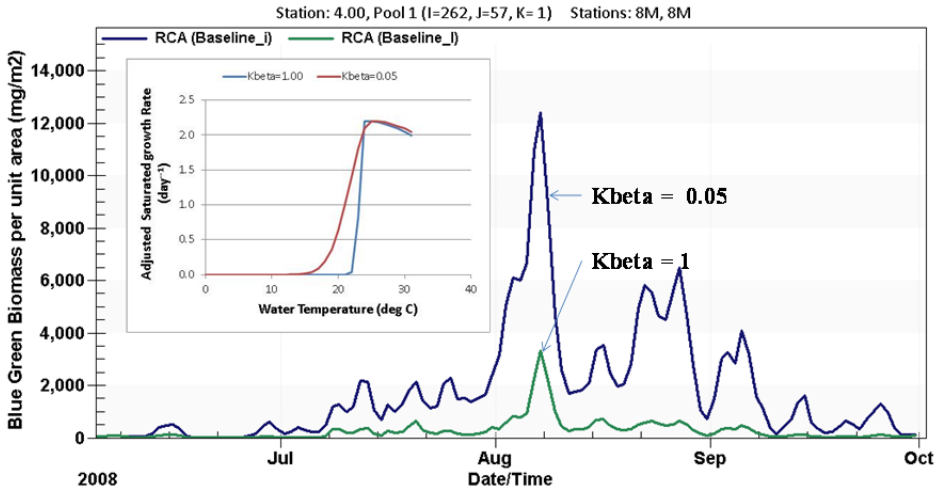

Figure B7-38: Sensitivity of predicted cyanobacteria depth-averaged biomass to changes in temperature curve.

A similar analysis was conducted to show the sensitivity of the model parameterization of the phosphorus half saturation constant that governs the nutrient limited growth rate for blue-greens. As shown in Figure B7-39, small changes in this value can affect the model predicted biomass, this time through an effect on nutrient-limited growth rate.

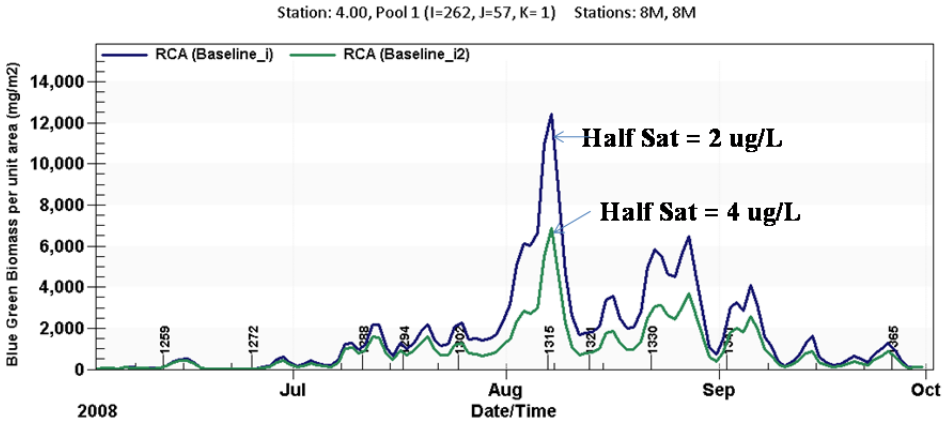

Figure B7-39: Sensitivity of predicted cyanobacteria depth-averaged biomass to changes in phosphorus half-saturation constant growth coefficient.

5. Conclusions and Recommendations

The WLEEM has provided confident load – response relationships to be developed for TP, SRP, total chlorophyll a, and cyanobacteria biomass in the Western Basin. The model accuracy is sufficient to support load management decisions for these response indicators. With respect to the cyanobacteria response metrics, using the load- response curves in Figures B7-26 and B7-27, a 50% reduction in either the July – September or the peak 30-day cyanobacteria biomass from the 2008 baseline values (3043 for the July – September biomass and 6206 for the peak 30-day biomass) will require a 50% reduction in the 2008 April –July TP load from the Maumee River.

But the process-based formulation of WLEEM allows a quantitative understanding of the various factors governing the load-response relationships. It demonstrates the relative importance of the Detroit River TP load for TP, SRP, and total chlorophyll a in the WLEB. However, it illustrates the overwhelming importance of the Maumee River TP load for control of HABs. It also demonstrates that elimination of only the SRP load from the Maumee River alone is insufficient to reduce cyanobacteria biomass to half its 2008 baseline value. The model also points out the sensitivity of cyanobacteria biomass to temperature and bioavailable phosphorus conditions in the Western Basin.

Finally, it is recommended that the load – response curves in Figures B7-26 and B7-27 for cyanobacteria biomass be used to establish a target spring Maumee River TP load reduction to achieve an established biomass target in the Western Basin. Reductions to other Western Basin tributary sources, including the Detroit River will not contribute greatly to the HABs control, but the Detroit River TP load is very important to the achievement of TP, SRP, and total chlorophyll a targets in the Western Basin and in Lake Erie as a whole.

6. References

Auer, M., Tomlinson, L., Higgins, S., *et al*. (2010). Great Lakes *Cladophora* in the 21st century: Same algae-different ecosystem. *J. Great Lakes Res*. 36: 248-255.

Bierman, V., Kaur, J., DePinto, J., *et al.* (2005). Modeling the role of zebra mussels in the proliferation of blue-green algae in Saginaw Bay, Lake Huron. J. Great Lakes Res. 31:32-55.

Bridgeman, Thomas. 2014. Email from Tom Bridgman to the University of Toledo on January 13, 2014 via email.

Bridgeman, T.B., J.D. Chaffin, and J.E. Filbrun. 2013. A novel method for tracking western Lake Erie Microcystis blooms, 2002-2011. Journal of Great Lakes Research. Vol. 39. Issue 1. Pp 83-89.

Booij, N., R.C. Ris, and L.H. Holthuijsen. 1999. "A third-generation wave model for coastal regions – Part I, Model description and validation." J. Geophys. Res., 104:C4, 7649-7666.

Delft University of Technology. 2006. SWAN User Manual: SWAN Cycle III, Version 40.51, Delft, The Netherlands, 137, available as http://www.citg.tudelft.nl/live/pagina.jsp?id=f928097d-81bb-4042-971b-e028c00e3326&lang=en

DePinto, J., H. Holmberg, T. Redder, et al. 2009. Linked hydrodynamic-sediment transport- water quality model for support of the Upper Mississippi River – Lake Pepin TMDL. Proceedings of the WEF Specialty Conference: TMDL 2009, Minneapolis, MN. Aug. 9-12.

Donigian, A.S. 2000. HSPF Training Workshop Handbook and CD. Lecture #19. Calibration and Verification Issues, Slide #19-22. EPA Headquarters, Washington Information Center, 10-14

January, 2000. Presented and prepared for U.S. EPA, Office of Water, Office of Science and Technology, Washington, D.C.

Donigian, A.S. 2002. Watershed Model Calibration and Validation: The HSPF Experience. WEF National TMDL Science and Policy 2002, November 13-16, 2002. Phoenix, AZ. WEF Specialty Conference Proceedings on CD-ROM.

GLOS. 2013. Point Query Tool for Hydrodynamic Model Results from the Great Lakes Coastal Forecasting System. Available online at http://glos.us/data-tools/point-query-tool-glcfs Accessed on December 1, 2013.

Hawley, N., T.H. Johengen, Y.R. Rao, S.A. Ruberg, D. Beletsky, S.A. Ludsin, B.J. Eadie, D.J. Schwab, T.E. Croley, and S.B. Brandt. 2006. "Lake Erie hypoxia prompts Canada-U. S. study." Eos, Transations American Geophysical Union, 87(32):313-319.

HydroQual .2004. User's Guide for RCA (Release 3.0). www.hydroqual.com/wr_rca.html.

James, S.C., C. Jones, and J.D. Roberts. 2005. "Consequence Management, Recovery & Restoration after a Contamination Event." Sandia National Laboratory report SAND2005-6797.

Jones, C. and W. Lick. 2001. "SEDZLJ: A sediment transport model." University of California – Santa Barbara. Santa Barbara, CA.

LimnoTech. 2010. Development, calibration, and application of the Lower Maumee River – Maumee Bay Model. Technical report for USACE-Buffalo District, Buffalo, NY. 127 pp.

LimnoTech. 2013. Development of an Integrated Modeling Approach for Quantifying the GLRI Deposition Metric: Pilot Application to Toledo Harbor. Technical report for USACE-Buffalo District, Buffalo, NY. 125 pp.

MDEQ. 2013. Michigan's Water Chemistry Monitoring Program: A Report of Statewide Spatial Patterns 2005-2009 and Fixed Station Status and Trends 1998-2008. MI/DEQ/WRD-13/005. Available online at http://www.michigan.gov/documents/deq/wb-swas-trend-05ccreport_203311_7.pdf

NOAA. 2013b. GLERL. "Great Lakes Coastal Forecasting System, GLCFS" http://www.glerl.noaa.gov/res/glcfs/.

TetraTech, Inc. 2007a. "The Environmental Fluid Dynamics Code User Manual: USEPA Version 1.01." June. URL: http://www.epa.gov/ceampubl/swater/efdc/EFDC-dl.html.

TetraTech, Inc. 2007b. "The Environmental Fluid Dynamics Code Theory and Computation – Volume 1: Hydrodynamics and Mass Transport." June. Fairfax, VA.

Thanh, P.H.X., M.D. Grace, and S.C. James. 2008. "Sandia National Laboratories Environmental Fluid Dynamics Code: Sediment Transport User Manual." Sandia National Laboratory report SAND2008-5621.

USEPA 2013. "Great Lakes Environmental Database (GLENDA)" Available online at: http://www.epa.gov/greatlakes/monitoring/data_proj/glenda/#query.

Young, I.R. 1999. "Wind Generated Ocean Waves." Eds. R. Bhattacharyya and M.E. McCormick. Ocean Engineering Series, Elsevier, Amsterdam, 288 pp.

APPENDIX B-8: ELCOM-CAEDYM Model

Serghei Bocaniov (bocaniov@umich.edu), Graham Sustainability Institute, University of Michigan
Luis Leon and Ram Yerubandi, S&T/WHERD/Integrated Modelling, Environment Canada.

Some of the material in this section (Appendix B-8) is being developed for publication and is not intended for distribution beyond the immediate objectives of the Annex 4 Workgroup at this time.

1. Model Description

Overview

ELCOM-CAEDYM is a coupled hydrodynamic and bio-geochemical model that consists of two models: a three-dimensional hydrodynamic model - the Estuary and Lake Computer Model (ELCOM; Hodges et al., 2000), and a bio-geochemical model - the Computational Aquatic Ecosystem Dynamics Model (CAEDYM; Hipsey and Hamilton, 2008).

The ELCOM is used for predicting the velocity, transport, mixing, temperature and salinity distribution in lakes and estuaries subjected to external environmental forcing such as tides, inflows and outflows, wind stress, surface heating or cooling. The three-dimensional hydrodynamic transport and mixing is simulated through solving the Navier-Stokes equations and scalar transport equations. Through coupling with CAEDYM, ELCOM can be used to simulate three-dimensional transport and interactions between physical, chemical and biological processes.

The CAEDYM can be used to simulate inorganic particles, dissolved oxygen, organic and inorganic nutrients (e.g. nitrogen, phosphorus, silica) and their fractions, phytoplankton, macroalgae and macrophytes, zooplankton, fish, mussels and clams, bacteria, metals (Al, Fe, Mn, etc.).

Structure/forcing functions/state variables/key relationship

Documentation and description of model equations, variables, forcing functions and parameter values were described in several publications:

- Description and application of ELCOM model (e.g. Hodges et al., 2000)
- ELCOM User guide (Hodges and Dallimore, 2014)
- ELCOM Science manual (Hodges and Dallimore, 2011)
- CAEDYM User guide (Hipsey et al., 2014)
- CAEDYM Science manual (Hipsey, 2014)
- additional CAEDYM equations (Leon et al., 2011; Bocaniov et al., 2014a)

Although CAEDYM model has 112 state variables in total, usually there is a minimum configuration of twelve state variable that are required for a simple water quality simulation (DO, PAR, EXTC, POP, PON, DOP, DON, POC, DOC, PO4, NH_4 and NO_3; see Table B8-1) though other of the remaining one hundred

variables maybe be enabled. For example, these variables can include TP, TN, TKN, PIP, PIN, DIC, SS, Chl-a, SiO_2, pH, BOD, COD, etc; see Table B8-1.

Table B8-1. List of state variables for a simple water quality simulation

Variables for a minimum configuration:		Variables that can be enabled (100 variables in total):	
Variable	Description	Variable	Description
DO	Dissolved oxygen	TP	Total phosphorous
PAR	Photosynthetically active radiation	TN	Total nitrogen
EXTC	Extinction coefficient	TKN	Total Kjeldahl nitrogen
POP	Particulate organic phosphorous	PIP	Particulate inorganic phosphorous
PON	Particulate organic nitrogen	PIN	Particulate inorganic nitrogen
DOP	Dissolved organic phosphorous	DIC	Dissolved inorganic carbon
DON	Dissolved organic nitrogen	SS	Suspended solids
POC	Particulate organic carbon	Chl-a	Chlorophyll-a
DOC	Dissolved organic carbon	SiO_2	Silica
PO_4	Filterable reactive phosphorous	pH	pH
NH_4	Ammonium	BOD	Biochemical oxygen demand
NO_3	Nitrate	COD	Chemical oxygen demand

The current ELCOM-CAEDYM setup for Lake Erie has been used in several recent publications (Leon et al., 2011; Bocaniov et al., 2014a; Liu et al., 2014). The model setup includes eleven major tributaries to Lake Erie (Detroit, Raisin, Maumee, Sandusky, Vermilion, Rocky, Cuyahoga, Grand [Ohio], Cattaraugus, Buffalo and Grand [Ontario] Rivers) and one outflow, the Niagara River. The computational grid in the model setup used a uniform horizontal grid of 2 km × 2 km and a non-uniformly spaced vertical grid with 45 layers of variable thickness. These vertical layers ranged from 0.5 m at the lake surface and near the bottom of the central basin to 5 m for the deepest layer in the east basin. To address the spatial variability of meteorological conditions across the lake, the computational domain was divided into six different domains: one for each of the west and east basins and four domains for the central basin. The model was run for 191 days from April 21 to October 28, 2008.

2. Data used for model input and evaluation (calibration, validation)

Data used for model input

Lake bathymetric data were obtained from the NOAA website (Schwab and Sellers, 1996). The data for the initial in-lake conditions were based on the observed data collected by the U.S. E.P.A. during the spring survey cruise in April 2008. Data for the inflows and outflow came from the variable datasets that include the STORET (U.S. E.P.A.) database, the U.S. Geological Survey (USGS) data, NOAA (Great Lakes Research Laboratory) database; Heidelberg College Water Quality Laboratory data; Water Survey of Canada (Environment Canada) database, and Grand River Conservation Authorities (GRCA) data. The nutrient loads to Lake Erie were calculated based on the loads from eleven major tributaries from April 21 to October 28 with TP and SRP loads scaled to match exact loads calculated by Dolan and Chapra (2012; e.g. EcoForeNodes for 2008 from Annex4 CTools). Atmospheric loads of phosphorus were not

taken into account. Meteorological data were obtained from Environment Canada (National Water Research Institute - NWRI) and NOAA National Data Buoy Center.

Data used for model evaluation

Model calibration for 2002 was performed on several datasets such as the University of Waterloo dataset (mainly for the east basin), U.S. E.P.A. Lake Erie Trophic Status project (Matisoff and Ciborowski, 2005), Environment Canada "Star Database", and the U.S. E.P.A. spring and summer survey cruises.

Model validation for 2008 was performed on the following datasets: the U.S. E.P.A. spring and summer survey cruises, Environment Canada "Star Database" and the University of Waterloo (Waterloo, Ontario, Canada) dataset for 2008. The latter includes data from three weekly cruises on Lake Erie (one lake-wide and two [central] basin-wide cruises) in mid/late summer of 2008, and high frequency measurements of water temperature and dissolved oxygen from the moored data loggers at several sites in the east basin (e.g. see Liu et al., 2014).

3. Calibration and confirmation approach and results

Model calibration

The Lake Erie ELCD model was calibrated with 2002 data (Leon et al., 2011; Bocaniov et al., 2014a). The model was calibrated by varying the model parameters within the range of published values for Lake Erie to provide the reasonable/acceptable predictions of the seasonal succession of five major phytoplankton groups in each of the basins as well as the temporal and spatial dynamics of water temperature, dissolved oxygen, total phytoplankton biomass, nutrients (nitrogen, phosphorous and silica) and their major fractions, suspended solids, light attenuation coefficient. The calibration results have already been presented in several publications (e.g. Leon et al., 2011; Bocaniov et al., 2014a) and this report includes some of the results presented in those publications. For example, the comparison of the observed and simulated epilimnetic concentrations of Chl-a, TP, Total Dissolved Phosphorus (TDP), Soluble Reactive Phosphorus (SRP), Soluble Reactive Silica (SRSi) and light attenuation coefficient (K_d) for station 938 in the east basin is presented in Figure B8-1, while Figures B8-2 and B8-3 show the lake wide horizontal distribution of simulated Chl-a and TP together with field observations.

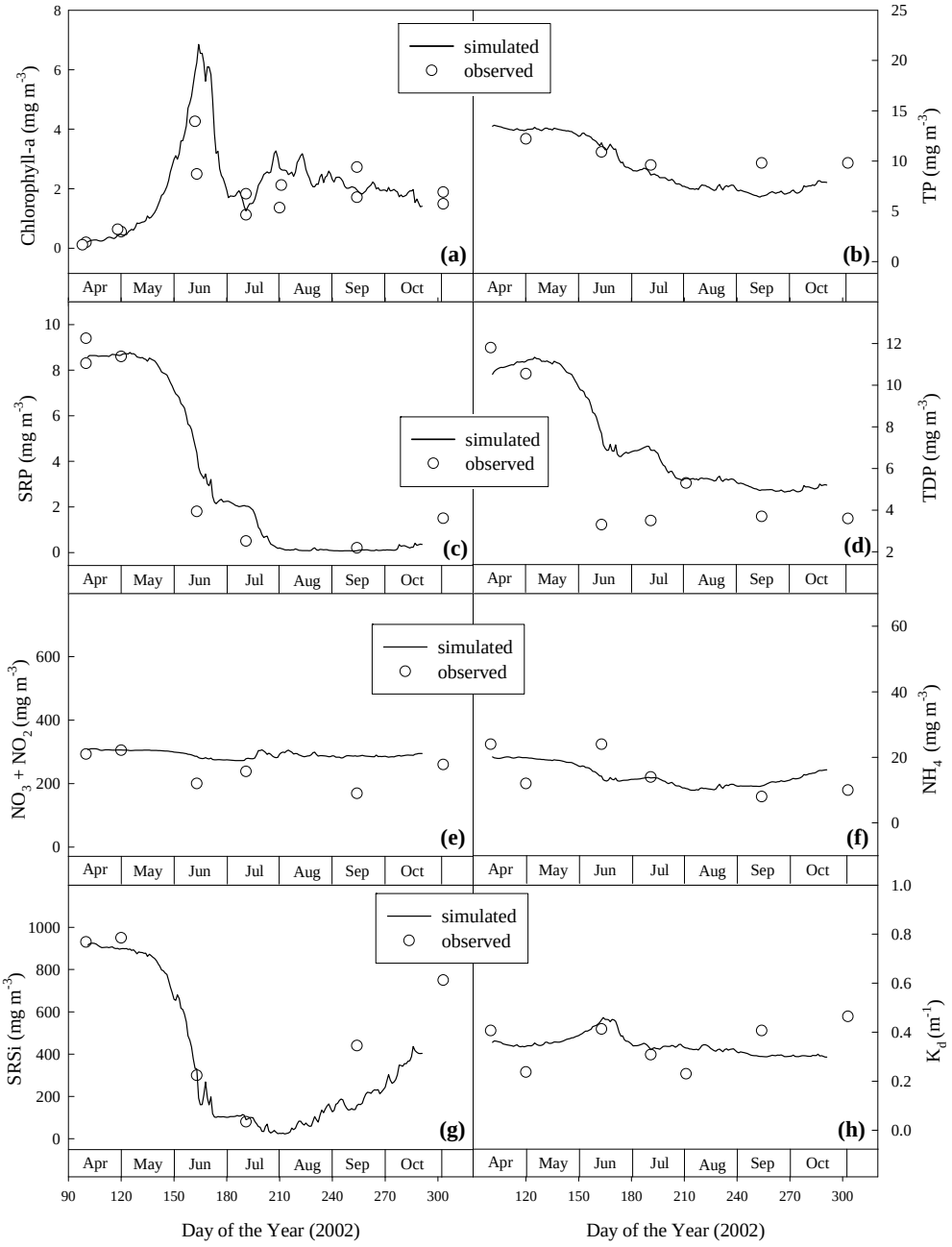

Figure B8-1: Calibration results for 2002 (Leon et al., 2011): time series output of predicted concentrations of Chl-a, TP, TDP, SRP, SRSi and K_d for the top 5 m of the surface mixed layer together with observations for station 938 (east basin) in 2002.

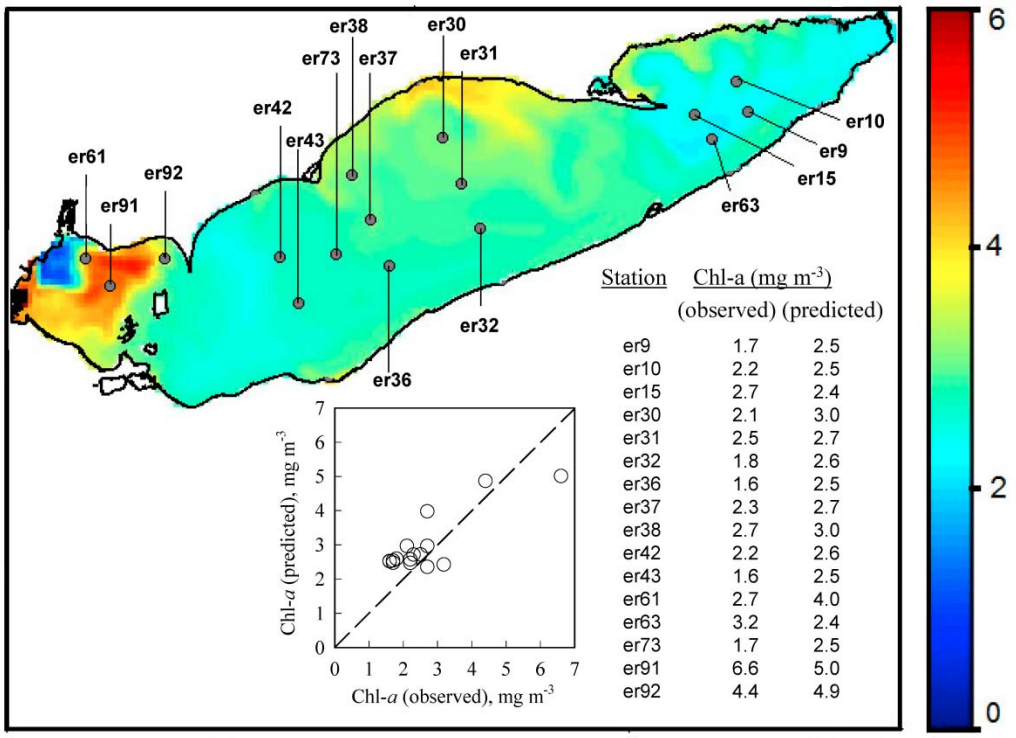

Station	Chl-a (mg m^{-3}) (observed)	(predicted)
er9	1.7	2.5
er10	2.2	2.5
er15	2.7	2.4
er30	2.1	3.0
er31	2.5	2.7
er32	1.8	2.6
er36	1.6	2.5
er37	2.3	2.7
er38	2.7	3.0
er42	2.2	2.6
er43	1.6	2.5
er61	2.7	4.0
er63	3.2	2.4
er73	1.7	2.5
er91	6.6	5.0
er92	4.4	4.9

Figure B8-2: Calibration results for 2002 (Leon et al., 2011): lake wide horizontal distribution of predicted epilimnetic chlorophyll-a concentrations (mg m^{-3}) with observed values for Aug 5–8, 2002.

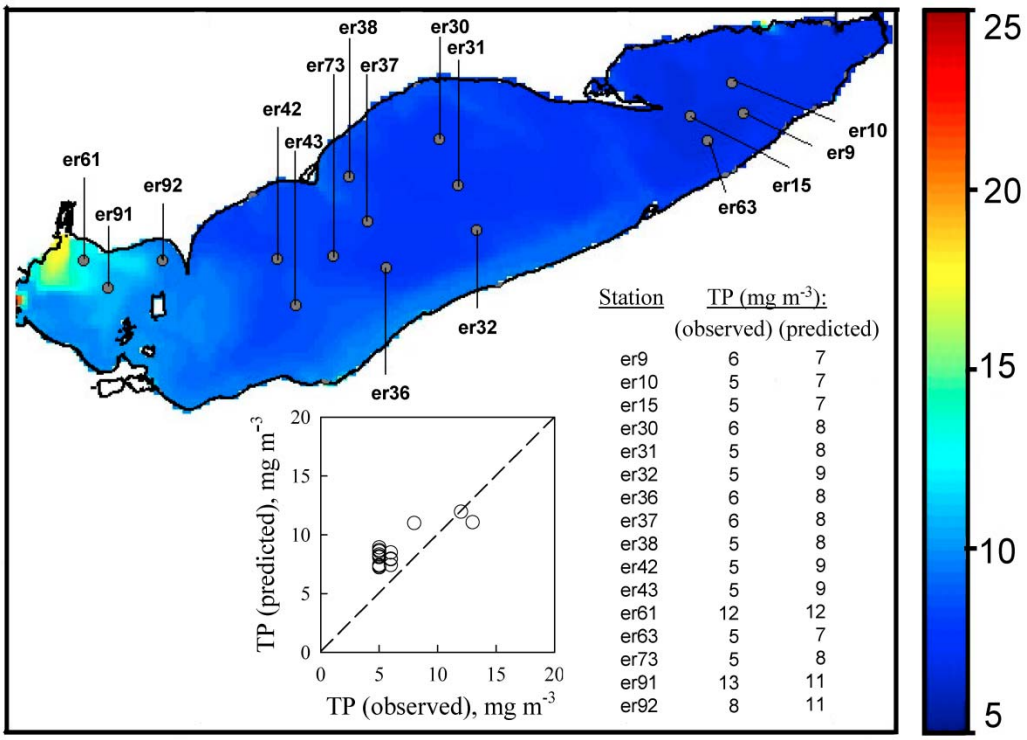

Station	TP (mg m^{-3}): (observed)	(predicted)
er9	6	7
er10	5	7
er15	5	7
er30	6	8
er31	5	8
er32	5	9
er36	6	8
er37	6	8
er38	5	8
er42	5	9
er43	5	9
er61	12	12
er63	5	7
er73	5	8
er91	13	11
er92	8	11

Figure B8-3: Calibration results for 2002 (Leon et al., 2011): lake wide horizontal distribution of predicted epilimnetic TP concentrations (expressed here as mg m^{-3}) with observed values for August 5–8, 2002.

Model validation

The Lake Erie ELCD model with the same set of parameters as in 2002 was ran and validated for other years: 2004/2005 (Oveisy et al., 2014), 2005 (Leon et al., 2013) and 2008 (Liu et al., 2014). While Oveisy et al. (2014) showed the ability of ELCD model to predict ice cover, general pattern of lake wide circulation, water temperatures, phytoplankton biomass and nutrients (TP), Leon and others (2013) presented the ability of ELCOM model to predict water temperatures in Lake Erie in 2005, while a more recent study (Liu et al., 2014) aimed at the validation of ELCOM predictions for 2008 for water temperatures at different depths and different locations (Figures B8-4 and B8-5). The ELCOM model with the same configuration was applied to a morphometrically different system without calibration and it provided a good match between the observed and simulated data for water currents and temperatures (Bocaniov et al., 2014b). Though a more detailed validation of model predicted water quality parameters is an ongoing work and will be a subject of upcoming several publications, this report presents some of the results showing the comparison against lake average surface water temperature (Figure B8-6a), basin-wide total phosphorous concentrations (Figure B8-6b-c) and dissolved oxygen at different locations and depths in the central basin (e.g. Sta. 341; Figure B8-7a-d).

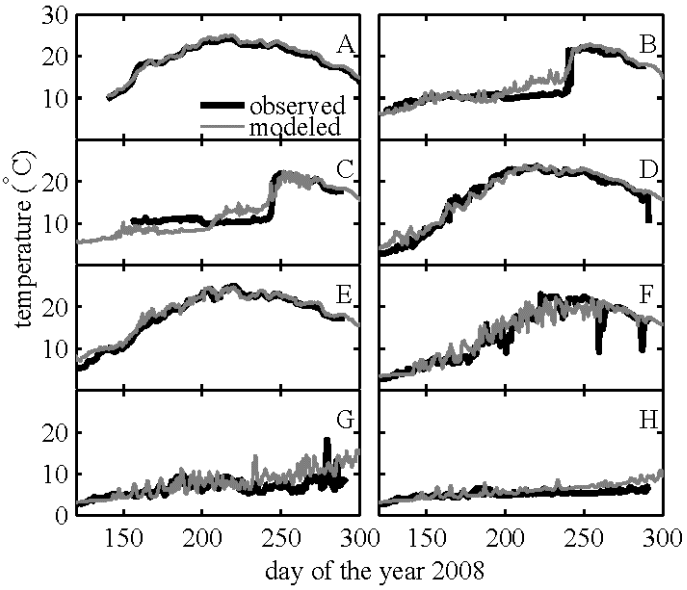

Figure B8-4: Validation of model predictions for 2008 (Liu et al., 2014): comparison of water temperatures at different locations: (A) averaged lake surface temperature, (B) Sta. 341 [west basin] at 15 m depth, (C) Sta. 1231 [central basin] at 16 m depth, (D) Sta. 84 [central basin] at 5 m depth, (E) Sta. 452 [east basin] at 9 m depth, (F) Sta. 452 at 20 m depth, (G) Sta. 452 at 30 m depth, and (H) Sta. 452 at 40 m depth.

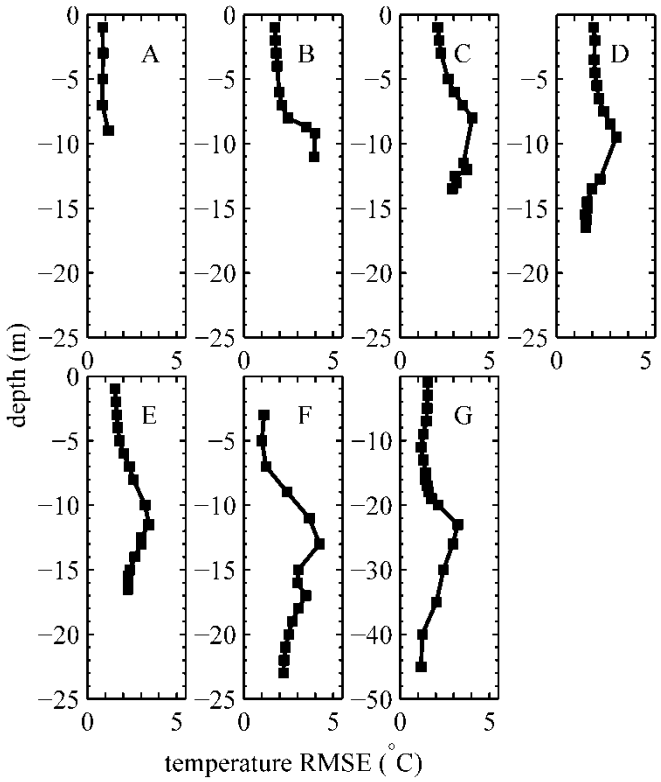

Figure B8-5: Validation of model predictions for 2008 (Liu et al., 2014): the vertical profiles of the root mean square error (RMSE) between the modeled and observed temperatures at Sta.: (A) 357 [west basin], (B) 1227 [central basin], (C) 1228 [central basin], (D) 341 [central basin], (E) 1231 [central basin], (F) 84 [central basin], and (G) 452 [east basin].

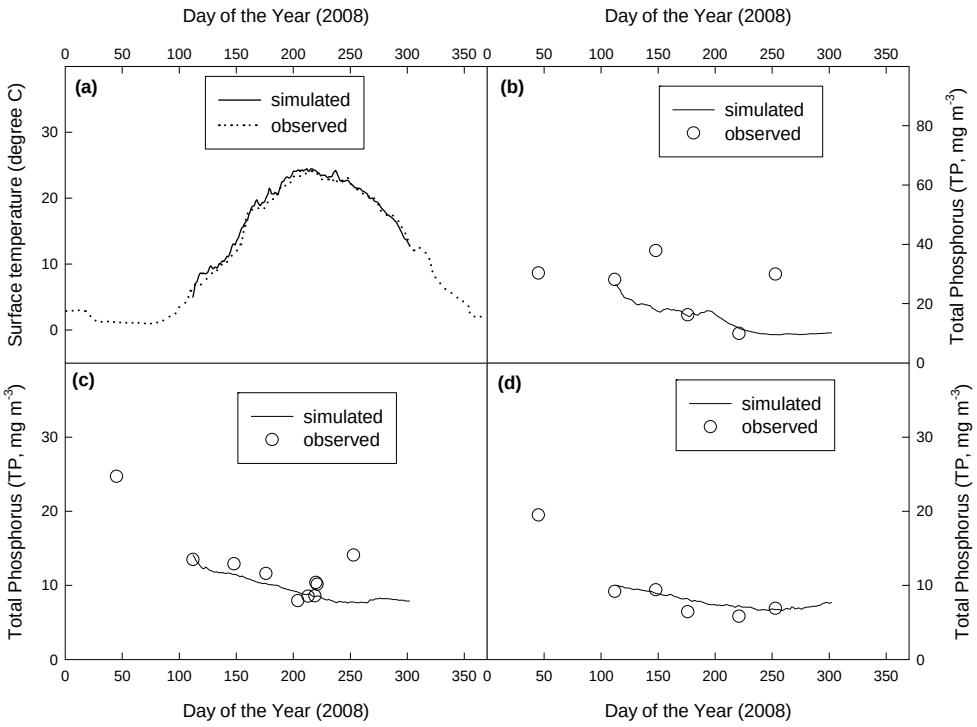

Figure B8-6: Validation of model predictions for 2008: simulated values together with observations for average lake surface temperature (a), and basin-wide concentrations of total phosphorus in west basin (b), central basin (c) and east basin (d).

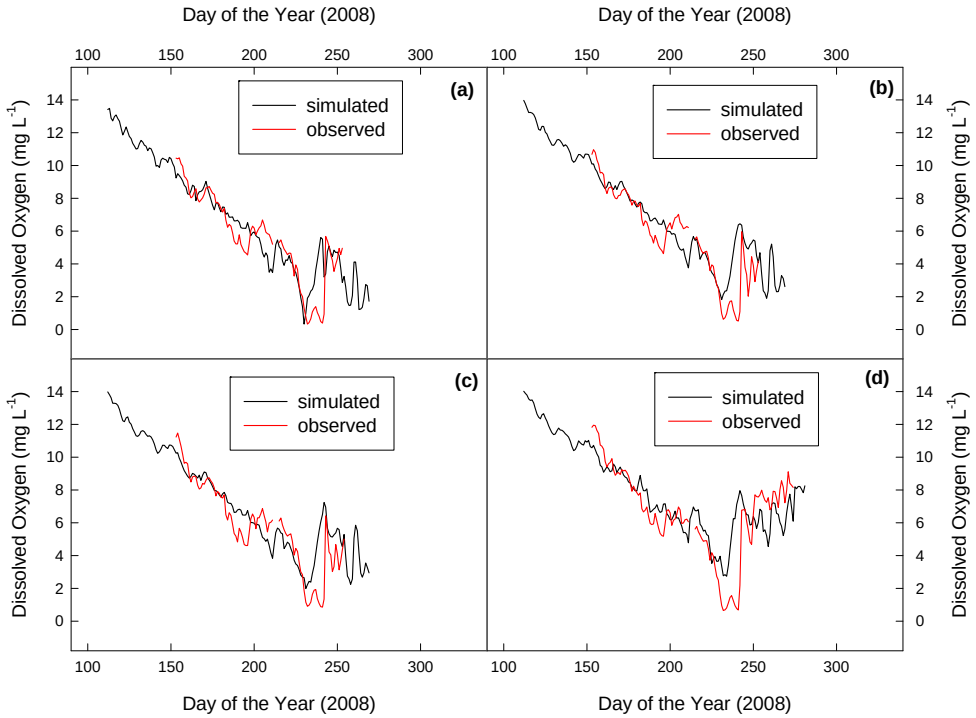

Figure B8-7: Validation of model predictions for 2008: simulated values together with the observations for the dissolved oxygen at Sta 341 (central basin) at 0.5 m above bottom (a), 1 m above bottom (b), 2 m above bottom (c), and 3 m above bottom (d).

4. Application Results

In this study we applied the three-dimensional (3D) ELCOM-CAEDYM model to Lake Erie to produce the load-response curves for Annex 4 modeling work.

Method

The load response curves presented in this report were developed separately for Total Phosphorous (TP) and Soluble Reactive Phosphorous (SRP) loading scenarios modifying the TP and/or SRP daily loads for the eleven modeled tributaries: Detroit, Raisin, Maumee, Sandusky, Vermilion, Rocky, Cuyahoga, Grand [Ohio], Cattaraugus, Buffalo and Grand [Ontario] rivers. TP is modeled as the sum of SRP, particulate organic phosphorous (POP), dissolved organic phosphorous (DOP) and particulate inorganic phosphorous (PIP). The load scenarios for both TP and SRP include the base case, +25%, -25%, -50%, -75% and -100% load adjustments. The base case TP and SRP loads are similar to the node values from the Annex 4 CTools files:

- 052913_EcoForeNodes_CY2008_TP_DMD_Final.xlsx
- 052813_EcoForeNodes_CY2008_DRP_DMD_Final.xlsx

SOD rates and hypoxia in the central basin. The full effect of load changes cannot be seen with such a short simulation period of 191 days since the water residence time of Lake Erie is almost three years (Bolsenga and Herdendorf, 1993). Previous studies have shown that the hypolimnetic oxygen depletion rates in the central basin of Lake Erie are driven by both the sediment oxygen demand (SOD) and water column oxygen demand (WOD) (e.g. Davis et al., 1987; Lam et al., 1987). The SOD rates are driven by the settling flux of organic matter, mostly phytoplankton, that is a function of lake productivity while the latter is a function of nutrient loads. Previous studies have also shown that there is a time lag of about 10 years or so between the change in nutrient loads and the observed change in the hypolimnetic oxygen that is driven by SOD and WOD (e.g. Charlton, 1987). Following the guidance obtained during the Ensemble modelling workshops, however, it was decided that SOD rates will be adjusted to capture the effects of changes in nutrient loads. We had to adjust the SOD rates assuming that they reach a new equilibrium with nutrients loads for a given nutrient load scenario.

The SOD rates are variable during the season as they are modified by temperature and the amount of dissolved oxygen present in the layer above sediments. In the present work, we used a static oxygen model that simulates the ambient sediment oxygen demand at any given temperature (SOD_T) as a function of the temperature and dissolved oxygen in the layer overlying the sediments (Eq. 1):

$$SOD_T = SOD_{20} \cdot f(T) \cdot f(DO) = SOD_{20} \cdot \theta^{T-20} \cdot \left[\frac{DO}{DO + K_{SOD}}\right] \qquad (1)$$

where, T is the temperature, °C; DO is the dissolved oxygen concentration in the layer above sediments, mg L^{-1}; SOD_{20} is the SOD rate at 20°C; θ is the temperature coefficient; and K_{SOD} is the constant that determines how the SOD is mediated under hypoxic conditions.

Our work on three-dimensional modeling of the hypoxia in Lake Erie in 2008 showed that the SOD_{20} of 1.2 gO_2 m^{-2} d^{-1} is an appropriate value not only to reproduce the ambient SOD rates (SOD_T) that are

similar to Rucinski et al. (2014) values (Table B8-2) but also to match the seasonal dynamics of the observed dissolved oxygen concentrations in both epilimnion and hypolimnion (e.g. Figure B8-7).

To determine the SOD_T for each of the nutrient loading scenario the following approach was used:

- As the water residence time in the central basin is about two years (Bolsenga and Herdendorf, 1993), we calculated the average Lake Erie load for 2008 and the preceding year and used the relationship between load and SOD rate (Rucinski et al., 2014) to determine the corresponding SOD_{20} for this load. This SOD_{20} value is based on the assumptions and limitations of one-dimensional model.

- Then, we used the same relationship (Rucinski at al., 2014) to determine the corresponding SOD_{20} for each of the loading scenarios and calculated the percent change compared to the one for the baseline scenario. We used the same percent change to apportion our SOD_{20} for the baseline scenario. The calculated SOD_{20} values for each of the loading scenarios are shown in Table B8-3.

Table B8-2. Comparison of the ambient SOD fluxes (SOD_T) calculated by CAYDEM model for the basic scenario (SOD_{20} = 1.2 gO_2 m^{-2} day^{-1}) with the values used in other studies at certain water temperatures (T) and dissolved oxygen concentrations (DO) that are typical for the hypolimnion in Lake Erie:

T = 5°C DO = 7 mg L^{-1}		T = 6°C DO = 6 mg L^{-1}		T = 7°C DO = 5 mg L^{-1}		T = 8°C DO = 4 mg L^{-1}		T = 9°C DO = 3 mg L^{-1}	
Our study	Literature value*	Our study	Literature value*	Our study	Literature value*	Our study	Literature value*	Our study	Literature value*
0.539	0.518	0.559	0.531	0.579	0.544	0.594	0.557	0.601	0.570

*Rucinski et al. (2014), please note that the SOD value in Rucinski et al. (2014) is independent of DO concentrations and depends only on temperature.

Table B8-3. Loading scenarios and maximum theoretical SOD rates (SOD_{20}):

TP load scenario	Max theoretical SOD* flux (SOD_{20}) ($g\ m^{-2}\ d^{-1}$)	SRP load scenario	Max theoretical SOD* flux (SOD_{20}) ($g\ m^{-2}\ d^{-1}$)
Base case	1.200	Base case	1.200
TP+25% (increase SRP same percentage also)	1.264	SRP+25% (increase SRP load only)	1.264
TP-25% (decrease SRP same percentage also)	1.106	SRP-25% (decrease SRP load only)	1.106

Table B8-3. (*Continued*)

TP-50% (decrease SRP same percentage also)	0.957	SRP-50% (decrease SRP load only)	0.957
TP load scenario	Max theoretical SOD* flux (SOD_{20}) ($g\ m^{-2}\ d^{-1}$)	SRP load scenario	Max theoretical SOD* flux (SOD_{20}) ($g\ m^{-2}\ d^{-1}$)
TP-75% (decrease SRP same percentage also)	0.681	SRP-75% (decrease SRP load only)	0.681
TP-100% (decrease SRP same percentage also)	0.559	SRP-100% (decrease SRP load only)	0.559

*Max SOD flux (SOD_{20}) is used by CAEDYM model to calculate the actual fluxes (SOD_T) depending on temperatures and DO concentrations of the overlaying water. See Table B8-2 for comparison of the actual SOD values with the literature values for the basic scenario.

The following approaches and assumptions were used to calculate the hypoxic area, averaged hypolimnetic DO concentration, the total number of the hypoxic days:

- Hypoxic area was defined as any area with the bottom DO concentration < 2 mg/L.
- The bottom layer hypolimnetic dissolved oxygen was defined using the following approach. First we identified any bottom cell at each output frequency (2 hours) that can be defined as the hypolimnion so that it satisfies our two major assumptions for the hypolimnetic layer: (i) has a temperature difference between the surface and bottom cells of the same vertical grid of more than 2 degrees (T_{surf} - T_{bot} >2°C) and has a temperature less than 14°C (T_{bot} < 14°C). Then, DO concentrations of the selected cells were averaged for each time step (2 hours) and day, and only those from August 1 to September 30 were used to derived the average hypolimnetic DO values for Aug-Sept.
- The number of hypoxic days (DO < 2 mg/L) is calculated over the entire period of simulations from April 21 to October 28 for any hypoxic area in the central basin exceeding the area of 746 km^2 to make the results comparable to those of 1-dimensional model.

Basin-wide total phytoplankton biomass. The phytoplankton biomass was calculated as the whole-basin biomass averaged over the entire depth of the water column for the period from June 1 to August 31, 2008. The phytoplankton biomass is expressed in mg m^{-3} (= µg L^{-1}) as Chlorophyll-a. The 100% load indicates the baseline scenario with no reduction in loads. The loads for the baseline scenario were determined as the whole lake loads for the period from January 1 to December 31 inclusive using the Dolan's data for TP and SRP (node values from the files in Annex 4 CTools). Atmospheric loads were not taken into account.

Basin-wide biomass of Cyanobacteria. The cyanobacteria biomass was determined as the average daily biomass for the top surface layer of the water column of the entire west basin to make it comparable with the satellite derived data and then extrapolated to the mean depth of the basin (7.4 m; Bolsenga and Herdendorf, 1993). The response curves for cyanobacteria were developed for both peak 30-day basin-wide biomass during the bloom and for basin wide average daily biomass averaged over July to

September. The former was calculated according to the method described in Stumpf et al. (2012). The biomass is expressed in metric tons (MT) as the dry weight per basin per day. The biomass of the cyanobacteria was plotted against the Spring Maumee River loads that were defined as the loads from the Maumee River for the period from April 21 to July 30 inclusive.

Load-Response curves

The following load-response curves are provided below for each load scenario:

- Average (August to September) extent of the hypoxic area in the central basin (Figure B8-8).
- Number of hypoxic days with DO < 2 mg L^{-1} in the central basin (Figure B8-9).
- Average hypolimnetic DO concentration in the central basin (Figure B8-10).
- Basin average (basin-wide) total chlorophyll-a concentration (June to August) for:
    - West basin (Figure B8-11);
    - Central basin (Figure B8-12);
    - East basin (Figure B8-13).
- Basin average (basin-wide) daily Cyanobacteria biomass (Jul 1 to Aug 31) expressed as the dry weight (DW) for the west basin:
    - mean concentration (July to September) (Figure B8-14);
    - 30-day averaged concentration during the bloom conditions (Figure B8-15).
- Seasonal dynamics of the hypoxic zone (DO < 2 mg L^{-1}) for some selected TP loading scenarios (TP, TP-25%, TP-50%, TP+25%) (Figure B8-16).

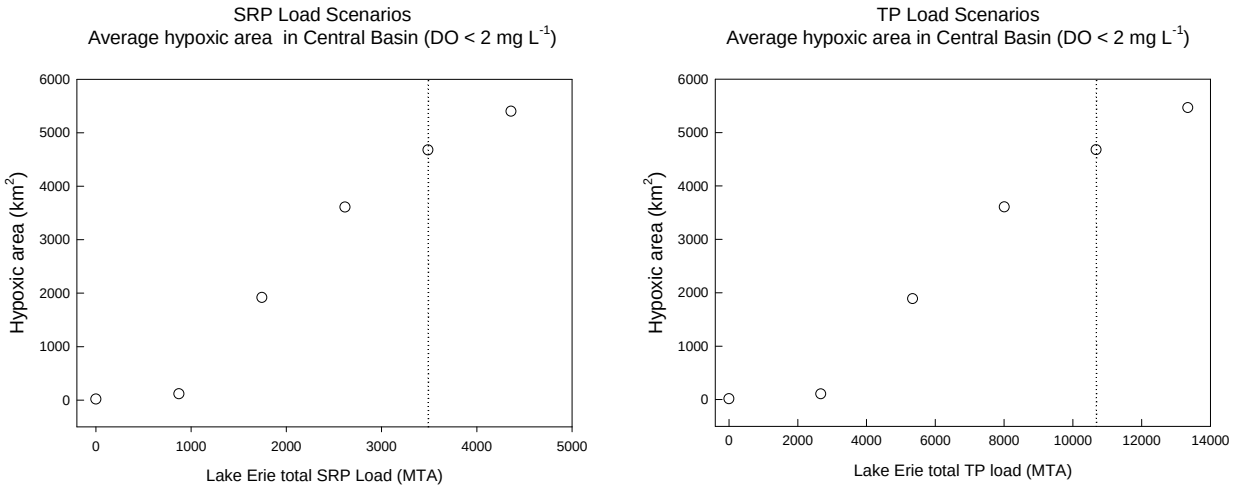

Figure B8-8: Average extent (August-September, 2008) of the hypoxic area for the central basin for SRP (left) and TP (right) load scenarios. The vertical dashed line indicates the load for the baseline scenario (no reduction in either SRP or TP loads).

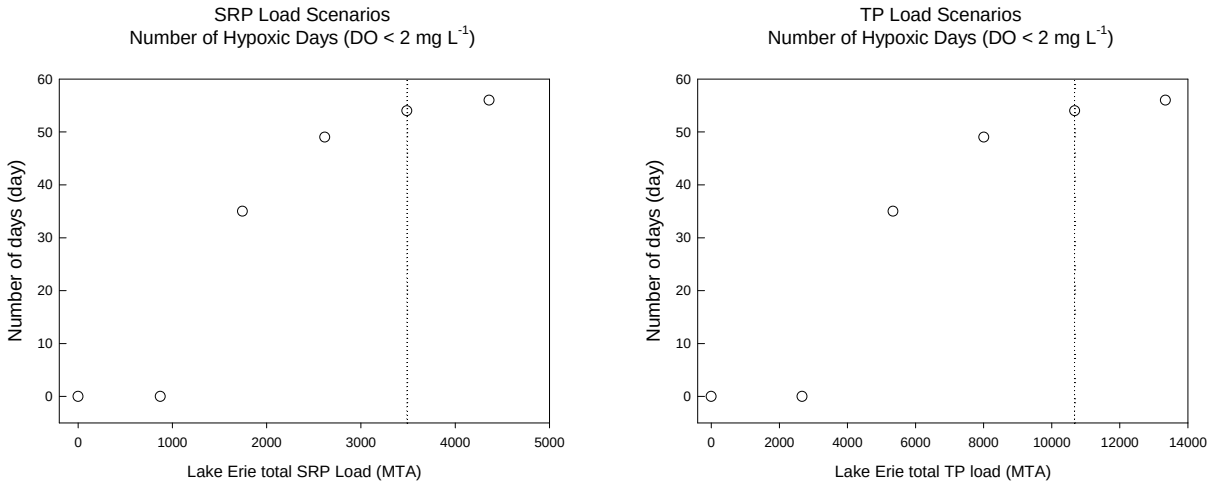

Figure B8-9: Number of total hypoxic days for central basin bottom layer for SRP (left) and TP (right) load scenarios. The vertical dashed line indicates the load for the baseline scenario (no reduction in either SRP or TP loads).

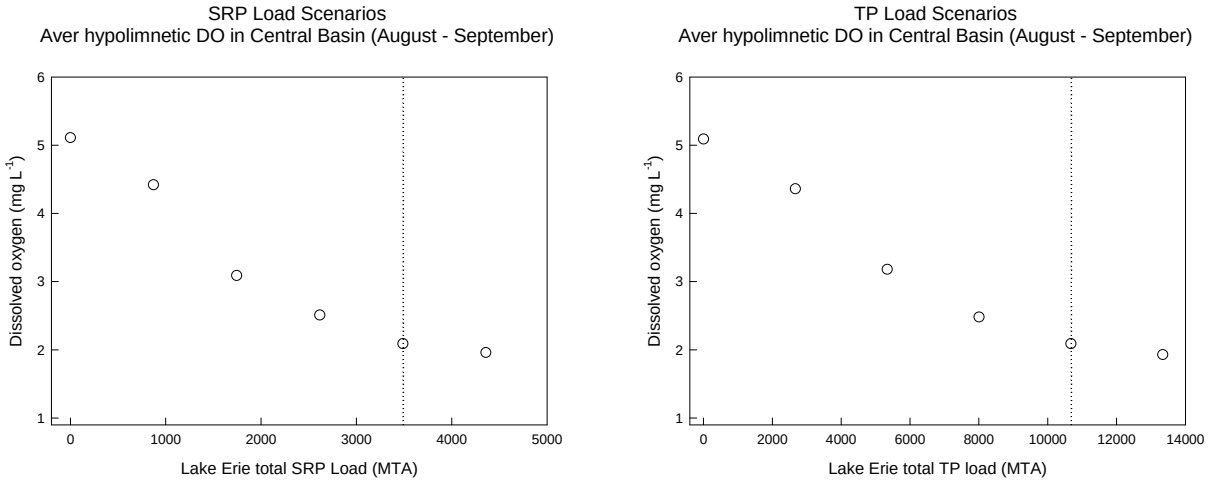

Figure B8-10: Central basin average hypolimnetic DO concentration (June-August, 2008) in the Central basin for SRP (left) and TP (right) load scenarios. The vertical dashed line indicates the load for the baseline scenario (no reduction in either SRP or TP loads).

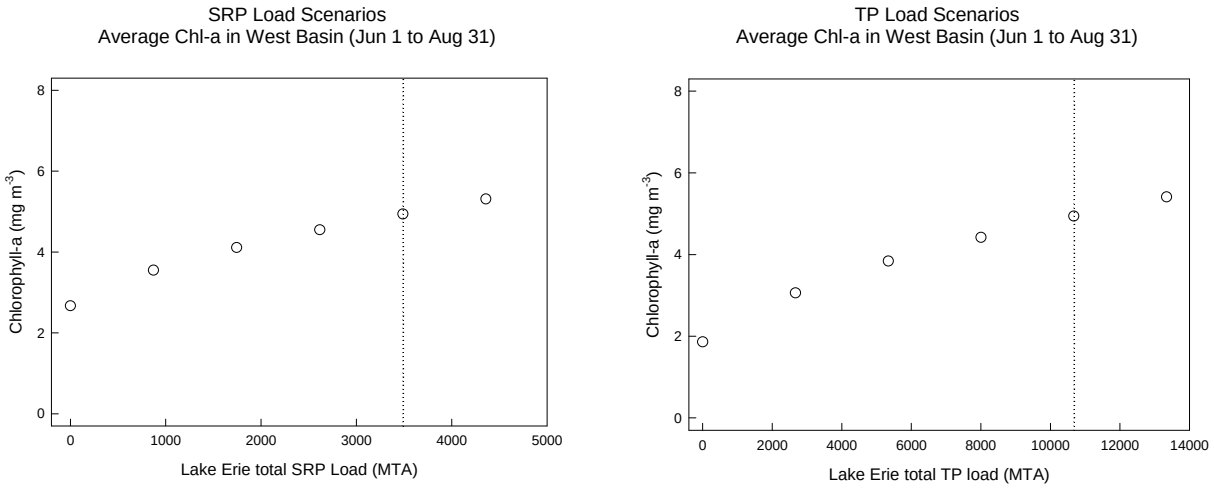

Figure B8-11: Average Chl-a concentration in West basin (June-August, 2008) for SRP (left) and TP (right) load scenarios. The vertical dashed line indicates the load for the baseline scenario (no reduction in either SRP or TP loads).

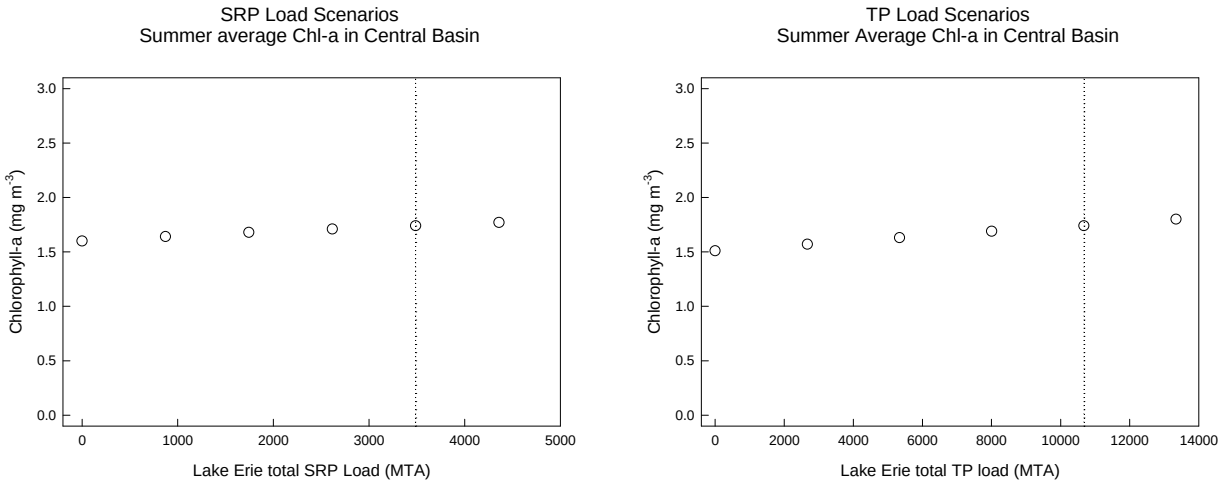

Figure B8-12: Average Chl-a concentration in Central basin (June-August, 2008) for SRP (left) and TP (right) load scenarios. The vertical dashed line indicates the load for the baseline scenario (no reduction in either SRP or TP loads).

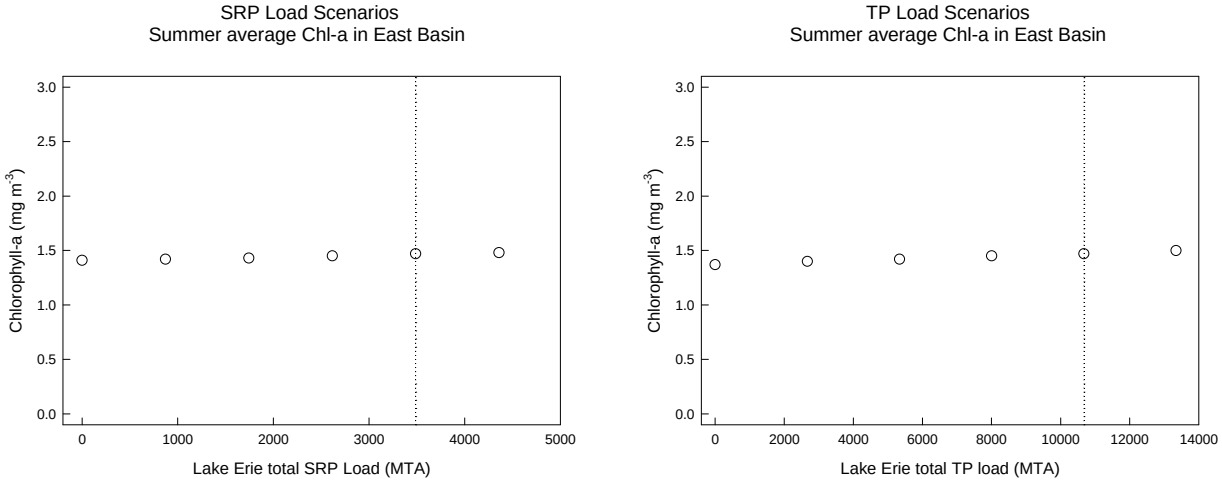

Figure B8-13: Average Chl-a concentration in East basin (June-August, 2008) for SRP (left) and TP (right) load scenarios. The vertical dashed line indicates the load for the baseline scenario (no reduction in either SRP or TP loads).

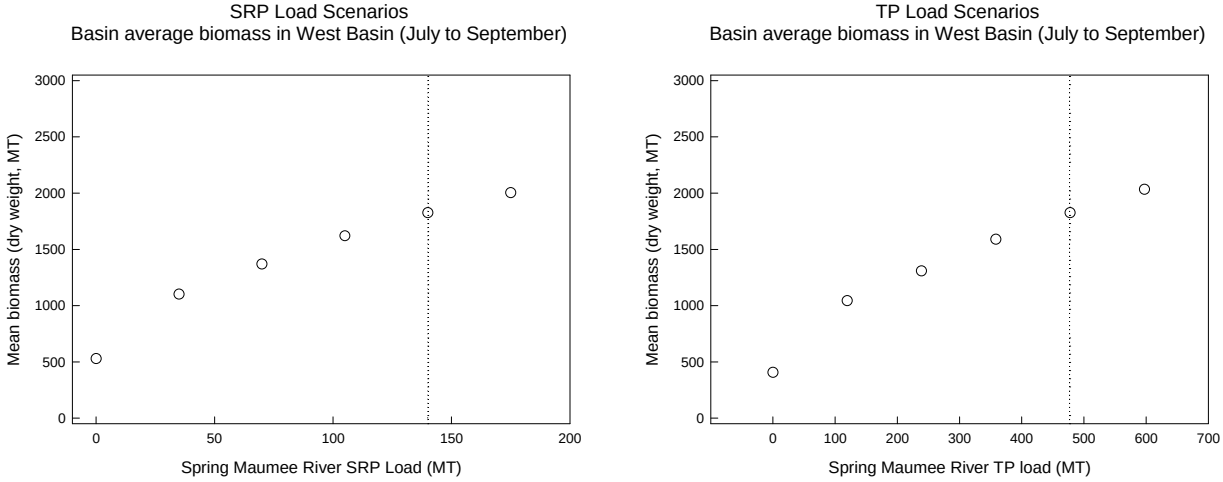

Figure B8-14: Mean basin averaged daily biomass of Cyanobacteria in the West basin as a function of the Spring (April 21 to July 31) Maumee River loads for SRP (left) and TP (right) load scenarios. The vertical dashed line indicates the load for the baseline scenario (no reduction in either SRP or TP loads).

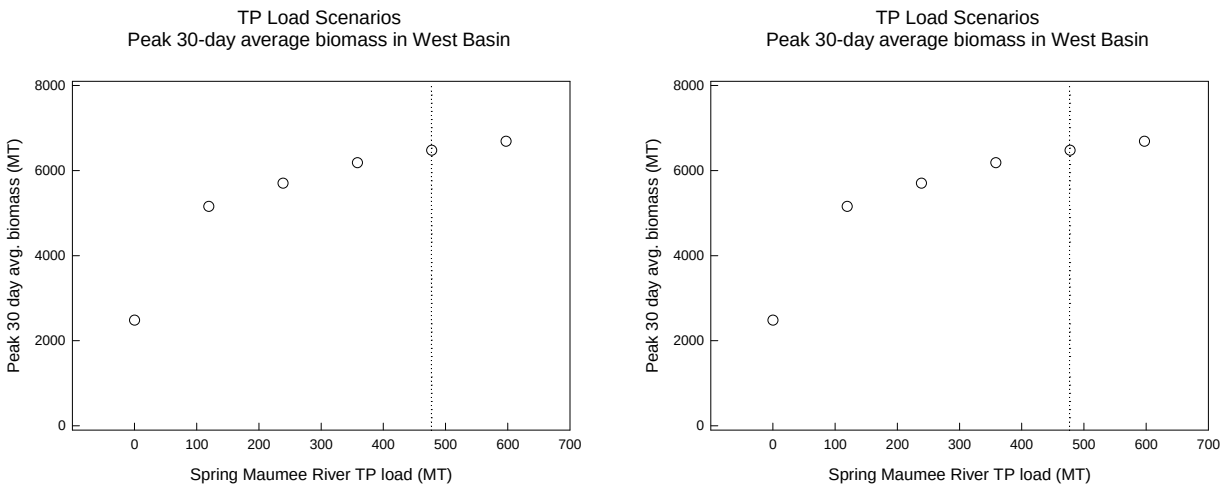

Figure B8-15: Peak 30-day basin averaged biomass of Cyanobacteria in the West basin for SRP (left) and TP (right) load scenarios. The vertical dashed line indicates the load for the baseline scenario (no reduction in either SRP or TP loads).

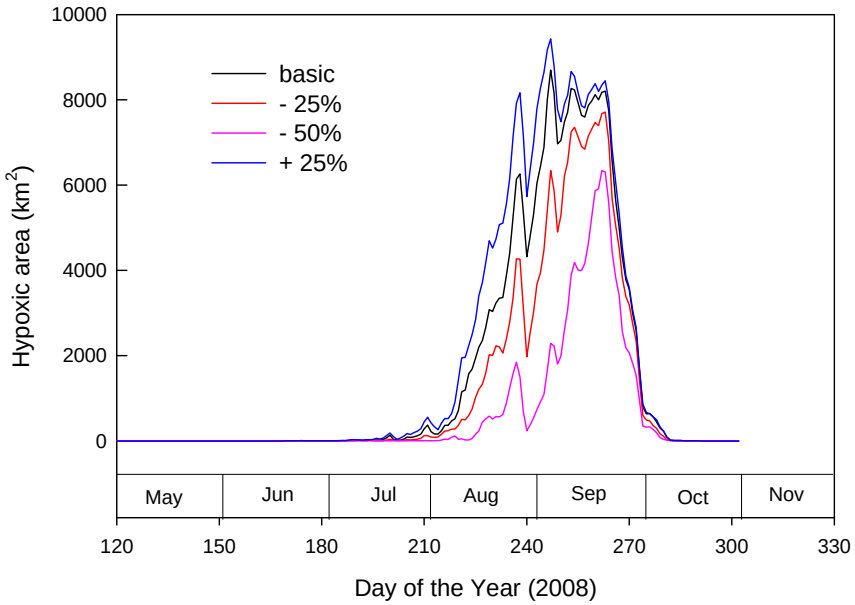

Figure B8-16: Seasonal dynamics of the hypoxic zone (DO < 2 mg L^{-1}) for some selected TP loading scenarios (TP, TP-25%, TP-50%, TP+25%).

Diagnosis/Interpretation

- The model provided reasonable and expected results in terms of the predicted extent of the hypoxic zone, basin-average biomass of cyanobacteria and total phytoplankton.

- The comparison of the load response curves for each of the water quality metrics showed a similar response for either SRP or TP load scenarios pointing out the importance of the soluble reactive portion of the TP for the lake biological processes.

- The model provided results that are in good agreement with the dissolved oxygen observations (e.g. Figure B8-7) and with the expected average extent of the hypoxic zone stressing the importance of the sediment oxygen demand (SOD) for the hypolimnetic oxygen depletion rates in the central basin of Lake Erie.

- The west basin is the most sensitive to variations in nutrient loads (e.g. Figure B8-11) as it has the shortest water residence time (51 days; Bolsenga and Herdendorf, 1993) that is shorter than the total simulation time (191 days). The central and east basins are less sensitive (Figures B8-12 and B8-13) as the water residence times of these basins are much longer than the simulation time, 635 and 322 days, respectively (Bolsenga and Herdendorf, 1993). In order to obtain reasonable estimates of concentrations in these basins, a 3D model has to be run for longer period.

Uncertainty/Sensitivity assessment

No uncertainty and sensitivity assessment have been conducted in this exercise. However, several applications in other lakes provide uncertainty and sensitivity of model results (Bruce et al., 2006; Gal et al., 2009; Makler-Pick et al., 2011).

5. Conclusions/recommendations

- One of the important findings of this study is that to reduce the average extent of the hypoxic zone in Lake Erie by 50%, approximately 17% reduction in SOD rates is needed that would correspond to about 40% reduction in phosphorus load based on the relationship of Rucinski et al. (2014).

- As the model results showed almost similar response for either SRP or TP load scenarios, management authorities should be aware of the importance of soluble phosphate (SRP) removal as other forms of phosphorus (e.g. particulate phosphorous) are less important in fueling in-lake biological processes.

- Concentration of cyanobacteria in the west basin are sensitive to the nutrient loads meaning that the nutrient abatement is a necessary step to reduce the severity of blooms.

- The averaging of the results at basin scale of a complex and dynamic 3D model defeats the power to explore the spatial variability of response in the lake. The 3D models are more suitable in studies on local management of nutrients from point and nonpoint sources that is not explored in this study.

- Because of the long residence time of the lake and due to shorter run times of this model for scenarios, the output would not be appropriate to provide input to the CGM model.

6. References

Bocaniov, S.A., Smith, R.E.H., Spillman, C.M., Hipsey, M.R., Leon, L.F., 2014a. The nearshore shunt and the decline of the phytoplankton spring bloom in the Laurentian Great Lakes: insights from a three dimensional lake model. Hydrobiologia 731, 151-172

Bocaniov, S.A., Ullmann, C., Rinke, K., Lamb, K., Boehrer, B., 2014b. Internal waves and mixing in a stratified reservoir: insights from three-dimensional modeling. Limnologica 49, 52–67

Bolsenga, S. J., Herdendorf, C. E. (Eds.), 1993. Lake Erie and Lake St. Clair Handbook. Wayne State University Press.

Bruce, L.C., Hamilton, D., Imberger, J., Gal, G., Gophen, M., Zohary, T., Hambright, K. D., 2006. A numerical simulation of the role of zooplankton in C, N and P cycling in Lake Kinneret, Israel. Ecol. Model. 193(3), 412-436.

Charlton, M.N., 1987. Lake Erie oxygen revisited. J. Great Lakes Res. 13(4), 697-708

Davis, W.S., Fay, L.A., Herdendorf C.E., 1987. Overview of USEPA/CLEAR Lake Erie sediment oxygen demand investigations during 1979. J. Great Lakes Res. 13(4), 731-737.

Dolan, D.M., Chapra, S.C., 2012. Great Lakes total phosphorus revisited: 1. Loading analysis and update (1994–2008). J. Great Lakes Res. 38(4), 730-740.

Gal, G., Hipsey, M.R., Parparov, A., Wagner, U., Makler, V., Zohary, T., 2009. Implementation of ecological modeling as an effective management and investigation tool: Lake Kinneret as a case study. Ecol. Model. 220(13), 1697-1718.

Hipsey, M.R., 2014. Computational aquatic ecosystem dynamics model: CAEDYM v3. User Guide. Centre for Water Research University of Western Australia. pp. 88

Hipsey M.R, Antenucci J.P, Hamilton D.P., 2014. Computational Aquatic Ecosystem Dynamics Model: CAEDYM v3. Science Manual. Centre for Water Research, University of Western Australia. pp. 111

Hodges B, Dallimore C., 2014. Estuary, Lake and Coastal Ocean Model: ELCOM v3.0 User Manual. Centre for Water Research, University of Western Australia. pp. 65

Hodges B, Dallimore C., 2011. Estuary, Lake and Coastal Ocean Model: ELCOM v2.2 Science Manual. Centre for Water Research, University of Western Australia. pp. 62

Hodges, B.R., Imberger, J., Saggio, A., Winters, K., 2000. Modeling basin scale waves in a stratified lake. Limnol. Oceanogr. 45: 1603–1620.

Lam, D.C.L., Schertzer, W.M., Fraser, A.S., 1987. Oxygen depletion in Lake Erie: modeling the physical, chemical, and biological interactions, 1972 and 1979. J. Great Lakes Res. 13(4), 770-781.

Leon, L.F., Antenucci, J.P., Rao, Y.R., McCrimmon, C., 2012. Summary performance of the estuary and lake computer model (ELCOM): application in the Laurentian and other Great Lakes. Water Qual. Res. J. Can. 47 (3-4), 252-267.

Leon, L.F., Imberger, J., Smith, R.E.H., Hecky, R.E., Lam, D.C. L., Schertzer, W.M., 2005. Modelling as a tool for nutrient management in Lake Erie: a hydrodynamics study. J. Great Lakes Res. 31(suppl. 2), 309-318.

Leon, L.F., Smith, R.E.H., Hipsey, M.R., Bocaniov, S.A., Higgins, S.N., Hecky, R.E., Antenucci, J.P., Imberger, J., Guildford, S.J., 2011. Application of a 3D hydrodynamic-biological model for seasonal and spatial dynamics of water quality and phytoplankton in Lake Erie. J. Great Lakes Res. 37(1), 41-53

Liu, W., Bocaniov, S.A., Lamb, K.G., Smith, R.E.H., 2014. Three dimensional modeling of the effects of changes in meteorological forcing on the thermal structure of Lake Erie. J. Great Lakes Res. (2014), http://dx.doi.org/10.1016/j.jglr.2014.08.002

Matisoff, G., Ciborowski, J.J.H., 2005. Lake Erie trophic status collaborative study. J. Great Lakes Res. 31 (suppl. 2), 1–10.

Oveisy, A., Rao, Y.R., Leon, L.F., Bocaniov, S.A. (2014). Three-dimensional winter modelling and the effects of ice cover on hydrodynamics, thermal structure and water quality in Lake Erie. J. Great Lakes Res. http://dx.doi.org/10.1016/j.jglr.2014.09.008.

Rucinski, D.K., Scavia, D., DePinto, J.V., Beletsky D., 2014. Modeling Lake Erie's hypoxia response to nutrient loads and meteorological variability. J. Great Lakes Res. http://dx.doi.org/10.1016/j.jglr.2014.02.003

Stumpf, R.P., Wynne T.T., Baker D.B., Fahnenstiel, G.L., 2012. Interannual variability of cyanobacterial blooms in Lake Erie. PloS one 7(8), e42444.

Schwab, D. J., Sellers, D.L., 1996. Computerized bathymetry and shorelines of the Great Lakes, NOAA Data Report ERL GLERL-16, NOAA, Ann Arbor, Mich.

Vardit Makler-Pick, V., Gal, G., Gorfine, M., Hipsey, M.R., Carmel, Y., 2011. Sensitivity analysis for complex ecological models: A new approach. Environ. Modell. Softw. 26, 124-134.

APPENDIX B-9: Great Lakes *Cladophora* Model

Martin T. Auer, Anika Kuczynski, Rasika K. Gawde, Michigan Technological University
Steven C. Chapra, Tufts University
Scott N. Higgins, International Institute for Sustainable Development

1. Motivation and Approach

Maintenance of levels of algal biomass below those constituting a nuisance condition is one of the Lake Ecosystem Objectives of Annex 4 (Nutrients) of the Great Lakes Water Quality Protocol of 2012. This Lake Ecosystem Objective is to be met by developing Substance Objectives for phosphorus concentrations in each of the Great Lakes to serve in establishing phosphorus loading targets. The U.S. and Canada, Parties to the 2012 Protocol, have been charged with setting target loads for Lake Erie by 2015.

An Annex 4 Workgroup has been empaneled and directed to utilize an ensemble modeling approach to develop the target loads. Nuisance growth of *Cladophora* in the nearshore waters of Lake Erie's eastern basin has been identified as one of the guiding Environmental Response Indicators (ERIs) for this effort. The appropriate metric for the *Cladophora* ERI is beach fouling, as it is detachment (sloughing) and accumulation that impact lakeshore aesthetics, contact recreation, wildlife and industrial use of cooling water. However, there is no regulatory standard characterizing acceptable levels of beach fouling by *Cladophora* and no *Cladophora*-related Substance Objective for phosphorus for use in establishing target loads. Here, we apply the Great Lakes *Cladophora* Model in establishing a phosphorus Substance Objective applicable to the *Cladophora* dynamic and characterize conditions in the eastern basin relative to that Substance Objective.

2. Model description

Overview

The Great Lakes *Cladophora* Model (GLCM; Tomlinson et al., 2010) is applied here to evaluate the impact of new Lake Erie target phosphorus loads on *Cladophora* growth in the eastern basin. The model is run for a range of soluble reactive phosphorus (SRP) concentrations and the maximum standing crop (gDW/m^2) and stored phosphorus content (P as %DW) of *Cladophora* calculated. SRP concentrations, measured for the eastern basin of Lake Erie (Dove and Chapra, 2015), are then utilized to characterize the state of the phosphorus-*Cladophora* dynamic for the 10-year interval 2002-2012. The SRP-*Cladophora* response curves developed are subsequently linked to a multi-basin Lake Erie TP model (Chapra and Dolan, 2012) to determine the maximum standing crop and stored phosphorus content of *Cladophora* for a range of total phosphorus loads to Lake Erie.

Model Structure

The Great Lakes *Cladophora* Model evolves from the framework developed by Canale and Auer (1982; and related papers), revised, calibrated and confirmed by Tomlinson et al. (2010) and applied by Auer et

al. (2010) in comparing historical and contemporary conditions of *Cladophora* growth. Further adjustment of biokinetic coefficients, with comparison to *Cladophora* metrics in Lakes Erie and Ontario, was made for the Annex 4 Workgroup application. The GLCM utilizes a mechanistic, mass balance approach based upon equations of state for two state variables: algal biomass and stored phosphorus,

$$\frac{dX}{dt} = [\mu - R - L] \cdot X \qquad [1]$$

where: X is the *Cladophora* biomass density (gDW/m^2), μ is the gross specific growth rate coefficient (1/day), R is the specific respiration rate coefficient (1/day) and L is the specific sloughing rate coefficient (1/day);

$$\frac{dS}{dt} = [\rho \cdot X - R \cdot S] \cdot X \qquad [2]$$

where: ρ is the phosphorus uptake coefficient (%P/day); The stored phosphorus content of the alga (Q, P as %DW) is then calculated as,

$$Q = \frac{S}{X} \cdot 100 \qquad [3]$$

Values for model coefficients are derived from field measurements and laboratory experiments and through model calibration (Canale and Auer, 1982; Tomlinson et al., 2010). The GLCM predicts *Cladophora* standing crop and production, the generation of sloughed biomass and stored phosphorus content as functions of light and temperature conditions and the availability of SRP.

3. Model calibration and confirmation

The GLCM was calibrated and confirmed at sites in the nearshore waters of Lake Huron (Harbor Beach, MI) and Lake Michigan (Milwaukee, WI) prior to application in support of phosphorus management in the Great Lakes (Tomlinson et al., 2010). These data sets are particularly useful for calibration-confirmation as they differ markedly in depth ($z \leq 2$m in Lake Huron, z = 9m in Lake Michigan) and nutrient status (Q = 0.2-0.5 %P in Lake Huron, $Q \leq 0.1$ %P in Lake Michigan). Model inputs include temperature, incident light (PAR) and the vertical light extinction coefficient; all of which were developed on a site-specific basis (Tomlinson et al., 2010). *Cladophora* biomass and stored phosphorus data for model calibration and confirmation were derived from field and laboratory studies described in Auer et al. (1982) and Tomlinson et al. (2010), respectively. The GLCM was calibrated (Lake Huron) and confirmed (Lake Michigan) by comparing model fit to field data. Model output successfully tracked both the magnitude of and temporal variation in algal standing crop and stored nutrient content; the performance of the GLCM is thus considered to be confirmed (Tomlinson et. al., 2010).

4. Model application

The calibrated and confirmed GLCM is now applied in simulating the response of *Cladophora* in the eastern basin of Lake Erie to changes in phosphorus loading to the lake as a whole. The approach for

accomplishing this is to develop relationships between SRP concentration and the *Cladophora* maximum standing crop and stored nutrient content. Output from a total phosphorus model developed by the Annex 4 Workgroup (Chapra and Dolan, 2012) and an empirical relationship between TP and SRP using data from Dove and Chapra (2015) are then utilized to identify the correspondence of various TP loads to those relationships.

Model Inputs

Model inputs required for application of the GLCM fall into one of four categories: site characteristics (depth and time interval of simulation), environmental forcing conditions (incident light, light extinction and temperature), initial conditions (*Cladophora* biomass and stored phosphorus content) and coefficients (see Tomlinson et al., 2010). Model inputs are detailed in Table B9-1, including their values and comments on their source and derivation.

Model Uncertainty/Sensitivity

Sensitivity analyses were performed to characterize model uncertainty in its application to the eastern basin of Lake Erie. The analysis was performed for seven model coefficients (K_m, $K_{s,max}$, Q_0, R_{max}, X_{max}, μ_{max}, and ρ_{max}; Tomlinson et al., 2010), varying them one at a time by ±10%. The resulting response, % change in *Cladophora* standing crop and stored phosphorus content (Figure B9-1), was then used as a metric of model uncertainty. The analysis indicated that stored phosphorus content is insensitive to model coefficient values (ΔQ <5%), a result of the large difference in the time scales of increase due to P-uptake and decrease due to partitioning through growth. Predicted algal standing crop was particularly sensitive to the value of the minimum cell quota (ΔX_{Q0} = 61%) and to the maximum gross growth and respiration rates ($\Delta X_{\mu max}$ = 61% and ΔX_{Rmax} = 54%). Model sensitivity to variation in Q_0 is carried forward in developing load-response curves as means of illustrating uncertainty.

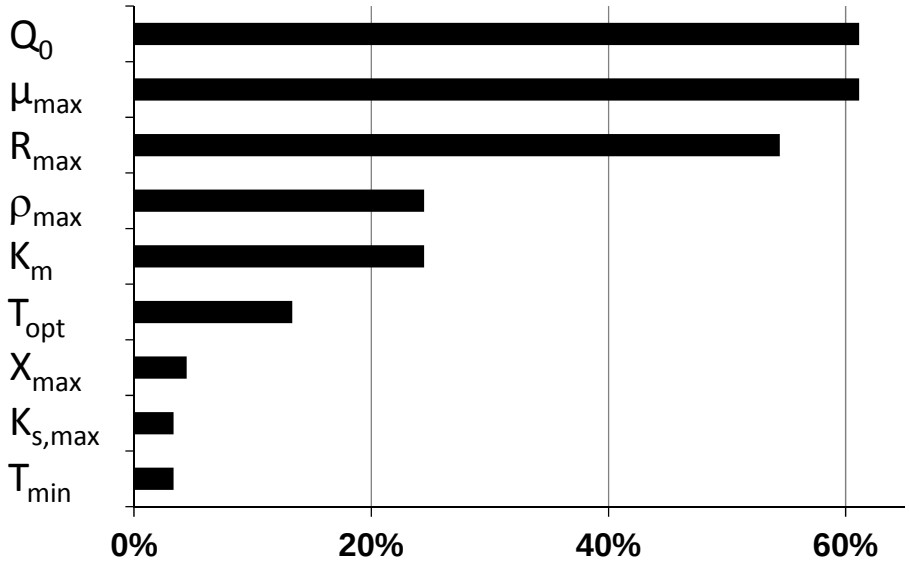

Figure B9-1: GLCM sensitivity analysis showing percent change in predicted *Cladophora* maximum standing crop corresponding to a ±10% change in selected model coefficients.

Table B9-1: Model inputs used to develop loading scenarios.

Model Inputs	Value	Units	Comments
Site Characteristics			
Depth	2	m	Optimal depth for growth in the Lake Erie eastern basin; Higgins et al., 2005
Time of simulation	30 May – 30 Aug		Growth season in Lake Ontario; Malkin et al., 2008
Forcing Conditions			
Incident light	Seasonal time series		NOAA/GLERL Real Time Meteorological Network; polynomial fit to hourly PAR data for 2002-2012, Muskegon, MI
Extinction coefficient	0.2	1/m	Clear water minimum, Higgins et al., 2005, Figure 2
Temperature	Seasonal time series		GLSEA2; polynomial fit to daily surface water values for Erie, PA, 2003-2013
Initial Conditions			
Biomass	1	gDW/m^2	Specified
Stored phosphorus	-	P as %DW	Initially Q_0, then re-run with equilibrium Q value for specified SRP
Coefficients			
μ_{max}	1.25	1/d	Determined by calibration to Lake Ontario; Higgins et al., 2012, Figure 2
R_{max}	0.45	1/d	Determined by calibration to Lake Ontario; Higgins et al., 2012, Figure 2
Q_0	0.04	P as %DW	Higgins et al. 2005, Table 1
K_m	177	mgP/m^3	Mean plus one S.D. of values measured by Auer and Canale 1982, Figure 11
X_{max}	315	gDW/m^2	Median maximum biomass for depths of 0-2 m, 2005; Higgins et al., 2005, Table 1

Load-Response Curves

The objective load-response curves is to link the management variable (here, phosphorus loads) to the ERI response (here, *Cladophora* biomass and nutrient content). This is a two-step process: first, defining the relationship between phosphorus loads and water column phosphorus concentrations and second developing a relationship between those concentrations and metrics of the *Cladophora* ERI.

Phosphorus Loads – for the first step, we utilize a mechanistic, mass balance model for total phosphorus in the Great Lakes developed by Chapra and Dolan (2012). Total phosphorus concentrations are calculated for the eastern basin of Lake Erie for a range of total TP loads to the lake. The model is run to steady state for the condition of the maximum total load for Lake Erie (16,334 MTA; Dolan and Chapra, 2012) and then a line is extended from that point to the origin (zero load), taking advantage of the linearity of the calculation (Figure B9-2).

In open lake applications, modeling and management efforts have utilized empirical models relating TP concentration to ERIs such as chlorophyll concentration, Secchi disk transparency and the rate of hypolimnetic oxygen depletion. The varying bioavailability of the TP analyte and the dynamic nature of meteorological and nutrient forcing conditions in the nearshore have led those modeling *Cladophora* (e.g. Canale and Auer, 1982; Higgins et al., 2005b; Malkin et al., 2008; Tomlinson et al., 2010) to pursue a mechanistic approach, focusing on the role of soluble reactive phosphorus, the form fully and freely available to algae. The adoption of an SRP-basis for the *Cladophora* ERI requires either: (a) utilization of an empirical relationship between TP and SRP or (b) development and application of a mechanistic, mass balance model for SRP in the nearshore.

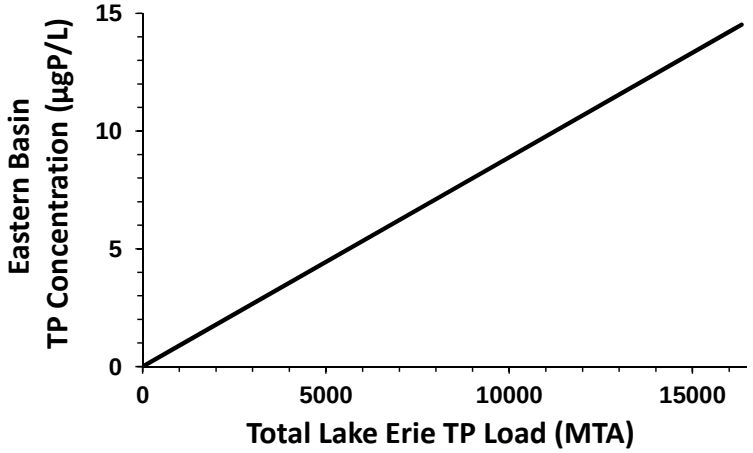

Figure B9-2: Relationship between the total Lake Erie TP load and the eastern basin TP concentration.

Here, we have chosen the first approach, drawing upon an empirical relationship between SRP and TP based on measurements made in the eastern basin of Lake Erie by Environment Canada from 1994-2012 (Figure B9-3; data of Dove and Chapra, 2015). This relationship may be applied in translating output from the TP model developed by Chapra and Dolan (2012) into the SRP concentrations required for application of the Great Lakes *Cladophora* Model (GLRC) to the *Cladophora* ERI. A non-linear fit to the data has been selected here to accommodate variation in the contribution of a refractory fraction to the

TP analyte and to recognize that the ability of phytoplankton to deplete SRP in phosphorus-poor systems.

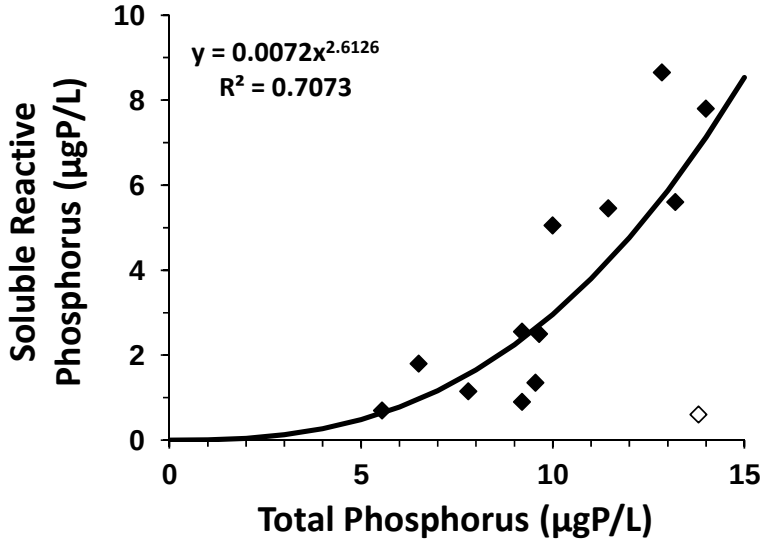

Figure B9-3: Empirical relationship between TP and SRP for 2002-2012 in the eastern basin of Lake Erie (data of Dove and Chapra, 2015).

Cladophora Response – the second step in developing a load–response curve for the *Cladophora* ERI involves application of the GLCM to relate the algal response (maximum standing crop and stored phosphorus content) to changes in the nutrient forcing condition (SRP concentration). Here, the GLCM is run for the June – August interval with forcing conditions, initial conditions and model coefficients as presented in Table B9-1. The response is simulated for algal colonization at 2m, a depth in the eastern basin characterized by abundant *Cladophora* growth (Higgins et al., 2005). Model runs yield two SRP-*Cladophora* ERI response curves: one for algal maximum standing crop and one for algal stored phosphorus content (Figure B-4). Four characteristic regions may be identified in the *Cladophora* response curve:

- *no growth* – *Cladophora* does not grow below a SRP concentration of ~0.5 µgP/L . Here, gross production is nutrient-limited to the point that metabolic demands cannot be satisfied, i.e. respiration > photosynthesis. This is the condition in the waters of Lake Superior which remains uncolonized by *Cladophora*;

- *P limitation* – above a SRP concentration of ~0._ µgP/L, model-predicted algal standing crop increases with increasing phosphorus levels in an essentially linear fashion. Here, incremental reductions in SRP can be expected to yield a concomitant reduction in *Cladophora* biomass, i.e. the system is sensitive to management; and

- *the 'hip'* – at a SRP concentration of ~2.0 µgP/L, the *Cladophora* response begins to depart from that linearity, tending toward a region of P-saturation. Movement of a system through the hip is an important signal of transition into or out of a condition that is sensitive to phosphorus management; and

- *P saturation* – moving above a concentration of 2.0 µgP/L, the *Cladophora* response asymptotically approaches the maximum standing crop dictated by its carrying capacity (self-shading, light limitation). Here, further increases in phosphorus availability have little impact on the *Cladophora* ERI. From a management perspective, a position in this region may be challenging because significant reductions in load fail to manifest themselves in a significant change in nuisance growth. This is misleading, however, because those reductions in phosphorus availability do serve to move the system toward the hip and into the region of P-limitation and a response by the *Cladophora* ERI.

The load-response curve for phosphorus and the *Cladophora* ERI is then developed by converting TP loads (with serial reduction, e.g. 10%, 25,%, 50%) to TP concentrations (Figure B9-2), TP concentrations to SRP concentrations (Figure B9-3) and SRP concentrations to the two *Cladophora* ERI metrics: maximum standing crop and stored nutrient content. Finally, a plot of the TP load (or load reduction) versus the two *Cladophora* ERI metrics represents the load-response relationship (Figure B9-5).

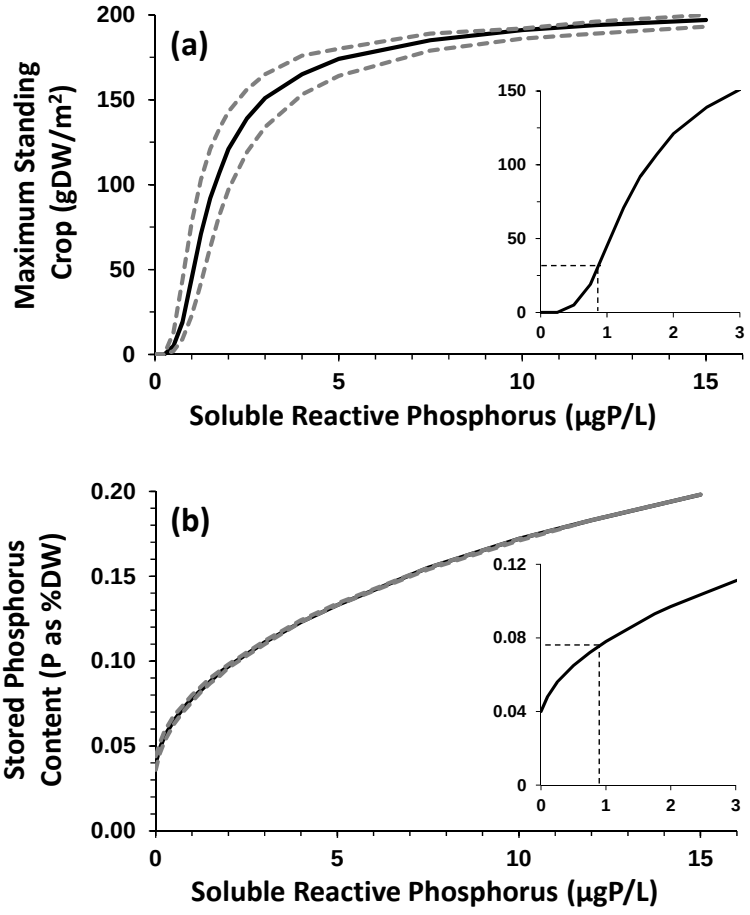

Figure B-4: Response curves for *Cladophora* growing at 2m depth in the eastern basin of Lake Erie: (a) maximum standing crop and (b) stored phosphorus content. Dashed lines illustrate the response to a ±10% in Q_0, the coefficient to which the model is most sensitive.

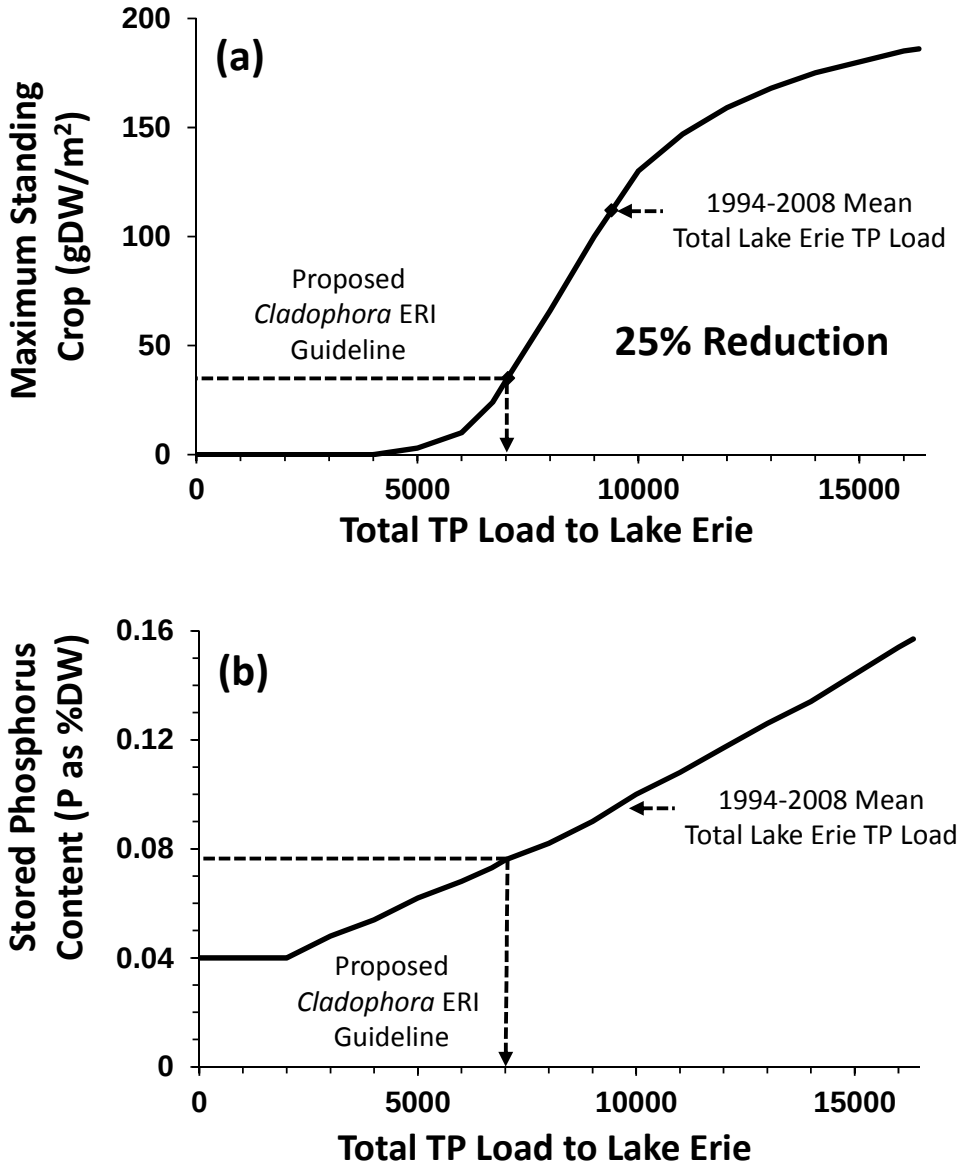

Figure **B-5:** Load-response curves for the *Cladophora* ERI in the eastern basin of Lake Erie: (a) maximum standing crop and (b) stored phosphorus content.

Diagnosis and Interpretation

Standards and Substance Objectives - there is no regulatory guidance, within the U.S. or Canada, relating to acceptable levels of *Cladophora* biomass and thus no Substance Objective for phosphorus relative to the *Cladophora* ERI has been established. In order to meet the Annex 4 Workgroup goal to provide a load-response curve for the *Cladophora* ERI, we propose a Substance Objective for phosphorus based on the SRP – *Cladophora* biomass response curve presented previously (Figure B9-4). We adopt an acceptable level of *Cladophora* biomass as 30±10 gDW/m^2, the average standing crop for five sites on Lake Ontario unimpacted by urban influences (Higgins et al., 2012). This biomass guidance value is comparable in magnitude to that proposed by Canale and Auer (1982) for avoidance of nuisance conditions of *Cladophora* growth in Lake Huron (50 gDW/m^2). Applying the GLCM, the proposed mean target biomass corresponds to an SRP level of 0.9 µgP/L (Figure B9-4, insets) and, using the regression equation presented as Figure B9-3, a TP level of 6.3 µgP/L.

Phosphorus and Cladophora in the Eastern Basin - phosphorus levels in the eastern basin of Lake Erie have met the proposed Substance Objective for TP twice (2000 and 2003) and SRP three times (1997, 2000 and 2008) in the past 40 years (Figure B9-6). While it is tempting to posit that SRP concentrations are now on the decline in the eastern basin, the juxtaposition of intervals of low (1997-2000 and 2008-2012) and high (2002-2007) SRP concentrations make it difficult to make that case. Rather, a high degree of variability in both SRP and TP is characteristic of the eastern basin with little or no downward trend in concentration in the past two decades. Considered from another perspective, the *Cladophora*-phosphorus dynamic has resided in the linear, P-limited range from 1994-2000 and 2008-2012, but lay beyond the 'hip' connecting the P-limited and P-saturated regions in the intervening years (2002-2007; Figure B9-7). Higgins et al. (2005) reported on surveys of ~100 km of shoreline at a depth of 2m in the eastern basin of Lake Erie where the standing crop of *Cladophora* averaged 281±144 gDW/m^2 in 1995, 158±101 gDW/m^2 in 2001 and 176±133 gDW/m^2 in 2002. These measurements represent some of the highest biomass values measured in the Great Lakes, levels of standing crop consistent with the elevated SRP concentrations noted by Dove and Chapra (2015; Figure 6b). Thus, the eastern basin of Lake Erie has historically been rich in phosphorus and has supported nuisance levels of *Cladophora* growth. Contemporary information on the phosphorus-*Cladophora* dynamic in the eastern basin is, however, limited with only one measurement of SRP since 2009 and, to our knowledge, no monitoring of *Cladophora* since 2002.

Impact of Load Management – The proposed Substance Objective proposed for the *Cladophora* ERI corresponds to a total TP loads to Lake Erie of 7000 MTA, as calculated here. Over the interval 1994-2008, total TP loads to Lake Erie have averaged 9388±2685 MTA. Thus a reduction in total TP load to Lake Erie of 25% would be required to meet the proposed phosphorus Substance Objective for the *Cladophora* ERI. It is recommended, however, that natural variability in the TP load (C.V. = 29%) be taken into account when establishing targets.

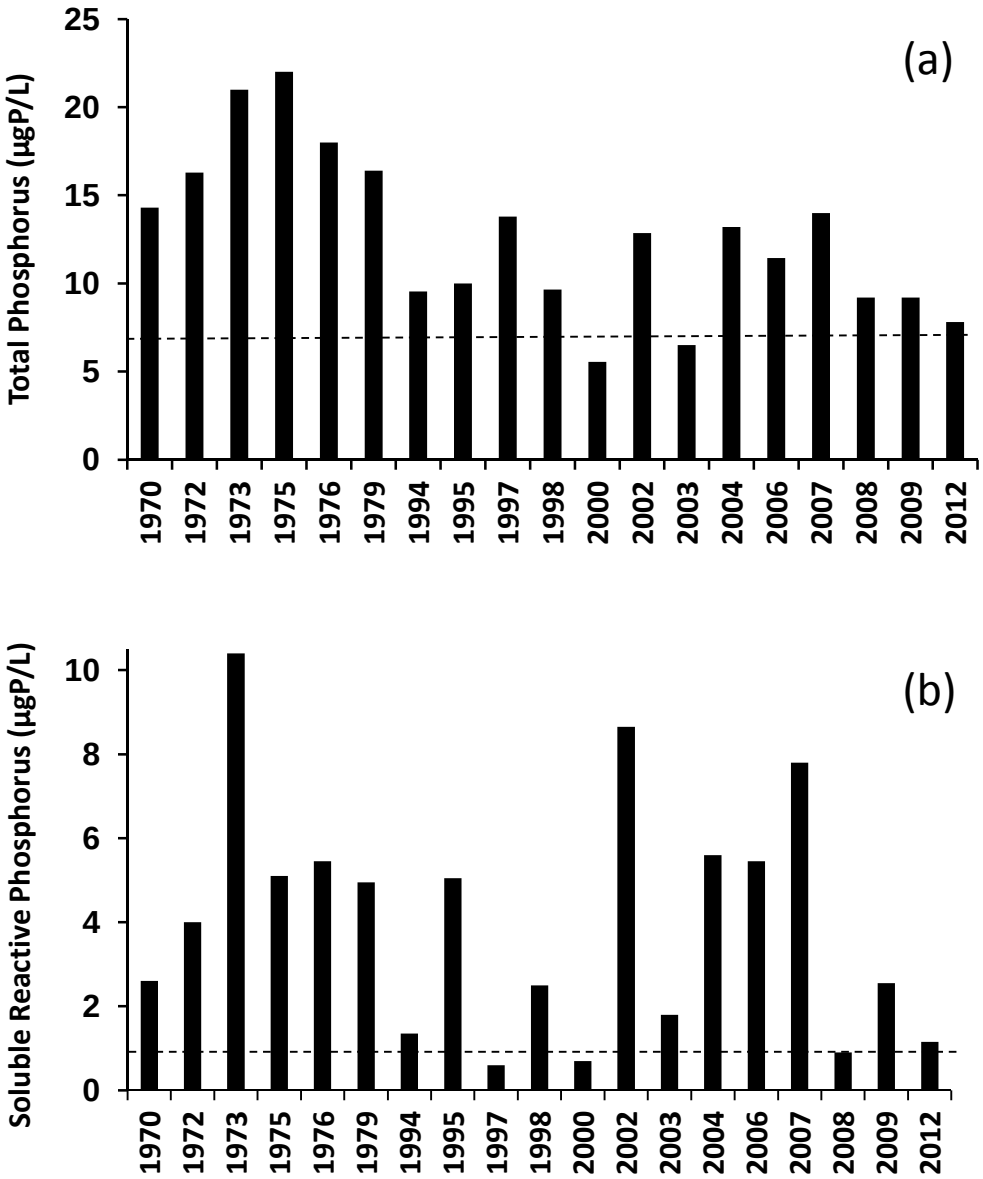

Figure B9-6: Concentrations of (a) TP and (b) SRP in the eastern basin of Lake Erie, 1970-2012 (EC data from Dove and Chapra 2015).

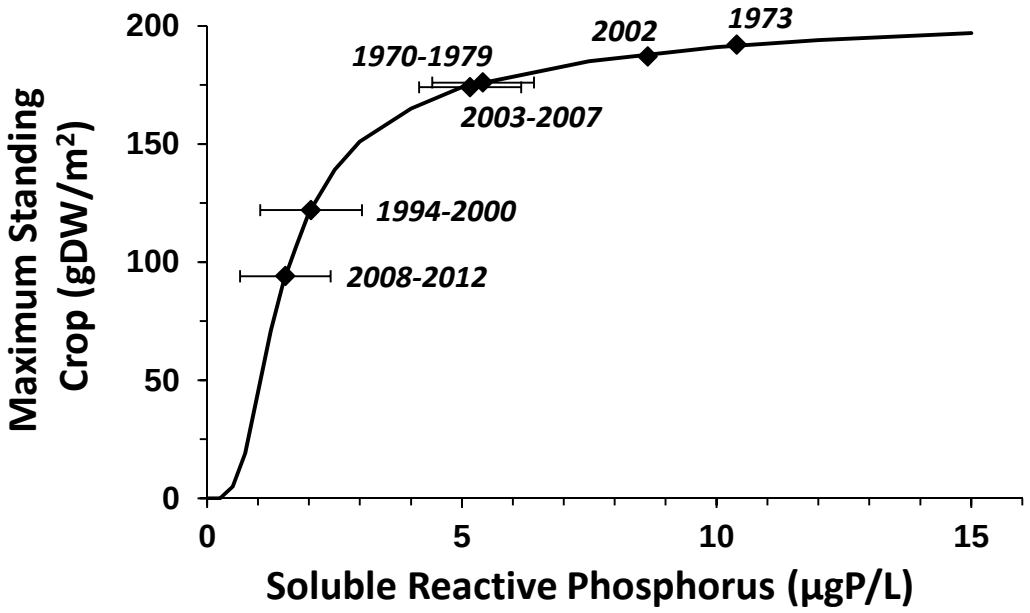

Figure B9-7: Mean SRP concentrations for the eastern basin of Lake Erie in relation to the maximum standing crop *Cladophora* ERI. Bars represent the standard deviation for mean SRP concentration for the interval shown.

Additional Considerations in the Nearshore **–** management of phosphorus in the offshore waters of the Great Lakes places its primary emphasis on well-mixed conditions, i.e. where tributary and point source inputs have become part of the larger water body and the system may be characterized and managed on a multi-basin or whole lake basis. In nearshore waters, those inputs have not yet been mixed with and assimilated by the larger water body and phosphorus concentrations will be higher and more variable than in offshore waters. The impact of a particular discharge may thus exist over an extended area of the nearshore where longshore currents transport phosphorus away from a source and initiate mixing with offshore waters. For this reason, P-management in relation to the *Cladophora* ERI must be addressed by integrating conditions in the well-mixed offshore boundary and the more spatially and temporally dynamic nearshore as impacted by tributaries and point sources.

Although not verified through regulatory monitoring, anecdotal evidence and satellite sensing (Figure B9-8) indicate that *Cladophora* is more abundant, more widely distributed and more likely to create nuisance conditions on the north shore (Canadian waters) of the eastern basin than along the south shore (U.S. waters). This would be consistent with the fact that the Grand River delivers TP and SRP loads of 200-350 and 50-150 MTA to the north shore (Shaker, 2014) while there are no tributary or point source discharges of this magnitude along the south shore. Measurements of SRP along the north shore to the east and west of the Grand River mouth (Figure B9-9; Joanna Majarreis, University of Waterloo, unpublished data), indicate that the Grand River discharge has the capacity to increase SRP concentrations in the Canadian nearshore well above offshore levels. Thus, it is not sufficient to address phosphorus dynamics with respect to the *Cladophora* ERI based simply on whole-lake or multi-basin

calculations. Instead, a 3D modeling framework must be employed where tributary and point source impacts and the attendant heterogeneity of the nearshore region may be taken into account.

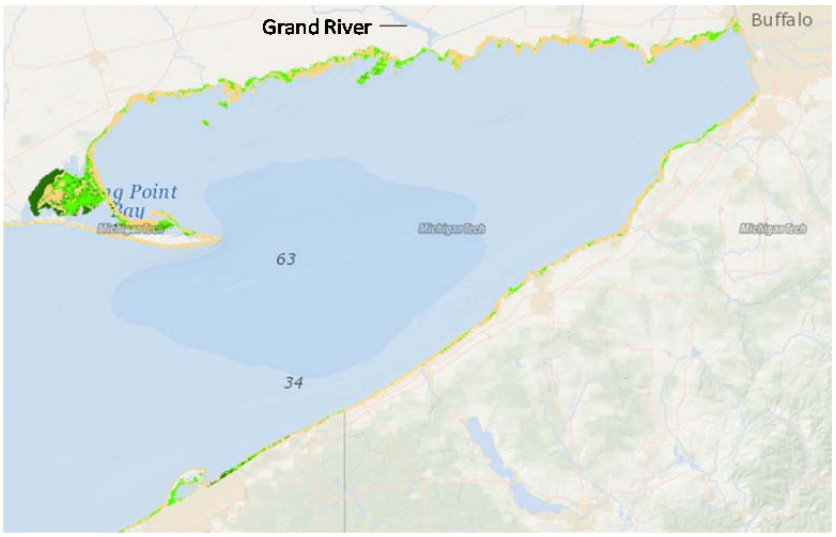

Figure B9-8: *Cladophora* distribution in the eastern basin of Lake Erie. Image acquired from the Michigan Tech Research Institute, http://geodjango.mtri.org/static/sav/.

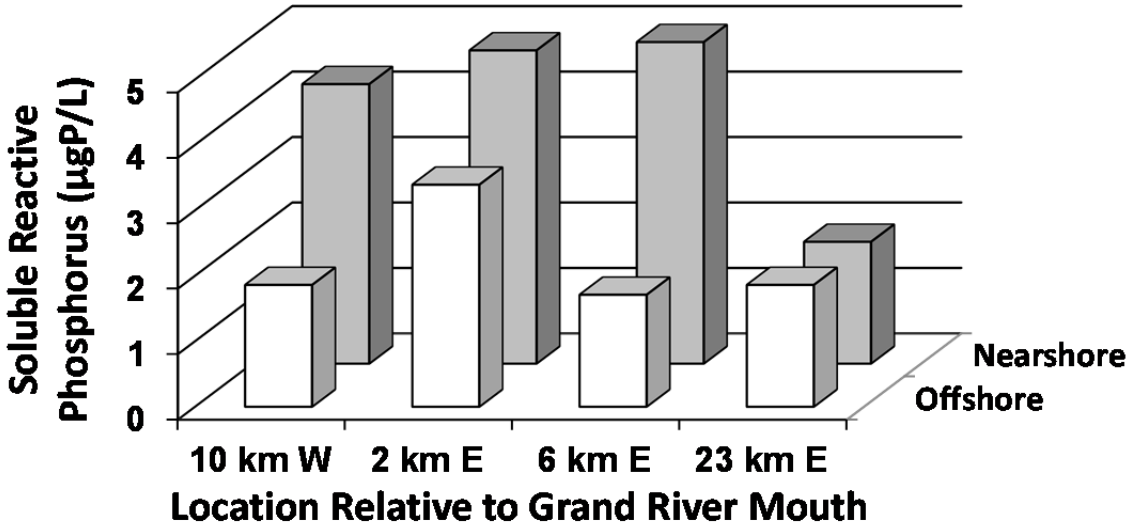

Figure B9-9: Mean surface water soluble reactive phosphorus concentrations for samples collected in May and June 2013 at nearshore (≤1 km) and offshore (~5 km) sites in the vicinity of the Grand River (unpublished data of Joanna Majarreis, University of Waterloo).

5. Conclusions/Recommendations

A peak biomass value for the *Cladophora* Environmental Response Indicator, 30 gDW/m^2, is proposed here as guidance for development of revised phosphorus loads for Lake Erie seeking to eliminate nuisance growth of the alga in the eastern basin. This *Cladophora* ERI value was then used in concert with the Great Lakes *Cladophora* model to establish a Substance Objective for soluble reactive

phosphorus, 0.9 µgP/L. Next, an empirical model based on measurements made in the eastern basin was used to convert the SRP Substance Objective for expression as total phosphorus, 6.3 µgP/L. Final, a mechanistic, multi-basin, mass balance model for total phosphorus in the Great Lakes was employed to establish the total TP load for Lake Erie corresponding to the TP-based expression of the phosphorus Substance Objective, 7000 MTA. We recommend that load, a 25% reduction from the average total TP load to Lake Erie for the period 1994-2008, as the revised load with respect to the *Cladophora* ERI. We believe it to be critical that water quality managers recognize the significant differences between nearshore and offshore environments and their respective ERIs. Because phosphorus discharges from tributaries and point sources pass through *Cladophora* habitat as they move toward mixing and assimilation with open waters, it is not sufficient to simply consider conditions in the open lake boundary to coastal environments. Thus, P-management in relation to the *Cladophora* ERI must utilize predictive tools, e.g. a 3D model, which can accommodate both nearshore-offshore exchange and the nearshore phosphorus dynamics nearshore as influenced by tributaries and point sources.

6. References

Auer, M. T. 1982. Ecological studies and mathematical modeling of *Cladophora* in Lake Huron: 1. Program description and field monitoring of growth dynamics. *Journal of Great Lakes Research*, 8(1): 73-83**.**

Auer, M.T., Tomlinson, L.M., Higgins, S.N., Malkin, S.Y., Howell, E.T. and H.A. Bootsma. 2010. Great Lakes *Cladophora* in the 21st Century: Same alga – different ecosystem. *Journal of Great Lakes Research*, 36: 248-255.

Canale, R.P. and M.T. Auer. 1982. Ecological studies and mathematical modeling of *Cladophora* in Lake Huron: 5. Model development and calibration. *Journal of Great Lakes Research*, 8(1):112-125**.**

Chapra, S.C. and Dolan, D.M. 2012. Great Lakes total phosphorus loads revisited: 2. Mass balance modeling. *Journal of Great Lakes Research*, 38(4): 741-754.

Dove, A. and Chapra, S.C. 2015. Long-term trends of nutrients and trophic response variables for the Great Lakes. In Review, *Limnology and Oceanography*.

Dolan, D.M. and Chapra, S.C. 2012. Great Lakes total phosphorus loads revisited: 1. Loading analysis and update (1994–2008). *Journal of Great Lakes Research*, 38(4): 730-740.

Higgins, S.N., Howell, E.T. and Hecky, R.E. 2005a. The Wall of Green: The status of *Cladophora glomerata* on the northern shores of Lake Erie's eastern basin, 1995–2002. *Journal of Great Lakes Research*, 31: 547-563.

Higgins, S.N., Hecky, R.E. and Guildford, S.J. 2005b. Modeling the growth, biomass, and tissue phosphorus concentration of *Cladophora glomerata* in Eastern Lake Erie: Model description and field testing. *Journal of Great Lakes Research*, 31: 439–455.

Higgins, S. N., Pennuto, C.M., Howell, E.T., Lewis, T.D. and Makarewicz, J.C. 2012. Urban influences on *Cladophora* blooms in Lake Ontario. *Journal of Great Lakes Research*, 38: 116–123.

Malkin, S.Y., Guildford, S.J., Hecky, R.E., 2008. Modeling the growth of *Cladophora* in a Laurentian Great Lake in response to changes due to the exotic invader *Dreissena* and to lake warming. Limnology and Oceanography, 53: 1111–1124.

Shaker, S. 2014. Historical Trends in Water Quality in the Grand River, Ontario: Reconstruction of Phosphorus Loadings. M.S. Thesis, Department of Earth and Environmental Sciences, University of Waterloo, Waterloo, Ontario, Canada. 43 pp.

Tomlinson, L.M., Auer, M.T. and H.A. Bootsma. 2010. The Great Lakes *Cladophora* Model: Development and application to Lake Michigan. *Journal of Great Lakes Research*, 36: 287-297.